HZDR-002

Wissenschaftlich-Technische Berichte
HZDR-002 2011 · ISSN 2191-8708

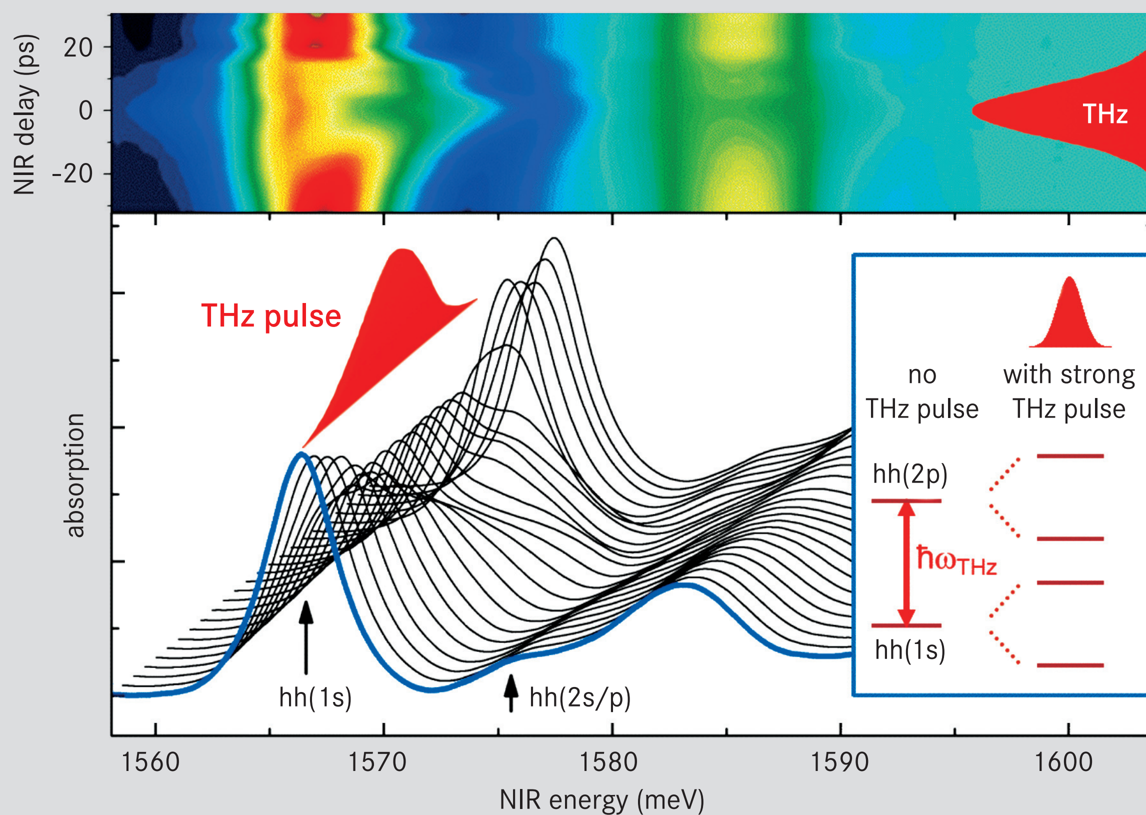

ANNUAL REPORT 2010

INSTITUTE OF ION BEAM PHYSICS AND MATERIALS RESEARCH

HZDR

HELMHOLTZ
ZENTRUM DRESDEN
ROSSENDORF

Wissenschaftlich-Technische Berichte
HZDR – 002
2011

HZDR

Annual Report 2010

Institute of Ion Beam Physics and Materials Research

Editors:

J. von Borany, J. Fassbender,
V. Heera, M. Helm

Cover Picture:

The cover picture illustrates the near-infrared absorption of excitonic transitions in semiconductor quantum wells under illumination with intense THz pulses of the free-electron laser. The THz light couples the hh(1s) and hh(2p) states resulting in a characteristic, intensity-dependent line splitting of the hh(1s) ground state at higher field strengths that is a manifestation of the intraexcitonic Autler-Townes effect. This splitting only occurs during the THz pulse, as shown in the waterfall and corresponding contour plot in the figure.

For further information see:
M. Wagner et al., Phys. Rev. Lett. **105**, 167401 (2010),
reprinted at pp. 16 – 19 of this Annual Report.

Helmholtz – Zentrum Dresden – Rossendorf e.V.

Institute of Ion Beam Physics and Materials Research

P.O. Box 51 01 19
01314 Dresden
Germany

Directors	Prof. Dr. M. Helm	Prof. Dr. J. Fassbender
Phone	+ 49 (351) 260 2260	+ 49 (351) 260 3096
Fax	+ 49 (351) 260 3285	+ 49 (351) 260 3285
Email	m.helm@hzdr.de	j.fassbender@hzdr.de

http://www.hzdr.de/FWI

Preface by the Directors

The Institute of Ion Beam Physics and Materials Research (IIM) is one of the six institutes of what was called Forschungszentrum Dresden-Rossendorf (FZD) until the end of 2010, but since this year 2011 is called "Helmholtz-Zentrum Dresden-Rossendorf (HZDR)". This change reflects a significant transition for us: it means that the research center is now member of the Helmholtz Association of German Research Centers (HGF), i.e., a real government research laboratory, with the mission to perform research to solve fundamental societal problems. Often to date those are called the "Grand Challenges" and comprise issues such as energy supply and resources, health in relation to aging population, future mobility, or the information society.

This Annual Report already bears the new corporate design, adequate for the time of its issueing, but reports results from the year 2010, when we were still member of the Leibniz Association (WGL). Our research is still mainly in the fields of semiconductor physics and materials science using ion beams. The institute operates a national and international Ion Beam Center, which, in addition to its own scientific activities, makes available fast ion technologies to universities, other research institutes, and industry. Parts of its activities are also dedicated to exploit the infrared/THz free-electron laser at the 40 MeV superconducting electron accelerator ELBE for condensed matter research. For both facilities the institute holds EU grants for funding access of external users.

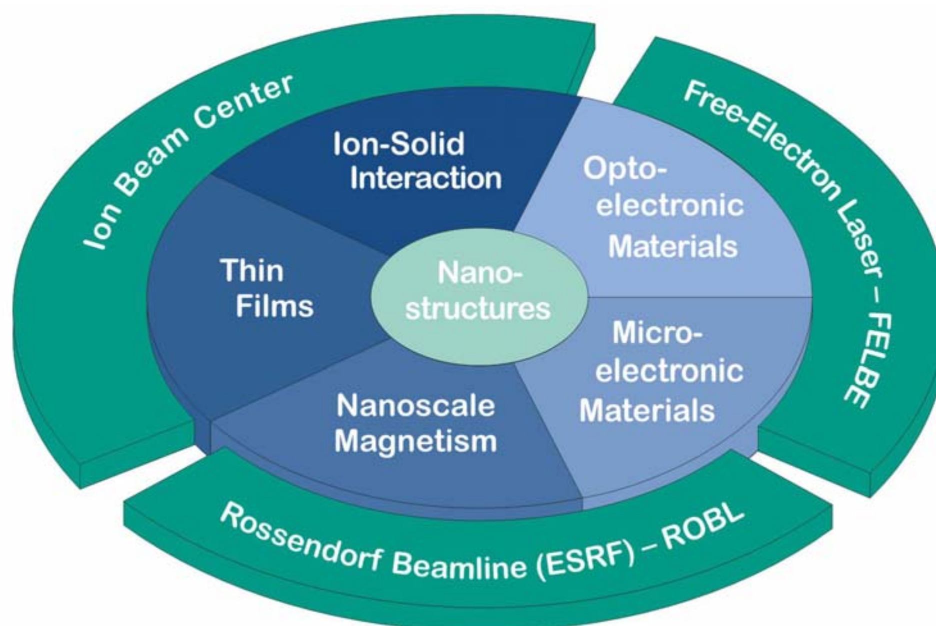

The diagram displays the presently six R&D topics of the institute, together with the associated larger-scale facilities providing access for external users. The research activities span a wide range of topics relevant for future information processing and energy technology, be it in the realm of nano-electronics, optoelectronics, magnetoelectronics, spintronics, and future photovoltaics.

The most significant change in the year 2010, however, was the official retirement of the institute's director for 17 years, Prof. Wolfhard Möller. He largely shaped the institute over those many years, not hesitating to initiate new research directions also beyond his own expertise. For all that we would like to express our sincere and deep gratitude to him. Yet Wolfhard Möller did not stop working, he still contributes strongly to the success of the EU I3 project SPIRIT, which he had initiated a few years back.

Other organizational changes include the new appointment of Dr. Jeffrey McCord as division head "Nanomagnetism" (after Jürgen Fassbender had become director of the institute) and the establishment of a new division "Nanostructures" headed by PD Dr. Sibylle Gemming. The new 6 MV

Tandetron accelerator was put into operation and replaces the old 5 MV tandem that was shut down after 38 (!) years of operation. The new machine will play the key role in our new activities in accelerator mass spectrometry (AMS) under guidance of Dr. Silke Merchel.

Highlights of last year's research are presented in this Annual Report through reprints of short papers that were published in leading international journals. In 2010, IIM staff published more than 140 papers in peer-reviewed journals, including Physical Review Letters, Nano Letters, Advanced Materials, Small, and of course a number of papers in Applied Physics Letters, some of which are reprinted in this Annual Report.

Concerning third-party funding the most remarkable achievement last year has been the extreme success with grants of the German Science Foundation (DFG). Probably motivated by the fact that starting in 2011, being a member of HGF, we have reduced eligibility for DFG grants, our scientific staff has made an exceptional effort in submitting excellent applications, finally resulting in a granted sum of more than two million Euro. Apart from this, the European I3 project SPIRIT is still running and funding transnational access to our ion beam facilities. Contracts with industry continue to play a major role as well, reflecting our spectrum from very basic to relevant applied research.

Finally we would like to cordially thank all partners, friends, and organizations who supported our progress in 2010. Special thanks are due to the Executive Board of the Helmholtz-Zentrum Dresden-Rossendorf, the Minister of Science and Arts of the Free State of Saxony, and the Minister of Education and Research of the Federal Government of Germany. Numerous partners from universities, industry and research institutes all around the world contributed essentially, and play a crucial role for the further development of the institute. Last but not least, the directors would like to thank all IIM staff for their efforts and excellent contributions in 2010.

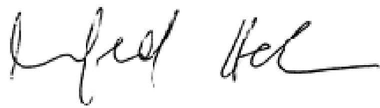

Prof. Manfred Helm

Prof. Jürgen Fassbender

Contents

Selected Publications

Copyright Remarks 9

X. Ou, P. Das Kanungo, R. Kögler, P. Werner, U. Gösele, W. Skorupa, and X. Wang …………….. 11
Carrier profiling of individual Si nanowires by scanning spreading resistance microscopy

M. Wagner, H. Schneider, D. Stehr, S. Winnerl, A.M. Andrews, S. Schartner, G. Strasser, and M. Helm …………………………………………………………………………………………. 16
Observation of the intraexciton Autler-Townes effect in GaAs/AlGaAs semiconductor quantum wells

J. Bhattacharyya, M. Wagner, M. Helm, M. Hopkinson, L.R. Wilson, and H. Schneider ………….. 20
Terahertz activated luminescence of trapped carriers in InGaAs/GaAs quantum dots

J. Potfajova, B. Schmidt, M. Helm, T. Gemming, M. Benyoucef, A. Rastelli, and O.G. Schmidt ….. 23
Microcavity enhanced silicon light emitting pn-diode

R. Skrotzki, J. Fiedler, T. Herrmannsdörfer, V. Heera, M. Voelskow, A. Mücklich, B. Schmidt, W. Skorupa, G. Gobsch, M. Helm, and J. Wosnitza ……………………………………………………. 26
On-chip superconductivity via gallium overdoping of silicon

G. Abrasonis, G.J. Kovács, M.D. Tucker, R. Heller, M. Krause, M.C. Guenette, F. Munnik, J. Lehmann, A. Tadich, B.C.C. Cowie ,L. Thomsen , M.M.M. Bilek, and W. Möller ……………….. 29
Sculpting nanoscale precipitation patterns in nanocomposite thin films via hyperthermal ion deposition

M. Vinnichenko, R. Gago, S. Cornelius, N. Shevchenko, A. Rogozin, A. Kolitsch, F. Munnik, and W. Möller ………………………………………………………………………………………... 32
Establishing the mechanism of thermally induced degradation of ZnO:Al electrical properties using synchrotron radiation

D. Markó, T. Strache, K. Lenz, J. Fassbender, and R. Kaltofen ……………………………………. 35
Determination of the saturation magnetization of ion irradiated Py/Ta samples using polar magneto-optical Kerr effect and ferromagnetic resonance

S. Zhou, D. Bürger, W. Skorupa, P. Oesterlin, M. Helm, and H. Schmidt …………………………... 38
The importance of hole concentration in establishing carrier-mediated ferromagnetism in Mn doped Ge

A.S. El-Said, R. Heller, F. Aumayr, and S. Facsko ……………………………………………………. 41
Pyramidal pits created by single highly charged ions in BaF_2 single crystals

M. Ranjan, T.H. Oates, S. Facsko, and W. Möller ……………………………………………………. 45
Optical properties of silver nanowire arrays with 35 nm periodicity

Statistics

Books …… 51

Journal Publications …… 51

Invited Conference Talks …… 60

Conference Contributions …… 62

Lectures / Talks …… 76

Organization of Workshops …… 79

Patents …… 79

PHD and Diploma Theses …… 79

Colloquia …… 80

Theory / Materials Science Seminar …… 81

Seminars …… 81

SPIRIT Visitors …… 84

FEL Visitors …… 85

ROBL-MRH Visitors …… 85

Other Guests …… 87

Laboratory Visits …… 88

Projects …… 90

Experimental Equipment …… 94

User Facilities …… 98

Services …… 101

Organigram …… 102

List of Personnel …… 103

Selected Publications

Copyright Remarks

The following journal articles are reprinted with kind permission from

X. Ou, P. Das Kanungo, R. Kögler, P. Werner, U. Gösele, W. Skorupa, and X. Wang
Carrier profiling of individual Si nanowires by scanning spreading resistance microscopy
Nano Letters, Vol. **10**, Issue 1, pp. 171-175
© 2010, American Chemical Society
doi: 10.1021/nl903228s

M. Wagner, H. Schneider, D. Stehr, S. Winnerl, A.M. Andrews, S. Schartner, G. Strasser, and M. Helm
Observation of the intraexciton Autler-Townes- Effect in GaAs / AlGaAs semiconductor quantum wells
Physical Review Letters Vol. **105**, Issue 16, Art.-No. 167401
© 2010, The American Physical Society
doi: 10.1103/PhysRevLett105.167401

J. Bhattacharyya, M. Wagner, M. Helm, M. Hopkinson, L.R. Wilson, and H.Schneider
Terahertz activated luminescence of trapped carriers in InGaAs / GaAs quantum dots
Applied Physics Letters, Vol. **97**, Issue 3, Art.-No. 031101
© 2010, American Institute of Physics
doi: 10.1063/1.3464163

J. Potfajova, B. Schmidt, M. Helm, T. Gemming, M. Benyoucef, A. Rastelli, and O.G. Schmidt
Microcavity enhanced silicon light emitting pn-diode
Applied Physics Letters, Vol. **96**, Issue 15, Art.-No. 151113
© 2010, American Institute of Physics
doi: 10.1063/1.3385153

R. Skrotzki, J. Fiedler, T. Herrmannsdörfer, V. Heera, M. Voelskow, A. Mücklich, B. Schmidt, W. Skorupa, G. Gobsch, M. Helm, and J. Wosnitza
On-chip superconductivity via gallium overdoping of silicon
Applied Physics Letters, Vol. **97**, Issue 19, Art.-No. 192505
© 2010, American Institute of Physics
doi: 10.1063/1.3509411

G. Abrasonis, G.J. Kovács, M.D. Tucker, R. Heller, M. Krause, M.C. Guenette, F. Munnik, J. Lehmann, A. Tadich, B.C.C. Cowie ,L. Thomsen , M.M.M. Bilek, and W. Möller
Sculpting nanoscale precipitation patterns in nanocomposite thin films via hyperthermal ion deposition
Applied Physics Letters, Vol. **97**, Issue 16, Art.-No. 163108
© 2010, American Institute of Physics
doi: 10.1063/1.3503967

M. Vinnichenko, R. Gago, S. Cornelius, N. Shevchenko, A. Rogozin, A. Kolitsch, F. Munnik, and W. Möller
Establishing the mechanism of thermally induced degradation of ZnO:Al electrical properties using synchrotron radiation
Applied Physics Letters, Vol. **96**, Issue 14, Art.-No. 141907
© 2010, American Institute of Physics
doi: 10.1063/1.3385024

D. Markó, T. Strache, K. Lenz, J. Fassbender, and R. Kaltofen
Determination of the saturation magnetization of ion irradiated Py / Ta samples using polar magneto-optical Kerr effect and ferromagnetic resonance
Applied Physics Letters, Vol. **96**, Issue 2, Art.-No. 022503
© 2010, American Institute of Physics
doi: 10.1063/1.3291051

S. Zhou, D. Bürger, W. Skorupa, P. Oesterlin, M. Helm, and H. Schmidt
The importance of hole concentration in establishing carrier-mediated ferromagnetism in Mn doped Ge
Applied Physics Letters, Vol. **96**, Issue 20, Art.-No. 202105
© 2010, American Institute of Physics
doi: 10.1063/1.0428770

A.S. El-Said, R. Heller, F. Aumayr, and S. Facsko
Pyramidal pits created by single highly charged ions in BaF_2 single crystals
Physical Review B, Vol. **82**, Issue 3, Art.-No. 033403
© 2010, The American Physical Society
doi: 10.1103/PhysRevB.82.033403

M. Ranjan, T.H. Oates, S. Facsko, and W. Möller
Optical properties of silver nanowire arrays with 35 nm periodicity
Optics Letters, Vol. **35**, Issue 15, pp. 2576 – 2578
© 2010, Optical Society of America
doi: 10.1364/OL.35002576

NANO LETTERS
pubs.acs.org/NanoLett

Carrier Profiling of Individual Si Nanowires by Scanning Spreading Resistance Microscopy

Xin Ou,*[,†,‡,§] Pratyush Das Kanungo,*[,†] Reinhard Kögler,[‡] Peter Werner,[†] Ulrich Gösele,[†] Wolfgang Skorupa,[‡] and Xi Wang[§]

[†] Max Planck Institute of Microstructure Physics, Weinberg 2, Halle D-06120, Germany, [‡] Institute of Ion Beam Physics and Materials Research, Forschungszentrum Dresden-Rossendorf e.V., P.O. Box 510119, 01314 Dresden, Germany, and [§] Shanghai Institute of Microsystem and Information Technology, Chinese Academy of Sciences, Shanghai 20050, China

ABSTRACT Individual silicon nanowires (NWs) doped either by ion implantation or by in situ dopant incorporation during NW growth were investigated by scanning spreading resistance microscopy (SSRM). The carrier profiles across the axial cross sections of the NWs are derived from the measured spreading resistance values and calibrated by the known carrier concentrations of the connected Si substrate or epi-layer. In the case of the phosphorus ion-implanted and subsequently annealed NWs, the SSRM profiles revealed a radial core−shell distribution of the activated dopants. The carrier concentration close to the surface of a phosphorus-doped NW is found to be by a factor of 6−7 higher than the value in the core and on average only 25% of the implanted phosphorus is electrically active. In contrast, for the in situ boron-doped NW the activation rate of the boron atoms is significantly higher than for phosphorus atoms. Some specific features of SSRM experiments of Si NWs are discussed including the possibility of three-dimensional measurements.

KEYWORDS Nanowire, carrier profile, SSRM, doping, implantation

Because of their unique physical properties, silicon nanowires (NWs) attracted major research interest in the past years.[1,2] One of the most promising applications of Si NWs is their integration in future CMOS circuits to scale down the microelectronics further to nanoelectronics.[3] Two key requirements for applying the NWs in electronic devices and circuits are controlled doping and precise carrier concentration profiling. Controlled doping of NWs has been demonstrated both by in situ doping[4−7] as well as by ion implantation.[8,9] However, in most cases only electrical transport measurements have been used to estimate the active carrier concentrations in the NWs.[4,5,7,9−11] Because of their nanometric size there is a lack of suitable characterization procedures for direct measurement of the active carrier concentration profiles in the NWs. Recently, atom probe tomography[12] was applied to quantify the total concentration distribution of the doping atoms in the NWs. Accumulation of the doping atoms toward the nanowire surface was reported, which shed some light on the dopant incorporation mechanism during in situ doping of vapor−liquid−solid NW growth. However, this method could not quantify the profile of the electrically active dopants in the NWs. Because of its cylindrical geometry and the high surface to volume ratio, the surface of a nanowire plays an important role in determining its electrical properties. One of the most critical surface effects for an unpassivated surface is the segregation of dopant atoms[13] at the Si/SiO_2 interface, which may modify the number of activated dopants in the volume.[13−17] The surface segregation of the active boron dopant in the NWs was reported by Raman scattering[18] and recently by electrical transport measurements in connection with surface etching.[19] Very recently the capabilities of mapping the active dopant concentration in Si NWs were demonstrated by using electron holography.[20] There is clearly an increasing need for direct measurements of the active dopant profile along the cross section of a single NW. In this paper, a direct visualization and quantification of the two-dimensional carrier concentration profiles is demonstrated for doped (both n- and p-type) individual vertical Si NWs of diameter ∼100 nm with scanning spreading resistance microscopy (SSRM).

SSRM[21,22] is based on the contact mode atomic force microscope. A constant force in terms of the deflection voltage is maintained between a conductive tip and the sample, measuring the local spreading resistance in the material in a nanoscale volume. This local spreading resistance is directly proportional to the local resistivity that can be converted to local carrier concentration using the standard carrier concentration versus resistivity curve.[23] The spatial resolution of SSRM mainly depends on the effective contact area between the tip and the sample that is determined by the radius of the tip (several tens of nanometers), the penetration depth into the sample and the nanoroughness of the tip (below 10 nm). Typically, SSRM can achieve a spatial resolution of about 10 nm[21] for a perfectly sharp and fresh tip and has a dynamic range of carrier concentration measured of $10^{15}-10^{20}$ cm^{-3}.[22]

* To whom correspondence should be addressed. E-mail: (X.O.) X.ou@fzd.de; (P.D.K.) kanungo@mpi-halle.de.
Received for review: 09/29/2009
Published on Web: 12/16/2009

© 2010 American Chemical Society

NANO LETTERS

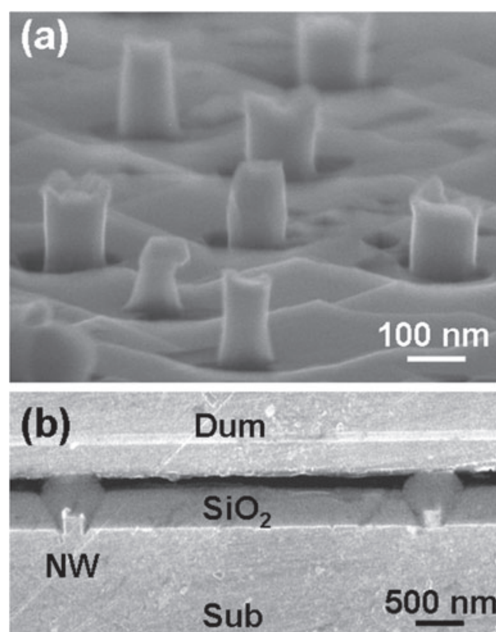

FIGURE 1. (a) SEM image of doped Si NWs with their Au caps removed by wet etching.(b) SEM image of the cross section of a SSRM specimen. The top part denoted as a dummy (Dum) wafer is glued to the sample containing the Si substrate (Sub) and NWs embedded in the SiO_2 matrix.

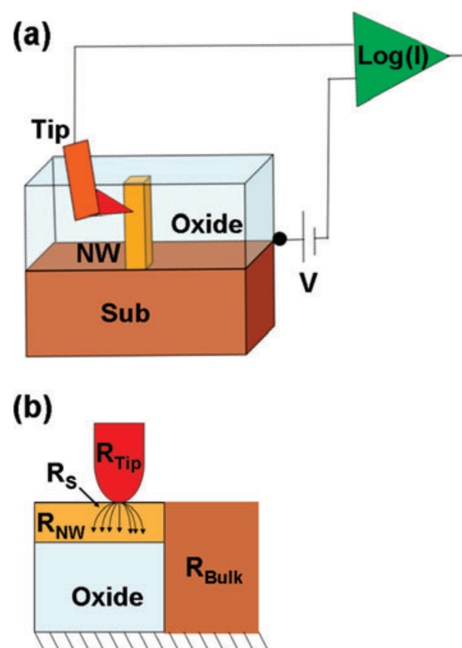

FIGURE 2. (a) Illustration of a SSRM measurement as applied for the investigation of a cross sectional specimen with Si NWs. Log(*I*) denotes the current amplifier. (b) Different resistors contributing to the electrical circuit.

The NWs of 50 to 250 nm in diameter and 100 to 400 nm in length were grown under ultrahigh vacuum (10^{-10} mbar) in a Riber SiVa45 MBE chamber using Au as the growth-initiator.[24] Doping of the NWs was carried out either by phosphorus ion implantation (for n-type) and subsequent rapid thermal annealing at 1100 °C for 30 s or by boron in situ incorporation during the growth of the NWs at 525 °C (for p-type). The substrate for the n-type NWs was n^+-Si (111) (resistivity ~ 0.001 Ω-cm) and for the p-type NWs p-Si (111) (resistivity ~ 10 Ω-cm). Details of the doping processes including the phosphorus implantation doses and energies are reported elsewhere.[5,9] The expected carrier concentration in the n-type NW was 10^{19} cm^{-3} (see Supporting Information) and in the p-type NW 10^{18} cm^{-3}.[5] Both of the NWs remained fully single-crystalline after doping as confirmed by transmission electron microscopy imaging (see Supporting Information). Figure 1a shows the typical morphology of the vertical Si NWs after removal of the Au droplet (remnants from the Au used for growth initiation) from the top of the NWs by wet etching. Generally, the columnlike NWs stand on an epitaxial layer of thickness of about 300 nm.[24] The grooves observed at the base of the NWs (Figure 1a) are formed due to surface diffusion of Si during the NW growth.[24]

To fabricate the specimen for cross sectional SSRM measurement without removing the NWs from the substrate, a layer of about 400 nm SiO_2 was deposited on the sample by magnetron sputtering to cover the NWs. Subsequently, the specimen was cut and glued by using the same preparation procedures as for the cross sectional transmission electron microscopy except for the Ar ion milling step. The specimen surface was lapped and ground with SiC powder and finally polished with diamond powder. A scanning electron microscopy (SEM) image of an SSRM specimen is shown in Figure 1b.

The scheme of the SSRM measurement is illustrated in Figure 2. An electrical circuit (Figure 2a) consists of the tip, the specimen including the NW embedded in the oxide matrix and the bulk substrate, and of a logarithmic current amplifier to read out the signal. The SSRM measurements were performed using a Veeco multimode atomic force microscope equipped with a conductive diamond coated Si tip. A constant bias voltage of −2.5 V was applied between the tip and the specimen to achieve a reasonable signal-to-noise ratio. The spreading resistance (R_S) comes from a very small volume underneath the tip (Figure 2b), and for an ideal Ohmic contact between a cylindrical tip and a flat sample surface it can be estimated by the formula $R_S = \rho/4a$,[25] where ρ is the resistivity and a is the "electrical radius", that is, the radius of the effective contact area between the tip and the sample. Please note that a can be orders of magnitude smaller than the physical radius of the tip.[26] SSRM is based on the assumption that the spreading resistance R_S is the dominating term in the measured serial resistor R

$$R = R_{Tip} + R_{Bulk} + R_{NW} + R_S \quad (1)$$

where R_{Tip} is the resistance of the probe tip, R_{NW} is the resistance of the Si NW, and R_{Bulk} is the resistance of the

© 2010 American Chemical Society

DOI: 10.1021/nl903228s | *Nano Lett.* **2010,** *10,* 171-175

NANO LETTERS

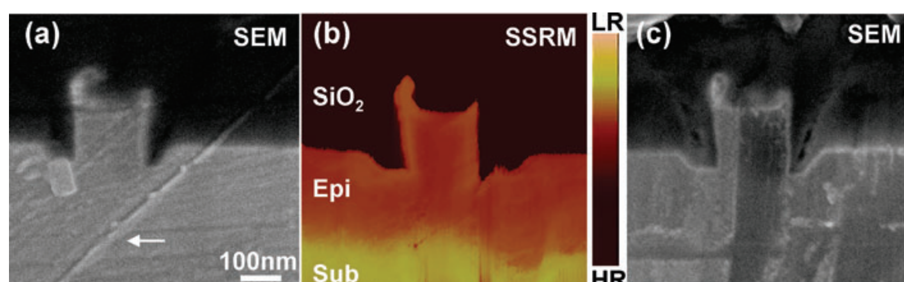

FIGURE 3. (a) SEM image of an individual phosphorus-doped NW before the SSRM measurement. The scratch indicated by an arrow was formed during the sample preparation. (b) Cross sectional SSRM image of the NW shown in (a). Dark and bright colors indicate high (HR) and low (LR) resistance which are scaled on the right side. The NW is connected to the Si substrate (Sub) via a Si epi-layer (Epi). The dark area surrounding the NW is the SiO_2 in which it is embedded. The scanning size is 800 × 800 nm^2. (c) SEM image taken after the SSRM measurement. This NW is the same as the one visible on the left side in Figure 1b.

substrate (including the epi-layer). R_{Bulk} can be neglected due to its very large cross section area as compared to the nanowire. In this case $R_S \gg R_{NW}$ holds $R \approx R_S$ in eq 1, that is, we can attribute the measured resistance entirely to the spreading resistance. The ratio R_{NW}/R_S only depends on the dimensions of the NW (see Supporting Information). It is worth noting that the SSRM images of the Si NW profiles shown in this paper are obtained for the condition of $R_S \gg R_{NW}$ due to the size of the investigated NW cross sections.

Figures 3 presents the SEM images and the corresponding SSRM image of the same phosphorus-doped NW. The consistence of the cross sections of the NW shown by the SEM images before (a) and after (c) the SSRM measurement and of the SSRM image demonstrates the high areal sensitivity of this SSRM measurement. The dark area surrounding the NW indicates the SiO_2 layer with high resistance (HR), and the brighter color shown in the substrate indicates a lower resistance (LR) there due to the high carrier concentration of 7.4×10^{19} cm^{-3} corresponding to its resistivity of 0.001 Ω-cm. The uniform medium dark color shown both in the epi-layer and in the bulk of the NW demonstrated their homogeneous doping to a similar level. This is in agreement with the transport of ions in matter (TRIM) calculations (see Supporting Information). Evidently, there is a brighter colored band at the side wall of the NW shown in Figure 3b. This indicates a lower resistance or higher conductivity there as compared to the bulk of the NW.

Averaged profiles of the spreading resistance (R_S) and carrier concentration in axial (AS) and radial (RS) directions are shown in Figure 4a,b. The R_S data were taken as a 512 × 512 data matrix from a 800 × 800 nm^2 area. R_S was converted to carrier concentration by an appropriate scaling (see Supporting Information) with the known resistivity of the substrate and using the standard carrier concentration vs resistivity curve for silicon.[23] The carrier concentrations along the axial and radial directions to the NW are shown by the right Y axis of Figure 4a,b, respectively. Figure 4a indicates, as expected, that the epi-layer and the bulk of NW are more than 1 order of magnitude less highly doped than the substrate. Figure 4b confirms a higher doping level close to the surface in comparison to the core region of the NW.

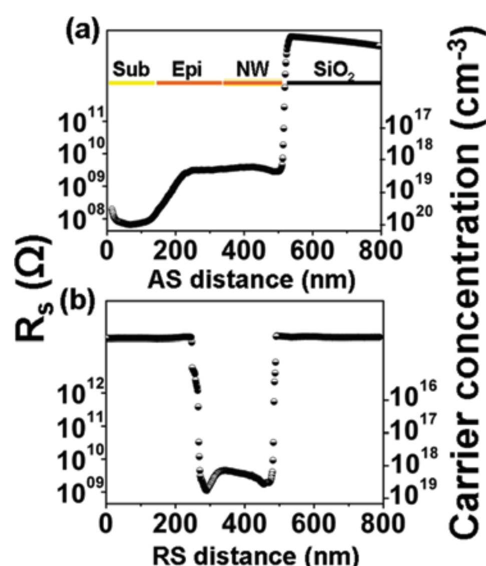

FIGURE 4. R_S profiles extracted from the SSRM image shown in Figure 3b. The profiles in axial direction (AS) and in radial direction (RS) are averaged over the whole Si NW. The carrier concentration (right scale) was converted from R_S values by calibration from the known resistivity (0.001 Ω-cm) of the Si substrate and using the standard carrier concentration vs resistivity curve (ref 23).

The more highly doped region extends from the surface to about 30 nm inside the NW, and the difference between the levels of this shell and the core is about a factor of 6−7. The significant discrepancy between the carrier concentrations of 2.5×10^{18} cm^{-3} average over the whole NW (Figure 4) and the expected average doping level of 10^{19} cm^{-3} is in agreement with recent current−voltage measurements.[9]

The unpassivated outer surface of a NW is normally covered by a thin layer of native SiO_2, and the dopants tend to be segregated at the Si/SiO_2 interface. Phosphorus generally piles up[13,27−31] at the Si/SiO_2 interface. After ion implantation, the redistribution of the phosphorus toward the Si/SiO_2 interface mainly occurs during the rapid thermal annealing and may be enhanced by the implantation damage induced transient enhance diffusion (TED).[28] This redistribution is responsible for the phosphorus loss in the core of the NW. The concentration of the phosphorus atoms in the shell close to the Si/SiO_2 interface can roughly be

© 2010 American Chemical Society

DOI: 10.1021/nl903228s | Nano Lett. 2010, 10, 171-175

estimated to be 1.9 × 10^{19} cm^{-3} by the assumption that phosphorus in the NW core is fully activated and the phosphorus concentration there is equal to the carrier concentration of 1.4 × 10^{18} cm^{-3} (Figure 4b). On the basis of this value only about 20% of the phosphorus atoms in the shell close to the surface are electrically active and detected by the SSRM. There is evidently an even stronger dopant deactivation directly at the NW surface. The phosphorus deactivation is due to (i) clustering of segregated dopant in the high concentration region,[31] (ii) dielectric mismatch,[14] and (iii) the surface states existing at the Si/SiO_2 interface of the NW.[11,16] The thickness of the surface region fully depleted by the interface states is calculated according to Seo's model[11] to be 2 nm. However, this thickness cannot be resolved by the present SSRM measurement since the distance between the neighboring data points is 1.6 nm and the spatial resolution is determined to be 4 nm by the measured width of a sharp thermally grown Si/SiO_2 interface.

Another important factor that can influence the dopant profiles in the Si NWs is the existence of the Au remaining from the growth-initiating phase. Au incorporated into the NW may serve as a p-type dopant forming an acceptor state at E_c-0.53 eV in Si and thereby can compensate the n-type carriers induced by phosphorus.[32] Although Au can be found on the surface of the NWs (see the TEM image in Supporting Information), Au incorporated during NW growth is negligible due to the very low Au solubility in Si which is below 10^{15} cm^{-3} at the growth temperature of 525 °C.[33] The Au in-diffusion into the NW during the postimplantation annealing is also limited by the low Au solubility in Si of 2 × 10^{16} cm^{-3}[33] at that temperature. Such level of Au was detected by Putnam et al.[34] in the volume of the Si NWs grown at 1000 °C by secondary ion mass spectrometry (SIMS). The low concentration restricts the role of Au in carrier compensation in the bulk of the NW by considering the level of the measured carrier concentration. However, the high concentration of the residual Au at the NW surface may contribute the phosphorus deactivation there, for instance, by forming of Au−P complexes.[32]

Figure 5 shows the SSRM image of an in situ boron-doped NW. The respective averaged R_S and carrier concentration profiles (see Supporting Information) in axial and radial directions are given in Figure 6a,b. In this case, the darker substrate implying a higher resistance as compared to the epi-layer and the NW is due to its lower doping level (1.3 × 10^{15} cm^{-3} corresponding to the resistivity of 10 Ω-cm) as compared to the expected doping level of 10^{18} cm^{-3} in the NW and epi-layer.[5] The dark lines in the epi-layer result from scratches and surface defects induced by mechanical polishing during the specimen preparation. Therefore, there is a strong fluctuation in the carrier concentration of the epi-layer (Figure 6a). It indicates the importance of a highly perfect specimen polishing without mechanical surface defects. In general, the extracted carrier concentrations in the NW (Figure 6) are approaching the expected doping level of 10^{18} cm^{-3}. The carrier profile along the radial direction in Figure 6b is relatively flat as compared to the one shown in Figure 4b indicating that the segregation effect for this investigated boron-doped NW is not as significant as for the phosphorus-doped one. This may result from the 1 order of magnitude lower doping level as compared to the phosphorus-doped NW, from the different doping process, and from the lower segregation coefficient of boron compared to phosphorus.[13] In addition, in contrast to the Figures 3b and 4b, the size of the scanning area in Figure 5 is increased to 2 × 2 μm^2 and thereby the distance between the data points is increased

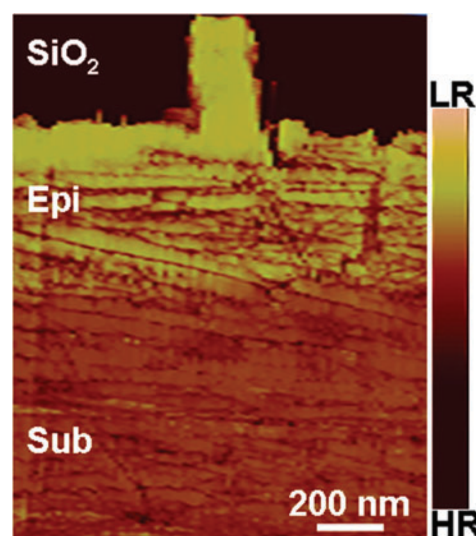

FIGURE 5. Cross sectional SSRM image of an in situ boron-doped NW. Note that the dark lines in the substrate and epi-layer are scratches resulting from the mechanical polishing. The image is taken from a scanning area with a size of 2 × 2 μm^2.

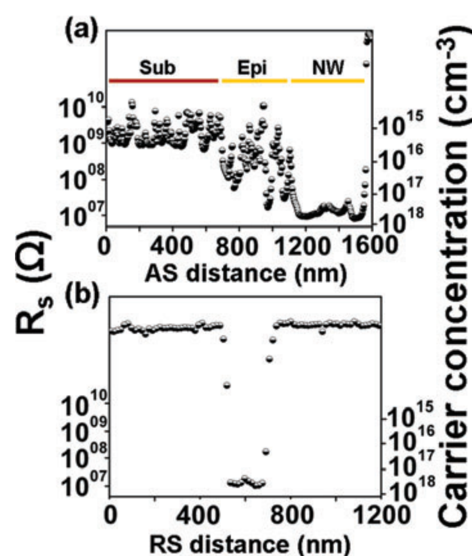

FIGURE 6. R_S profiles extracted from the SSRM image shown in Figure 5. The profiles in axial direction (AS) and in radial direction (RS) are averaged over the whole NW. The carrier concentration (right *Y* axis) was converted from R_S values by calibration from the known resistivity (0.04 Ω-cm) of the epi-layer and using the standard carrier concentration vs resistivity curve (ref 23).

© 2010 American Chemical Society

DOI: 10.1021/nl903228s | Nano Lett. 2010, 10, 171-175

NANO LETTERS

to 7.8 nm. This reduces the visibility of the effects of dopant segregation and deactivation directly at the NW surface. Nevertheless, the activation rate for boron atoms incorporated in situ during the NW growth is estimated to be 65−70%, which is much higher than for the implanted phosphorus atoms.

Although the investigated NWs here are of larger diameter (∼180 nm) compared to the preferable size for the future logic application. SSRM can be applied for carrier profiling in small diameter NWs (∼10 nm) as well. However, one has to carefully interpret the data as the smaller diameter NWs will have a higher resistance (R_{NW}) that may lead to an overestimation of R_S and affect the accuracy of the extracted carrier concentration from the SSRM measurement. Nevertheless, this effect can be quantitatively considered (see Supporting Information) by a correction approach. It was reported that a spatial resolution as high as 1 nm was achieved in carrier profiling of the ultrashallow junctions by the SSRM characterization in vacuum ambient.[35]

By repeated scanning of the same NW with a controlled force, the tip can abrade some material from the surface of the measured NW cross section. In Figure 3c, the change of the surface after the SSRM investigation is well visible in comparison to the status before (Figure 3a). In this way, the tip gradually moves deeper through the volume of the NW. By measuring the cross sections at different depths of the same NW in succession a three-dimensional (3D) carrier profiling of the NW can potentially be obtained by using an appropriate projection of the two-dimensional profiles along the depth scale. Further investigations regarding 3D SSRM are in progress.

In summary, the electrical properties of cross sections of individual NWs were investigated by SSRM. The carrier profiles of the NWs were determined from the measured spreading resistance with an appropriate calibration by the known resistivity of the underlying Si substrate or the epilayer. Close to the surface region of a phosphorus-doped NW the carrier concentration was found to be higher than in the core. In comparison, the concentration profile of the investigated boron-doped NW shows a higher electrical activation rate of the boron atoms as compared to the phosphorus atoms.

Acknowledgment. The authors gratefully acknowledge Elfi Christalle (FZD) for SEM measurements and Sigred Hopfe (MPI-Halle) for the SSRM specimen preparations.

Supporting Information Available. The analysis of the influence of the nanowire resistance in the spreading resistance measurements, a cross-sectional TEM micrograph of the phosphorus-implanted Si NW with the TRIM simulation, and the calibration technique used to obtain the carrier concentrations from the measured spreading resistance values. This material is available free of charge via the Internet at http://pubs.acs.org.

REFERENCES AND NOTES

(1) Cui, Y.; Zhong, Z.; Wang, D.; Wang, W. U.; Lieber, C. M. *Nano Lett.* **2003**, *3*, 147.
(2) Law, M.; Goldberger, J.; Yang, P. *Annu. Rev. Mater. Res.* **2004**, *34*, 83.
(3) Appenzeler, J.; Knoch, J.; Bjoerk, M. T.; Riel, H.; Schmid, H.; Riess, W. *IEEE Trans. Electron Devices.* **2008**, *55*, 2827.
(4) Cui, Y.; Duan, X.; Hu, J.; Lieber, C. M. *J. Phys. Chem. B* **2000**, *104*, 5213.
(5) Kanungo, P. D.; Zakharov, N.; Bauer, J.; Breitenstein, O.; Werner, P.; Gösele, U. *Appl. Phys. Lett.* **2008**, *92*, 263107.
(6) Wang, Y.; Lew, K. K.; Ho, T. T.; Pan, L.; Novak, S. W.; Dickey, E. C.; Redwing, J. M.; Mayer, T. S. *Nano Lett.* **2005**, *5*, 2139.
(7) Yu, J.-Y.; Chung, S.-W.; Heath, J. R. *J. Phys. Chem. B* **2000**, *104*, 11864.
(8) Hoffmann, S.; Bauer, J.; Ronning, C.; Stelzner, Th.; Michler, J.; Ballif, C.; Sivakov, V.; Christiansen, S. H. *Nano Lett.* **2009**, *9*, 1341.
(9) Kanungo, P. D.; Kögler, R.; Nguyen-Duc, K.; Zakharov, N.; Werner, P.; Gösele, U. *Nanotechnology* **2009**, *20*, 165706.
(10) Ingole, S.; Aella, P.; Manandhar, P.; Chikkannanavar, S. B.; Akhadov, E. A.; Smith, D. J.; Picraux, S. T. *J. Appl. Phys.* **2008**, *103*, 104302.
(11) Seo, K.; Sharma, S.; Yasseri, A. A.; Stewart, D. R.; Kamins, T. I. *Electrochem. Solid-State Lett.* **2006**, *9*, G69.
(12) Perea, D. E.; Hemesath, R. E.; Schwalbach, E. J.; Lensch-Falk, J. L.; Voorhees, P. W.; Lauhon, L. J. *Nat. Nanotechnol.* **2009**, *4*, 315.
(13) Grove, A. S.; Leistiko, O.; Sah, S. H. *J. Appl. Phys.* **1964**, *35*, 2695.
(14) Bjoerk, M. T.; Schmid, H.; Knoch, J.; Riel, S.; Riess, W. *Nat. Nanotechnol.* **2009**, *4*, 103.
(15) Peelaers, H.; Partoens, B.; Peeters, F. M. *Nano Lett.* **2006**, *6*, 2781.
(16) Schmidt, V.; Senz, S.; Gösele, U. *Appl. Phys. A* **2007**, *86*, 187.
(17) Ferna'ndez-Serra, M. V.; Adessi, C.; Blase, X. *Phys. Rev. Lett.* **2006**, *96*, 166805.
(18) Imamura, G.; Kawashima, T.; Fujii, M.; Nishimura, C.; Saitoh, T.; Hayashi, S. *Nano Lett.* **2008**, *8*, 2620.
(19) Xie, P.; Hu, Y. J.; Fang, Y.; Huang, J. J.; Lieber, C. M. *Proc. Nat. Acad. Sci. U.S.A.* **2009**, *106*, 15254.
(20) Den Hertog, M. I.; Schmid, H.; Cooper, D.; Rouviere, J. L.; Björk, T. M.; Riel, H.; Rivallin, P.; Karg, S.; Riess, W. *Nano Lett.* **2009**, *9* (11), 3837.
(21) Wolf, P. D.; Geva, M.; Hantschel, T.; Vandervorst, W.; Bylsma, R. B. *Appl. Phys. Lett.* **1998**, *73*, 2155.
(22) Maknys, K.; Douherets, O.; Anand, S. *Appl. Phys. Lett.* **2003**, *83*, 2184.
(23) Pierret, R. F. *Advanced Semiconductor Fundamentals*, 2nd ed.; Prentice Hall: Upper Saddle River, NJ, 2003; p 191.
(24) Werner, P.; Zakharov, N. D.; Gerth, G.; Schubert, L.; Gösele, U. *Int. J. Mater. Res.* **2006**, *97*, 1008.
(25) Schroder, D. K. *Semiconductor Material and Device Characterization*, 3rd ed.; John Wiley & Sons: New York, 2006.
(26) Eyben, P.; Degryse, D.; Vandervorst, W. In *Characterization and Metrology for ULSI Technology*, Proceedings of the International Conference on Characterization and Metrology for ULSI Technology, Richardson, Texas, March 15–18, 2005; Seiler, D. G., Diebold, A. C., McDonald, R., Ayre, C. R., Khosla, R. P., Zollner, S., Secula, E. M., Eds.; AIP Conference Proceedings; American Institute of Physics: Melville, NY, 2005; Vol. 788, p 264.
(27) Schwarz, S. A.; Barton, R. W.; Ho, C. P.; Helms, C. R. *J. Electrochem. Soc.* **1981**, *128*, 1101.
(28) Gfiffin, P. B.; Crowder, S. W.; Knight, J. M. *Appl. Phys. Lett.* **2003**, *67*, 482.
(29) Duffy, R.; Venezia, V. C.; Loo, J.; Hopstaken, M. J. P.; Verheijen, M. A.; Maas, G. C. J.; Tamminga, Y.; Dao, T.; Demeurisse, C. *Appl. Phys. Lett.* **2005**, *86*, No. 081917.
(30) Chang, R. D.; Tsai, J. R. *J. Appl. Phys.* **2008**, *103*, No. 053517.
(31) Schroer, E.; Uematsu, M. *Jpn. J. Appl. Phys.* **1999**, *38*, 7.
(32) Weman, H.; Henry, A.; Begum, T.; Monemar, B.; Awadelkarim, O. O.; Lindstrom, J. L. *J. Appl. Phys.* **1989**, *65*, 137.
(33) Trumbore, F. A. *Bell Syst. Tech. J.* **1960**, *39*, 205.
(34) Putnam, M. C.; Filler, M. A.; Kayes, B. M.; Kelzenberg, M. D.; Guan, Y.; Lewis, N. S.; Eiler, J. M.; Atwater, H. A. *Nano Lett.* **2008**, *8*, 3109.
(35) Zhang, L.; Tanimoto, H.; Adachi, K.; Nishiyama, A. *IEEE Electron Device Lett.* **2008**, *9*, 799.

© 2010 American Chemical Society

PRL **105,** 167401 (2010) PHYSICAL REVIEW LETTERS week ending 15 OCTOBER 2010

Observation of the Intraexciton Autler-Townes Effect in GaAs/AlGaAs Semiconductor Quantum Wells

Martin Wagner,[1] Harald Schneider,[1] Dominik Stehr,[1] Stephan Winnerl,[1] Aaron M. Andrews,[2] Stephan Schartner,[2] Gottfried Strasser,[2] and Manfred Helm[1]

[1]*Institute of Ion Beam Physics and Materials Research, Forschungszentrum Dresden-Rossendorf, P.O. Box 510119, 01314 Dresden, Germany*

[2]*Micro- and Nanostructure Center, TU Wien, Floragasse 7, 1040 Vienna, Austria*

(Received 11 May 2010; published 12 October 2010)

The near-infrared transmission of a semiconductor multiple quantum well is probed under intense terahertz illumination. We observe clear evidence of the intraexcitonic Autler-Townes effect when the terahertz beam is tuned near the $1s$-$2p$ transition of the heavy-hole exciton. The strongly coupled effective two-level system has been driven with terahertz field strengths of up to 10 kV/cm resulting in a Rabi energy of ≈ 0.6 times the transition energy. The induced near-infrared spectral changes at low intensities are qualitatively explained using a basic two-level model.

DOI: 10.1103/PhysRevLett.105.167401 PACS numbers: 78.67.De, 42.50.Hz, 73.21.Fg, 78.40.Fy

A fundamental problem in light-matter interaction is the coupling of an intense, monochromatic electromagnetic wave with a quantum mechanical two-level system. Many aspects of this scenario have been thoroughly investigated with atomic systems in connection with a third energy level, for instance, electromagnetic induced transparency (EIT) [1], lasing without inversion [2], and the Autler-Townes (or ac Stark) effect. The latter manifests itself in dressed light-matter states leading to a line splitting in a resonantly driven system [3,4]. Clear data on solid state systems, in particular, semiconductors, are more scarce, a reason being the short coherence times and the broad linewidths in these latter systems. A number of reports over the past decade have presented observations of various quantum optical phenomena in semiconductors, such as Rabi oscillations, the time-domain equivalent of the Autler-Townes effect, between donor states [5], interband transitions in quantum dots [6], intersubband transitions in quantum wells (QWs) [7], and intraexcitonic transitions in the midinfrared [8]. In the frequency domain, EIT [9,10] and gain without inversion [11] have been investigated as well as the Autler-Townes effect [12,13], but all in relation to QW intersubband transitions. Recently the latter phenomenon was also studied in quantum dots dressed by an interband excitation [14], and even in macroscopic Josephson junction based qubits [15,16], with both structures exhibiting small linewidths.

Particularly interesting systems are excitons in semiconductors, representing essentially the hydrogen problem energetically scaled down by a factor of 1000. Here we report the observation of the Autler-Townes effect of the intraexcitonic $1s$-$2p$ absorption in semiconductor QWs. Since the $1s$-$2p$ energy lies in the 10 meV (or THz) range, we can easily reach a regime where the dipole interaction energy and the ponderomotive energy approach the same order as the transition energy, a highly nonperturbative regime requiring much higher intensities in atomic systems or for band gap transitions [17,18].

As a simplified description, we consider a monochromatic wave coupled to a two-level system, where the states get "dressed" by the light field, leading to (e.g., [19])

$$\hbar\omega_{1'} = \hbar\omega_1 - \hbar\Omega' \quad \text{and} \quad \hbar\omega_{2'} = \hbar\omega_2 + \hbar\Omega', \qquad (1)$$

with $\Omega' = \frac{1}{2}\Delta \pm \frac{1}{2}\sqrt{\Delta^2 + \Omega^2}$ in the rotating-wave approximation (RWA), which requires $\Omega \ll \omega$. Here $\Delta = \omega - \omega_{21}$ is the detuning from the resonance frequency ω_{21}, and $\Omega = |\mu_{21}E|/\hbar$ denotes the Rabi frequency with the dipole matrix element μ_{21} and the electric field amplitude E. On resonance the original states split into doublets of energy $\hbar\omega_{1,2} \pm \hbar\Omega/2$, as sketched in Fig. 1(a).

Here we probe the near-infrared (NIR) transmission of an undoped GaAs/AlGaAs multiple quantum well (MQW) around the heavy-hole (HH) exciton while modulated via intense, in-plane polarized THz light. In-plane polarized THz light couples effectively to the $1s$-$2p$ excitonic transition, as has been exploited in sideband generation [20,21], for the dynamical Franz-Keldysh effect [22], and for a determination of the dephasing time of the $1s$-$2p$ transition [23]. Tuning the narrow band THz pump near the $1s$-$2p$ resonance we observe clear signatures of a strongly coupled two-level system, i.e., an anticrossing of the dressed states depending on the THz photon energy and an intensity dependent Rabi splitting on resonance. Our investigations thus represent the first unambiguous observation of an intraexcitonic Autler-Townes effect.

The hydrogen-atom like $1s$ and $2p$ levels of the quantum well heavy-hole exciton are sketched in Fig. 1(b). Unlike the optically "bright" $1s$ and $2s$ states, the "dark" $2p$ state cannot be accessed in NIR transmission experiments because of quantum mechanical selection rules; however, it lies very close to the $2s$ state. Using optical-pump

 © 2010 The American Physical Society

PRL 105, 167401 (2010) PHYSICAL REVIEW LETTERS week ending 15 OCTOBER 2010

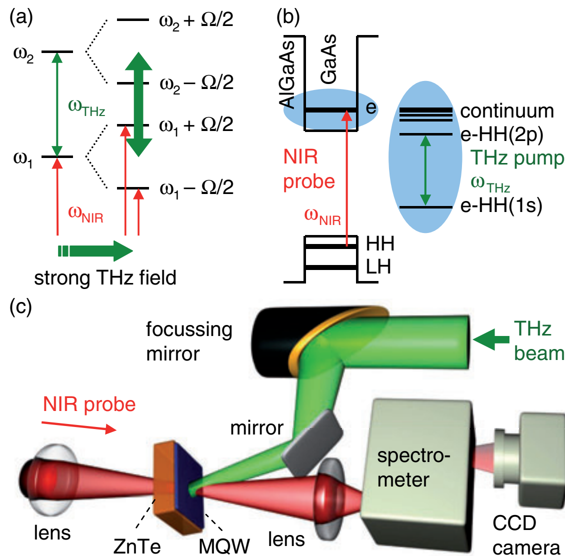

FIG. 1 (color online). (a) Autler-Townes splitting on resonance ($\omega_{THz} = \omega_{21}$) where the original states split by the Rabi frequency Ω. (b) Energy band diagram of a GaAs/AlGaAs quantum well with the electron (e) and heavy-hole (HH) and light-hole (LH) states. The THz pump beam is tuned to the $1s$-$2p$ transition of the e-HH exciton. (c) Experimental geometry.

THz-time-domain spectroscopy [24], the $1s$-$2p$ transition energy in our sample was determined to lie at $\hbar\omega_{21} \approx$ 9 meV with a linewidth of 3 meV (FWHM).

Figure 1(c) displays the experimental setup. Broadband NIR light from a 12-fs Ti:sapphire laser (Femtolasers: Femtosource Scientific sPro) is focused at an angle of $\approx 15°$ to the surface normal on the MQW film consisting of 60 periods of 8.2-nm thick GaAs quantum wells, separated by 19.6-nm thick barriers of $Al_{0.34}Ga_{0.66}As$. The substrate has been removed by wet etching, and the film of size 4×4 mm^2 was glued to a NIR transparent $\langle 100 \rangle$-oriented ZnTe substrate. The transmitted light is analyzed by a grating spectrometer and a charge-coupled device camera. Strong THz light from the free-electron laser (FEL) FELBE of the Forschungszentrum Dresden-Rossendorf is focused and overlapped with the NIR probe spot at normal incidence on the sample. The NIR laser is synchronized and its repetition rate is reduced to 13 MHz, the same as of the FEL. The timing jitter between NIR and FEL pulses can be estimated to 1–2 ps, much shorter than the typical FEL pulse duration of 20–35 ps (FWHM). Their temporal overlap is adjusted via a rf phase shifter. The NIR probe light is attenuated to a peak intensity below 100 W/cm^2 in order not to modify the sample's absorption spectrum. The sample is kept in a liquid He flow cryostat at low temperature (near 10 K). Even at the highest presented THz peak intensities, the lattice temperature stays below 15 K, as determined by the small spectral shift (< 0.3 meV) of the main exciton line when the NIR probe pulse is delayed by 300 ps with respect to the FEL pulse. Such spectral shifts due to a FEL induced lattice heating are already corrected for in the following spectra. In the experiment transmission spectra of the sample are recorded and normalized by the ZnTe substrate transmission before the absorption is calculated as the negative logarithm thereof.

In Fig. 2 absorption spectra are displayed for different time delays (in equidistant intervals of ≈ 2.7 ps) between the NIR probe and the FEL pump pulses with the THz photon energy at $\hbar\omega_{THz} = 10.5$ meV close to the $1s$-$2p$ resonance. Probing 32 ps before the FEL pulse arrives (red bottom curve) reveals an unperturbed spectrum where the relevant states are indicated. Shifting the NIR probe pulse closer in time to the center of the FEL pulse drastically modifies the sample's absorption with a strong decrease at the e-HH($1s$) state and a minor decrease at the e-LH($1s$) state. But most strikingly the e-HH($1s$) exciton line splits, as is discussed in detail in the following paragraphs. Comparing the spectra with those obtained at the temporal overlap for different THz average powers, one can deduce a FEL pulse envelope with a nearly bandwidth-limited pulse width of ≈ 27 ps (FWHM), as shown on the right-hand side in the contour plot. We find that the absorption change occurs adiabatically on a time scale of several picoseconds, limited by the FEL pulse width and promising ultrafast optical switching or modulation.

Since the Autler-Townes effect manifests itself by a unique dependency on THz peak intensity and photon energy, we vary these parameters at the temporal overlap between pump and probe pulses, as shown in Fig. 3. For THz photon energies below the $1s$-$2p$ resonance

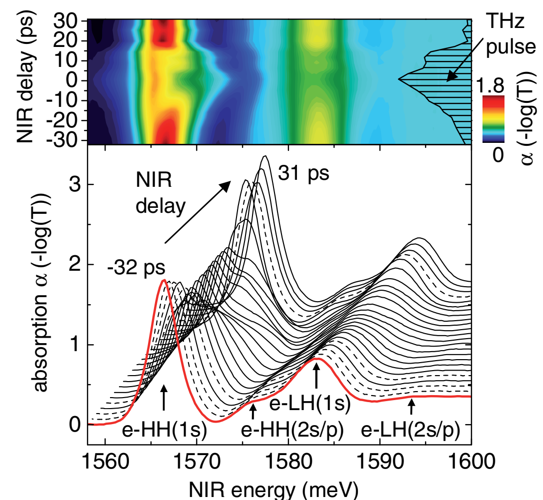

FIG. 2 (color online). Absorption at 10 K for different time delays between NIR probe and FEL pump pulses at a THz photon energy of 10.5 meV and a THz peak intensity of 500 kW/cm^2. The traces in the waterfall plot (bottom) are equally spaced in time. A few traces are interpolated between adjacent ones (dashed lines). Absorption peaks are labeled (lower red line). Above, the corresponding contour plot is shown. The right-hand inset displays the THz pulse intensity envelope.

PRL **105,** 167401 (2010) PHYSICAL REVIEW LETTERS week ending 15 OCTOBER 2010

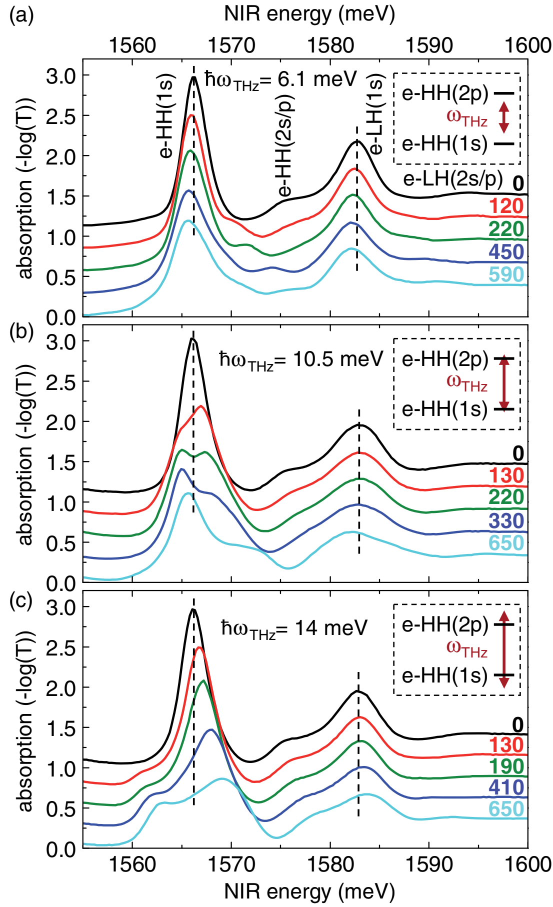

FIG. 3 (color online). Absorption spectra for different THz photon energies. Photon energies are tuned (a) below, (b) near, and (c) above resonance, as sketched in the insets. The low-temperature (10 K) spectra are vertically offset and labeled by THz peak intensities (in $\mathrm{kW/cm^2}$). Vertical dashed lines mark the undriven e-HH($1s$) and e-LH($1s$) exciton resonances. Note that the given absolute THz peak intensities are estimated to be accurate within $\pm 30\%$ for different THz photon energies, whereas at the same photon energy relative intensities are accurate to $\pm 10\%$.

[$\hbar\omega_{\mathrm{THz}} = 6.1$ meV in Fig. 3(a)], we clearly notice a small additional absorption peak evolving at 1570 meV and shifting to higher NIR energies with increasing THz peak intensity, while the main e-HH($1s$) peak slightly shifts towards lower energies. Its broadening could be explained by a beginning field ionization of the excitons, as known for strong in-plane dc electric fields [25]. Near resonance [$\hbar\omega_{\mathrm{THz}} = 10.5$ meV, Fig. 3(b)] we observe a distinct splitting of the e-HH($1s$) absorption line. Note that the largest peak separation of 6 meV at 650 $\mathrm{kW/cm^2}$ represents a significant fraction of the THz photon energy and the $1s$-$2p$ transition energy, a regime far beyond the RWA. An interesting but unexplained effect is the reversal of the relative absorption strengths of the dressed states with increasing pump intensity; i.e., consistent with a THz photon energy $\hbar\omega_{\mathrm{THz}} > \hbar\omega_{21}$ the less absorptive dressed state lies on the low-energy side for 130 $\mathrm{kW/cm^2}$, while it is found on the high-energy side above 330 $\mathrm{kW/cm^2}$, characteristic for $\hbar\omega_{\mathrm{THz}} < \hbar\omega_{21}$. In between we find a symmetric splitting at 220 $\mathrm{kW/cm^2}$ implying $\hbar\omega_{\mathrm{THz}} \approx \hbar\omega_{21}$. This reversal indicating a dynamic blueshift of the $1s$-$2p$ resonance is also present in the delay dependent absorption spectra in Fig. 2 for the time steps of 14.5–17.2 ps, and -10.2–-15.7 ps, respectively. Above resonance [$\hbar\omega_{\mathrm{THz}} = 14$ meV, Fig. 3(c)] a FEL induced peak appears below the e-HH($1s$) peak that is now blueshifted with increasing THz peak intensity. Compared to the unperturbed case, we observe a 20-fold increase in transmission at the e-HH($1s$) exciton for 650 $\mathrm{kW/cm^2}$, i.e., a large transmission change suitable for an optical modulator. We note that similar but much weaker signatures are seen at the e-LH($1s$) state, which will not be discussed further here.

Figure 4(a) displays the measured peak positions obtained from a two-line fit around the undriven e-HH($1s$) exciton (marked as dashed horizontal line) for different THz photon energies at ≈ 130 $\mathrm{kW/cm^2}$. These data points agree reasonably well with the anticrossing behavior (solid red lines) predicted by the simple two-level model according to Eq. (1) where the resonance energy $\hbar\omega_{21} = 9$ meV enters and the Rabi frequency was fitted to $\Omega = 0.25\omega_{21}$. Away from resonance the peak separation is largest and the absorption strength (indicated by a gray scale) is most pronounced for the dressed state closest to the undriven e-HH($1s$) exciton. Close to resonance the separation is smallest and the absorption strength is shared equally.

On resonance the two-level model predicts a splitting proportional to the Rabi energy and hence to the THz field, which is confirmed in Fig. 4(b) for $\hbar\omega_{\mathrm{THz}} = 10.5$ meV. The linearity is preserved up to a THz peak intensity of

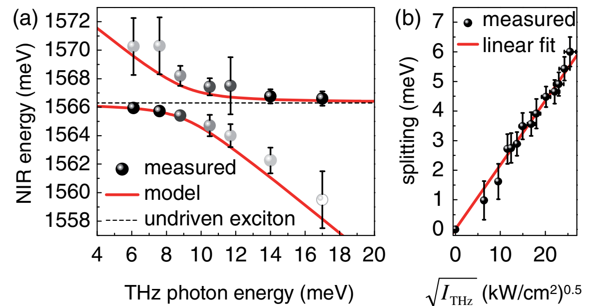

FIG. 4 (color online). Experiment-model comparison. (a) Measured peak positions for different THz photon energies at a THz peak intensity $I_{\mathrm{THz}} \approx 130$ $\mathrm{kW/cm^2}$. The absorption strength is indicated by a gray scale (more absorption for dark points). Error bars denote deviations based on several measurements and the uncertainty in the THz peak intensity. Solid red lines represent the calculation according to Eq. (1) (see text). (b) Separation between the split peaks for $\hbar\omega_{\mathrm{THz}} = 10.5$ meV near resonance. Vertical error bars are related to the error in the fitted peak positions, the horizontal ones to the uncertainty in the THz peak intensity.

650 kW/cm^2 with a Rabi energy $\Omega \approx 0.6\omega_{21}$, well beyond the RWA of our model. Assuming an intensity to field relation $I_{THz} = \frac{1}{2}\epsilon_0 c_0 n E_{THz}^2$ from a plane wave with a refractive index $n \approx 3.61$ [26], we estimate a THz field strength of $E_{THz} \approx 10$ kV/cm within the sample (30% reflection losses). Apparently, the simple two-level model holds true up to this moderate field strength. Note that the ponderomotive energy $U_p = e^2 E_{THz}^2/(4m^* \omega_{THz}^2)$ [22] as the mean oscillatory energy of an electron in the light field is 3 meV and thus of the same order as the Rabi energy, the exciton transition energy, and the ionization energy E_i, an extremely nonperturbative regime with a Keldysh parameter $\gamma = \sqrt{E_i/(2U_p)}$ near unity. We emphasize that despite large linewidths it is possible to study this complex regime in a quantum well exciton exposed to intense THz pulses, whereas it is difficult to address this region experimentally in atomic spectroscopy with its much larger level separations.

Differences from a simple two-level system are expected for our configuration since (i) the system comprises many excitonic levels and continuum states interacting with the THz radiation, (ii) the RWA breaks down, and this happens earlier for lower THz photon energies, (iii) exciton field ionization starts [25], and (iv) the dynamical Franz-Keldysh effect can occur in our experimental geometry [22]. What also cannot be explained within the two-level model is the peak reversal as a function of THz intensity [Fig. 3(b)]. Consequently, a more precise theoretical treatment, based on the full semiconductor Bloch equations [27,28], seems more applicable.

However, the measured Autler-Townes splitting can be compared quantitatively with the Rabi energy estimated from the dipole matrix element. Since the exciton behaves similar to a hydrogen atom, we evaluate the hydrogen $1s$-$2p$ transition matrix element $\mu_{21} = 0.745 e a_0^*$ [19] (with charge e). The exciton wave function is compressed in the quantum well growth direction. Hence the effective Bohr radius $a_0^* = 0.25(\alpha - 1)^2 m_e \varepsilon a_0/\mu^*$ depends on the fractional dimension α [29]. With $\varepsilon = 13$, Bohr radius a_0, reduced exciton mass $\mu^* = 0.059 m_e$, and $\alpha \approx 2.43$ for our system [30], we find $\mu_{21} \approx 44$ eÅ and a Rabi energy of 2.4 meV for a THz field strength of $E_{THz} \approx 5.4$ kV/cm, corresponding to a peak intensity of 200 kW/cm^2. Experimentally we observe an Autler-Townes splitting of 3 meV, which is in good agreement with the calculated value from simplified considerations.

In conclusion, we have reported a remarkably large absorption change and induced line splitting in the near-infrared spectral region around the e-HH($1s$) exciton when modulated at THz frequencies in a normal-incidence geometry at low temperature. The signatures are observed on a time scale of several picoseconds and are interpreted as an intraexcitonic ac Stark effect originating from the dressing of the excitonic $1s$ and $2p$ states by the THz field. The system has been driven up to a THz field strength of ≈ 10 kV/cm with a Rabi energy of ≈ 0.6 times the transition energy, a region well beyond the rotating-wave approximation and with a Keldysh parameter near unity. Moreover, the appearance of dressed states in this regime indicates a remarkably weak coupling of the $2p$ state to the continuum. Finally, with a 20-fold transmission change during picosecond pulses our approach provides a simple scheme for an ultrafast, normal-incidence optical modulator.

We thank P. Michel and his FELBE team for their dedicated support, as well as W. Seidel, F. Peter, and J. Kono for friendly cooperation and fruitful discussions. The Vienna group is supported by the Austrian FWF (SFB IR-ON).

[1] K.-J. Boller, A. Imamoğlu, and S. E. Harris, Phys. Rev. Lett. **66**, 2593 (1991).
[2] A. S. Zibrov *et al.*, Phys. Rev. Lett. **75**, 1499 (1995).
[3] S. H. Autler and C. H. Townes, Phys. Rev. **100**, 703 (1955).
[4] J. S. Bakos, Phys. Rep. **31**, 209 (1977).
[5] B. E. Cole *et al.*, Nature (London) **410**, 60 (2001).
[6] A. Zrenner *et al.*, Nature (London) **418**, 612 (2002).
[7] C. W. Luo *et al.*, Phys. Rev. Lett. **92**, 047402 (2004).
[8] S. Leinss *et al.*, Phys. Rev. Lett. **101**, 246401 (2008).
[9] G. B. Serapiglia *et al.*, Phys. Rev. Lett. **84**, 1019 (2000).
[10] M. C. Phillips *et al.*, Phys. Rev. Lett. **91**, 183602 (2003).
[11] M. D. Frogley *et al.*, Nature Mater. **5**, 175 (2006).
[12] J. F. Dynes *et al.*, Phys. Rev. Lett. **94**, 157403 (2005).
[13] S. G. Carter *et al.*, Science **310**, 651 (2005).
[14] X. Xu *et al.*, Science **317**, 929 (2007).
[15] M. Baur *et al.*, Phys. Rev. Lett. **102**, 243602 (2009).
[16] M. A. Sillanpää *et al.*, Phys. Rev. Lett. **103**, 193601 (2009).
[17] O. D. Mücke *et al.*, Phys. Rev. Lett. **87**, 057401 (2001).
[18] Q. T. Vu *et al.*, Phys. Rev. Lett. **92**, 217403 (2004).
[19] P. W. Milonni and J. H. Eberly, *Lasers* (John Wiley & Sons, New York, 1988).
[20] J. Kono *et al.*, Phys. Rev. Lett. **79**, 1758 (1997).
[21] M. Wagner *et al.*, Appl. Phys. Lett. **94**, 241105 (2009).
[22] K. B. Nordstrom *et al.*, Phys. Rev. Lett. **81**, 457 (1998).
[23] A. D. Jameson *et al.*, Appl. Phys. Lett. **95**, 201107 (2009).
[24] R. A. Kaindl *et al.*, Nature (London) **423**, 734 (2003).
[25] D. A. B. Miller *et al.*, Phys. Rev. B **32**, 1043 (1985).
[26] J. N. Heyman, R. Kersting, and K. Unterrainer, Appl. Phys. Lett. **72**, 644 (1998).
[27] M. Kira and S. W. Koch, Prog. Quantum Electron. **30**, 155 (2006).
[28] J. T. Steiner, M. Kira, and S. W. Koch, Phys. Rev. B **77**, 165308 (2008).
[29] X.-F. He, Phys. Rev. B **43**, 2063 (1991).
[30] H. Mathieu, P. Lefebvre, and P. Christol, Phys. Rev. B **46**, 4092 (1992).

APPLIED PHYSICS LETTERS **97**, 031101 (2010)

Terahertz activated luminescence of trapped carriers in InGaAs/GaAs quantum dots

J. Bhattacharyya,[1,a)] M. Wagner,[1] M. Helm,[1] M. Hopkinson,[2] L. R. Wilson,[3] and H. Schneider[1]
[1]*Institute of Ion Beam Physics and Materials Research, FZD-Rossendorf, D-01314 Dresden, Germany*
[2]*EPSRC National Centre for III-V Technology, University of Sheffield, Sheffield S1 3JD, United Kingdom*
[3]*Department of Physics and Astronomy, University of Sheffield, Sheffield S3 7RH, United Kingdom*

(Received 5 May 2010; accepted 19 June 2010; published online 19 July 2010)

Optical properties and interdot transfer dynamics of trapped carriers in InGaAs quantum dots (QDs) are investigated. Time resolved photoluminescence (PL) was measured for time-delayed interband and intraband excitations. Terahertz activated luminescence (TAL) from trapped carriers having lifetimes of ~ 250 ns at 8 K, was observed. Spectral shift of the TAL with respect to the PL showed the trionic nature of the PL in the n-doped QDs. With increasing terahertz excitation intensity, the TAL increased and reached saturation. The activation energy associated with the trapped carrier decay was quite close to the intersublevel transition energy (~ 20 meV) indicating trapping in the QDs. © *2010 American Institute of Physics*. [doi:10.1063/1.3464163]

Study of carrier dynamics in semiconductor quantum dots (QDs) is essential for the understanding and improvement of their performances as optoelectronic devices. Time resolved photoluminescence (PL) measurements have been extensively used to investigate the lifetimes and relaxation mechanisms of carriers in the QDs.[1–4] In these experiments, the initial carrier distribution depends on the excitation energies. For nonresonant excitation, the electron-hole pairs are generated in the barrier or the wetting layer (WL) of the self-assembled QD systems. These carriers rapidly relax into the QDs by phonon scattering and then recombine giving PL signals corresponding to the QD transitions. During the relaxation process, the carriers can be trapped in QDs with no appropriate partners to recombine.[5] Trapping of carriers in the potential fluctuations in the WL has also been reported earlier.[6] These long-lived trapped carriers are found to have significant influence on the PL transients, resulting in modification of PL decay rates[5] and increased rise times.[7] The dependences of the PL transients on the temperature and excitation intensity[7–9] have been used to investigate the influence of trapped carriers which relax by interdot transfer via the WL (Ref. 10) or tunneling to the adjacent QDs.[7,11] Study of the optical properties of these long-lived carriers from the PL transients requires measurements with long time window and high sensitivity. We propose a technique to probe these carriers using a streak-camera based detection enabling simultaneous time- and energy-resolved measurements.

In this report we present our investigation of trapped carriers where we isolated the luminescence from the trapped carriers from the regular PL, enabling a direct study of their distribution and dynamics. We studied the trapped carriers in InGaAs/GaAs QD ensembles using terahertz induced PL measurements. Using temporally separated laser pulses for interband and intraband excitations, we observed terahertz activated luminescence (TAL) from the trapped carriers.

The self-assembled InGaAs QD samples were grown on (100) GaAs using molecular beam epitaxy, in the Stranski–Krastranow growth mode. The sample studied consisted of 80 layers of QDs separated by 50 nm wide GaAs barriers to ensure structural and electrical isolation between the layers. Using postgrowth annealing at 850 °C, the intersublevel transition energy in the conduction band was redshifted from 55 meV (for the as-grown sample) to 20 meV and the intradot relaxation time was increased from a few picoseconds to 60 ps.[12] From atomic force microscope measurements of an uncapped reference sample, the QD density was estimated to be about 4×10^{10} cm^{-2} with an average base diameter of 20 nm and height of about 5 nm, before capping. The QDs were n-doped by a Si-layer grown ~ 2 nm below the QD layers, providing an average doping of one electron per dot. Time-resolved PL quenching measurements were performed using a tunable mode-locked Ti:sapphire laser (TSL), emitting ~ 4 ps long pulses, for interband excitation. Emission from a free-electron laser (FEL) with a pulse width of ~ 10 ps was synchronized to the TSL and used to induce intradot transitions resulting in quenching of the PL and other effects as will be discussed shortly. The TSL spot size on the sample was ~ 80 μm in diameter (full width at half maximum) with an average power of 1 mW. Both the laser pulses were incident at an angle of $\sim 15°$ on the sample. A pulse picker, triggered by the FEL pulses, was used to reduce the repetition rate of the TSL (78 MHz) to match with that of the FEL (13 MHz). By tuning the pulse picker, any of the six pulses from the TSL could be chosen which enabled us to introduce a relative time delay (Δt) up to 76.9 ns between the TSL and FEL pulses. Finer adjustments in the time delay were made using a mechanical delay unit. Time- and wavelength-resolved detection of the luminescence was done by a Hamamatsu streak camera coupled to a spectrometer. The sample was cooled in a He cryostat enabling measurements at different temperatures.

A schematic of the sequence of the laser pulses incident on the sample is shown in Fig. 1(a). Using the mechanical delay unit, the FEL pulse was set at 1.2 ns before the TSL pulse. Therefore the effective delay of the FEL pulse with respect to the previous TSL pulse, i.e., $\Delta t = 75.2$ ns. Figure 1(b) shows the measured PL transient at 5 K corresponding to the ground state recombination in the QDs, for interband

a)Electronic mail: j.bhattacharyya@fzd.de.

 © 2010 American Institute of Physics

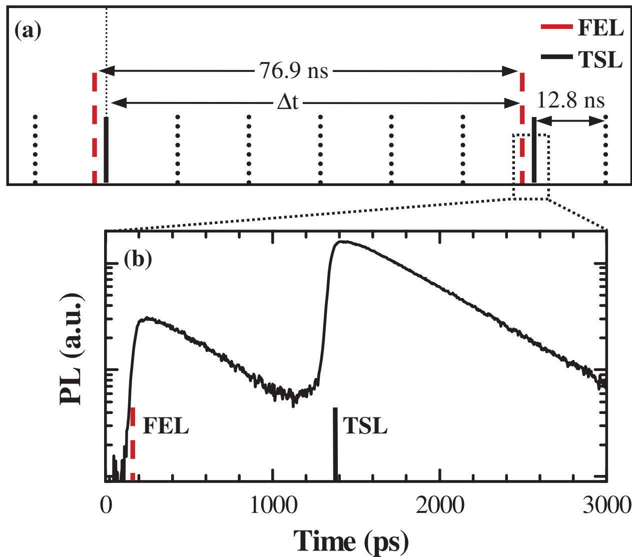

FIG. 1. (Color online) (a) Schematic showing the pulse sequence of the TSL (black lines) and the FEL (red dashed lines). The dotted black lines correspond to the TSL pulses suppressed by the pulse picker. (b) Luminescence transient at 5 K as measured by the streak camera for TSL and FEL excitation wavelengths of 802 nm at 1 mW and 61.4 μm at 74 mW, respectively, showing PL and TAL.

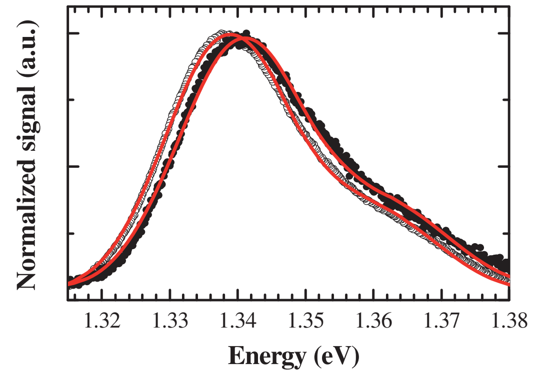

FIG. 2. (Color online) Normalized PL (open circles) and TAL (solid circles) spectra measured at 5 K for TSL and FEL excitation wavelengths of 802 nm (in the barrier) at 1 mW and 61.4 μm at 74 mW, respectively. The solid lines are the Gaussian fits.

excitation in the GaAs barrier. The signal around 1400 ps is the PL emission excited by the TSL pulse. The FEL was tuned to the conduction band $s-p_x$ intersublevel transition energy of the QDs at 20 meV (61.4 μm). The feature at 200 ps corresponds to the TAL due to the FEL pulse. For measurements where larger Δt was required, different TSL pulses [shown by dotted lines in Fig. 1(a)] were chosen by the pulse picker. However, the streak camera being triggered at 78 MHz repetition rate of the TSL, the temporal position of the laser pulses in the streak camera image appeared unchanged. Measurements were done for different interband excitation energies. TAL was observed only for TSL excitation in the barrier or the WL. This suggested that the TAL originated either from carriers trapped in the WL interfaces or from the lone carriers trapped in the QDs. For interband excitation below the WL energy, the carriers were generated in pairs within the same dots. Therefore the existence of lone trapped carriers in the dots or interfaces was negligible, leading to the absence of TAL signal. The measured rise times of the PL and TAL were limited by the resolution of our experiment which was ~35 ps. Monoexponential fits to the luminescence decay (τ_{PL}) gave similar decay times of 500 ps for both signals which are associated with the ground state recombination rate.

Isolation of the trapped carrier luminescence from the PL enabled us to investigate the spectral response of the TAL. The PL spectrum in Fig. 2 shows two peaks which arise from the ground state and first excited state transitions in the QD ensemble. The spectrum for the TAL is similar to that of the PL except that it is blueshifted with respect to the PL emission and is weaker in intensity. We performed measurements for different intensities of the FEL and fitted the luminescence spectra with two Gaussians each (as shown in Fig. 2) to get an estimate of the emission energies and intensities. Figure 3(a) shows the variation in the peak energies of the PL and TAL with the FEL power at 10 K. The blueshift of the TAL decreases with increasing FEL power. We observed a maximum ground state energy shift of ~4 meV which corresponds well with the trion renormalization energy in InAs.[13,14] With an average doping of one electron per dot, the emitted PL is expected to be trionic. Since the FEL energy is resonant with the electron $s-p_x$ transition, the interdot transfer occurs primarily for electrons. The transferred electron recombines when it arrives in a QD having a hole which makes the TAL signal predominantly excitonic. With increasing FEL intensity, the number of detrapped carriers increases, making the transition more trionic. The TAL intensity increases and reaches saturation and this is accompanied by an equivalent decrease in the PL intensity such that the total remains nearly constant. This demonstrates the influence of long-lived carriers on the PL. The excited state tran-

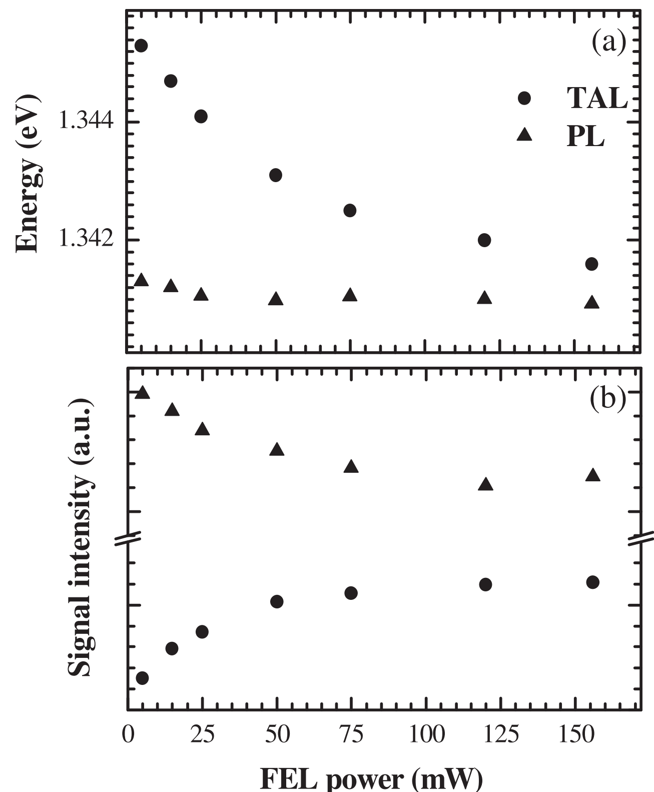

FIG. 3. The ground state transition (a) energy and (b) intensity of the QD ensemble at 10 K plotted as a function of FEL excitation power. The triangles and circles correspond to PL and TAL, respectively.

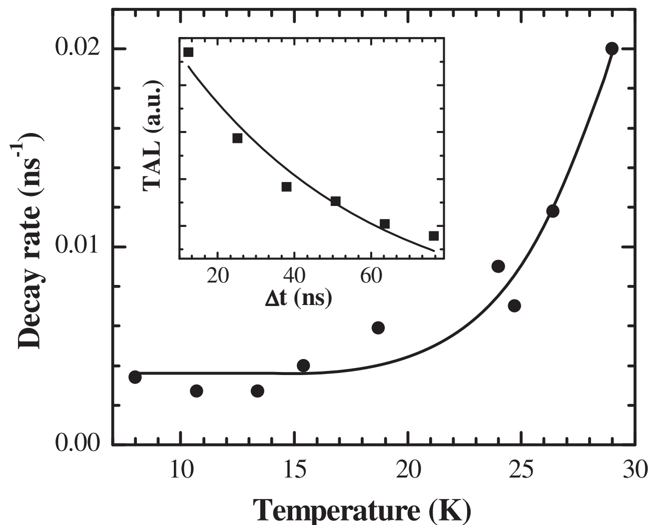

FIG. 4. Temperature dependence of the trapped carrier decay rates $(1/\tau_{tc})$. The line represents an Arrhenius fit giving an activation energy of 17 ± 3 meV. The inset shows a typical TAL decay with Δt at 29 K, fitted with a monoexponential function.

sition also showed similar behavior but with weaker magnitudes (not shown here).

As mentioned earlier, the carriers can be trapped in the WL interfaces or the QDs. To distinguish between these two possibilities we performed PL quenching measurements using FEL pulses detuned from the intersublevel transition energy. For FEL energy of 29 meV (42 μm) we found that the TAL intensity was drastically reduced. If the majority of the carriers were trapped in the WL interfaces, the FEL photons with higher energy would still be able to release the carriers into the continuum, which would relax into the QDs and emit TAL signals. However, for carriers trapped in the QDs, due to the delta-like density of states of the QDs, the FEL energy is required to match the intersublevel transition energy to excite the trapped carriers from s to p_x states in the QDs. The excited carriers have appreciable tunneling probability into adjacent QDs. When the carrier reaches a QD with another appropriate carrier, it can recombine radiatively. This emitted luminescence gives rise to the TAL signal.

As a further verification of our understanding we performed measurements to estimate the activation energy of the transfer mechanism of the trapped carriers. Apart from the TAL decay time (τ_{PL}) as mentioned earlier, another relevant lifetime is the trapped carrier lifetime (τ_{tc}) which results in a change in the TAL peak intensity as a function of the time delay between FEL and TSL pulses (Δt). Monoexponential fits to the TAL decay curves (see inset of Fig. 4) gave us an estimate of τ_{tc} at a given temperature. Measurements were done at different sample temperatures and the corresponding decay rates $(1/\tau_{tc})$ are plotted in Fig. 4. The temperature range was limited to 30 K, since the temperature dependence of the PL intensity (without FEL pulses) initially increased and reached saturation at around 30 K and later decreased. Similar behavior for PL have been reported for QDs (Ref. 15) where the initial increase was attributed to the trapped carrier luminescence, which fits to our description. Beyond 30 K, the trapped carriers were depleted and other thermal effects dominated. An Arrhenius fit of the decay rates gave an activation energy of 17 ± 3 meV. This value is quite close to the $s-p_x$ intersublevel transition energy, confirming that a majority of the carriers were trapped in the QDs. The background decay rate $1/\tau_{tc}\sim0.004$ ns^{-1} $(\tau_{tc}\sim250$ ns) is attributed to the weak interdot tunneling,[16] which is independent of the temperature.

In conclusion, we showed that time-resolved PL measurements with two-color pulsed laser excitations can be used to probe long lived carriers trapped in QD systems. The decrease in the TAL signal with increasing delay between the FEL and TSL pulses enabled us to directly measure the decay of the trapped carrier population. This gave an estimate of the trapped carrier lifetime without any influence of the radiative recombination lifetimes. Comparison of the spectral responses of the TAL and PL showed the excitonic and trionic nature of the transitions, respectively. From the temperature and FEL intensity dependent measurements we found that the carriers were trapped in the QDs.

Author J.B. acknowledges the financial support from Alexander von Humboldt foundation. The research leading to these results has received funding from the European Community's Seventh Framework Programme (FP7/2007-2013) under Grant Agreement No. 226716. The authors are grateful to P. Michel and the FELBE team for their dedicated support.

[1] M. Paillard, X. Marie, E. Vanelle, T. Amand, V. K. Kalevich, A. R. Kovsh, A. E. Zhukov, and V. M. Ustinov, Appl. Phys. Lett. **76**, 76 (2000).
[2] H. Yu, S. Lycett, C. Roberts, and R. Murray, Appl. Phys. Lett. **69**, 4087 (1996).
[3] S. Malik, E. C. Le Ru, D. Childs, and R. Murray, Phys. Rev. B **63**, 155313 (2001).
[4] Yu. I. Mazur, B. L. Liang, Zh. M. Wang, D. Guzun, G. J. Salamo, G. G. Tarasov, and Z. Ya. Zhuchenko, J. Appl. Phys. **100**, 054316 (2006).
[5] A. S. Shkolnik, L. Ya. Karachinsky, N. Yu. Gordeev, G. G. Zegrya, V. P. Evtikhiev, S. Pellegrini, and G. S. Buller, Appl. Phys. Lett. **86**, 211112 (2005).
[6] C. Lobo, R. Leon, S. Marcinkevicius, W. Yang, P. C. Sercel, X. Z. Liao, J. Zou, and D. J. H. Cockayne, Phys. Rev. B **60**, 16647 (1999).
[7] J. W. Tomm, T. Elsaesser, Y. I. Mazur, H. Kissel, G. G. Tarasov, Z. Y. Zhuchenko, and W. T. Masselink, Phys. Rev. B **67**, 045326 (2003).
[8] L. Brusaferri, S. Sanguinetti, E. Grilli, M. Guzzi, A. Bignazzi, F. Bogani, L. Carraresi, M. Colocci, A. Bosacchi, P. Frigeri, and S. Franchi, Appl. Phys. Lett. **69**, 3354 (1996).
[9] R. Chen, H. Y. Liu, and H. D. Sun, J. Appl. Phys. **107**, 013513 (2010).
[10] Z. Ma, K. Pierz, J. Hübner, and W. W. Rühle, Physica E (Amsterdam) **28**, 203 (2005).
[11] A. Tackeuchi, Y. Nakata, s. Muto, Y. Sugiyama, T. Usuki, Y. Nishikawa, N. Yokoyama, and O. Wada, Jpn. J. Appl. Phys., Part 2 **34**, L1439 (1995).
[12] E. A. Zibik, T. Grange, B. A. Carpenter, N. E. Porter, R. Ferreira, G. Bastard, D. Stehr, S. Winnerl, M. Helm, H. Y. Liu, M. S. Skolnick, and L. R. Wilson, Nature Mater. **8**, 803 (2009).
[13] A. D. Ashmore, J. J. Finley, R. Oulton, P. W. Fry, A. Lemaître, D. J. Mowbray, M. S. Skolnick, M. Hopkinson, P. D. Buckle, and P. A. Maksym, Physica E (Amsterdam) **13**, 127 (2002).
[14] P. A. Dalgarno, J. M. Smith, J. McFarlane, B. D. Gerardot, K. Karrai, A. Badolato, P. M. Petroff, and R. J. Warburton, Phys. Rev. B **77**, 245311 (2008).
[15] W. H. Jiang, X. L. Ye, B. Xu, H. Z. Xu, D. Ding, J. B. Liang, and Z. G. Wang, J. Appl. Phys. **88**, 2529 (2000).
[16] J. Rihani, V. Sallet, N. Yahyaoui, J. C. Harmand, M. Oueslati, and R. Chtourou, J. Lumin. **129**, 251 (2009).

APPLIED PHYSICS LETTERS **96**, 151113 (2010)

Microcavity enhanced silicon light emitting pn-diode

J. Potfajova,[1,a)] B. Schmidt,[1] M. Helm,[1] T. Gemming,[2] M. Benyoucef,[3] A. Rastelli,[3] and O. G. Schmidt[3]
[1]*Institute of Ion Beam Physics and Materials Research, Forschungszentrum Dresden-Rossendorf, P.O. Box 510119, 01314 Dresden, Germany*
[2]*Institute for Complex Materials, IFW Dresden, P.O. Box 270116, 01171 Dresden, Germany*
[3]*Institute for Integrative Nanosciences, IFW Dresden, P.O. Box 270116, 01171 Dresden, Germany*

(Received 16 November 2009; accepted 15 March 2010; published online 15 April 2010)

An electrically driven silicon light emitting diode with two distributed Bragg reflectors is reported. The active material is a Si pn-junction fabricated by boron ion implantation into an n-type silicon-on-insulator wafer. The cavity with a thickness of a few wavelengths is formed by amorphous Si/SiO_2 multilayer stacks. A strong narrowing and enhancement of the electroluminescence at a resonant wavelength of $\lambda=1146$ nm is observed with a quality factor of $Q=143$ and a finesse of $F=11$. © *2010 American Institute of Physics*. [doi:10.1063/1.3385153]

Achieving efficient light emission from silicon is a key challenge of today's optoelectronics, since it would open the way for all-silicon based integrated optoelectronic circuits. This could enable implementation of high-throughput optical interconnects as well as add new functionalities to integrated circuits. Large progress has been made during the past decade, culminating in the report of optical gain,[1] an optically pumped Si Raman Laser,[2] and recent hopes for a Ge-on-Si laser.[3] However, as long as no Si pn-junction laser is available, efforts also have to concentrate on increasing the efficiency of Si based luminescent devices. In two milestone papers it has been shown that B^+ ion implanted Si pn-junctions[4,5] operated in forward direction can exhibit electroluminescence (EL) efficiencies as large as 0.1% to 1% at room temperature, several orders of magnitude higher than the usual efficiency of of 10^{-6} for band gap emission in silicon.

It is well known that the performance of light emitting diodes (LED) can be significantly improved by integrating them into a resonant optical cavity or microcavity.[6] In particular, a microcavity gives rise to a higher spectral purity, better directionality, and higher efficiency of the emission.[7] This has been demonstrated for Si based structures almost exclusively by optical excitation, i.e., photoluminescence, using various active materials such as crystalline Si,[8] porous Si,[9] Si nanocrystals,[10] Er^{3+} ions together with Si nanocrystals[11] or Ge self-assembled quantum dots[12] in microcavities. However, there are only very few reports on electrically driven luminescence from Si based microcavities.[9,13] This is partly due to the fact that in Si technology distributed Bragg reflector (DBR) multilayer stacks are usually based on SiO_2 and another materials (e.g., Si_3N_4, a-Si). SiO_2 is a highly insulating material, rendering electrical injection difficult. An alternative route has been the incorporation of Si light emitters into photonic crystal structures.[14–16] Such a Si based LED has been reported in Ref. 17.

Here we report an electrically driven Si LED with two DBRs. The active material is a Si pn-junction fabricated by B^+ ion implantation[18] into the n-type device layer of a silicon-on-insulator (SOI) wafer. The cavity, formed from amorphous silicon and silicon dioxide (a-Si/SiO_2) multilayer stacks, leads to a strong narrowing and enhancement of the electroluminescence.

The devices were fabricated on a commercial 100 mm SOI wafer with a thickness and resistivity of the active n-type (001)Si device layer of (2 ± 0.5) μm and $1-5$ Ω cm, respectively. The thickness of the buried SiO_2 layer given by the manufacturer was (200 ± 10) nm. Using multiple oxidation and oxide removal the device layer was thinned down to an average thickness of 1300 nm, which would correspond to a 4λ cavity, however, there was a significant thickness gradient variation across the wafer. This thickness was chosen as a compromise between high cavity finesse and mechanical stability of the targeted membrane. Also the cavity should be thick enough to guarantee at least one cavity mode within the natural emission. Subsequently the Si layer was implanted with B^+ ions of 30 keV energy at a fluence of 4×10^{15} cm^{-2}, an optimum value for efficient near band gap light emission.[18] In order to contact the n-Si layer, n^+-regions were formed from the top around the p^+ layer by P^+ ion implantation (fluence 5×10^{14} cm^{-2}, energy 25 keV). After furnace annealing at 1050 °C for 20 min, Al contacts were evaporated and lithographically patterned. A schematic cross section of the device at this stage of the fabrication can be seen in Fig. 1(a). It represents an LED on SOI, where the SOI acts as a low-finesse cavity.

In order to produce devices with a high-quality cavity, the silicon substrate and buried oxide layer of every second device on the same SOI wafer were removed by etching with potassium hydroxide (KOH) and buffered hydrofluoric acid (HF), respectively. The remaining non-etched devices act as

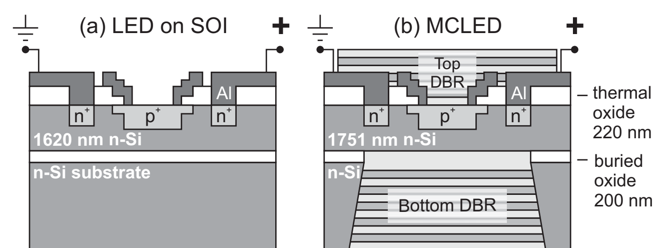

FIG. 1. Scheme of (a) LED on SOI and (b) MCLED.

a)Electronic mail: j.potfajova@fzd.de.

 © 2010 American Institute of Physics

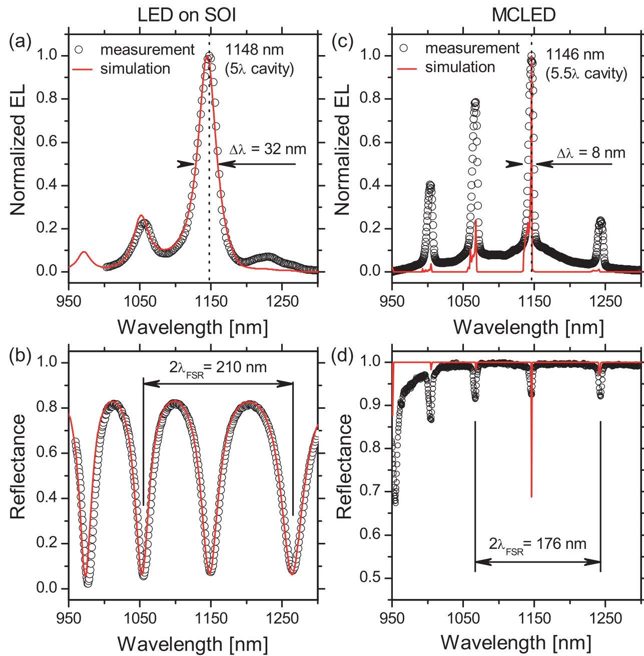

FIG. 2. (Color online) EL and reflectance of the LED on SOI in (a) and (b), and of the MCLED in (c) and (d), respectively. The black symbols represent the measured values and the red lines are the simulation results. The EL was recorded at a diode forward current of 30 mA.

reference LEDs. DBRs consisting of 3.5 pairs and 5.5 pairs of about 200 nm SiO_2/80 nm a-Si were deposited on the top and the bottom of the thin silicon device membrane, respectively. The asymmetry results in preferential emission from the top of the device. A sketch of the final microcavity-enhanced LED (MCLED) is displayed in Fig. 1(b). Actual thicknesses of all a-Si and SiO_2 layers forming the top and the bottom DBR, obtained from transmission electron microscopy, ellipsometry, and infrared spectroscopy, are (70 ± 7) nm and (193 ± 10) nm, respectively.

In the following we present results obtained on selected LEDs on SOI and MCLEDs. Both devices have a square shape of 50×50 μm^2 size and their actual thicknesses were 1620 nm and 1751 nm, respectively. It turned out that thinner devices (1330 nm thick) did not exhibit good electrical diode characteristics. The EL measurements on forward-biased pn-junctions were performed using a long-working-distance objective with a magnification of 20× and a numerical aperture of $N_A=0.4$. For comparison also the reflectance was recorded using infrared spectroscopy.

Figure 2 shows the results for the LED on SOI and the MCLED. For the LED on SOI the reflectance [Fig. 2(b)] is consistent with a low-quality Fabry–Perot cavity formed by a 1620 nm thick Si layer bounded by air and SiO_2 at the top and bottom, respectively. The EL [Fig. 2(a)] shows a main peak at $\lambda=1148$ nm and some weaker satellite peaks, which still lie within the natural emission spectrum of the Si band gap luminescence. Note that the natural spectrum cannot be accessed in this SOI device but it is known from experiments on similarly prepared bulk Si pn-diodes[19] to have an full-width at half-maximum (FWHM) of approximately 80 nm. In contrast, the emission from the SOI is narrowed to 32 nm. The main peak at 1148 nm corresponds to the 5λ-resonance of the cavity.

The MCLED exhibits the striking effect of the high-quality cavity with the two Bragg mirrors. Again EL as well as reflectance are plotted in Figs. 2(c) and 2(d), respectively. Now the main emission has a FWHM of only 8 nm and the peak is located at $\lambda=1146$ nm, which corresponds to a quality factor of $Q=\lambda/\Delta\lambda=143$. The finesse, F, defined as the ratio between free spectral range (88 nm) and linewidth, is deduced to F=11. A fit (see below) reveals that the main peak is related to the 5.5λ-resonance of the cavity with a thickness of 1751 nm.

All spectra were simulated using the UNIMCO program code,[20] which assumes laterally homogeneous structures. It does not take into account any layer thickness variation, surface roughness or inhomogeneous nor pn-junction boundaries. The optical constants of sputter deposited a-Si and SiO_2 films of the DBR stacks were determined from the ellipsometry measurements to be 3.564 and 1.449, respectively, at the wavelength of 1150 nm.

In the EL simulation the diode design plays an important role. In our design the p^+-region covers only the area of 50×50 μm^2 and from secondary ion mass spectrometry we know that during postimplantation annealing the boron diffuses to a depth of about 950 nm. The n^+-contacts are placed around the p^+n-junction. The current flows between p^+- and n^+-areas mostly parallel to the surface, which is the shortest path. Therefore the recombination preferentially takes place along the circumference of the p^+ area. This fact was also experimentally observed by laterally resolved EL measurements. A normalized measured EL spectrum of a Si pn-diode prepared under the same conditions[19] with a FWHM of about 80 nm and the maximum located at the wavelength 1138 nm has been taken as an input for the calculation. The best agreement between the calculated EL and the data measured from the LED on SOI and the MCLED were achieved, if we assume a thickness of 375 nm of the emitting zone (around an antinode of the electric field amplitude). The acceptance angle of the optical system (with $N_A=0.4$) is $2\theta=48°$. The positions and the intensities of the EL resonant peaks depend on the angle of light extraction. Increasing of the extraction angle shifts the EL to the smaller wavelengths and decreases the EL intensity. The FWHM of the calculated resonance peak increases from the value of 1 up to 4 nm, if in the simulation a collection angle of 48° ($\theta=0°\pm24°$) is taken into account. The average extracted EL spectra are compared to the experimental values in Fig. 2. A very good agreement between the EL measurement (full black circles) and the simulation (red solid lines) is obtained in the case of the LED on SOI [Fig. 2(a)]. Certain quantitative differences between the measurement and the simulation of the MCLED [Fig. 2(c)] are visible, nevertheless the position of the peaks is very close to measurements and the FWHM of the measured resonant maximum of $\Delta\lambda=8$ nm is only by a factor of 2 higher than the calculated value.

Up to now we have discussed only the spectral shape of the emission spectra. However, it is of course desirable to know the emission enhancement resulting from the microcavity effect. In Fig. 3 the measured EL spectrum of the MCLED (full black circles) is compared with the EL spectrum of the LED on SOI (open red circles). Both of these devices were fabricated on the same SOI wafer and the EL measurements were performed using the same experimental setup and same measurement parameters (forward current =30 mA). We can evaluate the enhancement by the Fabry–Perot resonator with respect to LED on SOI. From the com-

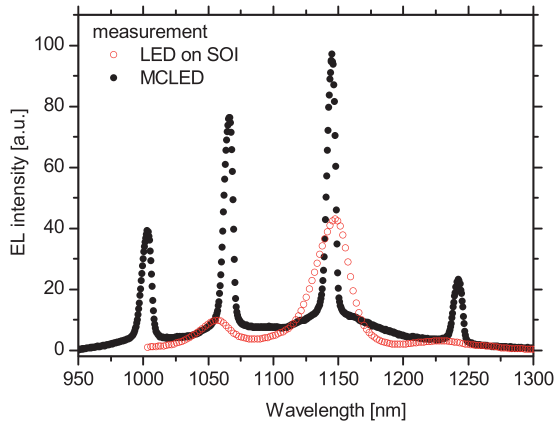

FIG. 3. (Color online) Direct comparison of the measured EL spectra of LED on SOI (red open circles) and MCLED (black full circles).

parison of the measured EL spectra of the LED on SOI and the MCLED in Fig. 3 (measured with the collection angle of $\theta = 0^\circ \pm 24^\circ$) the following conclusions can be drawn: Compared to the bulk LED on SOI, the EL intensity of the MCLED at the resonance wavelength of $\lambda = 1146$ nm is enhanced by a factor of 2.3. The relative enhancement appears even stronger for the side modes, the reason for which is not clear at present. This fact is partially responsible also for enhancement of the spectrally integrated emission[21] by a factor of 1.65. Note that we focus on the relative spectral enhancement induced by the Bragg mirrors in the SOI device, as measured in our experimental setup with a given collection angle. The MCLED showed the expected angular dependence, namely an intensity drop and a blueshift, measured up to a tilt angle of 15° (not shown here). For the parameters of the present cavity, no significant increase in the integrated extracted efficiency is expected. We cannot give reliable numbers for absolute efficiencies at this stage, but we know that the quantum efficiency of our light emitting devices on SOI wafers is definitely lower compared to 0.12% published by Sun *et al.*[18] The present device is thus mainly regarded as a proof of concept.

In conclusion, we have demonstrated a 5.5λ microcavity enhanced Si LED emitting at a resonant wavelength of 1146 nm with a quality factor of Q=143. As a reference, an LED in the device layer of the same SOI substrate without DBRs has been evaluated. An enhancement of the electroluminescence due to the microcavity effect has been demonstrated. Future efforts should be directed toward an even thinner cavity: With a thickness of less than 3–4λ only one cavity mode would remain within the natural emission linewidth, thus leading to emission of a single narrow line.

We thank the staff of the ion beam center and the clean room of FZD for the ion implantation and the device preparation, respectively, as well as J. M. Sun and T. Dekorsy for helpful discussions in the early stages of this work.

[1] L. Pavesi, L. Dal Negro, C. Mazzoleni, G. Franzo, and F. Priolo, Nature (London) **408**, 440 (2000).
[2] H. S. Rong, R. Jones, A. S. Liu, O. Cohen, D. Hak, A. Fang, and M. Paniccia, Nature (London) **433**, 725 (2005).
[3] J. Liu, X. Sun, L. C. Kimerling, and J. Michel, Opt. Lett. **34**, 1738 (2009).
[4] M. A. Green, J. Zhao, A. Wang, P. J. Reece, and M. Gal, Nature (London) **412**, 805 (2001).
[5] W. L. Ng, M. A. Lourenco, R. M. Gwilliam, S. Ledain, G. Shao, and K. P. Homewood, Nature (London) **410**, 192 (2001).
[6] N. E. J. Hunt, E. Schubert, R. Logan, and G. J. Zydzik, Appl. Phys. Lett. **61**, 2287 (1992).
[7] H. Benisty, H. D. Neve, and C. Weisbuch, IEEE J. Quantum Electron. **34**, 1612 (1998).
[8] D. Sotta, E. Hadji, N. Magnea, and E. Delamadeleine, J. Appl. Phys. **92**, 2207 (2002).
[9] S. Chan and P. Fauchet, Appl. Phys. Lett. **75**, 274 (1999).
[10] A. Belarouci and F. Gourbilleau, J. Appl. Phys. **101**, 073108 (2007).
[11] F. Iacona, G. Franzo, E. C. Moreira, and F. Priolo, J. Appl. Phys. **89**, 8354 (2001).
[12] J. S. Xia, K. Nemoto, Y. Ikegami, Y. Shiraki, and N. Usami, Appl. Phys. Lett. **91**, 011104 (2007).
[13] J. Potfajova, J. M. Sun, S. Winnerl, T. Dekorsy, W. Skorupa, B. Schmidt, M. Helm, S. Mantl, and U. Breuer, Electron. Lett. **40**, 904 (2004).
[14] M. Zelsmann, E. Picard, T. Charvolin, E. Hadji, M. Heitzmann, B. Dal'zotto, M. E. Nier, C. Seassal, P. Rojo-Romeo, and X. Letartre, Appl. Phys. Lett. **83**, 2542 (2003).
[15] M. Fujita, Y. Tanaka, and S. Noda, IEEE J. Sel. Top. Quantum Electron. **14**, 1090 (2008).
[16] M. Makarova, V. Sih, J. Warga, R. Li, L. Dal Negro, and J. Vuckovic, Appl. Phys. Lett. **92**, 161107 (2008).
[17] C. D. Presti, A. Irrera, G. Franz, I. Crupi, F. Priolo, F. Iacona, G. Di Stefano, A. Piana, D. Sam Filippo, and P. G. Fallica, Appl. Phys. Lett. **88**, 033501 (2006).
[18] J. M. Sun, T. Dekorsy, W. Skorupa, B. Schmidt, and M. Helm, Appl. Phys. Lett. **83**, 3885 (2003).
[19] J. M. Sun, T. Dekorsy, W. Skorupa, B. Schmidt, A. Mücklich, and M. Helm, Phys. Rev. B **70**, 155316 (2004).
[20] UniCAD, Inc., UNIMCO 4.0 User Manual—The unique CAD tool for LED, OLED, RCLED, VCSEL, and optical coating (2002–2005).
[21] N. E. J. Hunt, E. F. Schubert, R. F. Kopf, D. L. Sivco, A. Y. Cho, and G. J. Zydzik, Appl. Phys. Lett. **63**, 2600 (1993).

APPLIED PHYSICS LETTERS **97**, 192505 (2010)

On-chip superconductivity via gallium overdoping of silicon

R. Skrotzki,[1,a)] J. Fiedler,[1,2] T. Herrmannsdörfer,[1] V. Heera,[1] M. Voelskow,[1]
A. Mücklich,[1] B. Schmidt,[1] W. Skorupa,[1] G. Gobsch,[2] M. Helm,[1] and J. Wosnitza[1]
[1]*Dresden High Magnetic Field Laboratory (HLD) and Institute of Ion Beam Physics and Materials Research, Forschungszentrum Dresden-Rossendorf (FZD), P.O. Box 51 01 19, D-01314 Dresden, Germany*
[2]*Experimental Physics, Institute of Physics, Ilmenau University of Technology, Weimarer Str. 32, 98693 Ilmenau, Germany*

(Received 30 August 2010; accepted 12 October 2010; published online 11 November 2010)

We report on superconducting properties of gallium-enriched silicon layers in commercial (100) oriented silicon wafers. Ion implantation and subsequent rapid thermal annealing have been applied for realizing gallium precipitation beneath a silicon-dioxide cover layer. Depending on the preparation parameters, we observe a sharp drop to zero resistance at 7 K. The critical-field anisotropy proofs the thin-film character of superconductivity. In addition, out-of-plane critical fields of above 9 T and critical current densities exceeding 2 kA/cm^2 promote these structures to be possible playgrounds for future microelectronic technology. © *2010 American Institute of Physics*. [doi:10.1063/1.3509411]

A new group of superconductors, i.e., covalent-bound materials, have recently attracted strong technological as well as fundamental interest in exploring the origin of its electronic ground state.[1–3] Although first investigations have been made already in the early 1960s,[4,5] renewed attention occurred in 2004 with the finding of superconductivity in the archetypical covalent-bound material diamond which had to be heavily doped with boron.[6] Motivated by this achievement, superconductivity under ambient pressure has also been found in the other group-IV semiconductors, silicon and germanium.[7,8] Doping beyond the metal-to-insulator transition has been proven to be the key challenge since equilibrium solubility and related dopant precipitation limit the charge-carrier density and thus exclude the formation of a superconducting condensate in these systems.[9] Successful doping techniques include high-pressure high-temperature synthesis,[10] gas immersion laser doping,[11] and ion implantation combined with subsequent annealing.[1,8] Since the latter is fully compatible with conventional semiconductor processing, we have followed the idea of using this technique to integrate superconducting structures in a semiconducting environment. Accessible mass production of superconducting on-chip heterostructures would bare the chance of quickly developing novel microelectronic or even nanoelectronic devices reaching from a simple designed superconducting quantum interface device to a possible future quantum computer.[1,12]

Within this work we focused on silicon, by far the most common semiconductor in microelectronic industry. Since heavy doping via boron, the most promising acceptor in terms of activation of charge carriers, only leads to critical temperatures not higher than 0.6 K,[13] we thus follow another approach aiming at applicability. We have chosen Ga for ion implantation to yield on-chip superconductivity not via doping but rather due to precipitation. The low solubility limit of Ga in silicon (0.1 at. %) (Ref. 14) and comparable high critical temperatures for various known Ga phases (up to 8.5 K) (Refs. 15–17) have motivated our choice.

As host material, a Czochralski-grown, n-type Si wafer with (100) orientation and resistivity of about 1 kΩ cm was used. On top of its surface, a 30 nm thick SiO_2 cover layer was deposited via sputtering to protect the Si surface during implantation and annealing. As a first step, a total gallium fluence of 4×10^{16} cm^{-2} has been implanted through the cover layer at ion energy of 80 keV. This resulted in a heavily doped amorphous Si layer of about 90 nm width. According to simulations of Stopping and Range of Ions in Matter,[18] a Ga peak concentration of 8×10^{21} cm^{-3} (14 at. %) has then been accumulated in a depth of 30 nm below the SiO_2/Si interface. After implantation, the wafers were cut into pieces of 1×1 cm^2. Rapid thermal annealing (RTA) for 60 s in flowing Ar atmosphere (3 standard liters per minute) has then been applied for each sample at constant temperatures between 500 and 900 °C in order to stimulate Si recrystallization and Ga precipitation.

For electrical measurements, gold contacts were sputtered on the corners of the samples and silver wires were attached to them. Hall-effect and resistivity measurements in Van der Pauw geometry[19] were performed with a LakeShore HMS 9709 Hall measurement system in the temperature range between 2 and 400 K at applied excitation currents of 1 mA and fields of 1 T. Further low-temperature resistivity measurements were done in a Physical Properties Measurement System from Quantum Design using a home-made demagnetization inset reaching temperatures as low as 80 mK. The structure of the implanted layer was investigated by means of high-resolution Rutherford backscattering spectrometry in channelling geometry (RBS/C) (Ref. 20) with 1.2 MeV He^+ ions and cross-sectional transmission electron microscopy (XTEM) using a FEI Titan 80–300 microscope.

The sheet resistances of various annealed samples are shown in Fig. 1 as a function of temperature. The contribution of the substrate dominates at high temperatures. At lower temperatures, the charge carriers of the substrate freeze out and the electrical transport is governed by the implanted layer. Quite evidently, the residual sheet resistance drops with applying higher annealing temperatures in a non-monotonous fashion from 11 kΩ/sq. at 550 °C down to 1 kΩ/sq. at 900 °C since an increasing effect of Ga-doping

a)Electronic mail: r.skrotzki@fzd.de.

 © 2010 American Institute of Physics

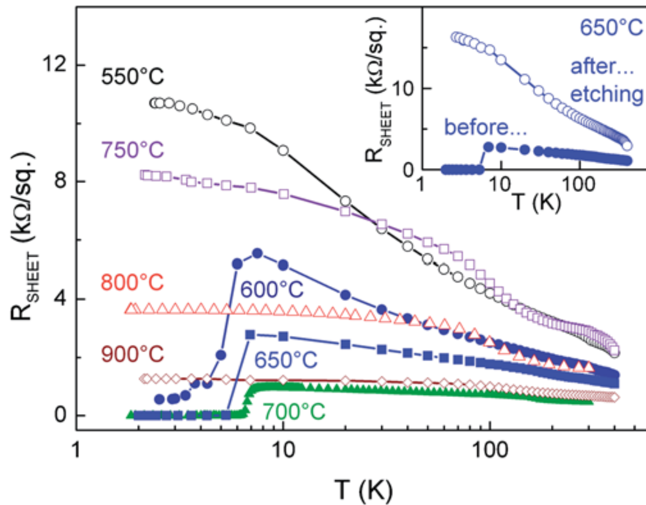

FIG. 1. (Color online) Temperature dependence of the sheet resistance for samples annealed at different temperatures. Within a narrow annealing-temperature window (600–700 °C), superconductivity at about 7 K is observed. The inset highlights the effect of etching away the SiO_2 cover including the segregated Ga layer.

in the near-surface Si region takes place. In a narrow window of annealing temperatures (600 to 700 °C), a superconducting resistivity drop starting at (7.02 ± 0.01) K is observed (using a 90% residual-resistivity criterion).

In order to study the evolution of the Ga distribution at different annealing temperatures, RBS/C has been performed. The distinct element contrast of this method allowed to determine the Ga depth profile plotted in Fig. 2. RTA between 500 and 700 °C results in the formation of a sharp Ga peak below the 30 nm SiO_2 cover layer. In that region, a narrow band (≈10 nm) of amorphous, Ga-containing precipitates of a few nanometers of size have been observed by preliminary XTEM results. These amorphous gallium precipitates evidently are the origin of superconductivity since similar observations for related Ga phases have been made in Refs. 21–23. However, at 800 °C and above the peak vanishes due to Ga out-diffusion through the SiO_2 cover layer which marks the upper limit of the annealing temperature

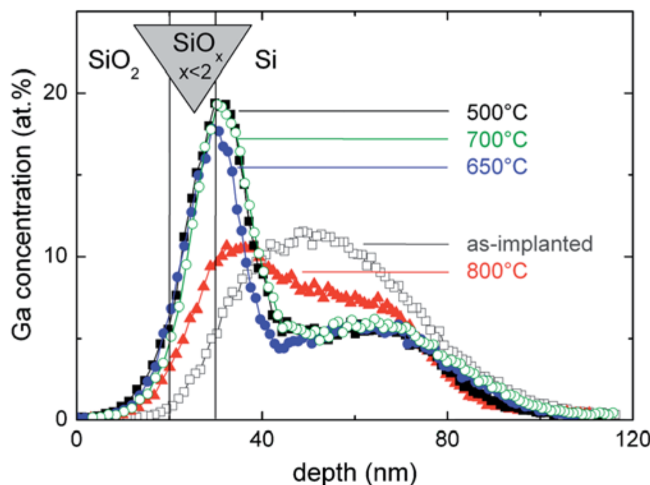

FIG. 2. (Color online) Calibrated Ga-concentration depth profiles obtained from RBS/C measurements. Upon annealing at temperatures up to 700 °C, a 10 nm wide Ga peak at the Si/SiO_2 interface appears. Annealing at higher temperatures leads to a Ga out-diffusion. Interface mixing results in a transition region between Si and SiO_2.

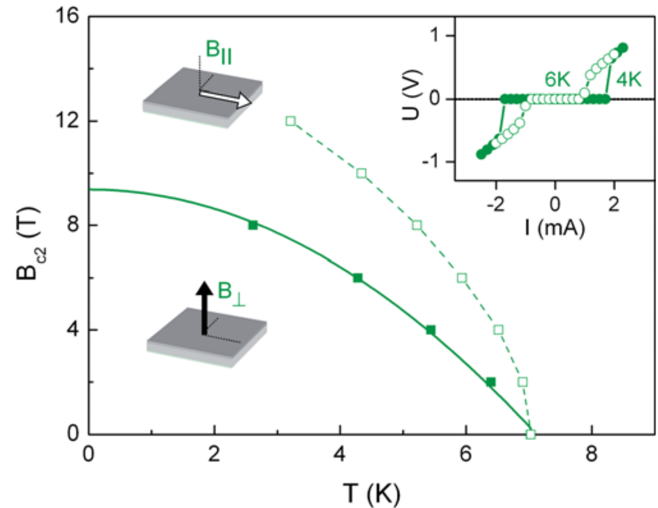

FIG. 3. (Color online) Temperature dependence of the upper critical field parallel (open squares) and perpendicular (filled squares) to the superconducting layer for a sample annealed at 700 °C. The solid line indicates a parabolic fit, while the dashed line is a guide to the eyes. The inset shows current-voltage characteristics at 4 K (closed circles) as well as 6 K (open circles) which reveal a critical current density of more than 2 kA/cm^2.

window where superconductivity is found. At first sight the absence of superconductivity for annealing temperatures below 600 °C appears surprising since RBS/C reveals a sharp Ga peak. A possible explanation is based on an observation reported in Ref. 21, where Jaeger *et al.* found that thin amorphous Ga films can only become superconducting if their low temperature sheet resistance does not exceed 6 kΩ/sq. Obviously, this scattering-induced threshold fits well to our observation for samples containing a segregated Ga layer.

To prove whether or not lower lying areas do affect superconductivity, we have etched away the SiO_2 cover including the Ga layer for a sample annealed at 650 °C (as confirmed by subsequent RBS/C analysis). As expected, superconductivity disappeared as can be seen in the inset of Fig. 1.

In order to investigate the thin-film character of superconductivity in the Ga-enriched layers, critical fields perpendicular and parallel to the layer have been measured for a sample annealed at 700 °C (Fig. 3). The out-of-plane critical fields follow a typical parabolic behavior with $B_{c2,per}(T=0)\approx 9.4$ T. Via $B_{c2,per}=\Phi_0/2\pi\xi_{GL}^2$ we obtain a Ginzburg–Landau coherence length $\xi_{GL}\approx 6$ nm. Additional magnetization measurements reveal $B_{c1,per}(T=1.8\text{ K})\approx 8\times 10^{-5}$ T which is related to a London penetration depth $\lambda_L\approx 3.7$ μm via $B_{c1,per}=\Phi_0/(4\pi\lambda_L^2)$ $[\ln(\lambda_L/\xi_{GL})+0.08]$. This results in a Ginzburg–Landau parameter $\kappa_{GL}=\lambda_L/\xi_{GL}\approx 618$, which clearly indicates a strong type-II character of superconductivity. Because the layer thickness d≈10 nm is much smaller than λ_L, an in-plane oriented field needs much less expulsion enthalpy and, thus, results in higher critical fields than in perpendicular geometry. Figure 3 shows that the in-plane critical fields $B_{c2,par}$ even reach the Pauli limit,[24] which in its simplest form is $B_{Pauli}=1.84\ T_c$ [T/K]≈12.9 T. This, vice versa, evidences the thin-layer character of superconductivity.

In addition to the high critical fields, also critical current densities up to 2 kA/cm^2 (inset of Fig. 3) have been observed. Combined with an easily accessible operating temperature of e.g. 4 K this offers good chances to adapt the

presented preparation technique for combining superconducting structures with semiconductor circuits. The application of selective SiO_2 etching or ion implantation through masks would allow for custom-designed circuits. This may pave the way for future "semi-super"-conducting devices.

The financial support by Deutsche Forschungsgemeinschaft under Contract No. HE 2604/7 is gratefully acknowledged. Part of this work was supported by EuroMagNET II, EU contract number 228043.

[1]T. Herrmannsdörfer, R. Skrotzki, V. Heera, O. Ignatchik, M. Uhlarz, A. Mücklich, M. Posselt, B. Schmidt, K.-H. Heinig, W. Skorupa, M. Voelskow, C. Wündisch, M. Helm, and J. Wosnitza, Supercond. Sci. Technol. **23**, 034007 (2010).
[2]X. Blasé, E. Bustarret, C. Chapelier, T. Klein, and C. Marcenat, Nature Mater. **8**, 375 (2009).
[3]K. Iakoubovskii, Cent. Eur. J. Phys. **7**, 654 (2009).
[4]M. L. Cohen, Phys. Rev. **134**, A511 (1964).
[5]C. S. Koonce and M. L. Cohen, Phys. Rev. **177**, 707 (1969).
[6]E. A. Ekimov, V. A. Sidorov, E. D. Bauer, N. N. Mel'nik, N. J. Curro, J. D. Thompson, and S. M. Stishov, Nature (London) **428**, 542 (2004).
[7]E. Bustarret, C. Marcenat, P. Achatz, J. Kacmarcik, F. Lévy, A. Huxley, L. Ortéga, E. Bourgeois, X. Blasé, D. Débarre, and J. Boulmer, Nature (London) **444**, 465 (2006).
[8]T. Herrmannsdörfer, V. Heera, O. Ignatchik, M. Uhlarz, A. Mücklich, M. Posselt, H. Reuther, B. Schmidt, K.-H. Heinig, W. Skorupa, M. Voelskow, C. Wündisch, R. Skrotzki, M. Helm, and J. Wosnitza, Phys. Rev. Lett. **102**, 217003 (2009).
[9]V. Heera, A. Mücklich, M. Posselt, C. Wündisch, B. Schmidt, R. Skrotzki, K. H. Heinig, T. Herrmannsdörfer, and W. Skorupa, J. Appl. Phys. **107**, 053508 (2010).
[10]N. Dubrovinskaia, R. Wirth, J. Wosnitza, T. Papageorgiou, H. F. Braun, N. Miyajima, and L. Dubrovinsky, Proc. Natl. Acad. Sci. U.S.A. **105**, 11619 (2008).
[11]D. Cammilleri, F. Fossard, D. Débarre, C. Tran Manh, C. Dubois, E. Bustarret, C. Marcenat, P. Achatz, D. Bouchier, and J. Boulmer, Thin Solid Films **517**, 75 (2008).
[12]L. DiCarlo, J. M. Chow, J. M. Gambetta, L. S. Bishop, B. R. Johnson, D. I. Schuster, J. Majer, A. Blais, L. Frunzio, S. M. Girvin, and R. J. Schoelkopf, Nature (London) **460**, 240 (2009).
[13]C. Marcenat, J. Kacmarcik, R. Piquerel, P. Achatz, G. Prudon, C. Dubois, B. Gautier, J. C. Dupuy, E. Bustarret, L. Ortega, T. Klein, J. Boulmer, T. Kocinewski, and D. Débarre, Phys. Rev. B **81**, 020501(R) (2010).
[14]F. A. Tumbore, Bell Syst. Tech. J. **39**, 205 (1960).
[15]E. V. Charnaya, C. Tien, K. J. Lin, C. S. Wur, and Yu. A. Kumzerov, Phys. Rev. B **58**, 467 (1998).
[16]E. V. Charnaya, C. Tien, M. K. Lee, and Yu. A. Kumzerov, J. Phys.: Condens. Matter **21**, 455304 (2009).
[17]D. Teske and J. E. Drumheller, J. Phys.: Condens. Matter **11**, 4935 (1999).
[18]J. F. Ziegler, J. P. Boersack, and U. Littmark, *The Stopping and Range of Ions in Solids* (Pergamon, New York, 1985).
[19]P. Blood and J. W. Orton, *The Electrical Characterization of Semiconductors: Majority Carriers and Electron States* (Academic, London, 1992).
[20]J. R. Tesmer, M. Nastasi, J. C. Barbour, C. J. Maggiore, and J. W. Mayer, *Handbook of Modern Ion Beam Analysis* (Materials Research Society, Pittsburgh, 1995).
[21]H. M. Jaeger, D. B. Haviland, A. M. Goldmann, and B. G. Orr, Phys. Rev. B **34**, 4920 (1986).
[22]J. B. Gosk, R. Puzniak, G. Strzelecka, A. Materna, A. Hruban, A. Wisniewski, A. Szewczyk, G. Kowalski, K. Korona, M. Kaminska, and A. Twardowski, Supercond. Sci. Technol. **21**, 065019 (2008).
[23]J. Hagel, M. T. Kelemen, G. Fischer, B. Pilawa, J. Wosnitza, E. Dormann, H. v. Löhneysen, A. Schnepf, H. Schnöckel, U. Neisel, and J. Beck, J. Low Temp. Phys. **129**, 133 (2002).
[24]A. M. Clogston, Phys. Rev. Lett. **9**, 266 (1962); B. S. Chandrasekhar, Appl. Phys. Lett. **1**, 7 (1962).

APPLIED PHYSICS LETTERS **97**, 163108 (2010)

Sculpting nanoscale precipitation patterns in nanocomposite thin films via hyperthermal ion deposition

Gintautas Abrasonis,[1,2,a)] György J. Kovács,[1] Mark D. Tucker,[2] René Heller,[1] Matthias Krause,[1,3] Mathew C. Guenette,[2] Frans Munnik,[1] Jan Lehmann,[1] Anton Tadich,[4] Bruce C. C. Cowie,[4] Lars Thomsen,[4] Marcela M. M. Bilek,[2] and Wolfhard Möller[1]

[1]*Forschungszentrum Dresden-Rossendorf, PF-510119, 01314 Dresden, Germany*
[2]*University of Sydney, New South Wales 2006, Australia*
[3]*Institut für Festkörperphysik, Technische Universität Dresden, 01062 Dresden, Germany*
[4]*Australian Synchrotron, 800 Blackburn Road, Clayton, Victoria 3168, Australia*

(Received 10 September 2010; accepted 28 September 2010; published online 19 October 2010)

Control of the morphology of self-organized nanostructures is the key issue in bottom-up approaches. Here, morphological transitions of precipitation patterns in C:Cu nanocomposite films are studied. The films have been grown by oblique incidence ionized physical vapor deposition. We show that the ion energy and directionality are transferred into the C–Cu phase separation process resulting in nanopattern formation and tilt. Increasing metal content induces the "tilted"-"lying" transition accompanied with Cu nanoparticle prolate-spherical-oblate shape transformations. The results allow the identification of metal subplantation as the key atomistic mechanism, and demonstrate the possibility to achieve nanoscale sculpting via energetic ion deposition. © *2010 American Institute of Physics*. [doi:10.1063/1.3503967]

Nanostructures determine material properties at the macroscale, and are therefore a key issue in thin film materials science. This is of particular importance for nanoscale multiphase films due to their multifunctionality and the combination of properties which cannot be predicted from the constituents alone.[1] Top-down approaches allow precise structure control at the nanoscale. However, their application for large scale nanomaterial fabrication is affected by the production time and price issues. Alternatively, bottom-up approaches rely on self-assembly and self-organization phenomena, and their control by external influences.[2] Film growth represents a large portfolio of interacting kinetic processes (surface and bulk diffusion, repeated nucleation, shadowing, etc.) which can be controlled by external parameters such as temperature, growth rate, presence of energetic species, etc.[3] In combination with the presence of thermodynamic forces toward phase separation, this results in a large variety of lateral or vertical compositional modulations such as dispersed nanoparticles (NPs),[3–5] encapsulated nanocolumns,[6–8] nanometric dendrites,[9] vertical superlattices,[10,11] or more complicated three-dimensional nanostructures.[12] Of these, nanoscale compositional patterns, showing a large degree of self-organization, deserve a special interest.

Recently, self-ordered structures have been observed in carbon-transition metal nanocomposite films grown by physical vapor deposition (PVD).[13–19] Precipitation patterns have been generated using a number of metals such as Ti,[18] Cr,[15] Fe,[14] Ni,[5,13] Cu,[13,17] Au,[14] Pt,[13] etc. The common feature is the presence of hyperthermal energetic species. However, there is no common agreement as to the driving atomistic processes involved, i.e., whether this is an interplay of nucleation, noncarbide forming metal surface segregation, ballistic diffusion and re-sputtering,[14] or confined to the near-surface layer spinodal decomposition[16] or radiation enhanced diffusion.[18] Contrary to the predictions of the above models, a recent study on the ionized PVD (iPVD) growth of C:Ni films has shown that at an oblique ion incidence the precipitation patterns tilt, and do not align with the film surface as the models predict, but rather align with the incident ions.[20] As a result, a consistent understanding of the driving mechanisms is currently still missing.

In this letter, we present a study on the oblique incidence iPVD growth of precipitation patterns in C:Cu films grown in a wide metal atomic ratio range. The C–Cu system has been chosen because of the almost complete immiscibility of the two elements.[4,21] Morphological transitions as a function of metal content are identified. This leads to the identification of energetic ion driven atomistic processes which are controlling the pattern formation and tilt.

The films were grown onto thermally oxidized Si substrates (SiO_2 layer thickness of ~500 nm) at room temperature by iPVD in the form of pulsed filtered cathodic vacuum arc (PFCVA).[5,22,23] For Cu (C), the pulse length, average arc current, and average filtering magnetic field were 0.35 ms (0.85 ms), ~1.3 kA (~1 kA), and ~45 mT (~34 mT), respectively, The pulsing frequency and a base pressure were 3 Hz and $\sim 1-5\times10^{-6}$ mbar, respectively. Deposition was performed by repeating C and Cu pulse sequences in a C:Cu ratio of 1:1 (×386 times), 2:5 (×162 times), 2:9 (×133 times), 1:7 (×217 times), and 1:10 (×178 times), followed by 15 C pulses. This gives film areal densities t and Cu atomic ratios $[t_{Cu}/(t_C+t_{Cu})]$ in the range of $\sim 7.0-8.6\times10^{17}$ atoms cm^{-2} and 16–80 at. %, respectively, as determined by Rutherford backscattering spectroscopy. According to Anders *et al.*,[24] the most probable native kinetic energies and average charge states for incoming C (Cu) ions are ~20 eV (~57 eV), and +1.0 (+2.0), respectively. Note that these values could be higher because of the significantly higher PFCVA currents used in this work.[20,25,26] An additional acceleration occurs when approaching the sample sur-

[a)]Author to whom correspondence should be addressed. Electronic mail: g.abrasonis@fzd.de. Tel.: +49 351 260 3578. FAX: +49 351 260 3285.

 © 2010 American Institute of Physics

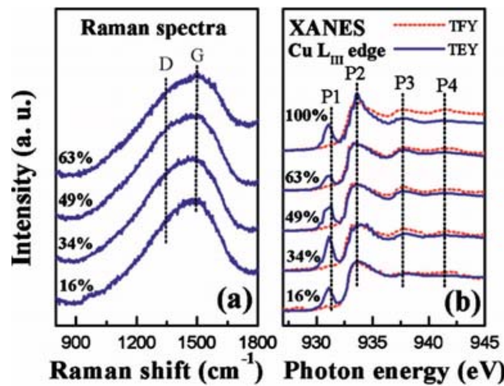

FIG. 1. (Color online) Raman (a) and XANES (b) spectra of the C:Cu films. Cu atomic ratio is shown above the respective curves. XANES in TEY (TFY) mode is plotted in solid (dotted) lines. Metal reference XANES spectrum is labeled with "100%."

face which is proportional to the difference between the plasma potential [estimate ~10 V (Refs. 5 and 23)] and the floating potential (−70 to −10 V but between −20 to −30 for most of the arc pulse[23]). Based on our previous work,[20] we estimate the ion incidence angle to be ~10°–15° from the sample surface normal. The morphology of the films was studied by cross-sectional transmission electron microscopy (XTEM) employing FEI Titan operated at 300 kV. The bonding structure of the carbon matrix was determined by Raman spectroscopy using 632.8 nm laser excitation light (Ref. 4). The chemical state of the dispersed Cu phase was determined by x-ray absorption near edge structure (XANES) at the Soft X-ray Spectroscopy Beamline, Australian Synchrotron, Clayton, Australia.[27] The data were acquired in the total electron yield (TEY) and total fluorescence yield (TFY) modes by recording the drain current from the sample and the intensity at a photodiode covered with an aluminum foil, respectively.

Raman spectra of the C:Cu films show a broad band in the wave number range of ~1000–1800 cm^{-1} with two features at ~1335 and 1500 cm^{-1}, commonly referred to as "D" and "G" peaks in the literature [see Fig. 1(a)].[28] The "D" and "G" peaks are due to the breathing and in-plane stretching vibrations, respectively. "G" mode originates from both sp^2 aromatic and olefinic structures while "D" mode only arises from sixfold rings. For disordered materials the relative intensity of the latter represents the degree of sixfold ring clustering. The absence of any sharp features, the low value of the G peak position (that of graphite is ~1580 cm^{-1}) and the weak intensity in the "D" peak region point toward a highly disordered nature of the matrix.[4,28] This is a result of the energetic deposition conditions and low growth temperature.[29] The increase in Cu content does not induce any substantial changes in the C phase. XANES of the Cu L_{III} edge [see Fig. 1(b)] shows a strong feature labeled P1 (absent in the bulk sensitive TFY mode) which is related to the surface oxidation and the P2-P4 triplet characteristic of metallic fcc Cu.[21] Independently of the Cu content, there is no considerable edge shift in the metal TFY XANES pointing to the absence of carbide. The low intensity of P3-P4 features in the film with the lowest metal content should be associated with the NP size effects on the Cu electronic structure.[21] The above observations show that a complete phase separation has taken place during the film growth resulting in the structure consisting of metallic Cu and dis-

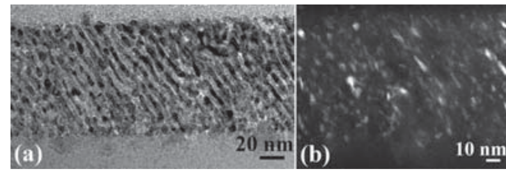

FIG. 2. Bright (a) and dark (b) field XTEM of C:Cu (34 at. %). The cross-sectional plane of the images contains or is close to the ion incidence direction.

ordered C. This is confirmed by XTEM which shows metal NPs encapsulated in the C matrix (see Fig. 2). The NPs are not distributed randomly but are ordered in layers whose period is ~8.7 nm. The layers are tilted with respect to the film surface by ~55°. This is consistent with the recent observations in iPVD grown C:Ni nanocomposite thin films.[20] Furthermore, the NPs tend to be elongated along the layers. This is in strong contrast to the observations in the literature where metal rich NPs elongated only in the direction of film growth have generally been reported.[3–6,8,14,30,31]

Changing the Cu content has a dramatic effect on the film morphology (see Fig. 3); the increase from 16 to 80 at. % results in an increase in the pattern periodicity from ~5.4 to ~17 nm. When increasing metal content from 16 to 34 at. %, period increases from ~5.4 to 8.7 nm with no significant changes in the pattern orientation (from ~65° to 55°). However, a further increase in the metal content to 49 at. % results in a drastic "tilted"-"lying" morphology transition. This transition is mirrored in the fast Fourier transform (FFT) images which show strong asymmetry for low metal contents, almost symmetrical diagonal correlations at 49 at. % and vertical correlations for larger Cu atomic ratios (see Fig. 3). Furthermore, the tilted-lying transition is accompanied by a strong change in NP shape from elongated-prolate toward near-spherical. Further increase in metal content from 49 to 63 at. % leads to an oblate NP shape but no

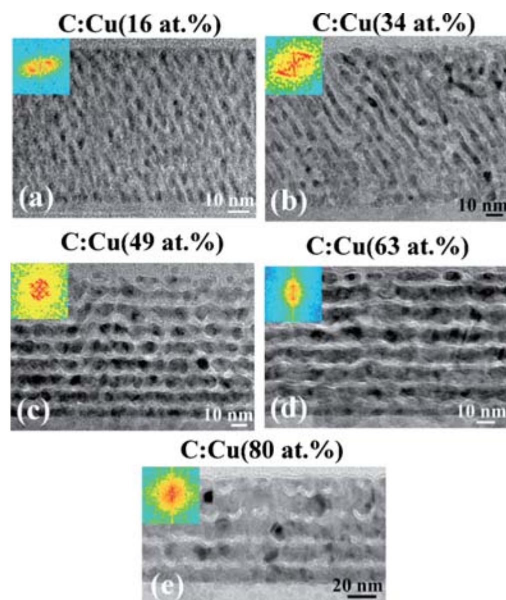

FIG. 3. (Color online) XTEM of the C:Cu films with different metal contents. The insets are FFTs of the respective XTEM images. The cross-sectional plane of the images [(a)–(c)] contains or is close to the ion incidence direction. Pattern periods are ~5.4 nm, 8.7 nm, ~10 nm, ~10 nm, and ~17 nm for the panels (a)–(e), respectively.

change in the period thickness. Merging of the NPs into a quasicontinuous layer and increase in periodicity is observed for the further metal content increase.

The results of this study show that the ion energy and directionality are transferred into a phase separation process, resulting not only in the formation of periodic structures, but also in their tilt following the direction of ion incidence. This is consistent with the recently reported results on the C–Ni system.[20] While C and Ni show a considerable mutual affinity by forming a metastable carbide,[5,20,30] the C–Cu system is totally immiscible under the current film growth conditions. This demonstrates that the ion directionality transfer on the periodic structure formation has a more general applicability. The above-observed transitions must be associated with physical effects as the C:Cu films show complete phase separation and no considerable changes in the chemical state or bonding structure. Any temperature induced diffusion effects[16,18] can be ruled out as they would result in the growth of metal nanocolumns and disappearance of the periodic structure.[5] The model for immiscible systems proposed by Gerhards *et al.*[14] assumes metal surface segregation and resputtering as the key factors controlling the pattern formation. This contradicts the observations of tilted structures in this study, as the metal surface segregation inevitably implies ordering in the film growth direction only. In a recent study, two following alternative explanations have been proposed:[20] heavy ion subplantation in a light matrix or anisotropic ballistic diffusion in the near surface layer. If the latter process were prevailing, anisotropic structures would be observed for all the possible film compositions. However, the tilting is lost when the amount of precipitate species reaches a certain critical value, thus excluding ion induced anisotropic diffusion as the driving mechanism. This is consistent with the following metal subplantation mechanism:[20] the initial metal ion directionality is rapidly lost when the ions penetrate into metal rich volumes which take progressively larger fractions of nanocomposite films concomitantly with the atomic ratio of the dispersed phase. On the other hand, the changes in the metal NP shape (prolate–spherical–oblate) remains unclear and necessitates further experimental and theoretical studies.

In summary, we have demonstrated that the ion energy and directionality during iPVD of C:Cu films is transferred into a phase separation process. It induces the formation of composition patterns and allows the control of their periodicity, orientation (tilted-lying) and NP morphology (elongated-spherical). The findings enable one to identify the energetic heavy metal ion subplantation as the key atomistic mechanism. As the underlying driving mechanism is of physical origin, it is believed that the results of this study are applicable to other immiscible or partially miscible systems, and present an alternative robust approach to sculpting the nanostructure of (multi)functional nanomaterials.

G.A. acknowledges the financial support of the Department of Education, Employment, and Workplace Relations, Canberra, Australia, in the Framework of Endeavor Research Fellowship, under Contract No. 837_2008. Financial support of the Saxonian Development Bank in the framework of the "European Centre for Emerging Materials and Processes" project is acknowledged (Project No. 13857/2379). The authors thank the Australian Synchrotron staff for support in performing the XANES measurements.

[1] P. M. Ajayan, L. S. Schadler, and P. V. Braun, *Nanocomposite Science and Technology* (Wiley-VCH, Weinheim, 2003).
[2] J. D. Halley and D. A. Winkler, Complexity **14**, 10 (2008).
[3] I. Petrov, P. B. Barna, L. Hultman, and J. E. Greene, J. Vac. Sci. Technol. A **21**, S117 (2003).
[4] M. Berndt, M. Krause, G. Abrasonis, A. Mucklich, F. Munnik, A. Kolitsch, and W. Moller, Plasma Processes Polym. **6**, S902 (2009).
[5] G. Abrasonis, G. J. Kovacs, L. Ryves, M. Krause, A. Mucklich, F. Munnik, T. W. H. Oates, M. M. M. Bilek, and W. Moller, J. Appl. Phys. **105**, 083518 (2009).
[6] N. Yasui, R. Horie, Y. Ohashi, K. Tanji, and T. Den, Adv. Mater. (Weinheim, Ger.) **19**, 2797 (2007).
[7] J. L. MacManus-Driscoll, P. Zerrer, H. Y. Wang, H. Yang, J. Yoon, A. Fouchet, R. Yu, M. G. Blamire, and Q. X. Jia, Nature Mater. **7**, 314 (2008).
[8] L. Mohaddes-Ardabili, H. Zheng, S. B. Ogale, B. Hannoyer, W. Tian, J. Wang, S. E. Lofland, S. R. Shinde, T. Zhao, Y. Jia, L. Salamanca-Riba, D. G. Schlom, M. Wuttig, and R. Ramesh, Nature Mater. **3**, 533 (2004).
[9] C. Corbella, B. Echebarria, L. Ramirez-Piscina, E. Pascual, J. L. Andujar, and E. Bertran, Acta Mater. **57**, 4948 (2009).
[10] P. Venezuela, J. Tersoff, J. A. Floro, E. Chason, D. M. Follstaedt, F. Liu, and M. G. Lagally, Nature (London) **397**, 678 (1999).
[11] J. H. He, C. A. Carosella, G. K. Hubler, S. B. Qadri, and J. A. Sprague, Phys. Rev. Lett. **96**, 056105 (2006).
[12] I. Daruka and J. Tersoff, Phys. Rev. Lett. **95**, 076102 (2005).
[13] W. Y. Wu and J. M. Ting, Chem. Phys. Lett. **388**, 312 (2004).
[14] I. Gerhards, H. Stillrich, C. Ronning, H. Hofsass, and M. Seibt, Phys. Rev. B **70**, 245418 (2004).
[15] P. E. Hovsepian, Y. N. Kok, A. P. Ehiasarian, R. Haasch, J. G. Wen, and I. Petrov, Surf. Coat. Technol. **200**, 1572 (2005).
[16] C. Corbella, B. Echebarria, L. Ramirez-Piscina, E. Pascual, J. L. Andujar, and E. Bertran, Appl. Phys. Lett. **87**, 213117 (2005).
[17] H. Zutz, D. Lyzwa, C. Ronning, M. Seibt, and H. Hofsass, Nucl. Instrum. Methods Phys. Res. B **267**, 1356 (2009).
[18] C. Q. Chen, Y. T. Pei, K. P. Shaha, and J. T. M. De Hosson, Appl. Phys. Lett. **96**, 073103 (2010).
[19] P. A. Chen, Thin Solid Films **204**, 413 (1991).
[20] G. Abrasonis, T. W. H. Oates, G. J. Kovacs, J. Grenzer, P. O. A. Persson, K. H. H. Heinig, A. Martinavicius, N. Jeutter, C. Baehtz, M. Tucker, M. M. M. Bilek, and W. Moeller, J. Appl. Phys. **108**, 043503 (2010).
[21] G. Abrasonis, A. Berndt, M. Krause, K. Kuepper, F. Munnik, A. Kolitsch, and W. Moller, J. Phys. Chem. C **112**, 17161 (2008).
[22] T. W. H. Oates, J. Pigott, D. R. McKenzie, and M. M. M. Bilek, Rev. Sci. Instrum. **74**, 4750 (2003).
[23] D. Andruczyk, R. N. Tarrant, B. W. James, M. M. M. Bilek, and G. B. Warr, Plasma Sources Sci. Technol. **15**, 533 (2006).
[24] A. Anders and G. Y. Yushkov, J. Appl. Phys. **91**, 4824 (2002).
[25] F. J. Paoloni and I. G. Brown, Rev. Sci. Instrum. **66**, 3855 (1995).
[26] R. Sanginés, A. M. Israel, I. S. Falconer, D. R. McKenzie, and M. M. M. Bilek, Appl. Phys. Lett. **96**, 221501 (2010).
[27] B. C. C. Cowie, A. Tadich, and L. Thomsen, AIP Conf. Proc. **1234**, 307 (2010).
[28] A. C. Ferrari and J. Robertson, Phys. Rev. B **61**, 14095 (2000).
[29] D. R. McKenzie, D. Muller, and B. A. Pailthorpe, Phys. Rev. Lett. **67**, 773 (1991).
[30] G. Abrasonis, R. Gago, M. Vinnichenko, U. Kreissig, A. Kolitsch, and W. Moller, Phys. Rev. B **73**, 125427 (2006).
[31] D. Babonneau, F. Pailloux, J. P. Eymery, M. F. Denanot, P. Guerin, E. Fonda, and O. Lyon, Phys. Rev. B **71**, 035430 (2005).

APPLIED PHYSICS LETTERS **96**, 141907 (2010)

Establishing the mechanism of thermally induced degradation of ZnO:Al electrical properties using synchrotron radiation

M. Vinnichenko,[1,a)] R. Gago,[2] S. Cornelius,[1] N. Shevchenko,[1] A. Rogozin,[1] A. Kolitsch,[1] F. Munnik,[1] and W. Möller[1]

[1]*Institute of Ion Beam Physics and Materials Research, Forschungszentrum Dresden-Rossendorf, P.O. Box 510119, 01314 Dresden, Germany*

[2]*Instituto de Ciencia de Materiales de Madrid, Consejo Superior de Investigaciones Científicas, E-28049 Madrid, Spain*

(Received 20 January 2010; accepted 18 March 2010; published online 7 April 2010)

X-ray absorption near edge structure and x-ray diffraction studies with synchrotron radiation have been used to relate the electrical properties of ZnO:Al films to their bonding structure and phase composition. It is found that Al-sites in an insulating metastable homologous $(ZnO)_3Al_2O_3$ phase are favored above a certain substrate temperature (T_S) leading to deterioration of both the crystallinity and the electrical properties of the films. The higher film resistivity is associated with lower carrier mobility due to increased free electron scattering. Lower metal to oxygen flux ratios during deposition expand the range of T_S at which low-resistivity films are obtained. © *2010 American Institute of Physics*. [doi:10.1063/1.3385024]

Requirements of thin film photovoltaic technology for transparent electrode (TE) materials extend well beyond achieving a combination of low electrical resistivity and high optical transmittance.[1] High-quality TE films have to be grown at low temperatures (<300 °C) while making them thermally stable at high processing temperatures. In contrast to the tin-doped indium oxide,[2] the resistivity of the much cheaper Al-doped ZnO (AZO) often increases significantly during either annealing[3] or growth at temperatures above a certain optimum value (typically, between 150 and 300 °C),[4–6] which limits the practical applications of AZO films. Outdiffusion of Al from substitutional sites in the ZnO wurtzite lattice and subsequent segregation of Al_2O_3 are believed to be the main reason for the degradation of film electrical properties.[3] However, experimental observations supporting this assumption are quite limited.[7] Conclusive evidence of phase segregation in AZO is lacking since its electrical properties and crystallinity deteriorate simultaneously above a certain deposition temperature[8] and, accordingly, the disordered film structure precludes a proper analysis using conventional methods.

The present work focuses on the investigation of the electrical properties of AZO films with respect to their bonding structure and phase composition probed by x-ray absorption near edge structure (XANES) and x-ray diffraction (XRD) using synchrotron radiation (SR). These methods are suitable for the characterization of highly disordered nanocrystalline films because XANES provides local-order information on the chemical environments at each elemental site whereas high-brilliance SR overcomes the limitation of XRD analysis with conventional laboratory sources.

AZO films were grown by reactive pulsed magnetron sputtering (RPMS) using the same experimental setup as described in Ref. 8 with two types of Zn–Al alloyed targets (Al concentrations c^T_{Al} of 1.7 ± 0.5 and 4.7 ± 1.7 at. %). The magnetron power and oxygen partial pressure, p_{O_2}, for different c^T_{Al} values are shown in Table I. AZO films of a 250–400 nm thickness were grown at T_S over the range of RT to 500 °C onto fused silica substrates for Hall-effect and XRD measurements, whereas 100 nm films were grown under similar conditions on conducting Si (100) for XANES.

The film thickness was determined by spectroscopic ellipsometry (M-2000FI, J.A Woolam Inc.). Electrical properties of the films were determined by RT Hall-effect measurements in van der Pauw geometry (HMS 3000, ECOPIA). Compositional analysis to infer the Al concentration in the films (c^F_{Al}) was performed by means of elastic recoil detection analysis (ERDA). The film structure was characterized by XRD using a D5000 (BRUKER AXS) diffractometer with Cu K_α radiation. The size of coherently diffracting domains, i.e., the coherence length (L) indicative of the grain size, was estimated from the wurtzite ZnO (002) peak with the aid of the Scherrer formula. Selected samples were further analyzed by XRD (wavelength of 0.154 nm) during isothermal annealing (920 °C, 2 h) at the European Synchrotron Radiation Facility.[9] Finally, the bonding structure of the films with elemental sensitivity to local environments of O, Zn, and Al sites was studied by XANES. Measurements with soft x-rays in the total electron yield mode were carried out at the synchrotron facility BESSY-II (Berlin, Germany). The sample signal was normalized to that of a gold grid located upstream the x-ray path.

TABLE I. Optimum substrate temperature (T_s^*) for different magnetron powers and oxygen partial pressures (p_{O_2}). In all cases, the p_{Ar} was of $(1.84\pm0.02)\times10^{-2}$ mbar.

c^T_{Al} (at. %)	P (W)	p_{O_2} (10^{-4} mbar)	T_S^* (°C)
4.7	181 ± 4	6.2 ± 0.7	200
4.7	156 ± 2	8.8 ± 0.2	250
1.7	106 ± 3	5.6 ± 0.2	300
1.7	98 ± 2	8.0 ± 0.2	450

a)Author to whom correspondence should be addressed. Electronic mail: m.vinnichenko@fzd.de. Tel.: +49 (0) 351 260 2374. FAX: +49 (0) 351 260 2703.

 © 2010 American Institute of Physics

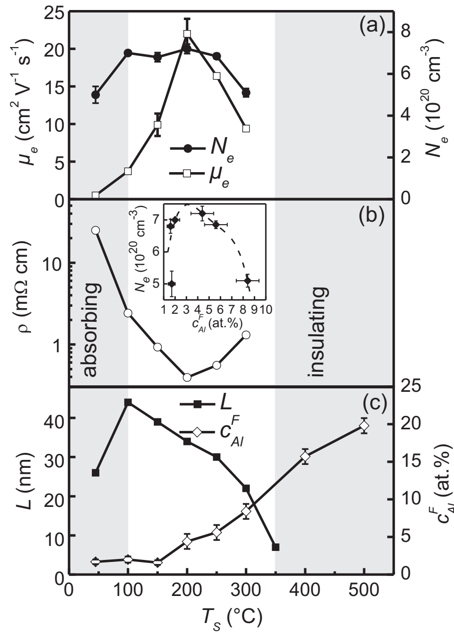

FIG. 1. Free electron mobility μ_e, density N_e (a), film resistivity ρ (b), coherence length L, and Al concentration of AZO films (c) vs substrate temperature at a fixed oxygen partial pressure of $(6.2 \pm 0.7) \times 10^{-4}$ mbar. Variation in N_e with $c^F{}_{\mathrm{Al}}$ is shown as inset in panel (b), being the dashed line only guide-to-the-eye.

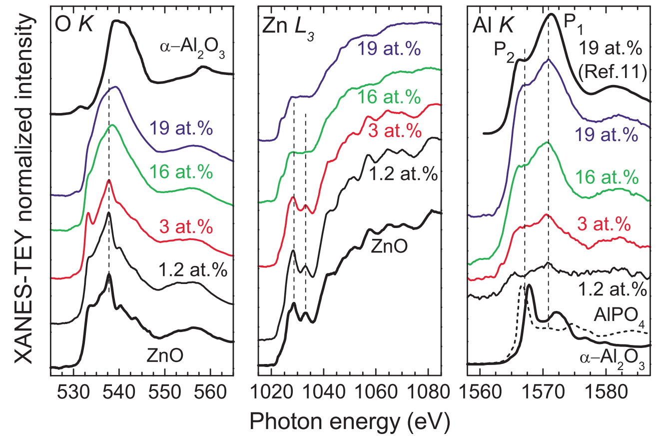

FIG. 2. (Color online) O K-, Zn L_3-, and Al K-edge XANES spectra of AZO films grown at T_S=400 °C ($c^F{}_{\mathrm{Al}}$=19 at. %), 350 °C (16 at. %), and 250 °C (3 at. %) using Zn–Al target with $c^T{}_{\mathrm{Al}}$=4.7 at. %, and at T_S=350 °C ($c^F{}_{\mathrm{Al}}$=1.2 at. %) using target with $c^T{}_{\mathrm{Al}}$=1.7 at. %. The spectra are shifted vertically for clarity. The reference spectra of ZnO, α-Al_2O_3 (from Refs. 10 and 12) and $AlPO_4$ (from Ref. 10) are shown for comparison, together with the spectra of a ZnO–Al_2O_3 film with 19 at. % Al adapted from Ref. 11.

Figures 1(a) and 1(b) show electrical properties of AZO films grown from the target with $c^T{}_{\mathrm{Al}}$=4.7 at. % as a function of T_S. Their electrical resistivity, ρ, decreases by a factor of more than 60 with T_S increasing from RT to an optimum value ($T_S{}^*$) of 200 °C [Fig. 1(b)]. Figure 1(a) indicates that this trend is mainly due to a strong increase in mobility, μ_e, while the density of free electrons, N_e, is nearly constant at $\sim 7.0 \times 10^{20}$ cm^{-3} for T_S between 100 and 250 °C. A further increase in T_S brings about a rise in ρ as a result of the rapidly decreasing μ_e, with N_e dropping by less than 30%. Finally, at $T_S \geq 350$ °C the films become insulating. This dependence of the electrical properties on T_S is characteristic of AZO films grown by various methods[4–6,8] and is accompanied by changes in the film crystallinity and composition [Fig. 1(c)]. The coherence length L [Fig. 1(c)], reaches a maximal value of 44 nm at 100 °C and decreases down to ~7 nm at 350 °C while $c^F{}_{\mathrm{Al}}$ increases from the values of ~2.0 at. % for $T_S \leq 150$ °C to almost 20 at. % at T_S =500 °C. Taking into account experimental errors, N_e does not change for $c^F{}_{\mathrm{Al}}$=2–6 at. % [see inset of Fig. 1(b)]. Increase of N_e values at $c^F{}_{\mathrm{Al}} \sim 2$ at. % for T_S rising from 45 to 100 °C may be related to an increase in the Al donor electrical activation.

Figure 2 shows O K-, Zn L_3-, and Al K-edge XANES spectra for AZO films with $c^F{}_{\mathrm{Al}}$ values ranging from 1.2 to 19 at. %. The films with $c^F{}_{\mathrm{Al}}$=3, 16, and 19 at. % have been synthesized at T_S and $c^T{}_{\mathrm{Al}}$ identical to those of the films characterized by Hall-effect (see Fig. 1), however, their $c^F{}_{\mathrm{Al}}$ values differ because of the small differences in the discharge parameters associated with the consumption of the metallic target during extended operation. XANES spectra of a film with $c^F{}_{\mathrm{Al}}$=1.2 at. % grown at T_S=350 °C and $c^T{}_{\mathrm{Al}}$ =1.7 at. % and of an undoped ZnO film grown in the same deposition system at T_S=500 °C are shown for comparison. The broadening of the O K-edge features with increasing $c^F{}_{\mathrm{Al}}$ is attributed to the formation of Al–O bonds and deterioration of the film crystalline quality, which agrees well with the XRD data [Fig. 1(c)]. This tendency also explains the significant broadening of the Zn L_3-edge in the films with $c^F{}_{\mathrm{Al}}$ of 16 and 19 at. %.

Comparison of the Al K-edge with those of reference $AlPO_4$ and α-Al_2O_3 compounds,[10] where Al has a coordination number (CN) of CN=4 or CN=6, respectively, can be used to identify the local arrangements of Al present in the AZO films. In particular, the feature at 1570.8 eV (P_1) is a fingerprint of the noticeable contribution from CN=6 sites, while the signal in the 1565–1568 eV range (P_2) is related to both CN=4 and 6 sites. Analysis of the contributions of both types of Al sites to the Al K-edge shape and its comparison with reference data[10,11] exclude the preferential formation of α-Al_2O_3 or spinel $ZnAl_2O_3$ compounds. This statement is also supported by the O K-edge shape, where the intensity does not increase significantly between 542 and 544 eV, as would be expected for the formation of α-Al_2O_3.[12] Moreover, the Al K-edge of the RPMS films is similar to that reported in Ref. 11 for pulsed laser deposited AZO films (see Fig. 2) and, therefore, can be interpreted in terms of a saturated solid solution. In this framework, the resulting XANES Al-K edge spectrum has been attributed to the formation of a metastable homologous phase $(ZnO)_mAl_2O_3$ (m=3).[11] The representative structure of this phase includes Zn and O layers which are similar to those of wurtzite ZnO with certain sheets of Zn replaced by Al sheets, either completely (CN=6) or partially (CN=4,5).[13]

The assumption of formation of the homologous phase is also supported by SR-based XRD, as shown in Fig. 3. A typical low-ρ AZO film (T_S=250 °C) is c-axis textured, with its diffraction pattern consisting mainly of the ZnO (002) peak at 2θ=34.52°. In the case of an insulating film (T_S =350 °C), the XRD pattern shows only a broader and weaker feature at a much lower 2θ value of ~33°. This indicates more than 4% larger interplanar distances in the c-axis direction in insulating AZO films as compared to undoped ZnO, which is in agreement with the estimates for

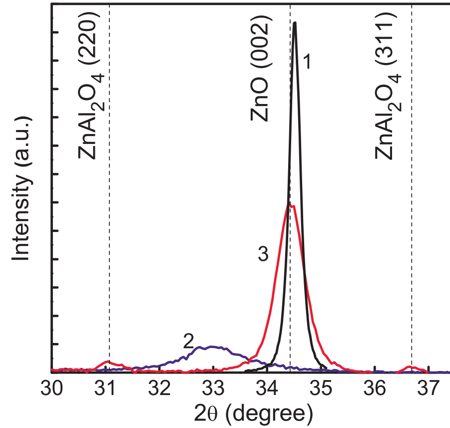

FIG. 3. (Color online) XRD patterns of ZnO:Al films deposited using Zn–Al target with c^{T}_{Al}=4.7 at. % at T_S=250 °C (1) and 350 °C (2). The XRD pattern of the 350 °C sample after isothermal annealing for 2 h at 920 °C (3) is also shown.

$(ZnO)_3Al_2O_3$ yielding a 2.3% to 12.7% increase.[11] In addition, as determined by ERDA, the composition of the insulating films grown at T_S=350–500 °C ranges from 12 to 20 at. % for Al, 34–24 at. % for Zn, and 54–56 at. % for O, which is close to the composition of $(ZnO)_3Al_2O_3$.

It is well-known[14] that Zn has a much higher vapor pressure than Al and the enthalpy of formation of ZnO bonds is much lower than that of Al_2O_3. Therefore, energy deposition during growth due to the elevated T_S and from the flux of energetic particles incident on the substrate causes preferential Zn desorption. This is supported by the observed increase in c^{F}_{Al} with increasing T_S [Fig. 1(c)]. It should be noted that the c^{F}_{Al} values are always close to or above the solid solubility limit of Al in ZnO, which is reported to be in the range 0.3–3 at. % depending on the preparation and characterization methods of the resulting ceramics.[11,15] Although decomposition of the obtained solid solution into ZnO and $ZnAl_2O_4$ is energetically more favorable, the highly nonequilibrium process of RPMS may trigger the formation of the $(ZnO)_3Al_2O_3$ homologous metastable phase. The metastable nature of this phase is confirmed by its transformation to a mixture of $ZnAl_2O_4$ spinel and ZnO upon isothermal annealing, as evidenced in the XRD pattern shown in Fig. 3.

The formation of $(ZnO)_3Al_2O_3$ is observed by XANES even in the film with the lowest c^{F}_{Al}, which has the lowest ρ and highest μ_e. However, for this sample the XANES Al *K*-edge spectrum shows a slight redshift in the P_2 peak as compared with the films of a higher Al concentration. This tendency might come from a detectable contribution of substitutional Al (CN=4), which correlates well with the obtained electrical properties. Except for this spectrum, the XANES Al *K*-edge is much the same for all samples, irrespective of the T_S and Al concentration. This indicates that the homologous $(ZnO)_3Al_2O_3$ phase is present in all the samples. Thus, deterioration of the film electrical properties and crystallinity at $T_S > T_S^*$ may be explained by the increased volume fraction of this undesirable phase, which scales with the Al incorporation. Formation of such phase impedes the crystal growth and increases volume fraction of grain boundaries, which may result in a higher density of electron traps and reduced μ_e observed for $T_S > T_S^*$. The homologous phase itself is expected to be insulating, similar to the $ZnAl_2O_4$ spinel due to significantly larger Zn–Zn distances than in ZnO,[16] with its inclusions being also able to scatter charge carriers.

As shown in Table I, a higher metal (Zn+Al) to oxygen flux ratio (e.g., high discharge power and/or low p_{O_2}) shifts T_S^* to much lower values. In this case, the deterioration of the film electrical properties and crystallinity also occurs at lower T_S values compared to the lower (Zn+Al)/O ratios. Therefore, formation of the undesirable homologous phase is favored at high metal to oxygen flux ratios, while low ratios are necessary to enable growth of low-ρ films at higher T_S.

In summary, the mechanism of the deterioration of crystallinity and electrical properties in AZO films prepared by RPMS at elevated T_S has been established. Increasing T_S above its optimum value leads to a higher Al concentration in the AZO films, which exceeds the solubility limit and triggers the formation of an insulating metastable homologous $(ZnO)_3Al_2O_3$ phase. This phase impedes crystal growth and causes a significant increase in free electron scattering. In order to enable the growth of low-ρ AZO films in a wider range of T_S, lower (Zn+Al)/O flux ratios should be used during deposition. The proposed approach to minimizing the influence of this undesirable phase may also be applied to other growth methods of AZO films involving high-energy particle bombardment.

We acknowledge HZB-BESSY II for provision of SR at SURICAT station and thank Dr. A. Vollmer for technical assistance and Dr. K. Ellmer for discussion. This research has been funded in part by Grant No. 226716 from the EC's 7th Framework Program (FP7/2007–2013), and Project Nos. CSD2008-0023 and FIS2009-12964-C05-04 from the Spanish Ministerio de Ciencia e Innovación.

[1] E. Fortunato, D. Ginley, H. Hosono, and D. C. Paine, MRS Bull. **32**, 242 (2007).
[2] A. Rogozin, M. Vinnichenko, N. Shevchenko, L. Vazquez, A. Mücklich, U. Kreissig, R. A. Yankov, A. Kolitsch, and W. Möller, J. Mater. Res. **22**, 2319 (2007).
[3] B. Szyszka, S. Jäger, J. Szczyrbowski, and G. Bräuer, Surf. Coat. Technol. **98**, 1304 (1998).
[4] K. H. Kim, K. C. Park, and D. Y. Ma, J. Appl. Phys. **81**, 7764 (1997).
[5] A. V. Singh, R. M. Mehra, N. Buthrath, A. Wakahara, and A. Yoshida, J. Appl. Phys. **90**, 5661 (2001).
[6] R. J. Hong, X. Jiang, B. Szyszka, V. Sittinger, and A. Pflug, Appl. Surf. Sci. **207**, 341 (2003).
[7] I. Sieber, N. Wanderka, I. Urban, I. Dörfel, E. Schierhorn, F. Fenske, and W. Fuhs, Thin Solid Films **330**, 108 (1998).
[8] S. Cornelius, M. Vinnichenko, N. Shevchenko, A. Rogozin, A. Kolitsch, and W. Möller, Appl. Phys. Lett. **94**, 042103 (2009).
[9] A. Rogozin, N. Shevchenko, M. Vinnichenko, F. Prokert, V. Cantelli, A. Kolitsch, and W. Moeller, Appl. Phys. Lett. **85**, 212 (2004).
[10] D. Cabaret, P. Sainctavit, P. Ildefonse, and A.-M. Flank, J. Phys.: Condens. Matter **8**, 3691 (1996).
[11] S. Yoshioka, F. Oba, R. Huang, I. Tanaka, T. Mizoguchi, and T. Yamamoto, J. Appl. Phys. **103**, 014309 (2008).
[12] G. S. Henderson, D. R. Neuville, and L. Cormier, Chem. Geol. **259**, 54 (2009).
[13] S. Yoshioka, K. Toyoura, F. Oba, A. Kuwabara, K. Matsunaga, and I. Tanaka, J. Solid State Chem. **181**, 137 (2008).
[14] Y. Okuno, H. Kato, and M. Sano, J. Cryst. Growth **171**, 39 (1997).
[15] H. Serier, M. Gaudon, and M. Menetrier, Solid State Sci. **11**, 1192 (2009).
[16] B. J. Ingram, G. B. Gonzalez, D. R. Kammler, M. I. Bertoni, and T. O. Mason, J. Electroceram. **13**, 167 (2004).

APPLIED PHYSICS LETTERS **96**, 022503 (2010)

Determination of the saturation magnetization of ion irradiated Py/Ta samples using polar magneto-optical Kerr effect and ferromagnetic resonance

D. Markó,[1] T. Strache,[1] K. Lenz,[1,a)] J. Fassbender,[1] and R. Kaltofen[2]
[1]*Institute of Ion Beam Physics and Materials Research, Forschungszentrum Dresden-Rossendorf e.V., P.O. Box 51 01 19, 01314 Dresden, Germany*
[2]*IFW Dresden, Institut für Integrative Nanowissenschaften, Helmholtzstr. 20, 01069 Dresden, Germany*

(Received 13 August 2009; accepted 18 December 2009; published online 11 January 2010)

Based on polar magneto-optical Kerr effect and frequency dependent ferromagnetic resonance measurements, a method has been found that allows for the quantitative determination of the saturation magnetization of samples with unknown effective magnetic volume. Conventional magnetometry cannot be used for this purpose. Thin Py/Ta multilayers with an overall Py thickness of 20 nm but different number of interfaces are used as test systems. By means of Ne ion irradiation the magnetic moment and the saturation magnetization are affected due to interfacial mixing. With both increasing ion fluence and increasing number of Py/Ta interfaces, a decrease of saturation magnetization is observed. © *2010 American Institute of Physics*. [doi:10.1063/1.3291051]

Ion beam irradiation and ion implantation of ferromagnetic films, multilayers, and nanostructured samples have proven to be a smart tool to tailor their magnetic properties and structural composition (see Refs. 1–3 and references therein). Transition metals like Ta are widely used as seed and cap layers in the design of spintronic devices like giant magnetoresistance effect sensors or magnetic random access memory) as Ta is chemically stable. It also helps to tune the post switching precessional motion of the magnetization.[4] In this context the structural and magnetic properties of various kinds of Py/Ta structures have been investigated.[5–11] It was shown experimentally[7,10] and verified theoretically[7,8,12] that Ta intermixing leads to magnetically dead layers of 0.6–1.2 nm in thickness. 12% of Ta intermixing are sufficient to suppress the magnetic moment of the Ni atoms in Py.[7] These dead layers make it difficult to determine the correct magnetic volume, which is needed to obtain the saturation magnetization $\mu_0 M_s$ from the magnetic moment measured, e.g., by superconducting quantum interference device (SQUID) magnetometry. This is especially true for multilayer samples which typically have a large number of interfaces. Therefore, the influence of ion irradiation on the saturation magnetization could only be investigated qualitatively up to now.[13,14]

Here we present a method to circumvent this problem. The saturation magnetization of Py/Ta (multilayer) samples is determined from polar magneto-optical Kerr effect (MOKE) and vector network analyzer ferromagnetic resonance (VNA-FMR) measurements even in the case of interfacial mixing due to ion irradiation, where SQUID magnetometry fails. We do not evaluate $\mu_0 M_s$ from calibrated MOKE measurements nor from its proportionality to the FMR amplitude, as these methods are cumbersome and error-prone. Instead, $\mu_0 M_s$ is directly determined from the magnetic anisotropy energy.

To test this method, three different sets of $\mathrm{Py(=Ni_{81}Fe_{19})/Ta}$ thin film systems with a varying number of Py/Ta interfaces were deposited on a $\mathrm{Si/SiO_2}$ substrate using dc magnetron sputtering on 3 inch wafers in a multisource high vacuum system (base pressure below 2×10^{-7} mbar) at an Ar pressure of 7.5×10^{-4} mbar. The thin film systems, referred to as $1\times$Py, $5\times$Py, and $10\times$Py, all contain a total of 20 nm Py. $1\times$Py consists of a single 20 nm thick Py layer. $5\times$Py samples are multilayers containing five times 4 nm Py each separated by 1 nm Ta. The $10\times$Py system is made of ten 2 nm Py layers each separated by 0.5 nm Ta layers (see Fig. 1). For all of the samples a 30.5–35 nm Ta seed layer has been prepared prior to deposition of the multilayers. The seed layer thickness was chosen such that the total amount of Ta including the 3 nm protective cap layer and the spacer layers corresponds to 38 nm. The films have been irradiated with Ne ions having an energy of 40 keV and the ion fluences were in the range of 5×10^{13} to 5×10^{16} $\mathrm{Ne/cm^2}$.

Figure 2(a) shows the ferromagnetic resonance frequency f of the $1\times$Py samples as a function of the applied magnetic field B_{ext} along the easy axis. While there is virtually no difference between the unirradiated sample and the samples irradiated with fluences up to 1×10^{15} $\mathrm{Ne/cm^2}$, a significant decrease of the resonance frequency f can be observed for fluences of 2.5×10^{15} $\mathrm{Ne/cm^2}$ and higher. Figure 2(b) depicts the three unirradiated samples. Here, the ferromagnetic resonance frequency f strongly decreases with an increasing number of Py/Ta repetitions, i.e., increasing number of interfaces.

The frequency versus field dependence, also known as Kittel equation, is given by

$$f = \frac{|\gamma|}{2\pi}\sqrt{B_{\mathrm{ext}}\left(B_{\mathrm{ext}} + \mu_0 M_{\mathrm{eff}} + \frac{K_{2\parallel}}{M_s}\right)}. \quad (1)$$

The key to determine $\mu_0 M_s$ from FMR measurements is the

FIG. 1. Sketch of the Py/Ta thin film systems: (a) $1\times$Py, (b) $5\times$Py, and (c) $10\times$Py.

[a)]Electronic mail: k.lenz@fzd.de.

 © 2010 American Institute of Physics

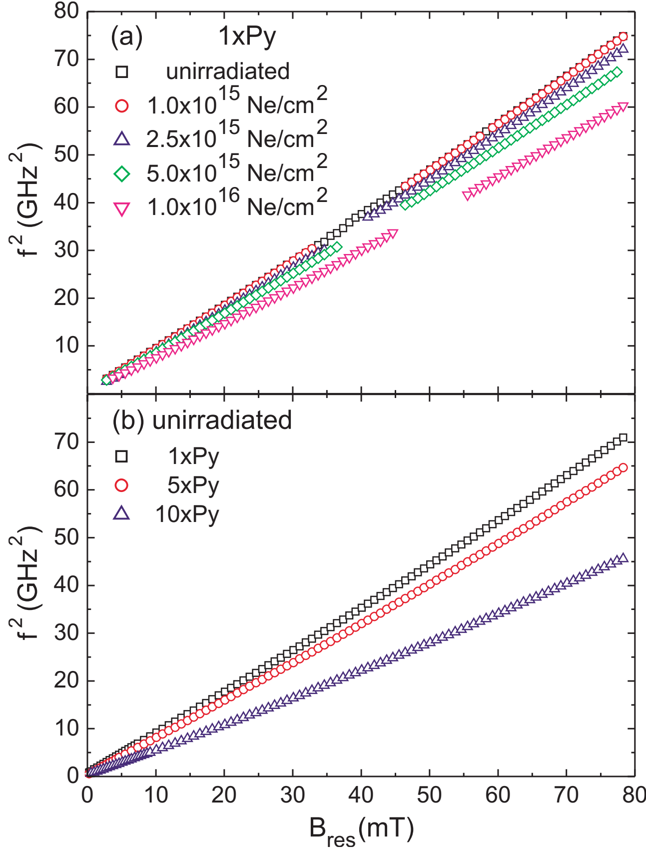

FIG. 2. (Color online) Microwave frequency squared vs the resonance field of (a) the irradiated $1\times$Py type samples and (b) the unirradiated samples.

effective magnetization $\mu_0 M_{\text{eff}} = \mu_0 M_s - 2K_{2\perp}/M_s$, which is the difference between shape anisotropy field and the uniaxial perpendicular anisotropy field, of Py. From the polar MOKE curves of selected $1\times$Py samples shown in Fig. 3 one can see that the samples do not have a perpendicular anisotropy, because there is no hysteresis. Hence, one can replace $\mu_0 M_{\text{eff}}$ by $\mu_0 M_s$ in Eq. (1) in order to determine $\mu_0 M_s$ by FMR. Now it becomes clear that a drop in saturation magnetization $\mu_0 M_s$ is responsible for the reduced resonance frequencies. From polar MOKE loops $\mu_0 M_s$ is obtained independently by determining the shape anisotropy field of the samples. This is the field value at which two

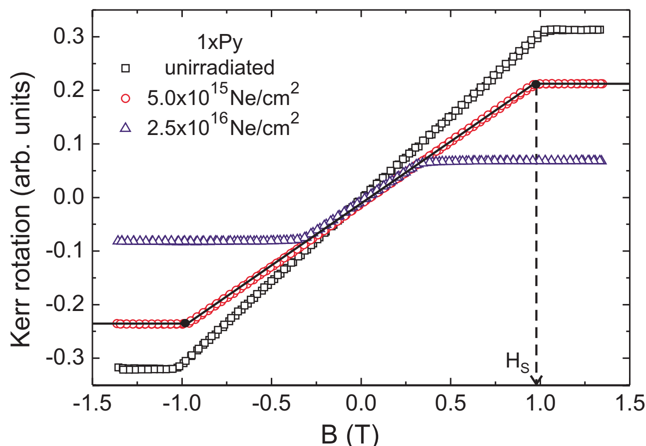

FIG. 3. (Color online) Polar MOKE measurements of selected $1\times$Py samples. The curves show no hysteresis which means that the samples do not have a perpendicular anisotropy.

TABLE I. Uniaxial in-plane anisotropy field $K_{2\parallel}/M_s$ and saturation magnetization $\mu_0 M_s$ (both in millitesla) determined from FMR.

Ion fluence (Ne/cm^2)	$1\times$Py		$5\times$Py		$10\times$Py	
	$K_{2\parallel}/M_s$	$\mu_0 M_s$	$K_{2\parallel}/M_s$	$\mu_0 M_s$	$K_{2\parallel}/M_s$	$\mu_0 M_s$
Unirradiated	0.70	1018	0.01	841	0.31	517
1.0×10^{14}	⋯	⋯	0.31	808	0.19	435
1.5×10^{14}	⋯	⋯	0.00	701	0.36	330
2.5×10^{14}	⋯	⋯	⋯	⋯	0.21	267
5.0×10^{14}	0.71	1022	⋯	⋯	⋯	⋯
1.0×10^{15}	0.65	1016	⋯	⋯	⋯	⋯
2.5×10^{15}	0.64	987	⋯	⋯	⋯	⋯
5.0×10^{15}	0.67	920	⋯	⋯	⋯	⋯
1.0×10^{16}	0.74	805	⋯	⋯	⋯	⋯

imaginary lines drawn to the horizontal "saturation branch" and steep "reversal region" of the hysteresis loop intersect (see Fig. 3).

SQUID magnetometry, like any other type of magnetometry, measures the magnetic moment $\vec{m}$ only. But calculating $\mu_0 M_s$ from $\vec{m}$ requires the knowledge of the exact effective Py volume, which is very difficult—if not impossible at all—to determine due to the increasing number of interfaces and their intermixing induced by ion irradiation. However, in our case, FMR and polar MOKE measurements allow $\mu_0 M_s$ to be determined without the knowledge of any effective Py thickness. The good agreement with the SQUID data of the unirradiated samples confirms this.

Using Eq. (1) the uniaxial in-plane anisotropy field $K_{2\parallel}$ and $\mu_0 M_s$ have been fitted. For the FMR analysis a g-factor for Py of $g=2.10$ (Ref. 15) was assumed for all samples as exact values for the irradiated samples are unknown. However, increasing g by 0.01 would decrease $\mu_0 M_s$ by 1% only. The results are given in Table I.

The samples possess a small uniaxial in-plane anisotropy that is slightly larger for the $1\times$Py samples than for the other two systems. It is virtually independent of the ion fluence and has only a minor contribution to the ferromagnetic resonance frequency f. Comparing the saturation magnetization of the unirradiated $1\times$Py and $10\times$Py samples, a reduction by a factor of 2 is found though all samples contain the same amount of Py. This behavior can be explained by taking into account the number of neighboring Ta atoms. In the $1\times$Py samples, the are only two interfaces and the number of neighboring Ta atoms is the smallest. However, in the $10\times$Py samples, there are already 20 interfaces and so many more Ni and Fe atoms have Ta atoms as neighbors. In this way, the deleterious effect of Ta on the ferromagnetic properties is becoming much stronger and leads to a reduction of the effective ferromagnetic film thickness by creating so-called magnetically dead layers close to the interfaces.[2,7,8,10,12]

Figure 4 shows $\mu_0 M_s$ as a function of the ion fluence of the samples determined independently from FMR, polar MOKE, as well as SQUID magnetometry. Data obtained from FMR and MOKE are consistent within error and also agree well with the SQUID data of the unirradiated samples. Note that no sort of normalization or scaling is involved in the determination of $\mu_0 M_s$.

In the case of $5\times$Py and $10\times$Py the decrease of $\mu_0 M_s$ already starts at very small ion fluences, whereas for $1\times$Py

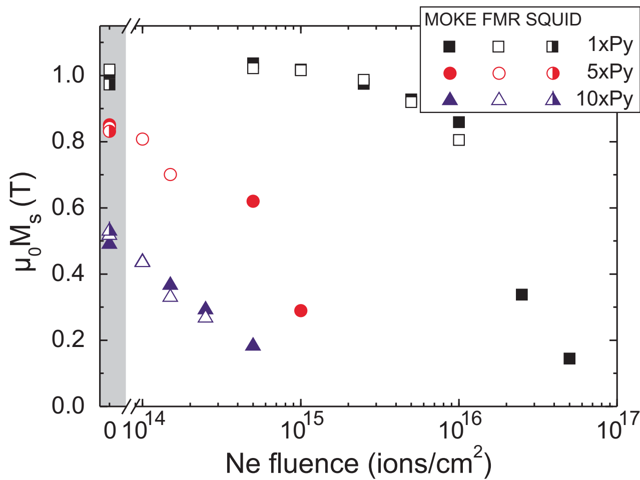

FIG. 4. (Color online) Comparison of saturation magnetization $\mu_0 M_s$ of the samples determined by FMR, polar MOKE, and SQUID magnetometry. The gray shaded area shows the data points of the unirradiated samples. The error bars of $\mu_0 M_s$ are 10% for the $10\times$Py, otherwise within symbol size.

$\mu_0 M_s$ remains almost unchanged for ion fluences up to 1×10^{15} Ne/cm^2. Just starting from ion fluences of 2.5×10^{15} Ne/cm^2 a significant decrease of $\mu_0 M_s$ sets in. As a result of the interfacial mixing the Ta concentration in Py increases and as it reaches 10–15 at. % an amorphization of the orginally polycrystalline $Ni_{81}Fe_{19}$ alloy takes place.[3] The critical ion fluence at which ferromagnetism completely vanishes depends on the number of interfaces and is 5×10^{16} Ne/cm^2 for the $1\times$Py samples, 0.5×10^{16} Ne/cm^2 for the $5\times$Py samples, and 0.1×10^{16} Ne/cm^2 for the $10\times$Py samples, respectively. In this case a significant amount of Py, but not necessarily the entire Py, is supposed to be amorphous.

In conclusion, using polar MOKE and VNA-FMR measurements, we have found a way to determine the saturation magnetization $\mu_0 M_s$ of samples with unknown effective magnetic volume. Py/Ta single- and multilayer films, each having a total Py thickness of 20 nm, were irradiated with Ne ions in order to modify their magnetic properties. With increasing ion fluence as well as an increasing number of Py/Ta interfaces, a decrease of saturation magnetization can be observed. However, the small uniaxial anisotropy of the samples remains virtually unaffected. Ne ion irradiation leads to a mixing and broadening of the interfaces and the Py/Ta stack undergoes a transition from being polycrystalline to amorphous at a critical fluence depending on the number of interfaces. The saturation magnetization is found to vanish at a Ta concentration of about 10–15 at. % in the Py layers.

We thank I. Winkler for the ion irradiation of the samples. This work was supported by Deutsche Forschungsgemeinschaft (Grant No. FA 314/3-1).

[1]C. Chappert, H. Bernas, J. Ferré, V. Kottler, J.-P. Jamet, Y. Chen, E. Cambril, T. Devolder, F. Rousseaux, V. Mathet, and H. Launois, Science **280**, 1919 (1998).
[2]J. Fassbender and J. McCord, J. Magn. Magn. Mater. **320**, 579 (2008).
[3]J. Fassbender, A. Mücklich, K. Potzger, and W. Möller, Nucl. Instrum. Methods Phys. Res. B **248**, 343 (2006).
[4]S. Ingvarsson, G. Xiao, S. S. P. Parkin, and R. H. Koch, Appl. Phys. Lett. **85**, 4995 (2004).
[5]H. Hurdequint, J. Magn. Magn. Mater. **310**, 2061 (2007).
[6]M. Mao, Q. Leng, Y. Huai, P. Johnson, M. Miller, H.-C. Tong, L. Miloslavsky, C. Qian, J. Wang, and H. Hedge, J. Appl. Phys. **85**, 5780 (1999).
[7]M. Kowalewski, W. H. Butler, N. Moghadam, G. M. Stocks, T. C. Schulthess, K. J. Song, J. R. Thompson, A. S. Arrott, T. Zhu, J. Drewes, R. R. Katti, M. T. McClure, and O. Escorcia, J. Appl. Phys. **87**, 5732 (2000).
[8]N. Y. Moghadam, G. M. Stocks, M. Kowalewski, and W. H. Butler, J. Appl. Phys. **89**, 6886 (2001).
[9]E. W. Hill, J. P. Li, and J. K. Birtwistle, J. Appl. Phys. **69**, 4526 (1991).
[10]G. H. Yu, H. C. Zhao, M. H. Li, F. W. Zhu, and W. Y. Lai, Appl. Phys. Lett. **80**, 455 (2002).
[11]M. Ueno and S. Tanoue, J. Vac. Sci. Technol. A **13**, 2194 (1995).
[12]N. Y. Moghadam and G. M. Stocks, Phys. Rev. B **71**, 134421 (2005).
[13]C. T. Rettner, S. Anders, T. Thomson, M. Albrecht, Y. Ideda, M. E. Best, and B. D. Terris, IEEE Trans. Magn. **38**, 1725 (2002).
[14]D. McGrouther and J. N. Chapman, Appl. Phys. Lett. **87**, 022507 (2005).
[15]J. P. Nibarger, R. Lopusnik, Z. Celinski, and T. J. Silva, Appl. Phys. Lett. **83**, 93 (2003).

APPLIED PHYSICS LETTERS **96**, 202105 (2010)

The importance of hole concentration in establishing carrier-mediated ferromagnetism in Mn doped Ge

Shengqiang Zhou,[1,2,a)] Danilo Bürger,[1] Wolfgang Skorupa,[1] Peter Oesterlin,[3] Manfred Helm,[1] and Heidemarie Schmidt[1]
[1]*Institute of Ion Beam Physics and Materials Research, Forschungszentrum Rossendorf, P.O. Box 510119, 01314 Dresden, Germany*
[2]*State Key Laboratory of Nuclear Physics and Technology, School of Physics, Peking University, Beijing 100871, China*
[3]*INNOVAVENT GmbH, Bertha-von-Suttner-Str. 5, 37085 Göttingen, Germany*

(Received 16 March 2010; accepted 21 April 2010; published online 18 May 2010)

In the present work, we have prepared Mn-doped Ge using different annealing approaches after Mn ion implantation, and obtained samples with hole concentrations ranging from 10^{18} to 2.1×10^{20} cm^{-3}, the latter being the highest reported so far. Based on the magnetotransport properties of Mn doped Ge, we argue that the hole concentration is a decisive parameter in establishing carrier-mediated ferromagnetism in magnetic Ge. © *2010 American Institute of Physics*. [doi:10.1063/1.3428770]

Mn doped GaAs (Ref. 1) and ZnTe (Ref. 2) are considered as the prototype diluted ferromagnetic semiconductors (FMS). In both systems, a large enough hole concentration is a prerequisite to establish the carrier-mediated ferromagnetism, which allows the electrical control over magnetism.[3] Practically, it is highly desirable to realize a FMS compatible with silicon technology. Whereas attempts to fabricate magnetically doped silicon (Si:Mn) have been rather discouraging,[4] germanium appears to be a promising candidate due to the well-accepted substitutional occupation of Mn in the Ge matrix.[5–8] The substitutional Mn ions produce double-acceptor levels and supply holes.[9]

The ferromagnetism in Ge:Mn has been nonquantitatively but plausibly explained by the formation of bound magnetic polarons (BMP).[10–13] According to the model by Kaminski and Das Sarma,[14] the percolation of BMP over the entire sample depends on the temperature and on the hole concentration. If GaAs:Mn can be any guide, a large enough hole concentration is required to establish carrier-mediated ferromagnetism.[15,16] For GaAs:Mn with 8.5% Mn, the critical hole concentration at 10 K is estimated to be 3×10^{19} cm^{-3} (Ref. 15). In Fig. 1 we summarize the hole concentration realized until now in Ge:Mn.[10,17–22,24] One can see that most of the values are well below the threshold value of 3×10^{19} cm^{-3}. Basically, this survey explains the lack of a correlation between magnetization and magnetotransport in Ge:Mn,[10,17–19,24,25] which is a hallmark of FMS.[2,26] Zhou *et al.*[27] shows that the positive magnetoresistance (MR) and the anomalous Hall resistance in Ge:Mn are likely related with a two-bandlike conduction. Furthermore, a correlation between magnetization and magnetotransport in Ge:Mn was observed at low temperatures when the hole concentration is large enough.[28]

In this article we present the magnetic and magnetotransport properties of Mn-doped Ge with hole concentrations ranging from 10^{18} to over 10^{20} cm^{-3}, which is achieved by applying different annealing approaches after ion implantation. We argue that the hole concentration is a decisive parameter in establishing the carrier-mediated ferromagnetism in Mn-doped Ge.

Nearly intrinsic, n-type Ge(001) wafers were implanted with Mn ions. The implantation energy and fluence were 100 keV and 30 keV, and 5×10^{16} cm^{-2} and 1×10^{16} cm^{-2}, respectively, resulting in a boxlike distribution of Mn ions with concentration around 10% over a depth of 100 nm. During implantation the wafers were flow-cooled with liquid nitrogen to avoid the formation of any Mn-rich secondary phase. A control wafer was implanted at 300 °C (100 keV, 5×10^{16} cm^{-2}), resulting in the formation of Mn_5Ge_3 crystalline precipitates during implantation.[29]

Flash lamp annealing (FLA) was performed with a pulse duration of 3 ms. The energy density was from 53.6 to 65.4 J/cm^2, which is enough for the implanted layer

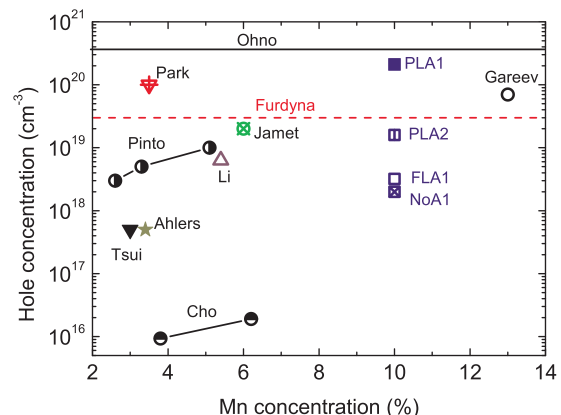

FIG. 1. (Color online) An overview of literature data showing the hole concentration vs Mn concentration in Ge:Mn. The four samples with 10% Mn are from this work, in which the hole concentration is determined from the ordinary Hall effect measured at 5 K. The other samples are from Park (Ref. 10), Jamet (Ref. 17), Tsui (Ref. 18), Gareev (Ref. 19), Pinto (Ref. 20), Li (Ref. 12), Cho (Ref. 21), and Ahlers (Ref. 22), for which the hole concentration is reported at room temperature. Except for the work by Cho (Ref. 21), all other Ge:Mn samples have been prepared by low-temperature molecular-beam epitaxy. The solid black line labeled "Ohno" is the hole concentration in a GaAs:Mn FMS with T_C=105 K (Ref. 23). The dashed red line "Furdyna" is the lowest hole concentration leading to ferromagnetism for GaAs:Mn (Ref. 15).

[a)]Electronic mail: s.zhou@fzd.de.

 © 2010 American Institute of Physics

TABLE I. Sample identification, Mn ion implantation temperature, annealing conditions, and hole-concentration. NoA1: implanted at a high temperature and nonannealed; FLA1: flash lamp annealed; PLA1 and PLA2: pulsed laser annealed.

Sample	Implantation temperature (°C)	Annealing conditions	Hole concentration (cm^{-3})
NoA1	300	⋯	2.0×10^{18}
FLA1	−40	3 ms, 59.4 J cm^{-2}	3.2×10^{18}
PLA2	−40	300 ns, 1.0 J cm^{-2}	1.6×10^{19}
PLA1	−40	300 ns, 1.5 J cm^{-2}	2.1×10^{20}

regrowth.[30] Pulsed laser annealing (PLA) was performed at Innovavent GmbH using a laser ASAMA 80–8 and an optical system VOLCANO. The pulse duration was 300 ns at a wavelength of 515 nm. The sample surface was scanned by a stripelike laser beam (2 mm×40 μm) with a frequency of 50 kHz. The introduced energy density amounted to 1.0 and 1.5 J/cm^2, which is enough for the liquid phase epitaxial regrowth. PLA has been used to fabricate GaAs:Mn and GaP:Mn FMS.[31–33] Magnetic properties were measured with a superconducting quantum interference device Quantum Design Magnetic Property Measurement System (MPMS) magnetometer. Magnetotransport properties were measured with a magnetic field applied perpendicularly to the film plane in van der Pauw geometry.

All samples presented in this work are listed in Table I. Figure 2(a) shows the zero-field cooling (ZFC)/field cooling (FC) magnetization curves. In general, all samples show an irreversibility in magnetization depending on their thermal history. This is the typical behavior of magnetic clusters. The low-concentration samples NoA1 and FLA1 reveal similar ZFC/FC curves with a peak at around 270 K, which corresponds to Mn_5Ge_3 precipitates. Mn_5Ge_3 has been confirmed by x-ray diffraction (not shown) in sample NoA1, that has been implanted with Mn at 300 °C (Table I). FLA with a pulse duration of 3 ms, as employed for sample FLA1, can effectively prevent the formation of MnAs precipitates in GaAs.[34] In sharp contrast, samples PLA1 and PLA2 annealed by a laser pulse have a large hole-concentration and display ZFC/FC curves significantly different from samples NoA1 and FLA1. The most noticeable feature is the ZFC peak in the temperature range from 60 to 70 K, which is related to Mn-rich regions in Ge.[10–12] The inset of Fig. 2(a) shows the remanent magnetization versus temperature for samples FLA1 and PLA1. Despite the large difference in ZFC/FC curves, a magnetic phase is observed for both samples at low temperature. This ferromagnetic phase is related with the coupling between diluted Mn ions in Ge.[11,13,17,35,36]

Note that the ZFC/FC curves of samples PLA1 and PLA2 also reveal a weak ferromagnetic component up to 260 K. This may be due to some small residual Mn_5Ge_3 precipitates. We have performed synchrotron x-ray diffraction measurements on both samples (not shown). PLA1 reveals a small peak close to $Mn_5Ge_3(002)$ but PLA2 reveals no extra peak besides the Ge phase. $Mn_{11}Ge_8$ has been observed in none of the samples.

Figure 2(b) shows the field-dependent magnetization at 5 K. Sample NoA1 exhibits the largest saturation magnetic moment, while the magnetization of sample PLA2 is smaller

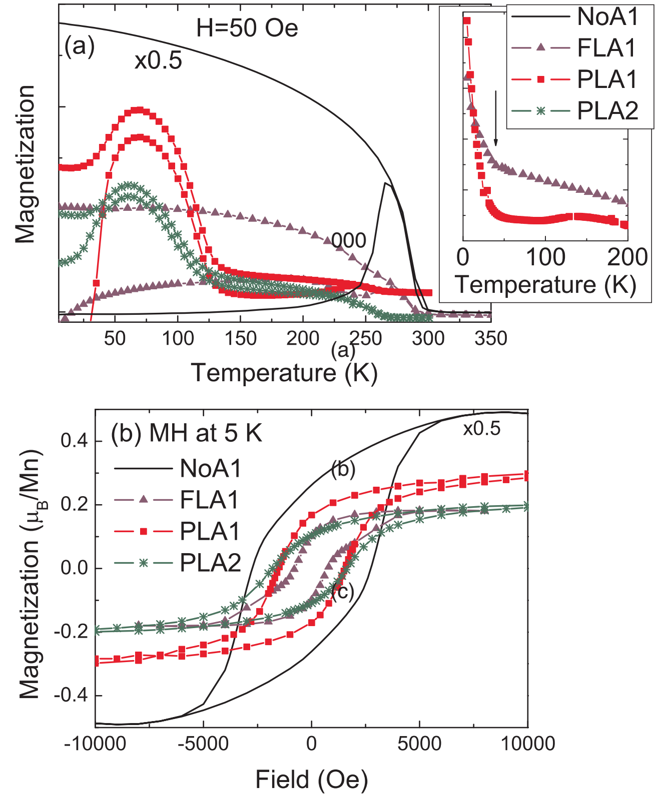

FIG. 2. (Color online) Magnetic properties of Mn-implanted Ge after different thermal processing: (a) Temperature-dependent magnetization after ZFC (lower branches) and after field cooling FC (upper branches). The inset shows the remanent magnetization vs temperature, and a low temperature magnetic phase is indicated by the arrow. The negative ZFC magnetization of sample PLA1 is due to the residual field in the superconducting magnet employed during magnetization measurements. (b) Magnetization at 5 K. Sample NoA1 containing Mn_5Ge_3 clusters exhibits the largest moment, while the other samples do not differ strongly.

than that of sample PLA1 and comparable to sample FLA1.

As shown in Fig. 2, samples PLA1 and PLA2 reveal similar magnetic properties. Moreover, the low temperature (below 30 K) ferromagnetic phase has been clearly observed in all of the investigated samples by us [see the inset of Fig. 2(a)], as well as by other groups.[11,13,17,35,36] However, we observed that the magnetotransport at low temperatures is much different. Figure 3(a) shows the MR at 5 K. Samples

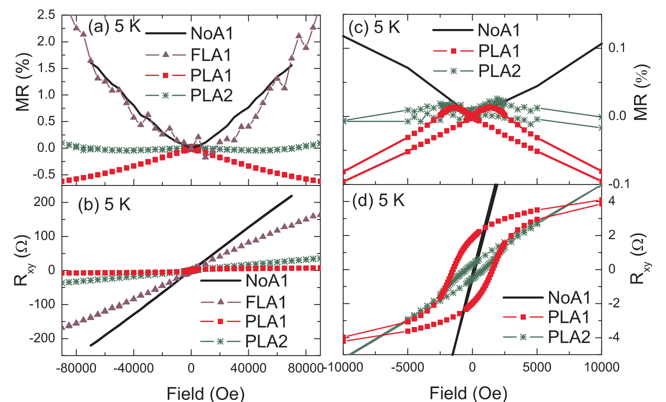

FIG. 3. (Color online) Magnetotransport properties of Mn-implanted Ge at 5 K: (a) MR, Samples PLA1 and PLA2 show a negative MR. (b) Hall resistance (R_{xy}). [(c) and (d)] Zoom-in of the low-field region of the MR and Hall curves. Samples PLA1 and PLA2 show hysteresis in MR and Hall curves, while samples NoA1 and FLA1 do not.

PLA1 and PLA2 have a negative MR but at large field the positive MR overcomes the negative one for sample PLA2. Figure 3(b) shows the Hall effect of different samples. The ordinary and anomalous Hall terms depend linearly on field and magnetization, respectively. At high fields, all samples exhibit a linear behavior, which allows the determination of the hole-concentration by a linear fitting of the Hall curve (see Table I and Fig. 1). The zoom-in of the MR and Hall curves in the low field region is shown in Figs. 3(c) and 3(d), respectively. Only samples PLA1 and PLA2 exhibit clear hysteretic MR and AHE curves (weak for sample PLA2). Compared with literature data (Fig. 1), the sample PLA1 reaches the largest hole-concentration. If the same set of carriers participate in ferromagnetic coupling and transport, one expects a large AHE, corresponding to the magnetization of the sample.[2,26] The hole concentration is the critical parameter for carrier-mediated ferromagnetism throughout the Ge:Mn sample. Only a large enough hole concentration (PLA1) gives rise to the carrier-mediated ferromagnetism throughout the Ge:Mn sample. The hole concentration of the other samples (PLA2, FLA1, and NoA1) is too small to mediate the ferromagnetism in Ge:Mn. A theoretical picture on the antiferromagnetic coupling between holes and Mn ions acting as double acceptors is given in Ref. 28.

In a summary, we present the magnetic and magnetotransport properties of a group of Ge:Mn samples with the hole concentration ranging from 10^{18} to 10^{20} cm^{-3}. The hole concentration is the critical parameter to establish carrier mediated ferromagnetism in Ge:Mn, as seen for GaAs:Mn.[1,15,16] A high-concentration codoping with a shallow acceptor[30] may allow to increase the hole-concentration further, possibly resulting in a dramatically increased Curie temperature.

Financial support from the Bundesministerium für Bildung und Forschung (Grant No. FKZ13N10144) is gratefully acknowledged. The authors acknowledge the support of Thomas Schumann for FLA.

[1] A. Van Esch, L. Van Bockstal, J. De Boeck, G. Verbanck, A. S. van Steenbergen, P. J. Wellmann, B. Grietens, R. Bogaerts, F. Herlach, and G. Borghs, Phys. Rev. B **56**, 13103 (1997).
[2] D. Ferrand, J. Cibert, A. Wasiela, C. Bourgognon, S. Tatarenko, G. Fishman, T. Andrearczyk, J. Jaroszyński, S. Koleśnik, T. Dietl, B. Barbara, and D. Dufeu, Phys. Rev. B **63**, 085201 (2001).
[3] H. Ohno, D. Chiba, F. Matsukura, T. Omiya, E. Abe, T. Dietl, Y. Ohno, and K. Ohtani, Nature (London) **408**, 944 (2000).
[4] S. Zhou, K. Potzger, G. Zhang, A. Mücklich, F. Eichhorn, N. Schell, R. Grötzchel, B. Schmidt, W. Skorupa, M. Helm, J. Fassbender, and D. Geiger, Phys. Rev. B **75**, 085203 (2007).
[5] P. Gambardella, L. Claude, S. Rusponi, K. J. Franke, H. Brune, J. Raabe, F. Nolting, P. Bencok, A. T. Hanbicki, B. T. Jonker, C. Grazioli, M. Veronese, and C. Carbone, Phys. Rev. B **75**, 125211 (2007).
[6] J.-S. Kang, G. Kim, S. C. Wi, S. S. Lee, S. Choi, S. Cho, S. W. Han, K. H. Kim, H. J. Song, H. J. Shin, A. Sekiyama, S. Kasai, S. Suga, and B. I. Min, Phys. Rev. Lett. **94**, 147202 (2005).
[7] S. Picozzi, L. Ottaviano, M. Passacantando, G. Profeta, A. Continenza, F. Priolo, M. Kim, and A. J. Freeman, Appl. Phys. Lett. **86**, 062501 (2005).
[8] S. Decoster, S. Cottenier, B. De Vries, H. Emmerich, U. Wahl, J. G. Correia, and A. Vantomme, Phys. Rev. Lett. **102**, 065502 (2009).
[9] H. H. Woodbury and W. W. Tyler, Phys. Rev. **100**, 659 (1955).
[10] Y. D. Park, A. T. Hanbicki, S. C. Erwin, C. S. Hellberg, J. M. Sullivan, J. E. Mattson, T. F. Ambrose, A. Wilson, G. Spanos, and B. T. Jonker, Science **295**, 651 (2002).
[11] D. Bougeard, S. Ahlers, A. Trampert, N. Sircar, and G. Abstreiter, Phys. Rev. Lett. **97**, 237202 (2006).
[12] A. P. Li, J. F. Wendelken, J. Shen, L. C. Feldman, J. R. Thompson, and H. H. Weitering, Phys. Rev. B **72**, 195205 (2005).
[13] A. P. Li, J. Shen, J. R. Thompson, and H. H. Weitering, Appl. Phys. Lett. **86**, 152507 (2005).
[14] A. Kaminski and S. Das Sarma, Phys. Rev. B **68**, 235210 (2003).
[15] S. U. Yuldashev, H. C. Jeon, H. S. Im, T. W. Kang, S. H. Lee, and J. K. Furdyna, Phys. Rev. B **70**, 193203 (2004).
[16] K. Khazen, H. J. von Bardeleben, J. L. Cantin, L. Thevenard, L. Largeau, O. Mauguin, and A. Lemaître, Phys. Rev. B **77**, 165204 (2008).
[17] M. Jamet, A. Barski, T. Devillers, V. Poydenot, R. Dujardin, P. Bayle-Guillemaud, J. Rothman, E. Bellet-Amalric, A. Marty, J. Cibert, R. Mattana, and S. Tatarenko, Nat. Mater. **5**, 653 (2006).
[18] F. Tsui, L. He, L. Ma, A. Tkachuk, Y. S. Chu, K. Nakajima, and T. Chikyow, Phys. Rev. Lett. **91**, 177203 (2003).
[19] R. R. Gareev, Y. V. Bugoslavsky, R. Schreiber, A. Paul, M. Sperl, and M. Döppe, Appl. Phys. Lett. **88**, 222508 (2006).
[20] N. Pinto, L. Morresi, M. Ficcadenti, R. Murri, F. D'Orazio, F. Lucari, L. Boarino, and G. Amato, Phys. Rev. B **72**, 165203 (2005).
[21] S. Cho, S. Choi, S. C. Hong, Y. Kim, J. B. Ketterson, B.-J. Kim, Y. C. Kim, and J.-H. Jung, Phys. Rev. B **66**, 033303 (2002).
[22] S. Ahlers, D. Bougeard, H. Riedl, G. Abstreiter, A. Trampert, W. Kipferl, M. Sperl, A. Bergmaier, and G. Dollinger, Physica E (Amsterdam) **32**, 422 (2006).
[23] T. Omiya, F. Matsukura, T. Dietl, Y. Ohno, T. Sakon, M. Motokawa, and H. Ohno, Physica E (Amsterdam) **7**, 976 (2000).
[24] A. P. Li, C. Zeng, K. van Benthem, M. F. Chisholm, J. Shen, S. V. S. N. Rao, S. K. Dixit, L. C. Feldman, A. G. Petukhov, M. Foygel, and H. H. Weitering, Phys. Rev. B **75**, 201201 (2007).
[25] C. Zeng, Z. Zhang, K. van Benthem, M. F. Chisholm, and H. H. Weitering, Phys. Rev. Lett. **100**, 066101 (2008).
[26] H. Ohno, H. Munekata, T. Penney, S. von Molnár, and L. L. Chang, Phys. Rev. Lett. **68**, 2664 (1992).
[27] S. Zhou, D. Bürger, M. Helm, and H. Schmidt, Appl. Phys. Lett. **95**, 172103 (2009).
[28] S. Zhou, D. Bürger, C. Baumgart, A. Mücklich, W. Skorupa, C. Timm, P. Oesterlin, M. Helm, and H. Schmidt, Phys. Rev. B **81**, 165204 (2010).
[29] S. Zhou, A. Shalimov, K. Potzger, N. M. Jeutter, C. Baehtz, M. Helm, J. Fassbender, and H. Schmidt, Appl. Phys. Lett. **95**, 192505 (2009).
[30] V. Heera, A. Mücklich, M. Posselt, M. Voelskow, C. Wündisch, B. Schmidt, R. Skrotzki, K. H. Heinig, T. Herrmannsdörfer, and W. Skorupa, J. Appl. Phys. **107**, 053508 (2010).
[31] M. A. Scarpulla, O. D. Dubon, K. M. Yu, O. Monteiro, M. R. Pillai, M. J. Aziz, and M. C. Ridgway, Appl. Phys. Lett. **82**, 1251 (2003).
[32] M. A. Scarpulla, B. L. Cardozo, R. Farshchi, W. M. H. Oo, M. D. McCluskey, K. M. Yu, and O. D. Dubon, Phys. Rev. Lett. **95**, 207204 (2005).
[33] D. Bürger, S. Zhou, M. Pandey, C. Viswanadham, J. Grenzer, O. Roshchupkina, W. Anwand, H. R. V. Gottschalch, M. Helm, and H. Schmidt, Phys. Rev. B **81**, 115202 (2010).
[34] D. Bürger, S. Zhou, J. Grenzer, H. Reuther, W. Anwand, V. Gottschalch, M. Helm, and H. Schmidt, Nucl. Instrum. Methods Phys. Res. B **267**, 1626 (2009).
[35] C. Jaeger, C. Bihler, T. Vallaitis, S. T. B. Goennenwein, M. Opel, R. Gross, and M. S. Brandt, Phys. Rev. B **74**, 045330 (2006).
[36] R. B. Morgunov, A. I. Dmitriev, and O. L. Kazakova, Phys. Rev. B **80**, 085205 (2009).

PHYSICAL REVIEW B **82**, 033403 (2010)

Pyramidal pits created by single highly charged ions in BaF_2 single crystals

A. S. El-Said,[1,2,*] R. Heller,[1] F. Aumayr,[3] and S. Facsko[1]
[1] *Institute of Ion Beam Physics and Materials Research, Forschungszentrum Dresden-Rossendorf, Bautzner Landstr. 400, 01328 Dresden, Germany*
[2] *Physics Department, Faculty of Science, Mansoura University, 35516 Mansoura, Egypt*
[3] *Institute of Applied Physics, Vienna University of Technology, 1040 Vienna, Austria*
(Received 23 April 2010; published 9 July 2010)

In various insulators, the impact of individual slow highly charged ions (eV-keV) creates surface nanostructures, whose size depends on the deposited potential energy. Here we report on the damage created on a cleaved BaF_2 (111) surface by irradiation with $4.5\times q$ keV highly charged xenon ions from a room-temperature electron-beam ion trap. Up to charge states $q=36$, no surface topographic changes on the BaF_2 surface are observed by scanning force microscopy. The hidden stored damage, however, can be made visible using the technique of selective chemical etching. Each individual ion impact develops into a pyramidal etch pits, as can be concluded from a comparison of the areal density of observed etch pits with the applied ion fluence (typically 10^8 ions/cm^2). The dimensional analysis of the measured pits reveals the significance of the deposited potential energy in the creation of lattice distortions/defects in BaF_2.

DOI: 10.1103/PhysRevB.82.033403 PACS number(s): 61.80.Jh, 34.35.+a, 61.72.J−, 68.37.Ps

Swift heavy ions (MeV-GeV kinetic energy) have become an important tool for structural modifications of various materials at the microscale and nanoscale for a wide range of applications in the last two decades.[1–4] One major limitation of using these high-energy ions is the damage creation in deep layers which in some applications should be avoided. The desire to confine the damage to the first few layers, which is essential for applications such as ion projection lithography, has stimulated the interest for the use of slow (eV-keV) highly charged ions (HCIs).[5] This type of ions is now readily available after recent developments in ion source technology leading to powerful ion sources such as the electron-beam ion trap (EBIT).[6,7] While electronic energy loss of swift heavy ions is the major cause of material modifications,[8,9] potential-energy deposition is dominating surface modifications by HCI.[10] During interaction with the solid surface HCI deposit their potential energy (the total ionization energy required for producing the high charge state from its neutral ground state) within a few femtosecond in a nanometer-sized volume close to the surface.[10–12] Initially the potential energy is deposited in the electronic subsystem of the target leading to strong electronic excitations. Strong electron-phonon coupling can then induce local surface modifications in various solids. Recently, HCI-induced surface modifications such as hillocks,[13–15] craters,[16] pits,[17] and calderalike structures[18] with nanometer dimensions have been demonstrated.[10]

The study of nanostructure formation on surfaces induced by HCI is a relatively new field and still requires a detailed comparison between materials with common and different properties, in order to develop a more general understanding of the underlying mechanisms. For this aim and motivated by our recent findings regarding surface nanostructuring of CaF_2 by means of HCI (Refs. 13 and 14), we selected BaF_2 as one of the ionic alkaline-earth fluorides (along with CaF_2 and SrF_2) which have a wide range of potential applications in microelectronic and optoelectronic devices such as high-k dielectrics and buffer layers in semiconductor-on-insulator structures.[19]

As samples for irradiation, we have used thin slabs ($10\times 10\times 0.5-1.0$ mm^3) cleaved along the (111) planes from single-crystal blocks of high-purity barium fluoride (from Korth Kristalle, Germany) grown from melt in an inert atmosphere. The samples were mounted in a vacuum chamber with base pressure of 10^{-9} mbar and irradiated at room temperature under normal incidence with highly charged isotope pure $^{129}Xe^{q+}$ ions of various charge states ($q=24-36$). A rectangular transmission electron microscopy grid was used to mask parts of the sample surface. The ions were extracted from the EBIT in pulsed mode at constant extraction voltage of 4.5 kV leading to kinetic energies of $4.5\times q$ keV. The selection of ions of specific charge-to-mass ratio was performed using a 90 analyzing magnet. The applied ion fluences were in the range of 10^9-10^{10} ions/cm^2 whereas etching experiments required lower fluence of about 10^8 ions/cm^2, which is small enough to avoid tracks overlapping and reasonably high for good statistics. The average beam flux varied between 10^4 and 10^6 ions/s. Irradiation parameters are listed in Table I (some of the ion parameters are estimated using SRIM 2008).[20]

After ion irradiation, the BaF_2 (111) crystal surfaces were inspected by scanning force microscopy (SFM). The measurements were performed in tapping mode under ambient conditions using Si sensors (cantilever resonance frequency $\approx$190 kHz). Additionally, we performed UHV-contact mode SFM measurements (using UHV Omicron AFM/STM) at constant force and Si tips with cantilever force constants of $\approx$0.2 N/m. Surprisingly, none of the used Xe^{q+} ($q=24-36$) ions were able to induce visible topographic changes on the irradiated surfaces. As a typical example, Fig. 1 shows the SFM topographic image of a BaF_2 surface irradiated with 1.26 keV/amu Xe^{36+} ions. The peak-to-peak roughness of the cleaved surfaces is $\approx$0.1 nm which would be enough for resolving ion-induced surface structures of sizes above the SFM detection limit ($\approx$0.1 nm and 1.0 nm for vertical and lateral dimensions, respectively).

To reveal the hidden damage not directly visible in the

 ©2010 The American Physical Society

TABLE I. Charge state (q), potential energy (E_{pot}), kinetic energy (E_{kin}), and the corresponding electronic $(dE/dx)_e$, and nuclear $(dE/dx)_n$ energy loss, range (R) of the Xe ions as well as the mean measured depth (D) of the etch pits.

q	E_{pot} (keV)	E_{kin} (keV/amu)	$(dE/dx)_e$ (keV/nm)	$(dE/dx)_n$ (keV/nm)	R (nm)	D (nm)
24+	7.3	0.84	0.30	2.36	39	16
28+	12.0	0.98	0.32	2.39	44	19
33+	21.2	1.16	0.35	2.42	51	22
36+	27.8	1.26	0.37	2.44	54	23

surface topography, chemical etching was performed using a 1 vol % solution of HNO_3 at room temperature without agitation. To avoid any possible size dependence on etching time, all samples were etched under identical conditions (i.e., same HNO_3 concentration, 5 s etching time). Because parts of the sample's surface were masked by a rectangular copper grid during irradiation, the observation of well-defined patterns is a straightforward evidence of successful chemical etching of damage induced by HCI projectiles. Moreover, one can easily differentiate between features created due to ion irradiation and naturally present dislocations which are also etchable.[21]

In Fig. 2(a), the SFM topographic image of a BaF_2 surface irradiated with 10^8 Xe^{36+} ions/cm^2 is shown after chemical etching. Due to the pattern of the used rectangular mask irradiated and masked regions can be clearly distinguished. In irradiated areas, etch pits of three-faced symmetric pyramidal depressions are revealed. This geometry originates from the (111) crystal lattice orientation of BaF_2. The mean width and depth of the created etch pits are about 1.6 μm and 23 nm, respectively. In nonirradiated regions, etched surfaces only occasionally show a few pits as a result of etching naturally present dislocations, whose size, however, is much larger than the one observed for etched ion tracks [Fig. 2(a)].

Figures 2(b)–2(d) shows further SFM images of BaF_2 samples etched after irradiation with $(4.5q \times \text{kV})$ Xe^{24+}, Xe^{28+}, and Xe^{33+}, respectively. In all cases, triangle-shaped etch pits were observed in the irradiated areas whose sizes increase with the incident ion charge state and whose number corresponds to the applied ion fluence. Figure 3 shows a magnified image and a line profile through one of the pits.

Table I summarizes the parameters of our irradiation experiments including the electronic energy loss, the nuclear energy loss, and the penetration depth calculated by SRIM.[20] The potential energy corresponding to the lowest (Xe^{24+}) and highest (Xe^{36+}) charge state used in our experiments differ by a factor of 3.8. In contrast to this, the difference in the kinetic energy is only a factor of 1.5 leading to a difference of only 25% in the electronic energy loss and an insignificant difference of 3% in the nuclear energy loss. However, at these low kinetic energies the electronic energy loss is already one order of magnitude smaller than the nuclear energy loss. Taking into account that the potential energy is deposited within the first few nanometer,[14] the dominant role of the potential energy for the damage creation becomes obvious.

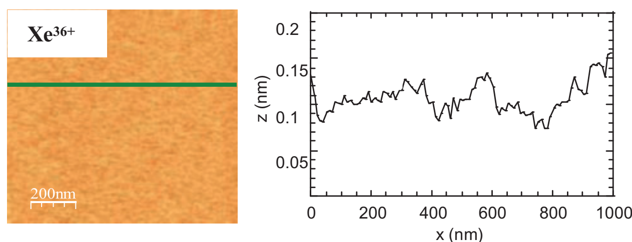

FIG. 1. (Color online) SFM topographic image and line scan of a BaF_2 (111) surface irradiated with 1.26 keV/amu Xe^{36+} ions (fluence 5×10^9 ions/cm^2). No topographic changes due to ion impact are visible.

In Fig. 4, the strong dependence of the mean size of the pits on potential energy is shown. The pit size is extracted from the SFM images by analyzing the width and depth of well-separated pits and calculating the removed volume (see Fig. 3). We note a nearly linear increase in pit volume with potential energy.

Before we interpret our findings for BaF_2 (111), we first compare them to results obtained during HCI irradiation of KBr (001) and CaF_2 (111) surfaces. For KBr (001) surfaces, the individual impacts of slow highly charged Xe ions induce nanometer-sized pitlike structures with lateral sizes of 10–25 nm and monatomic depth, which are visible in SFM without chemical etching.[17] For CaF_2 (111) surfaces, no topographic changes are visible in the SFM images up to a certain Xe-ion charge state ($q \leq 28$) while above this threshold permanent nanosized hillocks with lateral sizes of 20–40 nm and 0.5–1.0 nm height appear on the surface.[13,14] On the contrary, for BaF_2 (111) surfaces no topographic changes are visible in the SFM images up to the highest Xe-ion charge state ($q=36$) used in our experiments (see Fig. 1). Nanostructures in the form of pyramidal pits can, however, be revealed after chemical etching. All three cases have in common, that the nanostructures can unambiguously be associated to individual ion impact events and that the size of the generated nanostructures strongly depends on the charge state and therefore on the potential energy deposited by the HCI into the surface.[13,14,17]

The decisive role of the potential energy for the formation of nanostructures can be explained taking into account the fact that damage creation in ion-surface collisions is strongly correlated with the form of energy deposition in the solid. For slow (keV) singly charged or neutral atoms, nuclear stopping dominates the energy loss. This energy transfer to

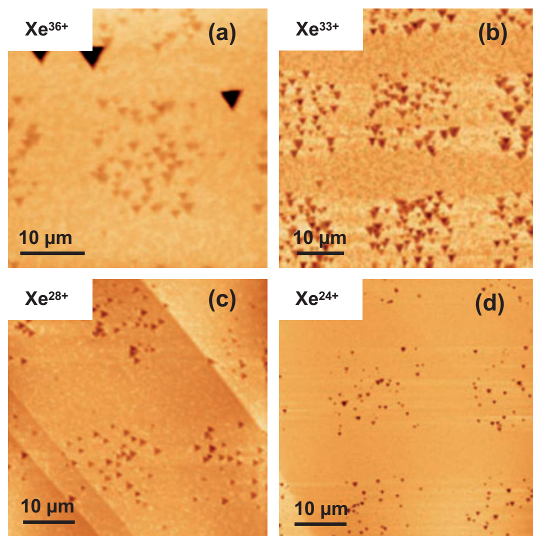

FIG. 2. (Color online) Scanning force micrographs of BaF_2 (111) surfaces after chemical etching. The samples were irradiated through a structured mask with (a) 4.5 keV/q Xe^{36+}, (b) Xe^{33+}, (c) Xe^{28+}, and (d) Xe^{24+} ions, respectively (fluence $\approx 10^8$ ions/cm^2).

target cores leads to atomic displacements and lattice vibrations in the target (phonons). On the other hand, slow highly charged ions transfer their potential energy via a series of Auger processes to the electronic subsystem of the target.[10–12] As a consequence, (i) a large number of electrons is emitted from the projectile into a shallow region close to the HCI impact zone,[22–24] (ii) inelastic interaction of these electrons with target atoms leads to a strong electronic excitation of a nanometer-sized region around the impact site,[10,11,25] i.e., generation of defects such as excitons, color centers, holes, etc., and production of further (secondary) electrons, and (iii) elastic collisions of these electrons with target atoms (electron-phonon coupling) heat the lattice in the surrounding of the impact site.

Modeling calculations for HCI impact on CaF_2 have shown that above a certain potential-energy threshold, the heating of the lattice atoms by these primary and secondary electrons can surpass the melting threshold of the solid.[14,26] Heat and pressure deforms the surface and after cooling

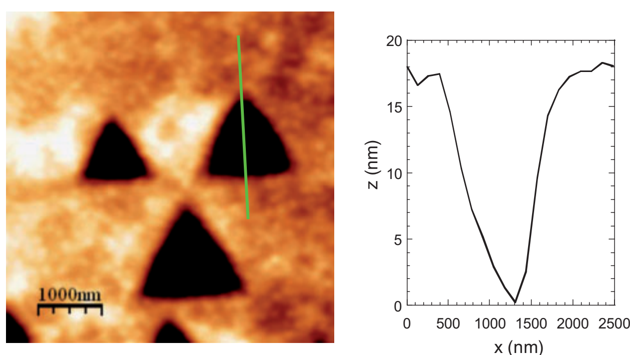

FIG. 3. (Color online) SFM image (left) of etched $4.5q \times$keV Xe^{28+} pits in BaF_2 (111). Line profile across one of the pits (right).

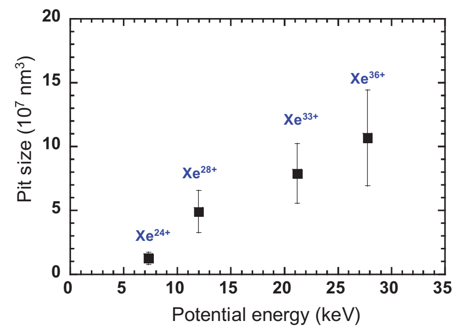

FIG. 4. (Color online) Mean size of etch pits as a function of potential energy of Xe^{q+} ions.

down a hillock remains at the surface. This melting threshold is obviously not (yet) reached for impact of Xe^{36+} on KBr and BaF_2. Since the melting temperatures are very similar in the case of CaF_2 and BaF_2 there have to be other reasons for this, which we can only speculate on (a) electron-transport properties, such as elastic and inelastic mean-free path could be different for both materials and transport the (electron) energy further away in the case of BaF_2 (resulting in a lower energy transferred to each target atom) (b) thermal conductivity of BaF_2 is higher than for CaF_2. So even if the same volume is heated by the electrons, this heat is more quickly carried away by heat conductivity or the hot zone is more effectively cooled from the surrounding material and therefore the zone does not melt. However, the strong electronic excitation will definitely lead to the generation of defects such as excitons, holes, color centers, etc., around the impact site also in these materials.

It is well known that even electron and photon impact on various ionic crystals can lead to color center creation and in further consequence to what is called electron- and photon-stimulated desorption.[27–29] The first steps include the production of holes and electron pairs. Because of the strong electron-phonon coupling of the ionic lattice, these defects become rapidly self-trapped (self-trapped exciton, self-trapped holes) (Refs. 30 and 31) and subsequently decay into color centers, i.e., an H center (an interstitial molecular halide ion) and an F center (an electron at an anion site). The independent diffusion of both centers and their subsequent recombination with the surface lead to the desorption of individual halide atoms and alkali (alkaline-earth) atoms, respectively.

This defect-induced desorption mechanism was also invoked to explain the interaction of singly[29] and multiply charged ions[11] with alkali-halide surfaces, in particular, to explain the effect of "potential sputtering," i.e., sputtering due to the potential energy of the projectile ions rather than their kinetic energy.[11,32–34] Also the pit formation during the interaction of HCI with KBr (001) (see above) was ascribed to this defect-induced desorption mechanism.[17] Contrary to the case of electrons, photons, or singly charged ions, however, the emission of a large number of electrons during the relaxation of HCI leads to a high density of defects close to the surface. As the defects diffuse, they combine to complex defect centers (e.g., F center agglomerates) from which in the case of KBr desorption is possible without the presence of step edges.[17]

As mentioned above, there is no reason to assume that the strong electronic excitation of the surface-near region due to the potential energy of the slow HCI should not induce similar defects and defect aggregates in BaF_2 and CaF_2 as well. However, in both cases the defects (or defect clusters) obviously do not result in pits visible in SFM images either because their diffusion is limited or the color centers remain (weakly) bound to the surface and do not lead to desorption. The impact region is, however, structurally weakened and can be preferentially attacked by a suitable etchant (as observed in our case for BaF_2).

In etching studies of swift heavy-ion tracks in alkali-halide surfaces, it was found that the etchability is related to the creation of large defect aggregates or even microdefects (clusters of few F centers) rather than single point defects (F and H centers).[35] The strong dependence of the mean size of etch pits as a function of potential energy of Xe^{q+} ions (Fig. 4) indicates that the electronic excitation induced by the HCI is able to create large defect aggregates at or close to the surface. Compared to the total ion range, the etch pits are only ≈40% deep (see Table I). This is a further hint that only in the beginning of the track (where the potential energy is deposited), etchable defect aggregates and clusters are produced while at the end of the ion track, point defects from the nuclear collision cascade prevail.

If our interpretation is correct, we should also be able to see similar structures after etching on CaF_2 (111) even below the (melting) threshold for hillock generation (see above). Indeed such etch pits have been found recently in preliminary experiments using Xe^{25+} projectile ion impact on CaF_2.[36] A more systematic study is currently in progress.

In conclusion, we have shown that in spite of no direct visible topographic surface modifications by HCI irradiation, surface and near surface lattice distortion are created in BaF_2 (111). The size of the revealed damage zone is strongly increasing with the deposited potential energy. The irradiation with slow HCI results in an extremely high and strongly localized dose distribution around the impact site. The etchability of the HCI-induced damage, suggests the efficient role of the deposited potential energy for the creation of defect aggregates rather than single point defects, an observation already made during swift heavy-ion irradiation.

A.S.E. thanks Alexander von Humboldt Foundation for financial support. This work was supported by the European project ITSLEIF (Grant No. RII3/026015).

*a.s.el-said@fzd.de; www.fzd.de

[1] M. Lang, F. X. Zhang, J. M. Zhang, J. Wang, B. Schuster, C. Trautmann, R. Neumann, U. Becker, and R. C. Ewing, Nature Mater. **8**, 793 (2009).
[2] A. Navitski, G. Mueller, V. Sakharuk, T. W. Cornelius, C. Trautmann, and S. Karim, Eur. Phys. J.: Appl. Phys. **48**, 30502 (2009).
[3] E. Akcöltekin, T. Peters, R. Meyer, A. Duvenbeck, M. Klusmann, I. Monnet, H. Lebius, and M. Schleberger, Nat. Nanotechnol. **2**, 290 (2007).
[4] T. W. Cornelius, J. Brötz, N. Chtanko, D. Dobrev, G. Miehe, R. Neumann, and M. E. T. Mollares, Nanotechnology **16**, S246 (2005).
[5] J. D. Gillaspy, D. C. Parks, and L. P. Ratliff, J. Vac. Sci. Technol. B **16**, 3294 (1998).
[6] F. Grossmann *et al.*, Nucl. Instrum. Methods Phys. Res. B **256**, 565 (2007).
[7] W. Meissl *et al.*, Rev. Sci. Instrum. **77**, 093303 (2006).
[8] A. S. El-Said *et al.*, Nucl. Instrum. Methods Phys. Res. B **256**, 313 (2007).
[9] K. Schwartz *et al.*, Phys. Rev. B **70**, 184104 (2004).
[10] F. Aumayr, A. S. El-Said, and W. Meissl, Nucl. Instrum. Methods Phys. Res. B **266**, 2729 (2008).
[11] F. Aumayr and H. P. Winter, Philos. Trans. R. Soc. London **362**, 77 (2004).
[12] T. Schenkel, A. V. Hamza, A. V. Barnes, and D. H. Schneider, Prog. Surf. Sci. **61**, 23 (1999).
[13] A. S. El-Said *et al.*, Nucl. Instrum. Methods Phys. Res. B **258**, 167 (2007).
[14] A. S. El-Said *et al.*, Phys. Rev. Lett. **100**, 237601 (2008).
[15] M. Terada *et al.*, Nucl. Instrum. Methods Phys. Res. B **235**, 452 (2005).
[16] M. Tona *et al.*, Surf. Sci. **601**, 723 (2007).
[17] R. Heller, S. Facsko, R. A. Wilhelm, and W. Moller, Phys. Rev. Lett. **101**, 096102 (2008).
[18] M. Tona *et al.*, J. Phys.: Conf. Ser. **58**, 331 (2007).
[19] M. Cao, C. Hu, and E. Wang, J. Am. Chem. Soc. **125**, 11196 (2003).
[20] J. F. Ziegler, P. Biersack, and U. Littmark, *The Stopping and Ranges of Ions in Solids* (Pergamon Press, Oxford, 1985).
[21] A. R. Patel and R. P. Singh, Jpn. J. Appl. Phys. **6**, 938 (1967).
[22] A. Arnau *et al.*, Surf. Sci. Rep. **27**, 113 (1997).
[23] H. P. Winter and F. Aumayr, J. Phys. B **32**, R39 (1999).
[24] F. Aumayr and H. P. Winter, Springer Tracts Mod. Phys. **225**, 79 (2007).
[25] S. Facsko, R. Heller, A. S. El-Said, W. Meissl, and F. Aumayr, J. Phys.: Condens. Matter **21**, 224012 (2009).
[26] C. Lemell *et al.*, Solid-State Electron. **51**, 1398 (2007).
[27] R. F. Haglund, Jr. *et al.*, Nucl. Instrum. Methods Phys. Res. B **13**, 525 (1986).
[28] M. Szymonski *et al.*, Surf. Sci. **260**, 295 (1992).
[29] N. Seifert *et al.*, Nucl. Instrum. Methods Phys. Res. B **101**, 131 (1995).
[30] R. T. Williams, K. S. Song, W. L. Faust, and C. H. Leung, Phys. Rev. B **33**, 7232 (1986).
[31] B. Such *et al.*, Phys. Rev. Lett. **85**, 2621 (2000).
[32] T. Neidhart, F. Pichler, F. Aumayr, HP. Winter, M. Schmid, and P. Varga, Phys. Rev. Lett. **74**, 5280 (1995).
[33] M. Sporn *et al.*, Phys. Rev. Lett. **79**, 945 (1997).
[34] G. Hayderer *et al.*, Phys. Rev. Lett. **86**, 3530 (2001).
[35] C. Trautmann, K. Schwartz, and O. Geiss, J. Appl. Phys. **83**, 3560 (1998).
[36] A. S. El-Said *et al.* (unpublished).

2576 OPTICS LETTERS / Vol. 35, No. 15 / August 1, 2010

Optical properties of silver nanowire arrays with 35 nm periodicity

Mukesh Ranjan,[1] Thomas W. H. Oates,[2] Stefan Facsko,[1,*] and Wolfhard Möller[1]

[1]*Institute of Ion Beam Physics and Materials Research, Forschungszentrum Dresden—Rossendorf e.V., P.O. Box 510119, 01314 Dresden, Germany*

[2]*Thin Film Physics, I. F. M., University of Linköping, S-581 83 Linköping, Sweden*

**Corresponding author: s.facsko@fzd.de*

Received January 13, 2010; revised June 3, 2010; accepted June 19, 2010; posted July 9, 2010 (Doc. ID 122661); published July 26, 2010

We present highly ordered Ag nanowire arrays with 35 nm periodicity grown on patterned templates. The optical properties measured using generalized ellipsometry exhibit strong anisotropy. Dielectric functions are calculated by fitting the Jones matrix elements with a biaxial layer model, accounting for both metallic behavior and localized surface plasmon resonances. The amplitude and wavelength maximum of the plasmon resonance perpendicular to the wires increase with increasing wire width and thickness. The dielectric coefficients of 10-mm-wide nanowires show a transition behavior from insulating in UV to metallic above 550 nm. Their potential application as polarization-dependent plasmonic-scattering transparent conductive electrodes is discussed. © 2010 Optical Society of America

OCIS codes: 310.6860, 240.6680, 240.2130, 160.1190.

Arrays of metallic nanowires have attracted much attention in the past several years owing to their unusual plasmonic and electrical properties and their potential in diverse applications such as nanosensors and plasmonic waveguides [1]. Recently, metal nanowires arrays have been proposed as transparent conductive electrodes (TCEs) in solar cells, LEDs, and displays owing to their high electrical-to-optical conductivity ratio [2,3]. One possible route to fabricate dense arrays of nanowires is by using nanostructured substrates, e.g., by extreme UV lithography or nanoimprint lithography, followed by shadow deposition of the metal wires [4]. Bottom-up production of templates has also been explored, including faceted or anodized alumina [5,6] and block copolymers. A fundamental issue connected to miniaturization of wires arrays is the divergence from macroscopic properties at the nanoscale [7]. The absorption and reflection of light with an electric field parallel to the wires (E_x) is increasingly reduced owing to the penetration of the electric fields through the wires. Additionally, polarization of the wires by light with electric field perpendicular to the wires (E_y) gives rise to localized plasmonic effects. The study of these effects in dense nanowire arrays is therefore of fundamental interest.

In this Letter we demonstrate the use of self-organized ion-beam sputtered ripple patterns on Si with periods of 35 nm as effective templates for Ag nanowire arrays formed by oblique angle deposition of evaporated Ag. At these dimensions, the effects of localized surface plasmon resonances (LSPRs) play a strong role in the optical properties of the layer. The ability to tune the plasmon resonance by varying the amount of deposited metal is demonstrated. The reflection properties of the arrays are measured using generalized ellipsometry (GE). By assuming the wire arrays to be an effective medium, the material dielectric functions are determined by fitting a biaxial model accounting for the metallic and localized plasmonic nature of the wires. Transmission properties are subsequently predicted and compared to measured transmission spectra of similar wire arrays on a transparent SiO_2 substrate.

We have previously reported on the growth of self-ordered nanoparticles and cobalt nanowires on prepatterned ripple surfaces [8]. Here we present Ag nanowire arrays and their optical characterization. Low-energy (<1 keV) ion bombardment at an optimized angle (67° to the surface normal for Si) leads to highly ordered ripple patterns on the substrate surface. The periodicity of such ripple patterns can be tuned by adjusting fluence and ion energy [8]. Ripples with a wavelength of 35 nm and an amplitude of 3 nm were prepared on Si (100) with a native oxide layer. The ripple quality was assessed using atomic force microscopy (AFM), an example of which is shown in Fig. 1(a). Ag was deposited perpendicularly to the ripples by electron beam evaporation at an incident angle of 70°. Ag grows in a Volmer–Weber mode on SiO_2, resulting in the formation of small islands. After further deposition, the clusters coalesce and eventually form a percolated network. Oblique angle deposition on rippled substrate results in cluster growth that is preferential along the ripples. Controlling

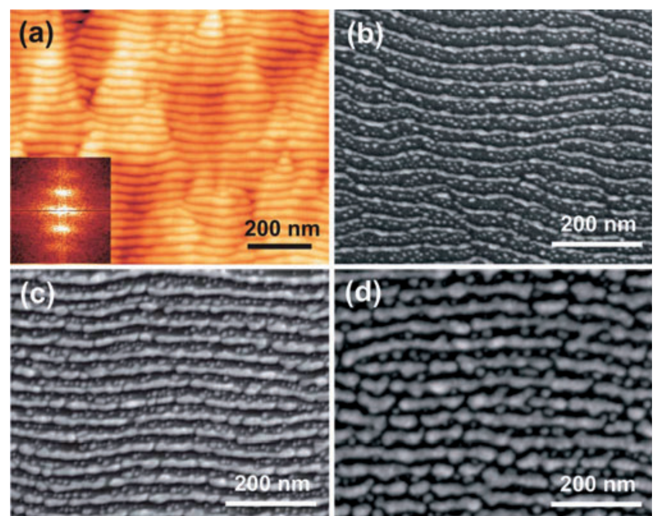

Fig. 1. (Color online) (a) AFM image of ripple patterns on silicon substrate and (b)–(d) silver nanowires decorating the ridges of the ripple patterns by oblique angle evaporation.

0146-9592/10/152576-03$15.00/0 © 2010 Optical Society of America

deposition rate and time leads to aligned particles and wires. At room temperature, nanowires of increasing width are formed at increasing deposition time. Scanning electron micrographs (SEMs) of three nanowire arrays of increasing width of 10 nm, 12.5 nm, and 15 nm are shown in Figs. 1(b)–1(d).

The reflectance properties were measured using GE. GE measures the ratio of the complex reflection coefficients, r_{ij} of polarized light with electric fields oriented parallel (p) and perpendicular (s) to the plane of incidence. The four complex valued coefficients define the 2×2 Jones matrix, which is sufficient to completely describe the reflection characteristics of ellipsometric analysis in nondepolarizing samples. In isotropic materials, the off-diagonal elements r_{ps} and r_{sp} are vanishingly small, so that standard ellipsometry is sufficient to determine the material dielectric functions. In anisotropic systems, such as we expect here, a proportion of incident p-polarized light is converted to s-polarized light (and vice versa), and the off-diagonal elements must be determined using GE [9]. The GE parameters Ψ_{ij} and Δ_{ij} are defined by

$$\frac{r_{pp}}{r_{ss}} = \tan \Psi_{pp} e^{i\Delta_{pp}},$$
$$\frac{r_{ps}}{r_{pp}} = \tan \Psi_{ps} e^{i\Delta_{ps}},$$
$$\frac{r_{sp}}{r_{ss}} = \tan \Psi_{sp} e^{i\Delta_{sp}}.$$

Measurement of the six independent parameters $(\Psi, \Delta)_{pp,ps,sp}$ that define the Jones matrix requires a sample orientation in which the plane of incidence of the light is neither parallel nor perpendicular to the ripple direction. Maximum off-diagonal elements are achieved using the chosen ripple rotation of 45° to the plane of incidence. Using a J. A. Woollam M2000 rotating compensator ellipsometer, the polarized reflection states were measured at multiple polarizer settings, from which the Jones matrix elements were extracted by linear regression. The resulting Jones matrix values corresponding to the samples shown in Figs. 1(b)–1(d) are plotted in Fig. 2. $\Psi_{pp,ps,sp}$ values are higher for thicker wires. Off-diagonal Jones matrix elements were found to be zero for the rippled substrate without Ag wires.

To determine the dielectric functions of the wire array, we first define the layer stack consisting of an Ag nanowire layer, a thin native SiO_2 layer, and the Si substrate in the ellipsometry software WVASE32. The Fresnel equations routinely used in ellipsometric analysis are not valid for the present anisotropic samples. We utilize the 4×4 matrix method described by Schubert [9]. The nanowire layer is a biaxially anisotropic layer with three independent optical axes (x, y, z) defined as parallel (x) and perpendicular (y) to the wires, and normal to the surface (z). The rotation of the substrate in the plane is accounted for by setting the Euler angle of rotation at 45°. Ag dielectric functions from the literature [10] are used as a basis for the three orthogonal dielectric functions $(\epsilon_x, \epsilon_y, \epsilon_z)$. These are fitted with a Drude component to account for the free electrons and a Tauc–Lorentz [11] component to approximate the interband transitions ($4d$–$5s$)

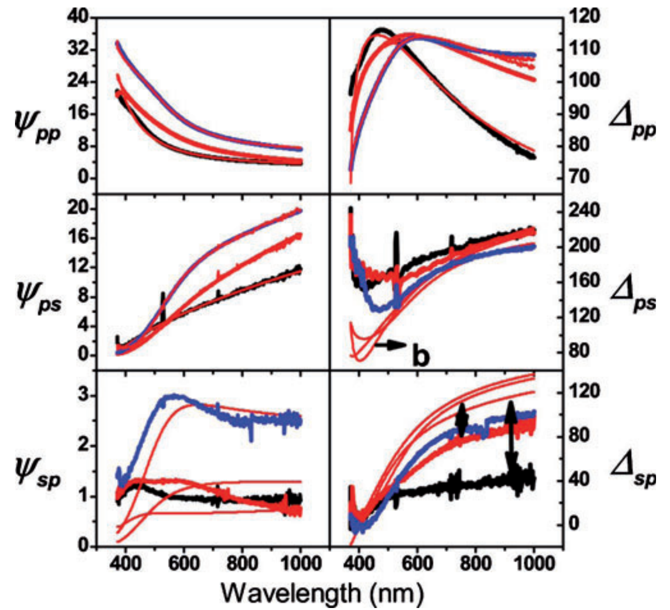

Fig. 2. (Color online) Measured values (thick curves) of the GE parameters, corresponding to Figs. 1(b) (black), 1(c) (red), and 1(d) (blue). The thin red curves represent the respective model results.

lying just outside the range of measurement at 3.8 eV. The Drude component is characterized by the metal plasma frequency, ω_p, which is proportional to the free electron concentration, and the broadening parameter, Γ, which is dominated by electron scattering from surfaces and crystal defects. For ϵ_x (parallel to the wires) and ϵ_z (normal to the surface), both ω_p and Γ are set as fitting parameters in the model. ω_p is expected to be below that of the bulk, because in both directions there is a large void content. Γ is expected to increase owing to increased surface scattering. For ϵ_y the Drude component is replaced by a Lorentzian function, which accounts for the LSPR expected from Ag elements of this dimension. A similar result is achieved by using a Drude model in a Maxwell–Garnett effective medium approximation [11]. Si and SiO_2 bulk dielectric functions are used for the other layers. A mean-square error (MSE) minimization algorithm is used to fit the model parameters to the measured elements of the Jones matrix. Although the model contains a number of simplifying assumptions, the result of the fitting (see Fig. 2) provides physically meaningful results with low parameter correlation and acceptable MSE values. The measured values of Ψ_{sp} are quite small, which amplifies the apparent difference with the fitted values. The model deviation from the measured values of Δ_{ps} and Δ_{sp} may be due to the simplifying assumptions of the rippled substrate.

Figure 3 shows the real and imaginary parts of the orthogonal dielectric functions $(\epsilon_x, \epsilon_y, \epsilon_z)$ of the three samples as determined from the GE fitting. Both ϵ_x and ϵ_z display predominantly metallic behavior, although ϵ_x of sample b is positive in the UV, indicating an insulating nature, while at wavelengths higher than 550 nm it is negative. ϵ_z is very close to the values of bulk Ag [10]. Note the strong resonance in the imaginary parts of ϵ_y due to the LSPR. The amplitude and wavelength maximum of the resonance increase with increasing wire

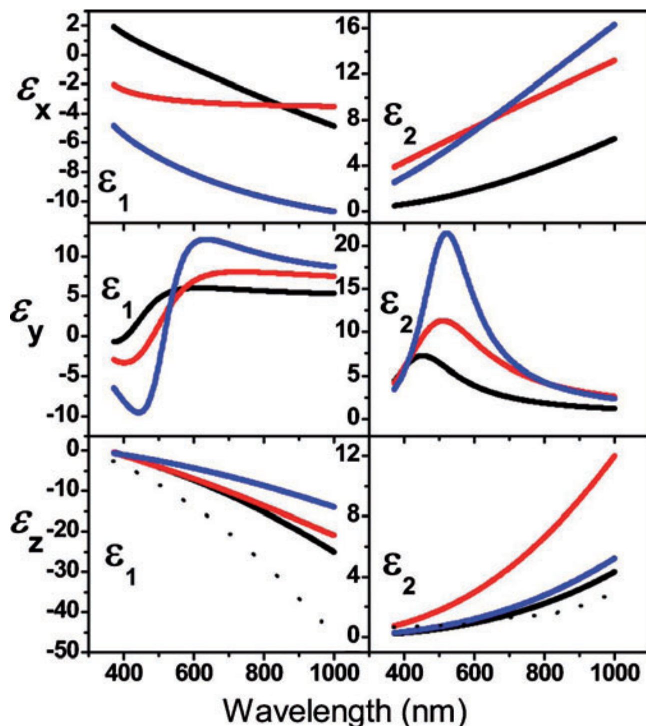

Fig. 3. (Color online) Biaxial dielectric functions of the arrays shown in Figs. 1(b) (black), 1(c) (red), and 1(d) (blue) determined by fitting GE measurements shown in Fig. 2. Black dotted curves are bulk Ag dielectric function.

thickness due to the increased proportion of Ag in the volume content of the layer [12]. Also note that the maximum values of the imaginary part of ϵ_y located at 520 nm are consistently higher than those of the imaginary part of ϵ_x across the measured range. This illustrates the strength of the absorption cross section of the LSPR.

Thus, armed with the biaxial dielectric functions of the layers, we may simulate the expected normal incidence transmission properties of nanowire arrays produced on transparent substrates. Figure 4(i) shows the simulated transmission of x-polarized, T_x, and y-polarized, T_y, light for the three arrays on a 0.1-mm-thick SiO_2 substrate. The main message is that for all three samples, the extinction ratio (T_x/T_y) is highly wavelength dependent. T_x is relatively constant across the range, the difference in magnitude being primarily dependent on the layer thickness of the Ag. T_y is small in the visible range near the LSPR maximum. However, in the IR it is above 80% for all three materials. In Fig. 4(ii), the measured transmission for Ag nanowires grown on rippled transparent SiO_2 substrate is shown. The good agreement with the calculated transmission spectra from Fig. 4(i) supports the validity of our model and of the determined dielectric functions.

The unusual plasmonic properties lead us to speculate on their application in photovoltaics. A desirable goal in this field is to utilize ultrathin metal films as the TCE. The

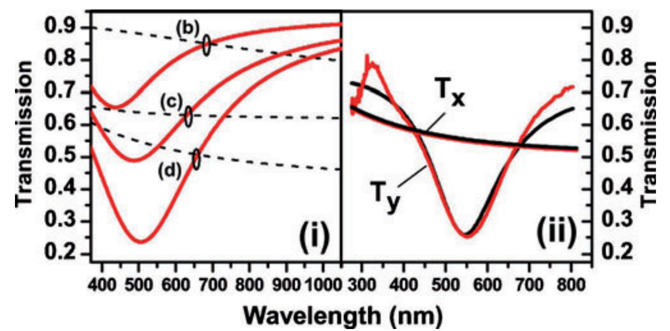

Fig. 4. (Color online) (i) Simulated transmission spectra of the three arrays from Fig. 1. Electric field vectors parallel, E_x (dashed black line) and perpendicular, E_y (solid red line) to the direction of the wires. (ii) Measured and modeled transmission spectra of Ag wires deposited on transparent SiO_2.

materials considered here would function not only as the TCE with transparencies above 80% over most of the measured spectral range (sample b) with bulk silver-like dielectric functions (high electrical conductivity) but also as a plasmonic scatterer to improve the light trapping in the absorption layer, as has been shown recently [13]. By combining the two elements into a single layer, the compactness can be increased. Alternatively, one may consider using these materials as polarized plasmonic color filters in LCDs. Finally, an easy upscaling of the production process for large-area production can be anticipated.

We acknowledge the financial support of the Deutsche Forschungsgemeinschaft (DFG) and E. Christalle and M. Fritzsche for SEM measurements.

References

1. S. Lal and S. Link, Nat. Photon. **1**, 641 (2007).
2. A. Kumar and C. Zhou, ACS Nano **4**, 11 (2010).
3. J. Y. Lee, S. T. Connor, Y. Cui, and P. Peumans, Nano Lett. **8**, 689 (2008).
4. Y. Ekinci, H. H. Solak, C. David, and H. Sigg, Opt. Express **14**, 2323 (2006).
5. G. Riveros, S. Green, A. Cortes, and E. A. Dalchiele, Nanotechnology **17**, 561 (2006).
6. S. Camelio, D. Babonneau, and L. Simonot, Europhys. Lett. **79**, 47002 (2007).
7. B. Lamprecht, G. Schider, and A. Leitner, Phys. Rev. Lett. **84**, 4721 (2000).
8. T. W. H. Oates, A. Keller, and S. Facsko, Appl. Phys. Lett. **93**, 063106 (2008).
9. M. Schubert, Phys. Rev. B **53**, 4265 (1996).
10. P. B. Johnson and R. W. Christy, Phys. Rev. B **6**, 4370 (1972).
11. H. Wormeester, E. S. Kooij, and B. Poelsema, Phys. Status Solidi A **205**, 756 (2008).
12. R. Doremus, Thin Solid Films **326**, 205 (1998).
13. V. E. Ferry, L. A. Sweatlock, D. Pacifici, and H. A. Atwater, Nano Lett. **8**, 4391 (2008).

Statistics

Books

1. Rebohle, L.; Skorupa, W.
Rare-earth implanted MOS devices for silicon photonics
Springer Verlag Berlin, 2010; ISBN: 978-3642144462

Publications

1. Abrasonis, G.; Kovács, G. J.; Tucker, M.; Heller, R.; Krause, M.; Guenette, M.; Munnik, F.; Lehmann, J.; Tadich, A.; Cowie, B. C. C.; Thomsen, L.; Bilek, M. M. M.; Möller, W.
Sculpting nanoscale precipitation patterns in nanocomposite thin films via hyperthermal ion deposition
Applied Physics Letters ***97****, 163108 (2010).*

2. Abrasonis, G.; Oates, T. W. H.; Kovacs, G.; Grenzer, J.; Persson, P. O. A.; H. Heinig, K.-H.; Martinavicius, A.; Jeutter, N.; Baehtz, C.; Tucker, M.; Bilek, M. M. M.; Möller, W.
Nanoscale precipitation patterns in carbon-nickel nanocomposite thin films: Period and tilt control via ion energy and deposition angle
Journal of Applied Physics ***108****, 043503 (2010).*

3. Altmaier, M.; Herpers, U.; Delisle, G.; Merchel, S.; Ott, U.
Glaciation history of Queen Maud Land (Antarctica) using in situ produced cosmogenic ^{10}Be, ^{26}Al and ^{21}Ne
Polar Science ***4****, 42 (2010).*

4. Ankiewicz, A. O.; Martins, J. S.; Carmo, M. C.; Grundmann, M.; Zhou, S.; Schmidt, H.; Sobolev, N. A.
Ferromagnetic resonance on metal nanocrystals in Fe and Ni implanted ZnO
Journal of Applied Physics ***107****, 09B518 (2010).*

5. Anwand, W.; Brauer, G.; Cowan, T. E.; Grambole, D.; Skorupa, W.; Cizek, J.; Kuriplach, J.; Prochazka, I.; Egger, W.; Sperr, P.
Structural characterization of H plasma-doped ZnO single crystals by positron annihilation spectroscopies
Physica Status Solidi (A) ***207****, 2415 (2010).*

6. Anwand, W.; Brauer, G.; Cowan, T. E.; Heera, V.; Schmidt, H.; Skorupa, W.; von Wenckstern, H.; Brandt, M.; Benndorf, G.; Grundmann, M.
Structural characterization of H plasma-doped ZnO single crystals by Hall measurements and photoluminescence studies
Physica Status Solidi (A) ***207****, 2426 (2010).*

7. Arnold, M.; Merchel, S.; Bourlès, Didier L.; Braucher, R.; Benedetti, L.; Finkel, Robert C.; Aumaître, G.; Gottdang, A.; Klein, M.
The French accelerator mass spectrometry facility ASTER: Improved performance and developments
Nuclear Instruments and Methods in Physics Research B ***268****, 1954 (2010).*

8. Balabanov, S.; Tsvetkova, T.; Borisova, E.; Avramov, L.; Bischoff, L.; Zuk, J.
Optical properties of Si^+ implanted PMMA
Journal of Physics: Conference Series ***233****, 012032-1 (2010).*

9. Beck, M.; Schäfer, H.; Klatt, G.; Demsar, J.; Winnerl, S.; Helm, M.; Dekorsy, T.
Impulsive terahertz radiation with high electric fields from an amplifier-driven large-area photoconductive antenna
Optics Express ***18****, 9251 (2010).*

10. Beckers, M.; Eriksson, F.; Lauridsen, J.; Baehtz, C.; Jensen, J.; Hultman, L.
Formation of basal plane fiber-textured Ti_2AlN films on amorphous substrates
Physica Status Solidi, Rapid Research Letters ***4****, 121 (2010).*

11. Bergeard, N.; Jamet, J.-P.; Ferré, J.; Mougin, A.; Fassbender, J.
Spin reorientation transition and phase diagram in an He^+ ion irradiated ultrathin Pt/Co(0.5 nm)/Pt film
Journal of Applied Physics ***108****, 103915 (2010).*

12. Berger, A.; Mangin, S.; McCord, J.; Hellwig, O.; Fullerton, E. E.
Cumulative minor loop growth in Co/Pt- and Co/Pd-multilayers
Physical Review B ***82****, 104423-1 (2010).*

13. Bernert, K.; Oestreich, Ch.; Bollmann, J.; Mikolajick, T.
The influence of bottom oxide thickness on the extraction of the trap energy distribution in SONOS (silicon-oxide-nitride-oxide-silicon) structures
Applied Physics A ***100****, 249 (2010).*

14. Bhattacharyya, J.; Wagner, M.; Helm, M.; Hopkinson, M.; Wilson, L. R.; Schneider, H.
Terahertz activated luminescence of trapped carriers in InGaAs/GaAs quantum dots
Applied Physics Letters ***97****, 031101 (2010).*

15. Bischoff, L.; Pilz, W.; Mazarov, P.; Wieck, A. D.
Comparison of bismuth emitting liquid metal ion sources
Applied Physics A ***99****, 145 (2010).*

16. Buljan, M.; Bogdanovic-Radovic, I.; Karlusic, M.; Desnica, U.; Radic, N.; Skukan, N.; Drazic, G.; Ivanda, M.; Gamulin, O.; Matej, Z.; Vales, V.; Grenzer, J.; Cornelius, T.; Metzger, H.; Holy, V.
Generation of an ordered Ge quantum dot array in an amorphous silica matrix by ion beam irradiation: Modeling and structural characterization
Physical Review B ***81****, 085321 (2010).*

17. Buljan, M.; Grenzer, J.; Holý, V.; Radić, N.; Mišić-Radić, T.; Levichev, S.; Bernstorff, S.; Pivac, B.; Capan, I.
Structural and charge trapping properties of two bilayer (Ge + SiO_2) / SiO_2 films deposited on rippled substrate
Applied Physics Letters ***97****, 163117 (2010).*

18. Buljan, M.; Grenzer, J.; Keller, A.; Radic, N.; Vales, V.; Bernstorff, S.; Cornelius, T.; Metzger, H.; Holy, V.
Growth of spatially ordered Ge nanoclusters in an amorphous matrix on rippled substrates
Physical Review B ***82****, 125316 (2010).*

19. Bürger, D.; Zhou, S.; Pandey, M.; Genzer, J.; Roshchupkina, O.; Anwand, W.; Reuther, H.; Gottschalch, V.; Helm, M.; Schmidt, H.
Application of pulsed laser annealing to ferromagnetic GaMnAs
Physical Review B ***81****, 115202 (2010).*

20. Chandramohan, S.; Strache, T.; Sarangi, S. N.; Sathyamoorthy, R.; Som, T.
Influence of implantation induced Ni-doping on structural, optical, and morphological properties of nanocrystalline CdS thin films
Materials Science and Engineering B ***171****, 16 (2010).*

21. Cherkouk, C.; Rebohle, L.; Skorupa, W.
Bioconjugation of the estrogen receptor hER(alpha) to a quantum dot dye for a controlled immobilization on the SiO_2 surface
Journal of Colloid and Interface Science / In press (2010).

22. Cizek, J.; Melikhzova, O.; Prochazka, I.; Kuriplach, J.; Kuzel, R.; Brauer, G.; Anwand, W.; Konstantinova, T. E.; Danilenko, I. A.
Defect studies of nanocrystalline zirconia powders and sintered ceramics
Physical Review B ***81****, 024116 (2010).*

23. Danesh, P.; Pantchev, B.; Wiezorek, J.; Schmidt, B.
Effect of keV ion irradiation on mechanical properties of hydrogenated amorphous silicon
Nuclear Instruments and Methods in Physics Research B ***268****, 2660 (2010).*

24. Das Kanungo, P.; Kögler, R.; Werner, P.; Gösele, U.; Skorupa, W.
A novel method to fabricate silicon nanowire p-n junctions by a combination of ion implantation and in-situ doping
Nanoscale Research Letters ***5****, 243 (2010).*

25. Davydok, A.; Biermanns, A.; Pietsch, U.; Grenzer, J.; Paetzelt, H.; Gottschalch, V.
X-ray diffraction from periodically patterned GaAs nanorods grown onto GaAs[111]B
Metallurgical and Materials Transactions A ***41****, 1191 (2010).*

26. Dupuy, J. C.; Dubois, C.; Prudon, G.; Gautier, B.; Kögler, R.; Akhmadaliev, S.; Perrat-Mabilon, A.; Peaucelle, C.
Isotopic Comparative Method (ICM) for the determination of variations of the useful ion yields in boron doped silicon as a function of oxygen concentration in the 0 - 10 at% range
Surface and Interface Analysis ***2010****, 42 (2010).*

27. El-Said, A. S.; Heller, R.; Aumayr, F.; Facsko, S.
Pyramidal pits created by single highly charged ions in BaF_2 single crystals
Physical Review B ***82****, 033403 (2010).*

28. Fan, J.; Ding, G.; Fung, S.; Xie, Z.; Zhong, Y.; Wong, K.; Brauer, G.; Anwand, W.; Grambole, D.; Ling, C.
Shallow acceptor and hydrogen impurity in p-type arsenic-doped ZnMgO films grown by radio frequency magnetron sputtering
*Semiconductor Science and Technology **25**, 085009 (2010).*

29. Fitting, H.-J.; Fitting Kourkoutis, L.; Roushdey, S.; Zamoryanskaya, M. V.; Schmidt, B.
Silicon nanocluster aggregation in SiO_2:Si layers
*Physica Status Solidi (A) **207**, 117 (2010).*

30. Fitting, H.-J.; Fitting Kourkoutis, L.; Salh, R.; Kolesnikova, E. V.; Zamoryanskaya, M. V.; von Czarnowski, A.; Schmidt, B.
Silicon cluster aggregation in silica layers
*Solid State Phenomena **156-158**, 529 (2010).*

31. Gago, R.; Vinnichenko, M.; Redondo-Cubero, A.; Czigany, Z.; Vazquez, L.
Surface morphology of heterogeneous nanocrystalline rutile/amorphous anatase TiO_2 films grown by reactive pulsed magnetron sputtering
*Plasma Processes and Polymers **7**, 813 (2010).*

32. Gemming, S.; Enyashin, A.; Frenzel, J.; Seifert, G.
Adsorption of nucleotides on the rutile (110) surface
*International Journal of Materials Research **101**, 758 (2010).*

33. Gemming, S.; Seifert, G.; Götz, M.; Fischer, T.; Ganteför, G.
Transition metal sulfide clusters below the cluster-platelet transition – theory and experiment
*Physica Status Solidi (B) **247**, 1069 (2010).*

34. Gordillo, N.; Rivera, A.; Grötzschel, R.; Munnik, F.; Güttler, D.; Crespillo, M. L.; Agulló-López, F.; González-Arrabal, R.
Compositional, structural and morphological modifications of N-rich Cu_3N films induced by irradiation with Cu^{8+} at 42 MeV
*Journal of Physics D: Applied Physics **43**, 345301 (2010).*

35. Hanisch, A.; Biermanns, A.; Pietsch, U.; Grenzer, J.; Facsko, S.
Xe ion beam induced ripple structures on differently oriented single-crystalline Si surfaces
*Journal of Physics D: Applied Physics **43**, 112001 (2010).*

36. Heera, V.; Mücklich, A.; Posselt, M.; Voelskow, M.; Wündisch, C.; Schmidt, B.; Skrotzki, R.; Heinig, K.-H.; Herrmannsdörfer, T.; Skorupa, W.
Heavily Ga-doped Germanium layers produced by ion implantation and flash lamp annealing - structure and electrical activation
*Journal of Applied Physics **107**, 053508-1 (2010).*

37. Henseler, P.; Erbe, A.; Köppl, M.; Leiderer, P.
Density reduction and diffusion in driven two-dimensional colloidal systems through microchannels
*Physical Review E **81**, 041402 (2010).*

38. Herrmannsdörfer, T.; Skrotzki, R.; Heera, V.; Ignatchik, O.; Uhlarz, M.; Mücklich, A.; Posselt, M.; Schmidt, B.; Heinig, K.-H.; Skorupa, W.; Voelskow, M.; Wündisch, C.; Helm, M.; Wosnitza, J.
Superconductivity in thin-film germanium in the temperature regime around 1 K
*Superconductor Science and Technology **23**, 034007 (2010).*

39. Hiller, D.; Götze, S.; Munnik, F.; Jivanescu, M.; Gerlach, J. W.; Vogt, J.; Pippel, E.; Zakharov, N.; Stesmans, A.; Zacharias, M.
Nitrogen at the Si-nanocrystal / SiO_2 interface and its influence on luminescence and interface defects
*Physical Review B **82**, 195401 (2010).*

40. Hiller, D.; Zierold, R.; Bachmann, J.; Alexe, M.; Yang, Y.; Gerlach, J. W.; Stesmans, A.; Jivanescu, M.; Müller, U.; Vogt, J.; Hilmer, H.; Löper, P.; Künle, M.; Munnik, F.; Nielsch, K.; Zacharias, M.
Low temperature silicon dioxide by thermal atomic layer deposition: Investigation of material properties
*Journal of Applied Physics **107**, 064314 (2010).*

41. Höglund, C.; Alling, B.; Birch, J.; Beckers, M.; Persson, P. O. Å.; Baehtz, C.; Czigány, Z.; Jensen, J.; Hultman, L.
Effects of volume mismatch and electronic structure on the decomposition of ScAlN and TiAlN solid solutions
*Physical Review B **81**, 2241011 (2010).*

42. Iida, K.; Haindl, S.; Thersleff, T.; Haenisch, J.; Kurth, F.; Kidszun, M.; Huehne, R.; Moench, I.; Schultz, L.; Holzapfel, B.; Heller, R.
Influence of Fe buffer thickness on the crystalline quality and the transport properties of

$Fe/Ba(Fe_{1-x}Co_x)_2As_2$ bilayers
*Applied Physics Letters **97**, 172507 (2010).*

43. Jacob, R.; Winnerl, S.; Schneider, H.; Helm, M.; Wenzel, M. T.; von Ribbeck, H.-G.; Eng, Lukas M.; Kehr, Susanne C.
Quantitative determination of the charge carrier concentration of sub-surface implanted silicon by IR-near-field spectroscopy
*Optics Express **18**, 26206 (2010).*

44. Kalinichenka, S.; Roentzsch, L.; Baehtz, C.; Kieback, B.
Hydrogen desorption kinetics of melt-spun and hydrogenated Mg90Ni10 and Mg80Ni10Y10 using in-situ synchrotron X-ray diffraction and thermogravimetry
*Journal of Alloys and Compounds **496**, 608 (2010).*

45. Kang, N.; Erbe, A.; Scheer, E.
Observation of negative differential resistance in DNA molecular junctions
*Applied Physics Letters **96**, 023701 (2010).*

46. Kanjilal, A.; Prucnal, S.; Minniti, M.; Skorupa, W.; Helm, M.; Facsko, S.
Crystalline ripples at the surface of ion eroded strained $Si_{0.8}Ge_{0.2}$ epilayers
*Journal of Applied Physics **107**, 073513 (2010).*

47. Kanjilal, A.; Prucnal, S.; Rebohle, L.; Voelskow, M.; Helm, M.; Skorupa, W.
Comparison of the room temperature 1.53 µm Er photoluminescence from flash lamp and furnace annealed Er-doped Ge-rich SiO_2 layers
*Journal of Applied Physics **107**, 113523 (2010).*

48. Kanjilal, A.; Rebohle, L.; Voelskow, M.; Helm, M.; Skorupa, W.
Controlling blue-violet electroluminescence of Ge-rich Er-doped SiO_2 layers by millisecond annealing using flash lamps
*Journal of Applied Physics **107**, 023114-1 (2010).*

49. Keller, A.; Facsko, S.
Ion-induced nanoscale ripple patterns on Si surfaces - theory and experiment
*Materials **3**, 4811 (2010).*

50. Keller, A.; Facsko, S.
Tuning the quality of nanoscale ripple patterns by sequential ion-beam sputtering
*Physical Review B **82**, 155444 (2010).*

51. Krausslich, J.; Hofer, S.; Zastrau, U.; Jeutter, N.; Baehtz, C.
Temperature dependence of lattice parameters of langasite single crystals
*Crystal Research and Technology **45**, 490 (2010).*

52. Krone, P.; Brombacher, C.; Makarov, D.; Lenz, K.; Ball, D.; Springer, F.; Rohrmann, H.; Fassbender, J.; Albrecht, M.
Nanocap arrays of granular $CoCrPt:SiO_2$ films on silica particles: Tailoring of the magnetic properties by Co^+ irradiation
*Nanotechnology **21**, 385703 (2010).*

53. Krstajic, P. M.; Peeters, F. M.; Helm, M.
Landau levels and magnetopolaron effect in dilute GaAs:N
*Solid State Communications **150**, 1575 (2010).*

54. Kumar, H.; Gosh, S.; Bürger, D.; Zhou, S.; Kabiraj, D.; Avasthi, D. K.; Grötzschel, R.; Schmidt, H.
Microstructure, electrical, magnetic, and extraordinary Hall effect studies in $Ni:SiO_2$ nanogranular films synthesized by atom beam sputtering
*Journal of Applied Physics **107**, 113913 (2010).*

55. Kunze, T.; Gemming, S.; Luschtinetz, R.; Pankoke, V.; Morawetz, K.; Seifert, G.
Electronic transport properties through thiophenes on switchable domains
*Physical Review B **81**, 115401 (2010).*

56. Kunze, T.; Gemming, S.; Numazawa, S.; Schreiber, M.
Low-temperature modeling for degenerate and frustrated Heisenberg systems with anisotropy
*Computer Physics Communications **181**, 806 (2010).*

57. Kutschan, B.; Morawetz, K.; Gemming, S.
Modeling the morphogenesis of brine channels in sea ice
*Physical Review E **81**, 036106 (2010).*

58. Liu, S.-P.; Weisbrod, S.; Tang, Z.; Marx, A.; Scheer, E.; Erbe, A.
Direct measurement of electrical transport through G-Quadruplex DNA with mechanically controllable

break junction electrodes
Angewandte Chemie - International Edition (2010).

59. Lorenz, K.; Magalhães, S.; Franco, N.; Darakchieva, V.; Barradas, N. P.; Alves, E.; Pereira, S.; Correia, M. R.; Munnik, F.; Martin, R. W.; O'Donnell, K. P.; Watson, I. M.
$Al_{1-x}In_xN$/GaN bilayers: structure, morphology and optical properties
Physica Status Solidi (B) ***247****, 1740 (2010).*

60. Männel, M.; Morawetz, K.; Lipavsky, P.
Multiple condensed phases in attractively interacting bose systems
New Journal of Physics ***12****, 033013 (2010).*

61. Markó, D.; Lenz, K.; Strache, T.; Kaltofen, R.; Fassbender, J.
Measuring the saturation magnetization in samples with unknown magnetic volume
IEEE Transactions on Magnetics ***46****, 1711 (2010).*

62. Markó, D.; Strache, T.; Lenz, K.; Fassbender, J.; Kaltofen, R.
Determination of the saturation magnetization from perpendicular magnetic anisotropy measurements of ion irradiated multilayers
Applied Physics Letters ***96****, 022503 (2010).*

63. Martins, R. M. S.; Musat, V.; Mücklich, A.; Franco, N.; Fortunato, E.
Characterization of mesoporous ZnO:SiO_2 films obtained by the sol-gel method
Thin Solid Films ***518****, 7002 (2010).*

64. Martins, R. M. S.; Schell, N.; Reuther, H.; Pereira, L.; Mahesh, K. K.; Silva, R. J. C.; Fernandes, F. M. B.
Texture development, microstructure and phase transformation characteristics of sputtered Ni-Ti Shape Memory Alloy films on TiN<111>
Thin Solid Films ***519****, 122 (2010).*

65. Martins, R. M. S.; Schell, N.; von Borany, J.; Mahesh, K. K.; Silva, R. J. C.; Braz Fernandes, F. M.
Structural evolution of magnetron sputtered shape memory alloy Ni–Ti films
Vacuum ***84****, 913 (2010).*

66. Masset, P. J.; Yankov, R.; Kolitsch, A.; Schütze, M.
Comparison of fluorination treatments to improve the high temperature oxidation resistance of TiAl alloys in SO_2 containing environments
Materials Science Forum ***638-642****, 1374 (2010).*

67. Melikhova, O.; Kuriplach, J.; Cizek, J.; Prochazka, I.; Brauer, G.; Anwand, W.
Investigation of hydrogen interaction with defects in zirconia
Journal of Physics: Conference Series ***225****, 012035 (2010).*

68. Menendez, E.; Garroni, S.; Lopez Ortega, A.; Estrader, M.; Liedke, M. O.; Fassbender, J.; Solsona, P.; Surinach, S.; Baro, M. D.; Nogues, J.
Magnetic measurements as a sensitive tool for studying dehydrogenation processes in hydrogen storage materials
Journal of Physical Chemistry C ***114****, 16818 (2010).*

69. Menendez, E.; Stinville, J. C.; Tromas, C.; Templier, C.; Villechaise, P.; Rivière, J. P.; Drouet, M.; Martinavicius, A.; Abrasonis, G.; Fassbender, J.; Baro, M. D.; Sort, J.; Nogues, J.
Out-of-plane magnetic patterning on austenitic stainless steels using plasma nitriding
Applied Physics Letters ***96****, 242509 (2010).*

70. Merchel, S.; Benedetti, L.; Bourlès, D. L.; Braucher, R.; Dewald, A.; Faestermann, T.; Finkel, R. C.; Korschinek, G.; Masarik, J.; Poutivtsev, M.; Rochette, P.; Rugel, G.; Zell, K.-O.
A multi-radionuclide approach for in-situ produced terrestrial cosmogenic nuclides: ^{10}Be, ^{26}Al, ^{36}Cl and ^{41}Ca from carbonate rocks
Nuclear Instruments and Methods in Physics Research B ***268****, 1179 (2010).*

71. Mironov, O. A.; Goiran, M.; Galibert, J.; Kozlov, D. V.; Ikonnikov, A. V.; Spirin, K. E.; Gavrilenko, V. I.; Isella, G.; Kummer, M.; von Känel, H.; Drachenko, O.; Helm, M.; Wosnitza, J.; Morris, R. J. H.; Leadley, D. R.
Cyclotron resonance of extremely conductive 2D holes in high Ge content strained heterostructures
Journal of Low Temperature Physics ***159****, 216 (2010).*

72. Miura, N.; Kozlova, N. V.; Dörr, K.; Freudenberger, J.; Schultz, L.; Drachenko, O.; Sawano, K.; Shiraki, Y.
Quantum transport and cyclotron resonance study of Ge/SiGe quantum wells in high magnetic fields
Journal of Low Temperature Physics ***159****, 222 (2010).*

73. Morawetz, K.; Maennel, M.
Impossibility to describe repulsion with contact interaction
Physics Letters A ***374****, 644 (2010).*

74. Nasdala, L.; Grambole, D.; Götze, J.; Kempe, U.; Váczi, T.
Helium irradiation study on zircon
Mineralogy and Petrology (2010).

75. Naydenova, Ts.; Atanasov, P.; Koleva, M.; Nedialkov, N.; Perriere, J.; Defourneau, D.; Fukuoka, H.; Obara, M.; Baumgart, C.; Zhou, S.; Schmidt, H.
Influence of vanadium concentration on the microstructure and magnetic properties of V-doped ZnO thin films
*Thin Solid Films **518**, 5505 (2010).*

76. Nazarov, A. N.; Tiagulskyi, S. I.; Tyagulskyy, I. P.; Lysenko, V. S.; Rebohle, L.; Lehmann, J.; Prucnal, S.; Voelskow, M.; Skorupa, W.
The effect of rare-earth clustering on charge trapping and electroluminescence in rare-earth implanted metal-oxide-semiconductor light-emitting devices
*Journal of Applied Physics **107**, 123112 (2010).*

77. Neve, S.; Masset, P. J.; Yankov, R. A.; Kolitsch, A.; Zschau, H.-E.; Schütze, M.
High temperature oxidation resistance of fluorine-treated TiAl alloys: Chemical vs. ion beam fluorination techniques
*Nuclear Instruments and Methods in Physics Research B **268**, 3381 (2010).*

78. Ney, A.; Opel, M.; Kaspar, T. C.; Ney, V.; Ye, S.; Ollefs, K.; Kammermeier, T.; Bauer, S.; Nielsen, K.-W.; Goennenwein, S. T. B.; Engelhard, M. H.; Zhou, S.; Potzger, K.; Simon, J.; Mader, W.; Heald, S. M.; Cezar, J. C.; Wilhelm, F.; Rogalev, A.; Gross, R.; Chambers, S. A.
Advanced spectroscopic synchrotron techniques to unravel the intrinsic properties of dilute magnetic oxides: The case of Co:ZnO
*New Journal of Physics **12**, 013020 (2010).*

79. Nomura, K.; Németh, Z.; Reuther, H.
^{57}Fe implantation effect of Sb doped SnO_2 films
*Journal of Physics: Conference Series **217**, 012118 (2010).*

80. Odor, G.; Liedke, B.; Heinig, K.-H.
Surface pattern formation and scaling described by conserved lattice gases
*Physical Review E **81**, 051114 (2010).*

81. Odor, G.; Liedke, B.; Heinig, K.-H.
Directed dimer diffusion describing the Kardar-Parisi-Zhang surface growth
*Physical Review E **81**, 031112 (2010).*

82. Oliveira, A. F.; Gemming, S.; Seifert, G.
Molecular dynamics simulations of BMP-2 adsorption on a hydrophobic surface
*Materials Science and Engineering Technology **41**, 1048 (2010).*

83. Orlowski, T.; Forstner, O.; Golser, R.; Kutschera, W.; Merchel, S.; Martschini, M.; Priller, A.; Steier, P.; Vockenhuber, C.; Wallner, A.
Comparison of detector systems for the separation of ^{36}Cl and ^{36}S with a 3-MV tandem
*Nuclear Instruments and Methods in Physics Research B **268**, 847 (2010).*

84. Ou, X.; Das Kanungo, P.; Kögler, R.; Werner, P.; Gösele, U.; Skorupa, W.; Wang, X.
Three-dimensional carrier profiling of individual Si nanowires by scanning spreading resistance microscopy
*Advanced Materials **22**, 4020 (2010).*

85. Ou, X.; Das Kanungo, P.; Kögler, R.; Werner, P.; Skorupa, W.; Gösele, U.; Wang, X.
Carrier profiling of individual Si nanowires by scanning spreading resistance microscopy
*Nano Letters **10**, 171 (2010).*

86. Pandey, B.; Ghosh, S.; Srivastava, P.; Kumar, P.; Kanjilal, D.; Zhou, S.; Schmidt, H.
Room temperature transparent ferromagnetism in 200 keV Ni^{2+} ion implanted PLD grown ZnO/sapphire film
*Journal of Applied Physics **107**, 023901 (2010).*

87. Pantchev, B.; Danesh, P.; Schmidt, B.; Grambole, D.; Bischoff, L.
Ion-beam induced hydrogen redistribution in a-Si:H-based triple layer structures
*Journal of Physics: Conference Series **253**, 012055 (2010).*

88. Pantchev, B.; Danesh, P.; Wiezorek, J.; Schmidt, B.
Nanoindentation-induced pile-up in hydrogenated amorphous silicon
*Journal of Physics: Conference Series **253**, 012054 (2010).*

89. Patschureck, C.; Kaltofen, R.; Mönch, I.; Schäfer, R.; Schultz, L.; McCord, J.
Magnetic domain compensation effect on the magneto-dynamic response of ferromagnetic elements
*Applied Physics Letters **97**, 052507 (2010).*

90. Pécz, B.; Stoemenos, J.; Voelskow, M.; Skorupa, W.; Dobos, L.; Pongrácz, A.; Battistig, G.
Ion implantation enhanced formation of 3C-SiC grains at the SiO2/Si interface after annealing in CO gas
*Journal of Physics: Conference Series **209**, 012045-1 (2010).*

91. Pellicer, E.; Varea, A.; Pane, S.; Nelson, Bradley J.; Menendez, E.; Estrader, M.; Surinach, S.; Baro, M. D.; Nogues, J.; Sort, J.
Nanocrystalline electroplated Cu-Ni: Metallic thin films with enhanced mechanical properties and tunable magnetic behavior
Advanced Functional Materials, 1 (2010).

92. Peter, F.; Winnerl, S.; Schneider, H.; Helm, M.
Excitation wavelength dependence of phase matched terahertz emission from a GaAs slab
*Optics Express **18**, 19574 (2010).*

93. Peter, S.; Günther, M.; Hauschild, D.; Grambole, D.; Richter, F.
Mid-frequency deposition of a-C:H films using five different precursors
*Vacuum **84**, 958 (2010).*

94. Philipp, P.; Schmidt, B.; Zier, M.
Charge carrier depth profiling of boron doped single crystalline silicon by Stepwise Oxidation Profiling (SWOP)
*AIP Conference Proceedings **1321**, 216 (2010).*

95. Pinto, S. R. C.; Rolo, A. G.; Gomes, M. J. M.; Ivanda, M.; Bogdanović-Radović, I.; Grenzer, J.; Mücklich, A.; Barber, D. J.; Bernstorff, S.; Buljan, M.
Formation of void lattice after annealing of Ge quantum dot lattice in alumina matrix
*Applied Physics Letters **97**, 173113 (2010).*

96. Potfajova, J.; Schmidt, B.; Helm, M.; Gemming, T.; Benyoucef, M.; Rastelli, A.; Schmidt, O. G.
Microcavity enhanced silicon light emitting pn-diode
*Applied Physics Letters **96**, 151113 (2010).*

97. Preoteasa, E.; Harangus, L.; Moldovan, A.; Dinescu, M.; Grambole, D.; Herrmann, F.
Proton mu-PIXE mapping, AFM imaging and size statistics of mineral granules in a dental composite
*X-Ray Spectrometry **39**, 208 (2010).*

98. Prucnal, S.; Rebohle, L.; Skorupa, W.
Blue electroluminescence of ytterbium clusters in SiO_2 by co-operative up-conversion
*Applied Physics B **98**, 451 (2010).*

99. Prucnal, S.; Turek, M.; Drozdziel, A.; Pyszniak, K.; Zhou, S. Q.; Kanjilal, A.; Zuk, J.; Skorupa, W.
Formation of InAs quantum dots in silicon by sequential ion implantation and flash lamp annealing
*Applied Physics B **101**, 315 (2010).*

100. Puzic, A.; Korhonen, T.; Kalantari, B.; Raabe, J.; Quitmann, C.; Juellig, P.; Bommer, L.; Goll, D.; Schuetz, G.; Wintz, S.; Strache, T.; Koerner, M.; Marko, D.; Bunce, C.; Fassbender, J.
Photon counting system for time-resolved experiments in multibunch mode
*Synchrotron Radiation News **23**, 26 (2010).*

101. Rafaja, D.; Wuestefeld, C.; Baehtz, C.; Klemm, V.; Dopita, M.; Motylenko, M.; Michotte, C.; Kathrein, M.
Effect of internal interfaces on hardness and thermal stability of nanocrystalline Ti0.5Al0.5N coatings
Metallurgical and Materials Transactions A (2010).

102. Ranjan, M.; Oates, T. W. H.; Facsko, S.; Möller, W.
Optical properties of silver nanowire arrays with 35 nm periodicity
*Optics Letters **35**, 2576 (2010).*

103. Rebohle, L.; Lehmann, J.; Prucnal, S.; Sunb, J. M.; Helm, M.; Skorupa, W.
Physical limitations of the electroluminescence mechanism in Terbium-based light emitters: Matrix and layer thickness dependence
*Applied Physics B **98**, 439 (2010).*

104. Reuther, H.; Müller, C.; Leonhardt, A.; Kutz, M. C.
Investigation of the formation of Fe-filled carbon nanotubes
*Journal of Physics: Conference Series **217**, 012098 (2010).*

105. Saly, M. J.; Munnik, F.; Winter, C. H.
Atomic layer deposition of CaB_2O_4 films using bis(tris(pyrazolyl)borate)calcium as a highly thermally

stable boron and calcium source
Journal of Materials Chemistry ***20**, 9995 (2010).*

106. Sandall, I. C.; Porter, N. E.; Wagner, M.; Schneider, H.; Winnerl, S.; Helm, M.; Wilson, L.
Terahertz optical sideband emission in self-assembled quantum dots
Applied Physics Letters ***96**, 201105 (2010).*

107. Sarakinos, K.; Music, D.; Mráz, S.; To Baben, M.; Jiang, K.; Nahif, F.; Braun, A.; Zilkens, C.; Konstantinidis, S.; Munnik, F.; Schneider, J. M.
On the phase formation of sputtered hafnium oxide and oxynitride films
Journal of Applied Physics ***108**, 014904 (2010).*

108. Scarlat, C.; Mok, K. M.; Zhou, S.; Vinnichenko, M.; Lorenz, M.; Grundmann, M.; Helm, M.; Schubert, M.; Schmidt, H.
Voigt effect measurement on PLD grown NiO thin films
Physica Status Solidi (C) ***7**, 334 (2010).*

109. Schlosser, M.; Iskra, P.; Abelein, U.; Lange, H.; Lochner, H.; Sulima, T.; Wiest, F.; Zilbauer, T.; Schmidt, B.; Eisele, I.; Hansch, W.
The impact ionization MOSFET (IMOS) as low-voltage optical detector
Nuclear Instruments and Methods in Physics Research A ***624**, 524 (2010).*

110. Schmidt, M.; Ellguth, M.; Schmidt, F.; Lüder, T.; von Wenckstern, H.; Pickenhain, R.; Grundmann, M.; Brauer, G.; Skorupa, W.
Defects in a nitrogen-implanted ZnO thin film
Physica Status Solidi (B) ***247**, 1220 (2010).*

111. Shalimov, A.; Zhou, S.; Roshchupkina, O.; Jeutter, N.; Baehtz, C.; Talut, G.; Reuther, H.; Potzger, K.
Multiple ferromagnetic secondary phases in Fe implanted yttria stabilized zirconia
Journal of Applied Physics ***108**, 024907 (2010).*

112. Sharma, M. K.; Kanjilal, A.; Voelskow, M.; Kanjilal, D.; Chatterjee, R.
Enhancement of ferromagnetism in Ni-implanted HfO_2 dielectric thin films
Nuclear Instruments and Methods in Physics Research B ***268**, 1631 (2010).*

113. Sharma, M.; Kanjilal, A.; Voelskow, M.; Kanjilal, D.; Chatterjee, R.
Room temperature ferromagnetism in Ni-doped HfO_2 thin films
Journal of Physics D: Applied Physics ***43**, 30 (2010).*

114. Skrotzki, R.; Fiedler, J.; Herrmannsdörfer, T.; Heera, V.; Voelskow, M.; Mücklich, A.; Schmidt, B.; Skorupa, W.; Gobsch, G.; Helm, M.; Wosnitza, J.
On-chip superconductivity via gallium overdoping of silicon
Applied Physics Letters ***97**, 192505 (2010).*

115. Spirin, K. E.; Ikonnikov, A. V.; Gavrilenko, V. I.; Kozlov, D. V.; Drachenko, O.; Schneider, H.; Helm, M.
The cyclotron resonance of holes in InGaAs/GaAs heterostructures with quantum wells in quantizing magnetic fields
Semiconductors ***44**, 1492 (2010).*

116. Steier, P.; Golser, R.; Kutschera, W.; Martschini, M.; Merchel, S.; Orlowski, T.; Priller, A.; Vockenhuber, C.; Wallner, A.
^{36}Cl exposure dating with a 3-MV tandem
Nuclear Instruments and Methods in Physics Research B ***268**, 744 (2010).*

117. Stöcker, H.; Zschornak, M.; Leisegang, T.; Shakhverdova, I.; Gemming, S.; Meyer, Dirk C.
Electric field mediated switching of mechanical properties of strontium titanate at room temperature
Crystal Research and Technology ***45**, 13 (2010).*

118. Svecova, B.; Nekvindova, P.; Mackova, A.; Malinsky, P.; Kolitsch, A.; Machovic, V.; Stara, S.; Mika, M.; Spirkova, J.
Study of Cu^+, Ag^+ and Au^+ ion implantation into silicate glasses
Journal of Non-Crystalline Solids ***356**, 2468 (2010.*

119. Talut, G.; Reuther, H.; Grenzer, J.; Mücklich, A.; Shalimov, A.; Skorupa, W.; Stromberg, F.
Spinodal decomposition and secondary phase formation in Fe-oversaturated GaN
Physical Review B ***81**, 155212 (2010).*

120. Tavares, C. J.; Marques, S. M.; Lanceros-Méndez, S.; Rebouta, L.; Alves, E.; Barradas, N. P.; Munnik, F.; Girardeau, T.; Riviére, J.-P.
N-doped photocatalytic titania thin films on active polymer substrates
Journal of Nanoscience and Nanotechnology ***10**, 1072 (2010).*

121. Templier, C.; Stinville, J. C.; Renault, P. O.; Abrasonis, G.; Villechaise, P.; Riviere, J. P.; Drouet, M.
Nitrogen interstitial induced texture depth gradient in stainless steel
Scripta Materialia ***63**, 496 (2010).*

122. Templier, C.; Stinville, J. C.; Villechaise, P.; Renault, P. O.; Abrasonis, G.; Riviere, J. P.; Martinavicius, A.; Drouet, M.
On lattice plane rotation and crystallographic structure of the expanded austenite in plasma nitrided AISI 316L steel
Surface and Coatings Technology ***204**, 2551 (2010).*

123. Thorn, A.; Ritter, E.; Sokolov, A.; Vorobjev, G.; Bischoff, L.; Herfurth, F.; Kester, O.; Pilz, W.; Thorn, D. B.; Ullmann, F.; Zschornack, G.
Optimization of the electron beam properties of Dresden EBIT devices for charge breeding
Journal of Instrumentation ***5**, C09006 (2010).*

124. Tibus, S.; Strache, T.; Springer, F.; Makarov, D.; Rohrmann, H.; Schrefl, T.; Fassbender, J.; Albrecht, M.
Magnetic properties of granular CoCrPt:SiO_2 films as tailored by Co^+ irradiation
Journal of Applied Physics ***107**, 093915 (2010).*

125. Tripathia, J. K.; Satpatib, B.; Liedke, M. O.; Guptad, A.; Som, T.
Effects of thermal annealing on structural and magnetic properties of thin Pt/Cr/Co multilayers
Journal of Magnetism and Magnetic Materials ***322**, 3464 (2010).*

126. Tsvetkova, T.; Balabanov, S.; Avramov, L.; Borisova, E.; Angelov, I.; Bischoff, L.
Photoluminescence of Si^+ and C^+ implanted polymers
Journal of Physics: Conference Series ***223**, 012033-1 (2010).*

127. Tsvetkova, T.; Balabanov, S.; Bischoff, L.; Krastev, V.; Avramova, P. Stefanov I.
X-ray photoelectron study of Si^+ ion implanted polymers
Journal of Physics: Conference Series ***253**, 012070-1 (2010).*

128. Turos, A.; Nowicki, L.; Stonert, A.; Pagowska, K.; Jagielski, J.; Mücklich, A.
Monte Carlo simulations of ion channeling in crystals containing extended defects
Nuclear Instruments and Methods in Physics Research B ***268**, 1718 (2010).*

129. Vinnichenko, M.; Gago, R.; Cornelius, S.; Shevchenko, N.; Rogozin, A.; Kolitsch, A.; Munnik, F.; Möller, W.
Establishing the mechanism of thermally induced degradation of ZnO:Al electrical properties using synchrotron radiation
Applied Physics Letters ***96**, 141907 (2010).*

130. Virsek, M.; Krause, M.; Kolitsch, A.; Mrzel, A.; Iskra, I.; Skapin, S. D.; Remskar, M.
The transformation pathways of $Mo_6S_2I_8$ nanowires into morphology-selective MoS_2 nanostructures
Journal of Physical Chemistry C ***114**, 6458 (2010).*

131. Voelskow, M.; Kanjilal, A.; Skorupa, W.
Subsecond melt processing for achieving SiGe surface layers
Current Applied Physics ***10**, 1309 (2010).*

132. Vogel, A.; Wintz, S.; Moser, J.; Bolte, M.; Strache, T.; Fritzsche, M.; Im, M.-Y.; Fischer, P.; Meier, G.; Fassbender, J.
Domain-wall pinning and depinning at soft spots in magnetic nanowires
IEEE Transactions on Magnetics ***46**, 1708 (2010).*

133. Voora, V.; Hofmann, T.; Brandt, M.; Lorenz, M.; Grundmann, M.; Ashkenov, N.; Schmidt, H.; Ianno, N.; Schubert, M.
Interface polarization coupling in piezoelectric-semiconductor ferroelectric heterostructures
Physical Review B ***81**, 195307-1 (2010).*

134. Wagner, M.; Schneider, H.; Stehr, D.; Winnerl, S.; Andrews, Aaron M.; Schartner, S.; Strasser, G.; Helm, M.
Observation of the intraexciton Autler-Townes effect in GaAs/AlGaAs semiconductor quantum wells
Physical Review Letters ***105**, 167401 (2010).*

135. Wunderlich, F.; Leisegang, T.; Weissbach, T.; Zschornak, M.; Dshemuchadse, J.; Lubk, A.; Führlich, T.; Welter, E.; Souptel, D.; Gemming, S.; Seifert, G.; Meyer, D. C.
EXAFS, XANES, and DFT study of the mixed-valence compound YMn_2O_5: Site-selective substitution of Fe for Mn
Physical Review B ***82**, 014409 (2010).*

136. Xu, Q.; Zhou, S.; Bürger, D.; Hochmuth, H.; Lorenz, M.; Grundmann, M.; Schmidt, H.
Electrical control of magnetoresistance in highly insulating Co-doped ZnO
Japanese Journal of Applied Physics ***49**, 043002 (2010).*

137. Xu, Q.; Zhou, S.; Wu, D.; Uhlarz, M.; Tang, Y.; Potzger, K.; Xu, M.; Schmidt, H.
Cluster spin glass behavior in Bi(Fe0.95Co0.05)O3
*Journal of Applied Physics **107**, 093920 (2010).*

138. Yang, K.; Bromberger, H.; Ruf, H.; Schäfer, H.; Neuhaus, J.; Dekorsy, T.; Villas-Boas Grimm, C.; Helm, M.; Biermann, K.; Künzel, H.
Passively mode-locked Tm,Ho:YAG laser at 2 µm based on saturable absorption of intersubband transitions in quantum wells
*Optics Express **18**, 6537 (2010).*

139. Zhang, W.; Peng, B.; Zhang, W.; Zhou, S.; Schmidt, H.
Ultra large coercivity in barium ferrite thin films prepared by magnetron sputtering
*Journal of Magnetism and Magnetic Materials **322**, 1859 (2010).*

140. Zhou, S.; Bürger, D.; Mücklich, A.; Baumgart, C.; Skorupa, W.; Timm, C.; Oesterlin, P.; Helm, M.; Schmidt, H.
Hysteresis in the magnetotransport of manganese-doped germanium: Evidence for carrier-mediated ferromagnetism
*Physical Review B **81**, 165204 (2010).*

141. Zhou, S.; Bürger, D.; Skorupa, W.; Oesterlin, P.; Helm, M.; Schmidt, H.
The importance of hole concentration in establishing carrier-mediated ferromagnetism in Mn doped Ge
*Applied Physics Letters **96**, 202105 (2010).*

142. Zhou, S.; Schmidt, H.
Mn-doped Ge and Si: A review of the experimental status
*Materials **3**, 5054 (2010).*

143. Zotti, Linda A.; Kirchner, T.; Cuevas, J.-C.; Pauly, F.; Huhn, T.; Scheer, E.; Erbe, A.
Revealing the role of anchoring groups in the electrical conduction through single-molecule junctions
*Small **6**, 1529 (2010).*

144. Zschintzsch, M.; Jeutter, N. M.; von Borany, J.; Krause, M.; Mücklich, A.
Reactive DC magnetron sputtering of (GeO_x-SiO_2) superlattices for Ge nanocrystal formation
*Journal of Applied Physics **107**, 034306 (2010).*

145. Zschornak, M.; Gemming, S.; Gutmann, E.; Weißbach, T.; Stöcker, H.; Leisegang, T.; Riedl, T.; Tränkner, M.; Gemming, T.; Meyer, D. C.
Surface modeling and chemical solution deposition of $SrO(SrTiO3)_n$ Ruddlesden–Popper phases
*Acta Materialia **58**, 4650 (2010)*

Invited Conference Talks

1. Abrasonis, G.
Self-organization during the growth of phase-separated nanostructured thin films
DPG Frühjahrstagung der Sektion Kondensierte Materie, 22.-26.03.2010, Regensburg, Germany

2. Abrasonis, G.
PVD growth of carbon-transition metal nanocomposites: From energetic condensation to periodic precipitation patterns
8th International Nanotechnology Symposium Nanofair 2010, 6.-7.07.2010, Dresden, Germany

3. Abrasonis, G.; Oates, T. W. H.; Kovacs, Gy. J.; Tucker, M.; Grenzer, J.; Persson, P. O. A.; Heinig, K.-H.; Martinavicius, A.; Jeutter, N.; Baethz, C.; Bilek, M. M. M.; Möller, W.
Synthesis and tilting of precipitation patterns in carbon-transition metal nanocomposite thin films by hyperthermal ion deposition
17th International Conference on Ion Beam Modification of Materials, 22.-27.08.2010, Montréal, Québec, Canada

4. Abrasonis, G.
PVD growth of carbon-transition metal nanocomposites: From energetic condensation to spin-dependent transport
International Conference "Radiation Interaction with Material and its Use in Technologies 2010", 20.-22.09.2010, Kaunas, Lithuania

5. Anwand, W.; Kanjilal, A.; Wagner, A.; Brauer, G.; Cowan, T.; Rebohle, L.; Cherkouk, C.; Skorupa, W.
Defect characterization of Er implanted, Ge-rich SiO_2 layers using slow positron implantation spectroscopy
International Workshop on Advanced Positron Beam Technology for Material Sciences, 15.-18.03.2010, Algiers, Algeria

6. Bischoff, L.; Heinig, K.-H.; Schmidt, B.; Facsko, S.; Pilz, W.
Crystalline Ge surface nanopatterns by erosion with heavy Bi- dimer and trimer ions
21th International Conference on the Application of Accelerators in Research and Industry, 8.-13.08.2010, Fort Worth, USA

7. Drachenko, O.
High field cyclotron resonance spectroscopy using quantum cascade lasers
14th Nanophysics and Nanoelectronics Symposium, 15.-19.03.2010, Nizhny Novgorod, Russia

8. Facsko, S.; Keller, A.; Ranjan, M.; Möller, W.
Surface nanostructures induced by low energy ion sputtering
International Conference on Metallurgical Coatings and Thin Films, 26.-30.04.2010, San Diego, USA

9. Facsko, S.; Wilhelm, R. A.; El-Said, A. S.; Heller, R.
Surface nanostructures induced by slow highly charged ions
EMMI Workshop "Physics Prospects at the ESR and HITRAP", 27.-30.06.2010, Eisenach, Germany

10. Facsko, S.
Impact of slow highly charged ions on insulating surfaces
24th International Conference on Atomic Collisions in Solids, 18.-23.07.2010, Krakow, Poland

11. Facsko, S.; Ranjan, M.; Keller, A.; Oates, Thomas W. H.; Fassbender, J.; Möller, W.
Ion-induced surface patterns as templates for thin film growth
12th International Conference on Plasma Surface Engineering, 13.-17.09.2010, Garmisch Partenkirchen, Germany

12. Fan, J. C.; Zhu, C. Y.; Yang, B.; Fung, S.; Beling, C. D.; Brauer, G.; Anwand, W.; Grambole, D.; Skorupa, W.; Wong, K. S.; Zhong, Y. C.; Ling, C. C.
A comprehensive study of the p-type conductivity formation in radio frequency magnetron sputtering grown arsenic-doped ZnO film
6th International Workshop on Zinc Oxide and Related Materials, 5.-7.08.2010, Changchun, China

13. Fassbender, J.; Liedke, M. O.; Körner, M.; Markó, D.; Lenz, K.; Facsko, S.
Ion-erosion-induced pattern as templates for layers with magnetic anisotropy and coupling
Joint European Magnetics Symposium 2010, 23.-28.08.2010, Krakow, Poland

14. Fassbender, J.; Strache, T.; Fritzsche, M.; McCord, J.; Basitz, M.; Mcvitie, S.
Magnetization reversal and artificial domains in hybrid magnetic materials
IEEE 7th International Symposium on Metallic Multilayers, 19.-24.09.2010, Berkeley, USA

15. Fassbender, J.; Strache, T.; Marko, D.; Wintz, S.; Lenz, K.; Keller, A.; Facsko, S.; McCord, J.
Nanomagnets – created and tailored by ions
6th Nanoscience and Nanotechnology Conference, 15.-18.06.2010, Izmir, Turkey

16. Gemming, S.
Transport in nanostructured materials
FAHL Academia 2010: Transparent and Flexible Electronics, 28.09.2010, Leipzig, Germany

17. Gemming, S.; Merchel, S.
Materials research at the FZD
1. Norwegian-German Sea-Ice Workshop, 6.-7.12.2010, Bremerhaven, Germany

18. Gemming, S.; Seifert, G.; Enyashin, A. N.
Simulating the bioavailability of carbon nanotubes
12th International and Interdisciplinary NRW Symposium "Biomaterials and Biomechanics", 17.-19.03.2010, Essen, Germany

19. Helm, M.
The basic physics of intersubband transitions – from the simple to the subtle
International Quantum Cascade Lasers School & Workshop, 30.08.-3.09.2010, Florenz, Italy

20. Helm, M.
Terahertz free-electron lasers and their applications for the spectroscopy of solids
THz radiation: Generation, Detection and Applications (Heraeus Seminar), 18.-21.04.2010, Bad Honnef, Germany

21. Ou, X.; Das Kanungo, P.; Kögler, R.
Doping of the Si nanowires
6th IUPAC International Symposium on Novel Materials and Their Synthesis, 11.-14.10.2010, Wuhan, China

22. Posselt, M.
Energetics and kinetics of defects, impurities, nanostructures and interfaces
11th IUMRS International Conference in Asia, 25.-28.09.2010, Qingdao, China

23. Potzger, K.
Ion beam induced ferromagnetism in semiconductors
17th International Conference on Ion Beam Modification of Materials, 22.-27.08.2010, Montreal, Canada, and
24. *8th International Conference Ion Implantation and Other Applications of Ions and Electrons, 14.-17.06.2010, Kazimierz Dolny, Poland, and*
25. *International Conference on Nanoscale Magnetism, 28.09.-2.10.2010, Istanbul, Turky*
26. Quitmann, C.; Raabe, J.; Puzic, A.; Wintz, S.; Fassbender, J.; Marriager, S.; Ingold, G.; Johnson, S.; Beaud, P.; Feidenhans'L, R.; Pressacco, F.; Back, Ch.
Dynamics of magnetic objects and ultra-fast phase transitions in RhFe
International Workshop on X-Ray spectroscopy of Magnetic Solids, 10.-11.06.2010, Oxfordshire, UK
27. Schmidt, B.; Heinig, K.-H.
Ion beam synthesis of nano-crystals for electronics and photonics
21st International Conference on the Application of Accelerators in Research and Industry, 8.-13.08.2010, Dallas/Fortworth, Texas, USA
28. Schmidt, B.; Heinig, K.-H.; Mücklich, A.; Akhmadaliev, C.; Ridgway, M.; Kluth, P.
Swift heavy ion beam shaping of Au and Ge nanoparticles in SiO_2
21st International Conference on the Application of Accelerators in Research and Industry, 8.-13.08.2010, Dallas/Fortworth, Texas, USA
29. Schmidt, H.
Spin manipulation in Co-doped ZnO
12th International Ceramics Congress, 6.-11.06.2010, Montecatini Terme, Italy
30. Schneider, H.
Semiconductor quantum structures for quadratic detection at mid-infrared and THz frequencies
Novel Quantum Structure Detectors for Opto-electronic Conversion 2010, 4.-6.01.2010, Sanya, China
31. Schneider, H.; Winnerl, S.; Drachenko, O.; Helm, M.; Liu, H. C.; Walther, M.; Faist, J.
Two-photon quantum well infrared photodetectors for terahertz autocorrelation
5th International Symposium on Ultrafast Phenomena & Terahertz Waves, 12.-16.09.2010, Xi'an, China
32. Skorupa, W.; Wündisch, C.; Posselt, M.; Heera, V.; Herrmannsdörfer, T.; Buca, D.; Mantl, D.; Haeberlein, S.; Fendler, R.; Gebel, T.
Advances in Si & Ge millisecond processing: From SOI to superconducting Ge
8th International Conference Ion Implantation and Other Applications of Ions and Electrons, 14.-17.06.2010, Kazimierz Dolny, Poland
33. Wagner, M.; Stehr, D.; Schneider, H.; Winnerl, S.; Helm, M.
Terahertz nonlinear optics of excitons in semiconductor quantum wells
20th International Conference on Applied Electromagnetics and Communications, 20.-23.09.2010, Dubrovnik, Croatia
34. Winnerl, S.; Hubrich, R.; Peter, F.; Schneider, H.; Helm, M.
Longitudinal fields in focused radially polarized terahertz beams
35th International Conference on Infrared, Millimeter and Terahertz Waves, 5.-10.09.2010, Rome, Italy

Conference Contribution

1. Abrasonis, G.; Oates, T. W. H.; Kovacs, G. J.; Grenzer, J.; Persson, P. O. A.; Heinig, K.-H.; Martinavicius, A.; Jeutter, N.; Baehtz, C.; Grötzschel, R.; Tucker, M.; Rosen, J.; Bilek, M. M. M.; Möller, W.
Tilting of self-organized layered arrays of encapsulated metal nanoparticles in C:Ni nanocomposite films by means of hyperthermal ion deposition
38th International Conference on Metallurgical Coatings & Thin Films, 2.-6.05.2010, San Diego, California, USA
2. Abrasonis, G.; Oates, T. W. H.; Kovacs, G. J.; Tucker, M.; Grenzer, J.; Persson, P. O. A.; Heinig, K.-H.; Martinavicius, A.; Jeutter, N.; Baethz, C.; Bilek, M. M. M.; Möller, W.
Tilting of precipitation patterns in carbon-transition metal nanocomposite thin films by hyperthermal ion deposition
2010 MRS Fall Meeting, 29.11.-3.12.2010, Boston, USA
3. Abrasonis, G.; Wintz, S.; Liedke, M. O.; Aksoy, F.; Liu, Z.; Kuepper, K.; Krause, M.
Environment controlled de-wetting kinetics of Rh-Pd bilayer/alloy thin films on silica: A physical approach to synthesize core-shell nanoparticles
2010 MRS Fall Meeting, 29.11.-3.12.2010, Boston, USA
4. Akhmadaliev, S.; Heller, R.; Kolitsch, A.; Merchel, S.; Möller, W.
DREAMS at FZD: The new accelerator mass spectrometry facility

6. Workshop Radiochemische Analytik bei Betrieb und Rückbau kerntechnische Anlagen, der Deklaration von Abfällen und im Strahlenschutz / 23.Seminar Aktivierungsanalyse und Gammaspektroskopie, 6.-8.09.2010, Dresden, Germany

5. Akhmadaliev, S.; Kolitsch, A.; Merchel, S.; Möller, W.
DREAMS - a universal AMS facility based on the 6 MV – Tandetron™ at FZD in Dresden
DPG Frühjahrstagung der Sektion Atome, Moleküle, Quantenoptik und Plasmen, 8.-12.03.2010, Hannover, Germany

6. Al-Motasem, A. T.; Posselt, M.; Bergner, F.
Nucleation of Cu-vacancy and Ni-vacancy clusters in bcc-Fe
10th International Conference on Computer Simulation of Radiation Effects in Solids, 19.-23.07.2010, Krakow, Poland

7. Al-Motasem, A. T.; Posselt, M.; Talati, M.; Bergner, F.
Thermodynamics of nanoclusters in bcc-Fe containing copper, nickel and vacancies
5th International Conference on Multiscale Materials Modeling, 4.-8.10.2010, Freiburg, Germany

8. Al-Motasem, A. T.; Posselt, M.; Bergner, F.
Nucleation of copper-vacancy clusters in bcc-Fe: An atomistic study
International Conference on Nuclear Materials 2010, 4.-7.10.2010, Karlsruhe, Germany

9. Anwand, W.; Kanjilal, A.; Wagner, A.; Butterling, M.; Brauer, G.; Cowan, T. E.; Rebohle, L.; Skorupa, W.
Defect characterization of Er implanted, Ge-rich SiO_2 layers using slow positron implantation spectroscopy
39th Polish Seminar on Positron Annihilation, 20.-25.06.2010, Kazimierz Dolny, Poland

10. Baehtz, C.; Jeutter, N.; Grenzer, J.; von Borany, J.
***In-situ* thin film and nano structure characterization at ROBL**
Congress on Materials Science and Engineering 2010, 24.-26.08.2010, Darmstadt, Germany

11. Baehtz, C.; von Borany, J.; Wirth, C. T.; Bayer, B. C.; Hofmann, S.
In-situ investigations at ROBL-MRH
12th European Powder Diffraction Conference, 27.-30.08.2010, Darmstadt, Germany

12. Ball, D.; Liedke, M. O.; Lenz, K.; Fritzsche, M.; Yilgin, R.; Keller, A.; Ranjan, M.; Facsko, S.; Fassbender, J.
Magnetic Anisotropy of Thin Magnetic Films on Nanometer Scale Silicon Ripples
8th International Nanotechnology Symposium Nanofair 2010, 6.-7.07.2010, Dresden, Germany

13. Basith, M.; Mcvitie, S.; Strache, T.; Fritzsche, M.; McCord, J.; Fassbender, J.
Magnetisation reversal processes in saturation magnetisation reduced stripes
Condensed Matter and Materials Physics Conference, 14.-16.12.2010, Warwick, UK

14. Batabyal, R.; Roy, A.; Roy, S.; Bischoff, L.; Dev, B. N.
Lateral straggling and its influence on lateral diffusion in implantation with a focused ion beam
24th International Conference on Atomic Collisions in Solids, 18.-23.07.2010, Krakow, Poland

15. Baumgart, C.; Müller, A.-D.; Müller, F.; Helm, M.; Schmidt, H.
Quantitative Kelvin probe force microscopy imaging on locally doped Si
DPG Frühjahrstagung der Sektion Kondensierte Materie, 22.-26.03.2010, Regensburg, Germany

16. Baumgart, C.; Müller, A.-D.; Müller, F.; Helm, M.; Schmidt, H.
Quantitative Kelvin probe force microscopy imaging on locally doped semiconductors
International Conference on Functional Nanocoatings, 28.-31.03.2010, Dresden, Germany

17. Baumgart, C.; Müller, A.-D.; Müller, F.; Helm, M.; Schmidt, H.
Quantitative Kelvin probe force microscopy on semiconductors under ambient conditions
8th International Nanotechnology Symposium Nanofair 2010, 6.-7.07.2010, Dresden, Germany

18. Baumgart, C.; Müller, A.-D.; Müller, F.; Helm, M.; Schmidt, H.
Quantitative Kelvin probe force microscopy imaging on locally doped semiconductors
10th International Conference on Nanostructured Materials, 13.-17.09.2010, Rome, Italy

19. Bhattacharyya, J.; Wagner, M.; Helm, M.; Hopkinson, M.; Wilson, L. R.; Schneider, H.
Direct evidence of long lived trapped carriers in InGaAs/GaAs quantum dots studied using terahertz-activated luminescence measurements
30th International Conference on the Physics of Semiconductors, 25.07.2010, Seoul, South Korea

20. Bhattacharyya, J.; Wagner, M.; Helm, M.; Hopkinson, M.; Wilson, L. R.; Schneider, H.
Effect of carrier redistribution on spin polarization in n-doped InGaAs quantum dot ensemble
6th International Conference on the Physics and Applications of Spin Related Phenomena in Semiconductors, 1.10.2010, Tokyo, Japan

21. Biermanns, A.; Hanisch, A.; Grenzer, J.; Facsko, S.; Metzger, T. H.; Pietsch, U.
X-ray scattering and diffraction from Xe-beam induced ripples in crystalline Si

Deutsche Tagung für Forschung mit Synchrotronstrahlung, Neutronen und Ionenstrahlen an Großgeräten, 24.-26.02.2010, Berlin, Germany

22. Bischoff, L.; Heinig, K.-H.; Schmidt, B.; Facsko, S.; Pilz, P.
Self-assembled ordered nanostructures on Ge by cluster irradiation
Workshop Ionenstrahlphysik, 29.-31.03.2010, Dresden, Germany

23. Bischoff, L.; Pilz, W.; Schmidt, B.
A bismuth liquid metal ion source for mass separated FIB applications
5. FIB Workshop of DGE, SSOM and ASEM, 28.-29.06.2010, Vienna, Austria

24. Bischoff, L.; Heinig, K.-H.; Schmidt, B.; Facsko, S.; Pilz, W.
Self-organization of Ge nanopattern under erosion with heavy Bi monomer and cluster ions
17th International Conference on Ion Beam Modification of Material, 22.-27.08.2010, Montreal, Canada

25. Böttger, R.; Bischoff, L.; Schmidt, B.; Krause, M.
Nanomachining of freestanding Si nanowires
Dresdner Barkhausen Symposium, 16.12.2010, TU Dresden, Germany

26. Buhl, M.; Körner, M.; Fritzsche, M.; Wiesenhütter, U.; Liedke, O.; Fassbender, J.
Herstellung und magnetische Charakterisierung von Co-Nanopartikel auf ionenstrahlerodierten Siliziumsubstraten
DPG Frühjahrstagung der Sektion Kondensierte Materie, 21.-26.03.2010, Regensburg, Germany

27. Buljan, M.; Grenzer, J.; Keller, A.; Radić, N.; Cornelius, T.; Metzger, T. H.; Holý, V.
Growth of quantum dot crystals in amorphous matrix on rippled substrates
DPG Frühjahrstagung der Sektion Kondensierte Materie, 21.-26.03.2010, Regensburg, Germany

28. Bürger, D.; Seeger, M.; Zhou, S.; Helm, M.; Schmidt, H.
Thermodynamical limits of diluted magnetic semiconductors
DPG Frühjahrstagung der Sektion Kondensierte Materie, 21.-26.03.2010, Regensburg, Germany

29. Bürger, D.; Zhou, S.; Pandey, M.; Grenzer, J.; Roshchupkina, O.; Anwand, W.; Reuther, H.; Gottschalch, V.; Helm, M.; Schmidt, H.
Modification of GaAs by Mn ion implantation towards semiconductor spintronic thin films
Workshop Ion Beam Physics, 29.-31.03.2010, Dresden, Germany

30. Bürger, D.; Seeger, M.; Zhou, S.; Skorupa, W.; Helm, M.; Schmidt, H.
Thermodynamical limits of diluted (magnetic) semiconductors
30th International Conference on the Physics of Semiconductors, 25.-30.07.2010, Seoul, South Korea

31. Cantelli, V.; Grenzer, J.; Jeutter, N.; von Borany, J.
In-situ grazing incidence scattering investigations during magnetron sputtering deposition of FePt/Ag nanocomposite layers
10th Biennial Conference on High Resolution X-Ray Diffraction and Imaging, 20.-23.09.2010, Warwick, UK

32. Chen, C. L.; Richter, A.; Talut, G.; Kögler, R.
Irradiation effects in FeCrAl ODS alloys
1st International Conference on Materials for Energy, 4.-8.07.2010, Karlsruhe, Germany

33. Cherkouk, C.; Rebohle, L.; Skorupa, W.; Helm, M.
Estrogen detection in waterish solutions by silicon based light emitters
E-MRS 2010 Spring Meeting, 7.-11.06.2010, Strasbourg, France

34. Cherkouk, C.; Rebohle, L.; Skorupa, W.; Helm, M.
Estrogen detection in water by silicon based light emitters
8th International Conference Ion Implantation and Other Applications of Ions and Electronics, 14.-17.06.2010, Kazimierz Dolny, Poland

35. Constantinescu, B.; Bugoi, R.; Munnik, F.; Pichon, L.
Micro-pixe studies for archaeological gold identification – the case of transylvanian gold and of dacian gold staters (kosons)
12th International Conference on Nuclear Microprobe Technology and Applications, 26.-30.07.2010, Leipzig, Germany

36. Cornelius, S.; Vinnichenko, M.; Kolitsch, A.; Möller, W.
High mobility Al-doped ZnO grown by reactive pulsed magnetron sputtering
International Conference on Functional Nanocoatings, 28.-30.03.2010, Dresden, Germany

37. Cornelius, S.; Vinnichenko, M.; Rogozin, A.; Shevchenko, N.; Kolitsch, A.; Möller, W.
Eigenschaften und Mikrostruktur von mittels gepulstem reaktivem Magentronsputtern abgeschiedenen Metalloxid-Schichten
PLASMA Germany, Frühjahrstagzung 2010, 5.-6.05.2010, Dresden, Germany

38. Cornelius, S.; Vinnichenko, M.; Shevchenko, N.; Kolitsch, A.; Möller, W.
Einfluss der Al-Konzentration auf Struktur und elektrische Eigenschaften von mittels reaktivem gepulstem Magnetronsputtern gewachsenen ZnO:Al Schichten
Workshop „Transparente leitfähige Oxide – Festkörperphysikalische Grundlagen und Technologie“, 1.-2.06.2010, Dresden, Germany

39. Cornelius, S.; Vinnichenko, M.; Kolitsch, A.; Möller, W.
Electrical transport in Al doped ZnO grown by reactive pulsed magnetron sputtering
5th Forum on New Materials (in the framework of 12th International Conference on Modern Materials and Technologies), 13.-18.06.2010, Montecatini Terme, Italy

40. Cornelius, S.; Vinnichenko, M.; Kolitsch, A.; Möller, W.
Influence of Al concentration on structure and electrical properties of polycrystalline and epitaxial Al-doped ZnO films grown by reactive pulsed magnetron sputtering
12th International Conference on Plasma Surface Engineering, 13.-17.09.2010, Garmisch Partenkirchen, Germany

41. Das Kanungo, P.; Ou, X.; Kögler, R.; Nikolai, Z.; Werner, P.; Skorupa, W.; Goesele, U.
Doping and electrical characterization of individual silicon nanowire
2010 MRS Spring Meeting, 5.-9.04.2010, San Fransisco, USA

42. Donchev, A.; Schütze, M.; Kolitsch, A.; Yankov, R.
Enhanced resistance of Ti-alloys against environmental attack by a combined Al- and F-treatment
139th Annual Meeting & Exhibition, The Minerals, Metals and Materials Society, 14.-18.02.2010, Seattle, USA

43. Donchev, A.; Schütze, M.; Kolitsch, A.; Yankov, R.
Protection of TiAl-components against high temperature oxidation with fluorine
Materials Science & Technology 2010 Conference and Exhibition and 112th Annual Meeting of the American Ceramics Society, 17.-21.10.2010, Houston, USA

44. Donchev, A.; Schütze, M.; Kolitsch, A.; Yankov, R.
Improved environmental resistance of Ti-alloys at elevated temperatures by a combined Al- and F-treatment
Materials Science & Technology 2010 Conference and Exhibition and 112th Annual Meeting of the American Ceramics Society, 17.-21.10.2010, Houston, USA

45. Donchev, A.; Schütze, M.; Kolitsch, A.; Yankov, R.
Comparison of different fluorine-treatments for improved high temperature oxidation resistance of TiAl-alloys
2010 MRS Fall Meeting, 29.11.-3.12.2010, Boston, USA

46. Drachenko, O.; Winnerl, S.; Schneider, H.; Helm, M.; Leotin, J.
Infrared magneto-spectroscopy using quantum cascade lasers
35th International Conference on Infrared, Millimeter and THz Waves, 5.-10.09.2010, Rome, Italy

47. Eberhardt, K.; Henkelmann, R.; Merchel, S.; Denecke, M. A.
GDCh Arbeitskreis Analytik mit Radionukliden und Hochleistungsstrahlenquellen
Deutsche Tagung für Forschung mit Synchrotronstrahlung, Neutronen und Ionenstrahlen an Großgeräten, 24.-26.02.2010, Berlin, Germany

48. Eder, F.; Neelmeijer, C.; Bichler, M.; Merchel, S.
Homogeneity study for obsidian provenancing by ion beam analysis
Workshop Ion Beam Physics, 29.-31.03.2010, Dresden, Germany

49. Eder, F.; Neelmeijer, C.; Bichler, M.; Merchel, S.
Obsidian homogeneity study for provenancing using ion beam- and neutron activation analysis
12th International Conference on Particle Induced X-ray Emission and its Analytical Applications, University of Surrey, 27.06.-2.07.2010, Surrey, UK

50. Eder, F.; Neelmeijer, C.; Bichler, M.; Merchel, S.
Studying obsidians from milos by complementary techniques: An application of ion beam and instrumental neutron activation analysis
6. Workshop Radiochemische Analytik bei Betrieb und Rückbau kerntechnische Anlagen, der Deklaration von Abfällen und im Strahlenschutz / 23.Seminar Aktivierungsanalyse und Gammaspektroskopie, 6.-8.09.2010, Dresden, Germany

51. Fassbender, J.; Möller, W.; Beyer, E.; Seifert, G.; Zellbeck, H.; Abrasonis, G.; Gemming, S.; Hübner, M.; Joswig, J.-O.; Krause, M.; Kunze, T.; Leson, A.; Makowski, S.; Posselt, M.; Weihnacht, V.
Nanostrukturierte Verschleißschutzschichten für den Automobilbau - von der Konzeption zur Anwendung
1. International Colloquium of the European Centre for Emerging Materials and Processes (ECEMP), 2.-3.12.2010, Dresden, Germany

52. Fiedler, J.; Heera, V.; Bischoff, L.; Facsko, S.; Heinig, K.-H.; Mücklich, A.; Posselt, M.; Reuther, H.; Schmidt, B.; Voelskow, M.; Wündisch, C.; Skorupa, W.; Gobsch, G.
Degradation of cover SiO_2 on Ge during Ga implantation
Workshop Ion Beam Physics, 29.-31.03.2010, Dresden-Rossendorf, Germany

53. Fischer, H.; Lindner, M.; Schickle, K.; Kirsten, A.; Seifert, G.; Oliveira, A.; Gemming, S.; Jennissen, H. P.; Zurlinden, K.; Meißner, M.; Müller-Mai, C.
BioMin - Funktionalisierte Mineraloberflächen: Sorptionsmechanismen von wachstumsstimulierenden Proteinen an Oberflächen von Knochenersatzwerkstoffen auf Calciumphosphatbasis
Symposium Mineral Surfaces - From Atomic Processes to Industrial Application, 26.-27.10.2010, Mainz, Germany

54. Fritzsche, M.; Keller, A.; Facsko, S.; Lenz, K.; Fassbender, J.
Annealing of silicon nanopatterns
DPG Frühjahrstagung der Sektion Kondensierte Materie, 21.-26.03.2010, Regensburg, Germany, and

55. *Workshop Ion Beam Physics, 29.-31.03.2010, Dresden, Germany*

56. Gago, R.; Redondo-Cubero, A.; Vinnichenko, M.; Vazquez, L.
Roughness evolution in amorphous silicon films grown by (biased) DC magnetron sputtering
12th International Conference on Plasma Surface Engineering, 13.-17.09.2010, Garmisch-Partenkirchen, Germany

57. Gemming, S.
Correlation of structure and conductance in nanowires and nanotubes
DPG Frühjahrstagung der Sektion Kondensierte Materie, 21.-26.03.2010, Regensburg, Germany

58. Gemming, S.; Schreiber, M.; Kunze, T.; Numazawa, S.
Low-temperature modelling for degenerate and frustrated Heisenberg systems with anisotropy
International Workshop on Perspectives in Highly Frustrated Magnetism, 19.-23.04.2010, Dresden, Germany

59. Gemming, S.
Correlation of structure and conductance in nanowires
26th European Crystallographic Meeting, 30.08.-2.09.2010, Darmstadt, Germany

60. Gemming, S.; Zschornak, M.; Weißbach, T.; Stöcker, H.; Meyer, D. C.; Gemming, T.; Lubk, A.; Spaldin, N. A.
Multifunctional oxides - Influence of defects on the ferroic properties
5th International Conference on Multiscale Materials Modelling, 4.-8.10.2010, Freiburg, Germany

61. Gieniusz, R.; Mazalski, P.; Kurant, Z.; Maziewski, A.; Liedke, M. O.; Fassbender, J.; Wawro, A.; Baczewski, L. T.
Modifications of magnetic properties of Pt/Co/Pt layers induced by Ga irradiations
Joint European Magnetic Symposia, 23.-28.08.2010, Krakow, Poland

62. Grenzer, J.; Cantelli, V.; Jeutter, N.; von Borany, J.
In-situ grazing incidence scattering investigations during magnetron sputtering deposition of FePt/Ag thin films
Deutsche Tagung für Forschung mit Synchrotronstrahlung, Neutronen und Ionenstrahlen an Großgeräten, 24.-26.02.2010, Berlin, Germany

63. Grenzer, J.; Cantelli, V.; Jeutter, N. M.; von Borany, J.
In-situ grazing incidence scattering investigations during magnetron sputtering deposition of FePt/Ag thin films
DPG Frühjahrstagung der Sektion Kondensierte Materie, 21.-26.03.2010, Regensburg, Germany

64. Grenzer, J.; Biermanns, A.; Akhmadaliev, C.; Bischoff, L.
X-ray Investigations on CoSi2 nano wires manufactured by focused ion beam synthesis
10th Biennial Conference on High Resolution X-Ray Diffraction and Imaging, 20.09.2010, Warwick, UK

65. Hanisch, A.; Biermanns, A.; Grenzer, J.; Pietsch, U.
Characterization of Xe ion-induced rippled structures on Si (001) in the medium ion energy range
DPG Frühjahrstagung der Sektion Kondensierte Materie, 22.-26.03.2010, Regensburg, Germany

66. Heera, V.; Herrmannsdörfer, T.; Skrotzki, R.; Ignatchik, O.; Uhlarz, M.; Fiedler, J.; Mücklich, A.; Voelskow, M.; Posselt, M.; Wündisch, C.; Heinig, K.-H.; Skorupa, W.; Wosnitza, J.; Helm, M.
Superconductivity in Ga-doped Germanium above 1 K
30th International Conference on the Physics of Semiconductors, 25.-30.07.2010, Seoul, South Korea

67. Heinig, K.-H.; Schmidt, B.; Mücklich, A.; Akhmadaliev, C.; Ridgeway, M.; Kluth, P.; Vredenberg, A.
Au and Ge nanoparticle shaping by swift heavy ion irradiation
Workshop Ion Beam Physics, 29.-31.03.2010, Dresden-Rossendorf, Germany

68. Heintze, C.; Bergner, F.; Kögler, R.; Lindau, R.
The influence of Helium and ODS on the irradiation-induced hardening of Eurofer 97 at 300°C

12th International Conference on Modern Materials and Technologies together with 5th Forum on New Materials, 13.-18.06.2010, Montecatini Terme, Italy

69. Järvi, T. T.; Pohl, D.; Rellinghaus, B.; Schultz, L.; Albe, K.; Kuronen, A.; Nordlund, K.; Fassbender, J.
Radiation effects in nanoparticles
5th International Conference on Multiscale Materials Modelling, 4.-8.10.2010, Freiburg, Germany

70. Kanak, J.; Stobiecki, T.; Powroznik, W.; Mazalski, P.; Sveklo, I.; Maziewski, A.; Liedke, M. O.; Fassbender, J.; Wawro, A.; Baczewski, L. T.
X-ray reflectivity investigations of Ga+ ion irradiated Pt/Co/Pt films
Joint European Magnetic Symposia, 23.-28.08.2010, Krakow, Poland

71. Kolitsch, A.; Yankov, R.; Donchev, A.
Improvement of the oxidation behaviour of complex shaped TiAl-alloys by plasma immersion ion implantation with fluorine
18th International Conference on Ion Implantation Technology, 6.-11.06.2010, Kyoto, Japan

72. Kosmata, M.; Munnik, F.; Heller, R.; Neelmeijer, C.
Quantitative Tiefenprofilelementanalyse mit Subnanometer Tiefenauflösung
6. Workshop Radiochemische Analytik bei Betrieb und Rückbau kerntechnische Anlagen, der Deklaration von Abfällen und im Strahlenschutz / 23.Seminar Aktivierungsanalyse und Gammaspektroskopie, 6.-8.09.2010, Dresden, Germany

73. Körner, M.; Liedke, M. O.; Strache, T.; Dzenisevich, S.; Keller, A.; Facsko, S.; Lenz, K.; Fassbender, J.
Tailoring the magnetic coupling of Fe/Cr/Fe trilayers by using substrates with nanometer scale ripples
8th International Nanotechnology Symposium Nanofair 2010, 6.-7.07.2010, Dresden, Germany

74. Krause, M.; Abrasonis, G.; Mücklich, A.; Kolitsch, A.; Möller, W.
Carbon:Vanadium (C:V) nanocomposite films for tribological applications
12th International Conference on Plasma Surface Engineering, 13.-17.09.2010, Garmisch-Partenkirchen, Germany

75. Kunze, T.; Gemming, S.; Posselt, M.; Erdogan, E.; Seifert, G.
Theoretical investigations of carbon-based nanocoatings
International Conference on Functional Nanocoatings, 28.-31.03.2010, Dresden, Germany

76. Kunze, T.; Posselt, M.; Gemming, S.; Seifert, G.
Nanotribology of lubricated carbon-based nanocoatings
5th International Conference on Multiscale Materials Modeling, 4.-8.10.2010, Freiburg, Germany

77. Kutschan, B.; Morawetz, K.; Gemming, S.
Modeling the morphogenesis of brine channels in sea ice
DPG Frühjahrstagung der Sektion Kondensierte Materie, 21.-26.03.2010, Regensburg, Germany

78. Lehmann, J.; Rebohle, L.; Kanjilal, A.; Voelskow, M.; Helm, M.; Skorupa, W.
Wear-out phenomena in Si-based light emitting devices with ion beam implanted europium
8th International Conference "Ion Implantation and Other Applications of Ions and Electrons", 14.-17.06.2010, Kazimierz Dolny, Poland

79. Lehmann, J.; Rebohle, L.; Kanjilal, A.; Voelskow, M.; Skorupa, W.; Helm, M.
Investigation of wear-out phenomena in Eu-implanted metal-oxide semiconductor light emitting devices
8th International Nanotechnology Symposium Nanofair 2010, 6.-7.07.2010, Dresden, Germany

80. Lenz, K.; Markó, D.; Strache, T.; Kaltofen, R.; Fassbender, J.
Determination of the saturation magnetization from perpendicular magnetic anisotropy measurements of ion irradiated multilayers
11th Joint MMM-Intermag Conference, 18.-22.01.2010, Washington DC, USA

81. Lenz, K.; Körner, M.; Liedke, M. O.; Fritzsche, M.; Cizmar, E.; Ranjan, M.; Facsko, S.; Fassbender, J.
Morphology induced magnetic anisotropy of thin films on nanoscale MgO- and Si-Ripples
IEEE 7th International Symposium on Metallic Multilayers, 19.-24.09.2010, Berkeley, CA, USA

82. Li, L.; Zhou, S. Q.; Bürger, D.; Fassbender, J.; Helm, M.; Schmidt, H.; Oesterlin, P.; Yao, S. D.
Activation of acceptor levels in Mn implanted Si by pulsed laser annealing
DPG Frühjahrstagung der Sektion Kondensierte Materie, 21.-26.03.2010, Regensburg, Germany

83. Li, L.; Zhou, S.; Bürger, D.; Roshchupkina, O.; Rushforth, A.; Campion, R. P.; Yao, S.; Grenzer, J.; Fassbender, J.; Helm, M.
Tailoring the magnetism of GaMnAs films by ion irradiation
Workshop Ion Beam Physics, 29.-31.03.2010, Dresden, Germany

84. Li, L.; Zhou, S.; Bürger, D.; Roshchupkina, O.; Rushforth, A.; Campion, R. P.; Yao, S.; Grenzer, J.; Fassbender, J.; Helm, M.
Tailoring the magnetism of GaMnAs films by ion irradiation
Trends in Spintronics and Nanomagnetism, 22.05.-27.10.2010, Lecce, Italy

85. Liedke, B.; Heinig, K.-H.; Facsko, S.; Möller, W.
Ion induced surface pattern evolution described by combined TRIM and kinetic Monte-Carlo simulation
Workshop Ion Beam Physics, 29.-31.03.2010, Dresden, Germany

86. Liedke, B.; Heinig, K.-H.; Facsko, S.; Möller, W.
Multiphysics program for ion-induced collision cascades and thermally activated phase separation: Intermetallic nanolayers by interface mixing
10th International Conference on Computer Simulation of Radiation Effects in Solids, 19.-23.07.2010, Kraków, Poland

87. Liedke, B.; Heinig, K.-H.; Facsko, S.; Möller, W.
Ion erosion induced surface patterning studied by combined trim and kinetic monte-carlo simulations
17th International Conference on Ion Beam Modification of Materials, 22.-27.08.2010, Montreal, Canada

88. Liedke, M. O.; Shalimov, A.; Fassbender, J.; Mazalski, P.; Maziewski, A.; Wawro, A.; Baczewski, L. T.
SQUID investigations of Ga+ irradiated epitaxial Pt/Co/Pt trilayers
Joint European Magnetic Symposia, 23.-28.08.2010, Krakow, Poland

89. Liskova, E.; Veis, M.; Visnovsky, S.; Mazalski, P.; Maziewski, A.; Liedke, M. O.; Fassbender, J.; Wawro, A.; Baczewski, L. T.
Influence of Ga+ irradiation on MO spectra of Pt/Co/Pt films
Joint European Magnetic Symposia, 23.-28.08.2010, Krakow, Poland

90. Lišková, E.; Veis, M.; Višpovský, Š.; Maziewski, A.; Mazalski, P.; Ferré, J.; Mougin, A.; Liedke, M. O.; Fassbender, J.
Magnetooptical spectroscopy of Ga+ irradiated Pt/Co/Pt sandwiches
IEEE 7th International Symposium on Metallic Multilayers, 19.-24.09.2010, Berkeley, CA, USA

91. Lubk, A.; Gemming, S.; Spaldin, N. A.
First-principles study of ferroelectric domain walls in multiferroic bismuth ferrite
DPG Frühjahrstagung der Sektion Kondensierte Materie, 21.-26.03.2010, Regensburg, Germany

92. Martin, N.; Mönch, I.; Schäfer, R.; Schultz, L.; McCord, J.
Improved vortex nucleation in truncated soft magnetic cones
55th Annual Conference on Magnetism & Magnetic Materials, 14.-18.11.2010, Atlanta, Georgia, USA

93. Martin, N.; Strache, T.; Mönch, I.; Schultz, L.; Fassbender, J.; McCord, J.
Competition of dipolar interactions and lateral exchange spring effect in NiFe elements
55th Annual Conference on Magnetism & Magnetic Materials, 14.-18.11.2010, Atlanta, Georgia, USA

94. Martinavicius, A.; Abrasonis, G.; Möller, W.
Interstitial nitrogen induced decomposition of austenitic stainless steel
International Conference "Radiation Interaction with Material and its Use on Technologies 2010", 20.-23.09.2010, Kaunas, Lithuania

95. Martins, R. M. S.; Schell, N.; Mahesh, K. K.; Silva, R. J. C.; Braz Fernandes, F. M.
In-situ X-ray diffraction studies during deposition of Ni-Ti films
E-MRS 2010 Spring Meeting, 7.-10.06.2010, Strasbourg, France

96. Martins, R. M. S.; Barradas, N.; Alves, E.; Henke, D.; Reuther, H.; Carmezim, M. J.; Silva, T. M.; Fernandes, J. C. S.
Ni-Ti surface modification for enhanced biocompatibility and corrosion performance in biomedical applications
E-MRS 2010 Spring Meeting, 7.-10.06.2010, Strasbourg, France

97. Martins, R. M. S.; Barradas, N.; Alves, E.; Henke, D.; Reuther, H.; Carmezim, M. J.; Fernandes, T. M.; Silva J. C. S.
Ni-Ti surface modification by plasma immersion ion implantation
11th International Symposium on Multiscale, Multifunctional and Functionally Graded Materials, 26.-29.09.2010, Guimarães, Portugal

98. Martins, R. M. S.; Barradas, N.; Alves, E.; Henke, D.; Reuther, H.; Carmezim, M. J.; Silva, T. M.; Fernandes, J. C. S.
Surface modification of Ni-Ti for biomedical applications by plasma-immersion ion implantation
MRS Fall Meeting, 29.11.-3.12.2010, Boston, MA, USA

99. Martins, R. M. S.; Schell, N.; Mahesh, K. K.; Silva, R. J. C.; Braz Fernandes, F. M.
***In-situ* X-ray diffraction studies during magnetron Co-sputtering of Ni-Ti shape memory alloy films**
MRS Fall Meeting 29.11.-3.12.2010, Boston, MA, USA

100. Martins, R. M. S.; Musat, V.; Mücklich, A.; Fortunato, E.
Characterization of mesoporous ZnO:SiO_2 films obtained by the sol-gel method
MRS Fall Meeting, 29.11.-3.12.2010, Boston, MA, USA

101. Mazalski, P.; Maziewski, A.; Tekielak, M.; Ferré, J.; Jaworowicz, J.; Mougin, A.; Liedke, B.; Liedke, M. O.; Fassbender, J.
Ga ion irradiation induced spin reorientations in Co films
4th Euro-Asian Symposium "Trends in MAGnetism": Nanospintronics, 28.06.-2.07.2010, Ekaterinburg, Russia

102. Mazalski, P.; Dobrogowski, W.; Maziewski, A.; Sveklo, I.; Fritzsche, M.; Liedke, M. O.; Fassbender, J.; Wawro, A.; Baczewski, L. T.
Alteration of magnetic anisotropy of Pt/Co/Pt trilayers by FIB irradiation
5th International Conference on Surfaces, Coatings and Nanostructured Materials, 19.-21.10.2010, Reims, France

103. McCord, J.; Mönch, I.; Strache, T.; Fassbender, J.; Mattheis, R.
Local patterning of damping by ion-irradiation in ferromagnetic-antiferromagnetic thin films
IEEE 7th International Symposium on Metallic Multilayers, 20.-24.09.2010, Berkeley, USA

104. McCord, J.; Strache, T.; Mönch, I.; Fassbender, J.; Mattheis, R.
Spatially controlled manipulation of damping in ferromagnetic thin films
Joint European Magnetic Symposia 2010, 27.08.2010, Krakow, Poland

105. Melikhova, O.; Cizek, J.; Kuriplach, J.; Prochazka, I.; Anwand, W.; Brauer, G.; Grambole, D.
Characterization of point defects in yttria stabilized zirconia single crystals
12th International Workshop on Slow Positron Beam Techniques for Solids and Surfaces, 1.-6.08.2010, Magnetic Island/North Queensland, Australia

106. Merchel, S.; Kolitsch, A.; Akhmadaliev, S.; Möller, W.
Bestimmung langlebiger Radionuklide mittels Beschleunigermassenspektrometrie (AMS) mit DREAMS
Deutsche Tagung für Forschung mit Synchrotronstrahlung, Neutronen und Ionenstrahlen an Großgeräten, 24.-26.02.2010, Berlin, Germany

107. Merchel, S.; Braucher, R.; Benedetti, L.; Bourlès, D.
New approaches investigating production rates of in-situ produced terrestrial cosmogenic nuclides
DPG Frühjahrstagung des Arbeitskreises Atome, Moleküle, Quantenoptik und Plasmen, 8.-12.03.2010, Hannover, Germany

108. Merchel, S.; Andermann, C.; Arnold, M.; Aumaître, G.; Bourlès, D.; Braucher, R.; Fuchs, M.; Gloaguen, R.; Klemm, K.; Martschini, M.; Schildgen, Taylor F.; Steier, P.; Wallner, A.; Yildirim, C.
Setting-up chemistry labs for accelerator mass spectrometry
6. Workshop Radiochemische Analytik bei Betrieb und Rückbau kerntechnische Anlagen, der Deklaration von Abfällen und im Strahlenschutz / 23.Seminar Aktivierungsanalyse und Gammaspektroskopie, 6.-8.09.2010, Dresden, Germany

109. Merchel, S.; Arnold, M.; Aumaître, G.; Bourlès, D.; Braucher, R.
How to get a new accelerator mass spectrometry (AMS) facility running: The chemistry part
10th European Conference on Accelerators in Applied Research and Technology, 13.-17.09.2010, Athens, Greece

110. Mok, K. M.; Du, N.; Schmidt, H.
Anisotropic magneto-optical response of metallic thin films probed by vector-magneto-optical generalized ellipsometry
3rd Nano Charm Workshop on Non-Destructive Real Time Process Control, 13.-15.10.2010, Berlin, Germany, and

111. *Trends in Spintronics and Nanomagnetism, 24.-28.05.2010, Lecce, Italy*

112. Moser, J.; Kobs, A.; Vogel, A.; Gerhardt, T.; Bolte, M.; Im, M.-Y.; Fischer, P.; Wintz, S.; Merkt, U.; Oepen, H. P.; Meier, G.
Controlled reduction of the nucleation field in Co/Pt multilayer wires
DPG Frühjahrstagung der Sektion Kondensierte Materie, 21.-26.03.2010, Regensburg, Germany

113. Möller, W.; Kolitsch, A.; Merchel, S.; Zier, M.; Spirit,-Team
Schnelle Ionen für Europa - Das SPIRIT-Projekt
Deutsche Tagung für Forschung mit Synchrotronstrahlung, Neutronen und Ionenstrahlen an Großgeräten, 24.-26.02.2010, Berlin, Germany

114. Munnik, F.; Heller, R.; Neelmeijer, C.
Hydrogen depth profiling with nanometre resolution
2nd International Conference on Functional Nanocoatings, 28.-31.03.2010, Dresden, Germany

115. Munnik, F.; González-Arrabal, R.; Romero, P.; Fernández, P.; Hernández, T.; Gonzalez, M.
μ-ERD and μ-PIXE characterization of H as-implanted and post-implanted annealed Oxide Dispersion Strengthened steel for fusion applications
12th International Conference on Nuclear Microprobe Technology and Applications, 26.-30.07.2010, Leipzig, Germany

116. Munnik, F.; Cabral, A. R.; Lehmann, B.; Radtke, M.; Reinholz, U.; Riesemeier, H.
Spatially-resolved detection of iodine in natural platinum–palladium nuggets: A comparison of PIXE and XRF
12th International Conference on Nuclear Microprobe Technology and Applications, 26.-30.07.2010, Leipzig, Germany

117. Neelmeijer, C.
Treasures as seen under proton irradiation
Analytica Conference 2010, 23.-25.03.2010, München, Germany

118. Neelmeijer, C.; Vieluf, M.; Kosmata, M.; Munnik, F.
High depth resolution analysis of elemental depth distributions in nanocoatings
2nd International Conference on Functional Nanocoatings, 28.-31.03.2010, Dresden, Germany

119. Neelmeijer, C.; Roscher, R.
Original version or not: PIXE-RBS testing of a Meissen porcelain box
Workshop Ionenstrahlphysik, 29.-31.03.2010, FZD, Germany

120. Neelmeijer, C.; Pietsch, U.; Ulbricht, H.
The enduring secret of Meissen Porcelain
38th International Symposium on Archaeometry, 10.-14.05.2010, Tampa, USA

121. Neelmeijer, C.; Roscher, R.
PIXE-RBS survey of a Meissen Porcelain snuffbox: First version or not?
12th International Conference on Particle Induced X-Ray Emission and its Analytical Applications, 27.06.-2.07.2010, Guildford, UK

122. Neudert, A.; Lai, Y. W.; Schäfer, R.; McCord, J.
Field and stress induced twin boundary motion in NiMnGa
E-MRS Strasbourg, 6.-11.06.2010, Strasbourg, France

123. Neudert, A.; Lai, Y. W.; McCord, J.
Twin boundary motion in NiMnGa upon pulsed field excitation
12th International Conference on New Actuators, 14.-16.06.2010, Bremen, Germany

124. Numazawa, S.; Heinig, K.-H.; Ranjan, M.; Facsko, S.
Mechanism of metal nanostructure self-ordering during oblique deposition on pre-patterned surfaces
DPG Frühjahrstagung der Sektion Kondensierte Materie, 21.-26.03.2010, Regensburg, Germany

125. Numazawa, S.; Heinig, K.-H.
Mechanism of selective nano structure formation on pre-patterned surfaces
10th International Conference on Computer Simulations of Radiation Effects in Solids, 19.-23.07.2010, Krakow, Poland

126. Numazawa, S.; Süle, P.; Heinig, K.-H.
Ion patterning of Si studied by kinetic Monte Carlo using ion damage from Molecular Dynamics calculations
17th International Conference on Ion Beam Modification of Materials, 22.-28.08.2010, Montréal, Canada

127. Ou, X.; Das Kanungo, P.; Kögler, R.; Werner, P.; Goesele, U.; Skorupa, W.
Doping of vertical Si nanowires and the carrier profiling
Workshop Ion Beam Physics, 29.-31.03.2010, Dresden, Germany

128. Ou, X.; Das Kanungo, P.; Kögler, R.; Werner, P.; Goesele, U.; Skorupa, W.
Doping of vertical Si nanowires and the carrier profiling
International Conference on Ion Implantation Technology, 6.-11.06.2010, Kyoto, Japan

129. Ou, X.; Das Kanungo, P.; Kögler, R.; Werner, P.; Goesele, U.; Skorupa, W.
Doping of vertical Si nanowires and the carrier profiling
E-MRS 2010 Spring Meeting, 6.-11.06.2010, Strasbourg, France

130. Ou, X.; Das Kanungo, P.; Kögler, R.; Werner, P.; Goesele, U.; Skorupa, W.
Doping of vertical Si nanowires and carrier profiling by scanning spreading resistance microscopy
2010 MRS Fall Meeting, 29.11.-3.12.2010, Boston, USA

131. Pagowska, K.; Ratajczak, R.; Stonert, A.; Turos, A.; Nowicki, L.; Sathish, N.; Jozwik, P.; Mücklich, A.
RBS\channeling and TEM study of damage buildup in ion bombarded GaN
8th International Conference Ion Implantation and Other Applications of Ions and Electrons, 14.-17.06.2010, Kazimierz Dolny, Poland

132. Pantchev, B.; Danesh, P.; Schmidt, B.; Grambole, D.; Bischoff, L.
Ion-beam induced hydrogen redistribution in a-Si:H-based triple layer structures
16th International School on Condensed Matter Physics "Progress in Solid State and Molecular Electronics, Ionics and Photonics", 29.08.-3.09.2010, Varna, Bulgaria

133. Pantchev, B.; Danesh, P.; Wiezorek, J.; Schmidt, B.
Nanoindentation-induced pile-up in hydrogenated amorphous silicon
16th International School on Condensed Matter Physics "Progress in Solid State and Molecular Electronics, Ionics and Photonics", 29.08.-3.09.2010, Varna, Bulgaria

134. Patschureck, C.; McCord, J.; Schäfer, R.; Mattheis, R.; Schultz, L.
Domain width effects on the magneto-dynamic response of CoFeB element arrays
Joint European Magnetic Symposia 2010, 25.08.2010, Krakow, Poland

135. Peplinski, B.; Adam, C.; Reuther, H.; Vogel, C.; Adamczyk, B.; Menzel, M.; Emmerling, F.; Simon, F.-G.
First identification of the tridymite form of AlPO4 in a municipal sewage sludge ash
European Powder Diffraction Conference, 27.-30.08.2010, Darmstadt, Germany

136. Philipp, P.; Schmidt, B.; Zier, M.
Charge carrier depth profiling of boron doped single crystalline silicon by stepwise oxidation profiling
18th International Conference on Ion Implantation Technology, 6.-11.06.2010, Kyoto, Japan

137. Posselt, M.
Evaluation of a new bond-ordered potential for Si
10th International Conference on Computer Simulations of Radiation Effects in Solids, 19.-23.07.2010, Krakow, Poland

138. Posselt, M.
Status of atomic-level simulations of solid phase epitaxial recrystallization of amorphous Si
5th International Conference on Multiscale Materials Modeling, Symposium Microstructure Modeling, 4.-8.10.2010, Freiburg, Germany

139. Posselt, M.; Al-Motasem, A.; Bergner, F.; Birkenheuer, U.
Atomistic study of copper-vacancy clusters in bcc-Fe
5th Forum on New Materials, 14.-18.06.2010, Montecatini Terme, Italy

140. Prochazka, I.; Cizek, J.; Anwand, W.; Brauer, G.; Grambole, D.; Schmidt, H.
Hydrogen-induced surface modifications of ZnO single crystals
12th International Workshop on Slow Positron Beam Techniques for Solids and Surfaces, 1.-6.08.2010, Magnetic Island/North Queensland, Australia

141. Prucnal, S.; Turek, M.; Drozdziel, A.; Pyszniak, K.; Wójtowicz, A.; Zhou, S. Q.; Kanjilal, A.; Shalimov, A.; Skorupa, W.; Zuk, J.
Optical and microstructural properties of self-assembled InAs quantum structures in silicon
E-MRS 2010 Spring Meeting, 7.-10.06.2010, Strasbourg, France

142. Prucnal, S.; Turek, M.; Drozdziel, A.; Pyszniak, K.; Wójtowicz, A.; Kanjilal, A.; Shalimov, A.; Skorupa, W.; Żuk, J.
Optical and microstructural properties of In(As,N) quantum structure made by ion implantation and flash lamp processing
8th International Conference Ion Implantation and Other Applications of Ions and Electrons, 14.-17.06.2010, Kazimierz Dolny, Poland

143. Prucnal, S.; Skorupa, W.; Abendroth, B.; Krockert, K.; Möller, H. J.
Solar cell emitters fabricated by plasma immersion ion implantation and flash lamp millisecond annealing
8th International Conference Ion Implantation and Other Applications of Ions and Electrons, 14.-17.06.2010, Kazimierz Dolny, Poland

144. Prucnal, S.; Skorupa, W.; Abendroth, B.; Krockert, K.; Möller, H. J.
Electro-optical properties of solar cell emitters fabricated by plasma immersion ion implantation and flash lamp millisecond annealing
26th European Photovoltaic Solar Energy Conference and Exhibition, 5.-9.09.2010, Valencia, Spain

145. Ranjan, M.; Facsko, S.; Möller, W.
Biaxial optical anisotropy of self aligned silver nanoparticles and nanowires
DPG Frühjahrstagung der Sektion Kondensierte Materie, 21.-26.03.2010, Regensburg, Germany

146. Ranjan, M.; Facsko, S.; Möller, W.
Self-Organisation of metal nanoparticles on ion beam produced ripple templates
Workshop Ion Beam Physics, 29.-31.03.2010, Dresden, Germany

147. Ranjan, M.; Oates, T. W. H.; Facsko, S.
Self-Organisation of metal nanoparticles and nanowires grown on ripple templates
Nanofair 2010, 6.-7.07.2010, Dresden, Germany

148. Ranjan, M.; Fritzsche, M.; Zhou, J.; Facsko, S.; Möller, W.
Self-assembled Ag nanoparticles on plasma sputtered hexagonally ordered GaSb nanodots
Plasma Surface Engineering, 13.-17.09.2010, Garmisch-Partenkirchen, Germany

149. Rebohle, L.; Kanjilal, A.; Skorupa, W.; Helm, M.
The inverse energy transfer between Ge nanocrystals and erbium in SiO_2 and its dependence on

microstructure
EMRS 2010 Spring Meeting, 6.-11.06.2010, Strasbourg, France

150. Rebohle, L.; Nazarov, A.; Tyagulskii, S.; Tyagulskii, I.; Lehmann, J.; Skorupa, W.
Correlation between the microstructure and the degradation of rare earth implanted Si-based light emitters
3rd International Meeting on Recent Developments in the Study of Radiation Effects in Matter, 24.-28.10.2010, Gramado, Brazil

151. Reiche, I.; Merchel, S.; Radtke, M.; Riesemeier, H.; Bevers, H.
Rare silverpoint drawings by Rembrandt in the focus of SR-XRF
Research Conference on X-ray techniques in the Investigations of the Objects of Cultural Heritage: Around Rembrandt and his Workshop, 13.-16.05.2010, Krakow, Poland

152. Reichel, D.; Skorupa, W.; Lerch, W.; Gelpey, J.
Temperature measurement in rapid thermal annealing
9th International Workshop on Subsecond Thermophysics, 22.-24.09.2010, Graz, Austria

153. Renno, A. D.; Merchel, S.; Michalak, P. P.; Munnik, F.; Wiedenbeck, M.
A development strategy for creating a suite of reference materials for the in-situ microanalysis of non-conventional raw materials
Fall Meeting 2010 of the American Geophysical Union, 13.-17.12.2010, San Francisco, USA

154. Richter, C.; Akhmadaliev, S.; Beyreuther, E.; Dammene, Y.; Karsch, L.; Laschinsky, L.; Leßmann, E.; Naumburger, D.; Schürer, M.; Sobiella, M.; Weber, A.; Pawelke, J.; Baumann, M.
Auf dem Weg zu systematischen radiobiologischen Experimenten mit laserbeschleunigten Protonen: Entwicklung, Charakterisierung und Einsatz eines integrierten Dosimetrie- und Zellbestrahlungssystems
19. Symposium - Experimentelle Strahlentherapie und Klinische Strahlenbiologie, 4.-6.03.2010, Dresden, Germany

155. Roshchupkina, O.; Grenzer, J.; Fritzsche, M.; Fassbender, J.
Structural investigations of the grain growth induced by focused-ion-beam irradiation in thin magnetic films
DPG Frühjahrstagung der Sektion Kondensierte Materie, 21.-26.03.2010, Regensburg, Germany

156. Roshchupkina, O. D.; Grenzer, J.; Strache, T.; Fritzsche, M.; Fassbender, J.
Grain growth induced by focused ion beam irradiation in thin magnetic films
10th Biennial Conference on High Resolution X-Ray Diffraction and Imaging, 20.-23.09.2010, University of Warwick, UK

157. Schmidt, B.; Heinig, K.-H.; Beyer, V.
Memory and electroluminescence properties of silicon nanocrystal MOS-FETs
18th International Conference on Ion implantation Technology, 6.-11.06.2010, Kyoto, Japan

158. Schmidt, H.
Electrical characterization of oxygen vacancies in oxides by means of space charge spectroscopy
Workshop on Positron Annihilation Spectroscopy, 19.10.2010, FZD, Germany

159. Schneider, S.; Bracht, H.; Klug, J.; Lundsgaard Hansen, J.; Nylandsted Larsen, A.; Bougeard, D.; Haller, E.; Posselt, M.; Wündisch, C.
The impact of interstitials on diffusion in germanium under proton irradiation
DPG Frühjahrstagung der Sektion Kondensierte Materie, 21.-26.03.2010, Regensburg, Germany

160. Schreiber, M.; Steinbach, G.; Gemming, S.
Density-functional investigation of the electronic structure at surfaces and interfaces of gallium phosphide
46. Symposium für Theoretische Chemie, 27.-30.09.2010, Münster, Germany

161. Strache, T.; Wintz, S.; Basith, M. A.; Martin, N.; Fritzsche, M.; Mönch, I.; Liedke, M. O.; Körner, M.; Markó, D.; Raabe, J.; Mcvitie, S.; McCord, J.; Fassbender, J.
Saturation magnetization modulated stripes embedded in a ferromagnetic matrix
DPG-Frühjahrstagung der Sektion Kondensierte Materie, 21.-26.03.2010, Regensburg, Germany

162. Strache, T.; Roshchupkina, O.; Fritzsche, M.; Basith, M. A.; McCord, J.; Fassbender, J.
Hybrid magnetic materials created by local ion irradiation
Workshop Ion Beam Physics, 29.-31.03.2010, Dresden, Germany

163. Strache, T.; Wintz, S.; Basith, M. A.; Martin, N.; Fritzsche, M.; Mönch, I.; Liedke, M. O.; Körner, M.; Markó, D.; Raabe, J.; Mcvitie, S.; McCord, J.; Fassbender, J.
Saturation magnetization modulated stripes embedded in a ferromagnetic matrix
Joint European Magnetic Symposia 2010, 27.08.2010, Kraków, Poland

164. Talati, M.; Posselt, M.; Bonny, G.; Al-Motasem, A. T.; Bergner, F.
Contribution of lattice vibrations to the thermodynamics of vacancy clusters in bcc-Fe
5th International Conference on Multiscale Materials Modeling, 4.-8.10.2010, Freiburg, Germany

165. Teichert, Ch.; Hou, Y.; Beinik, I.; Chen, X.; Hsu, Y. F.; Djurisic, A. B.; Anwand, W.; Brauer, G.
Scanning probe microscopy-based characterization of ZnO nanorods
IEEE International NanoElectronics Conference, 3.-8.01.2010, Hong Kong, China

166. Thorn, A.; Ritter, E.; Sokolov, A.; Vorobjev, G.; Bischoff, L.; Herfurth, F.; Kester, O.; Pilz, W.; Thorn, D. B.; Ullmann, F.; Zschornack, G.
Optimization of the Electron Beam Properties of Dresden EBIT for Charge Breeding
International Symposium on Electron Beam Ion Sources and Traps, 18.-23.07.2010, Stockholm, Sweden

167. Tromas, C.; Stinville, J. –C.; Menendez, E.; Villechaise, P.; Nogues, J.; Sort, J.; Templier, C.; Riviere, J. –P.; Martinavicius, A.; Abrasonis, G.
Anisotropy of the elastic and magnetic properties of expanded austenite in AISI 316L stainless steel
12th International Conference on Plasma Surface Engineering, 13.-17.09.2010, Garmisch-Partenkirchen, Germany

168. Tsvetkova, T.; Balabanov, S.; Bischoff, L.; Krastev, V.; Avramova, P. Stefanov I.
X-ray photoelectron study of Si+ ion implanted polymers
16th International School on Condensed Matter Physics "Progress in Solid State and Molecular Electronics, Ionics and Photonics", 29.08.-3.09.2010, Varna, Bulgaria

169. Tyschenko, I. E.; Cherkov, A. G.; Voelskow, M.; Popov, V. P.
Ion-beam synthesis of InSb nanocrystals within the buried SiO_2 layer of silicon-on-insulator structure
18th International Conference on Ion implantation Technology, 6.-11.06.2010, Kyoto, Japan

170. Vinnichenko, M.; Cornelius, S.; Gago, R.; Krause, M.; Shevchenko, N.; Rogozin, A.; Munnik, F.; Kolitsch, A.; Möller, W.
Effect of secondary phase formation on electrical and optical properties of Al-doped ZnO
EFDS-Workshop „Transparente leitfähige Oxide - Festkörperphysikalische Grundlagen und Technologie", 1.-2.06.2010, Dresden, Germany

171. Vinnichenko, M.; Cornelius, S.; Krause, M.; Gago, R.; Munnik, F.; Sergeev, O.; Chakanga, K.; von Maydel, K.; Kolitsch, A.; Möller, W.
Effect of secondary phase formation on optical properties of the Al-doped ZnO
3rd International Symposium on Transparent Conductive Materials, 17.-21.10.2010, Analipsi / Hersonissos, Crete, Greece

172. Vinnichenko, M.; Gago, R.; Cornelius, S.; Rogozin, A.; Shevchenko, N.; Kolitsch, A.; Möller, W.
Mechanism of electrical properties degradation of ZnO:Al films during growth at elevated temperatures
5th Forum on New Materials (in the framework of 12th International Conference on Modern Materials and Technologies), 13.-18.06.2010, Montecatini Terme, Italy

173. Vinnichenko, M.; Gago, R.; Cornelius, S.; Rogozin, A.; Shevchenko, N.; Munnik, F.; Kolitsch, A.; Möller, W.
Thermally-induced formation of secondary phases in ZnO:Al films grown by reactive pulsed magnetron sputtering
12th International Conference on Plasma Surface Engineering, 13.-17.09.2010, Garmisch-Partenkirchen, Germany

174. Voelskow, M.; Grambole, D.; Skorupa, W.; Kanjilal, A.; Kumar, M.; Chatterjee, R.; Milikisiyants, S.; Lakshmi, K. V.; Singh, J. P.
Measurement of the hydrogen concentration in indium oxide tubular nanostructures
Workshop Ion Beam Physics, 29.-31.03.2010, Dresden-Rossendorf, Germany

175. Voelskow, M.; Stoimenos, I.; Rebohle, L.; Skorupa, W.
The formation of near surface SiGe layers with combined high-dose ion implantation and flash-lamp annealing
E-MRS 2010 Spring Meeting, 7.-10.06.2010, Strasbourg, France

176. Vogel, A.; Wintz, S.; Moser, J.; Bolte, M.; Strache, T.; Fritzsche, M.; Im, M.-Y.; Fischer, P.; Meier, G.; Fassbender, J.
Domain-wall pinning and depinning at soft spots in magnetic nanowires
IEEE 7th International Symposium on Magnetic Multilayers, 19.-24.09.2010, Berkeley, USA

177. Wagner, M.; Schneider, H.; Stehr, D.; Winnerl, S.; Helm, M.; Roch, T.; Andrews, A. M.; Schartner, S.; Strasser, G.
Terahertz induced intra-excitonic Autler-Townes effect in semiconductor quantum wells
30th International Conference on the Physics of Semiconductors, 25.-30.07.2010, Seoul, South Korea

178. Wagner, M.; Golde, D.; Stehr, D.; Schneider, H.; Helm, M.; Andrews, A. M.; Roch, T.; Strasser, G.; Kira, M.; Koch, S. W.
Fano signatures in the intersubband THz response of GaAs/AlGaAs quantum wells after interband

photoexcitation
30th International Conference on the Physics of Semiconductors, 25.-30.07.2010, Seoul, South Korea

179. Wagner, M.; Schneider, H.; Stehr, D.; Winnerl, S.; Andrews, A. M.; Schartner, S.; Strasser, G.; Helm, M.
Terahertz nonlinear optics using intraexcitonic quantum well transitions: Sideband generation and AC stark splitting
10th International workshop on Nonlinear Optics and Excitation Kinetics in Semiconductors, 16.-19.08.2010, Paderborn, Germany

180. Weißbach, T.; Leisegang, T.; Lubk, A.; Meyer, D. C.; Gemming, S.
Electronic structure and magnetism in $YFeMnO_5$
DPG Frühjahrstagung der Sektion Kondensierte Materie, 21.-26.03.2010, Regensburg, Germany

181. Wenisch, R.; Forrer, D.; Gross, S.; Casarin, M.; Montagner, D.; Vittadini, A.; Helm, M.; Tondello, E.; Gemming, S.
Spectroscopic and theoretical investigations on Pd(II) and Pt(II) dithiocarbamates
DPG Frühjahrstagung der Sektion Kondensierte Materie, 21.-26.03.2010, Regensburg, Germany

182. Wiemann, R.; Kosmata, M.; Vieluf, M.; Hanf, D.; Liechtenstein, V. Kh.; Grötzschel, R.
Ladungsabhängigkeit des Bremsvermögens und der Umladungsquerschitte von leichten MeV Schwerionen in ultradünnen DLC Kohlenstofffolien
Deutsche Tagung für Forschung mit Synchrotronstrahlung, Neutronen und Ionenstrahlen an Großgeräten, 24.-26.02.2010, Berlin, Germany

183. Wieser, M.; Grebing, J.; Höwler, M.; Bernert, K.; Schmidt, B.; Fassbender, J.; Erbe, A.
Electrical contacting of vertical nanostructures
DPG Frühjahrstagung der Sektion Kondensierte Materie, 21.-26.03.2010, Regensburg, Germany

184. Wiest, F.; Eggert, T.; Fojt, R.; Höllt, L.; Knobloch, J.; Pahlke, A.; Pahlke, S.; Stötter, R.; Schmidt, B.; Lange, H.
Silicon sensors realized by KETEK in co-operation with FZD
Workshop Ion Beam Physics, 29.-31.03.2010, Dresden-Rossendorf, Germany

185. Wilde, C.; Möller, W.; Neidhardt, J.
Effect of temperature on the retention of 2 keV Cs^+ ions in Si
Workshop Ion Beam Physics, 29.-31.03.2010, Dresden-Rossendorf, Germany

186. Wilhelm, R. A.; Heller, R.; El-Said, A. S.; Facsko, S.
Surface modification on KBr (001) with slow highly charged ions
International Symposium on Electron Beam Ion Sources and Traps,7.-10.04.2010, Stockholm, Sweden

187. Winnerl, S.; Helm, M.; Malic, E.; Knorr, A.
Relaxation dynamics in graphene investigated in the mid- and far-infrared spectral range
Begutachtungskolloquium zum Schwerpunktprogram "Graphen" der DFG, 21.-22.01.2010, Bad Honnef, Germany

188. Winnerl, S.; Schneider, H.; Stehr, D.; Helm, M.; Seidel, W.; Michel, P.; Zibik, E. A.; Carpenter, B. A.; Porter, N. E.; Wilson, L. R.; Grange, T.; Ferreira, R.; Bastard, G.; Liu, H. C.; Y. Song, C.; Bründermann, E.
Time-resolved terahertz spectroscopy and imaging at the FELBE free-electron laser facility
International Forum on Terahertz Spectroscopy and Imaging, 2.-3.03.2010, Kaiserslautern, Germany

189. Winnerl, S.; Hubrich, R.; Peter, F.; Schneider, H.; Helm, M.
The spatial structure of longitudinal and transversal fields in focussed terahertz beams
DPG Frühjahrstagung der Sektion Kondensierte Materie, 22.-26.03.2010, Regensburg, Germany

190. Winnerl, S.; Hubrich, R.; Peter, F.; Helm, M.; Schneider, H.
Longitudinal THz electric fields in the focus of radially polarized beams
5th International Symposium on Ultrafast Phenomena & Terahertz Waves, 12.-16.09.2010, Xi'an, China

191. Winnerl, S.; Orlita, M.; Plochocka, P.; Schneider, H.; Helm, M.; Kossacki, P.; Potemski, M.; Sprinkle, M.; Berger, C.; de Heer, W. A.
Relaxation dynamics in epitaxial graphene probed at low excitation energies
2nd International Symposium on the Science and Technology of Epitaxial Graphene, 14.-17.09.2010, Amelia Island, USA

192. Wintz, S.; Vogel, A.; Moser, J.; Bolte, M.; Strache, T.; Fritzsche, M.; Im, M.-Y.; Fischer, P.; Meier, G.; Fassbender, J.
Domain-wall pinning and depinning at magnetic soft spots in nanowires
11th Joint MMM-Intermag Conference, 18.-22.01.2010, Washington D.C., USA

193. Wintz, S.; Puzic, A.; Strache, T.; Körner, M.; Bunce, C.; Markó, D.; Grebing, J.; Fritzsche, M.; Moench, I.; Mattheis, R.; Erbe, A.; Raabe, J.; Quitmann, C.; Fassbender, J.
Magnetization dynamics of coupled vortices
IEEE 7th International Symposium on Magnetic Multilayers, 19.-24.09.2010, Berkeley, USA

194. Wündisch, C.; Posselt, M.; Schmidt, B.; Heera, V.; Mücklich, A.; Skorupa, W.; Clarysse, T.; Simoen, E.; Hortenbach, H.
Doping of germanium by ion implantation and flash lamp annealing
Workshop Ion Beam Physics, 29.-31.03.2010, Dresden, Germany

195. Yankov, R. A.; Kolitsch, A.; Munnik, F.; von Borany, J.
Formation of an alumina-containing scale for the surface protection of TiAl alloys and Ti against environmental degradation at elevated temperatures
12th International Conference on Modern Materials and Technologies and 12th International Ceramic Congress, 6.-11.06.2010, Montecatini Terme, Italy

196. Yankov, R. A.; Kolitsch, A.; Munnik, F.; von Borany, J.
Suppression of oxygen-induced embrittlement in Ti by plasma immersion ion implantation (PIII)-based processing
12th International Conference on Plasma Surface Engineering, 13.-17.09.2010, Garmisch-Partenkirchen, Germany

197. Yankov, R. A.; Kolitsch, A.; Munnik, F.; von Borany, J.; Donchev, A.; Schütze, M.
Surface protection of TiAl alloys and Ti against high-temperature environmental degradation
Dresdner Werkstoffsymposium Werkstoffe der Energietechnik, 9.-10.12.2010, Dresden, Germany

198. Zeil, K.; Metzkes, J.; Kraft, S.; Kluge, T.; Bussmann, M.; Schmidt, B.; Zier, M.; Schramm, U.; Cowan, T.; Sauerbrey, R.
Laser proton acceleration from mass limited targets
4th International Conference on Superstrong Fields in Plasmas, 3.-9.10.2010, Varenna, Italia

199. Zhou, S.; Bürger, D.; Baumgart, C.; Skorupa, W.; Timm, C.; Oesterlin, P.; Helm, M.; Schmidt, H.
Hysteresis in the magneto-transport of Manganese-doped Germanium: Evidence for carrier-mediated ferromagnetism
30th International Conference on the Physics of Semiconductors, 25.-30.07.2010, Seoul, South Korea

200. Zhou, S.; Bürger, D.; Baumgart, C.; Skorupa, W.; Timm, C.; Oesterlin, P.; Helm, M.; Schmidt, H.
Manganese doped Germanium: From clustering to carrier-mediated ferromagnetism
International Conference on Physics and Applications of Spin Related Phenomena in Semiconductors, 1.-4.08.2010, Tokyo, Japan

201. Zhou, S.; Bürger, D.; Skorupa, W.; Timm, C.; Oesterlin, P.; Helm, M.; Schmidt, H.
Manganese implanted Germanium: From clustering to carrier-mediated ferromagnetism
17th International Conference on Ion Beam Modification of Materials, 22.-27.08.2010, Montreal, Canada

202. Zier, M.; Reinholz, U.; Riesemeier, H.; Radtke, M.; Munnik, F.
Ions and X-rays: Unique partners for accurate stopping power determination of ^{15}N ions in Si for hydrogen depth profiling
Deutsche Tagung für Forschung mit Synchrotronstrahlung, Neutronen und Ionenstrahlen an Großgeräten, 24.-26.02.2010, Berlin, Germany

203. Zschintzsch, M.; Jeutter, N.; Mücklich, A.; von Borany, J.; Sahle, C.
Self-organized formation of Ge nanocrystals out of (GeO_x-SiO_2) superlattice structures
2010 MRS Spring Meeting, 5.-9.04.2010, San Francisco, California, USA

204. Zschintzsch, M.; Jeutter, N.; von Borany, J.; Mücklich, A.; Sahle, C.
Confined Ge nanocrystals in an oxide matrix for multiple bandgap solar cells
8th International Nanotechnology Symposium Nanofair 2010, 6.-7.07.2010, Dresden, Germany

205. Zschintzsch, M.; Jeutter, N.; von Borany, J.; Mücklich, A.; Sahle, C.
Multiple bandgap solar cells based on confined Ge nanocrystals in an oxide matrix
25th European Phototvoltaic Solar Energy Conference and 5th World Conference on Photovoltaic Energy Conversion, 6.-10.09.2010, Valencia, Spain

206. Zschornak, M.; Gutmann, E.; Weißbach, T.; Leisegang, T.; Meyer, D. C.; Gemming, S.
DFT modelling of $SrO(SrTiO_3)_n$ Ruddlesden-Popper surfaces
DPG Frühjahrstagung der Sektion Kondensierte Materie, 21.-26.03.2010, Regensburg, Germany

207. Zschornak, M.; Richter, C.; Stöcker, H.; Leisegang, T.; Gemming, S.; Meyer, D. C.
Polarization dependent diffraction anomalous fine structure of rutile TiO_2 (001) and (111) reflections
DPG Frühjahrstagung der Sektion Kondensierte Materie, 21.-26.03.2010, Regensburg, Germany

208. Zschornak, M.; Gutmann, E.; Stöcker, H.; Shakverdova, I.; Meyer, D. C.; Gemming, S.
Modeling of Ruddlesden-Popper surfaces and oxygen vacancies in strontium titanate
International Conference on Advanced Materials Modelling, 7.-10.07.2010, Nantes, France

209. Zschornak, M.; Richter, C.; Novikov, D.; Stöcker, H.; Leisegang, T.; Gemming, S.; Meyer, D. C.
Oxygen vacancy contribution on the polarization dependent DAFS of Rutile TiO_2
26th European Crystallographic Meeting, 30.08.-2.09.2010, Darmstadt, Germany

210. Zybell, S.; Schneider, H.; Wagner, M.; Winnerl, S.; Köhler, K.; Helm, M.
Time-resolved photoluminescence from undoped GaAs/$Al_{0.35}Ga_{0.65}As$ quantum wells quenched by pulsed midinfrared radiation
DPG Frühjahrstagung der Sektion Kondensierte Materie, 21.-26.03.2010, Regensburg, Germany

Lectures / Talks

1. Abrasonis, G.
Ion-assisted phase separation during the growth of carbon-transition metal nanocomposite thin films
Seminar Talk, Département Physique et Mécanique des Matériaux, Institut P', UPR 3346 CNRS, Université de Poitiers, 7.12.2010, Futuroscope Chasseneuil Cedex, France

2. Baehtz, C.
Synchrotron radiation in materials science
Seminar Talk, TU Bergakademie Freiberg, 3.05.2010, Freiberg, Germany

3. Ball, D.; Fassbender, J.; Lenz, K.; Markó, D.; Körner, M.; Fritzsche, M.; Strache, T.; Mücklich, A.; Albrecht, M.; Makarov, D.; Tibus, S.; Krone, P.**Investigating the magnetic properties of tailored bit patterned media using ferromagnetic resonance** *Group Seminar, TU München, 9.06.2010, München, Germany*

4. Baumgart, C.
Quantitative KPFM measurements on Silicon nanowire structures
Workshop FZD/FZJ: Silicon Nanowire Structures, 29.04.2010, Dresden, Germany

5. Baumgart, C.; Helm, M.; Schmidt, H.
Quantitative Kelvin probe force microscopy on semiconductors
2. Wissenschaftliches Seminar des Dresdner Fraunhofer-Clusters Nanoanalytik, 05.08.2010, Dresden, Germany

6. Bischoff, L.
Focused ion beams
SPIRIT Tutorial "Ion Implantation and Irradiation", 13.-14.12.2010, Dresden, Germany

7. Bischoff, L.; Heinig, K.-H.
Selbstorganisierte Oberflächenmuster auf Germanium durch schwere Clusterionen
DFG Forschergruppe 845 Projektantragsrunde, 20.-21.05.2010, Leipzig, Germany

8. Borany, J. von
Next jump of energy efficiency of photovoltaics technology - not only a vision!
7th Innovationsforum for Automation, 21.-22.01.2010, Dresden, Germany

9. Borany, J. von; Schmidt, B.
Ionenimplantierte Halbleiterstrukturen fuer die Strahlungssensorik
Innovationsforum Sonden fuer Hydrogeologie und Rohstofferkundung, 24.09.-25.10.2010, Dresden, Germany

10. Borany, J. von
High-energy ion implantation für Si device applications
SPIRIT Tutorial "Ion Implantation and Irradiation", 13.-14.12.2010, Dresden, Germany

11. Bürger, D.; Zhou, S.; Baumgart, C.; Skorupa, W.; Timm, C.; Oesterlin, P.; Helm, M.; Schmidt, H.
Hysteresis in the magneto-transport of manganese-doped germanium: Evidence for carrier-mediated ferromagnetism
47. Punktdefekttreffen, 7.-8.10.2010, Dresden, Germany

12. Facsko, S.
Surface nanostructures induced by low energy ion sputtering
Birck Nanoscience Center Seminar, 28.04.201, West Lafayette, Indiana, USA

13. Facsko, S.
Surface patterning by low energy ion sputtering
Seminar der Physikfakultät, 25.11.2010, Cosenza, Italy

14. Fiedler, J.; Heera, V.; Skrotzki, R.; Herrmannsdörfer, T.; Voelskow, M.; Mücklich, A.; Schmidt, B.; Posselt, M.; Skorupa, W.; Helm, M.; Gobsch, G.
Superconductivity in Group IV Semiconductors
Punktdefekttreffen, 7.-8.10.2010, Dresden, Germany

15. Gemming, S.
Density-functional theory within multi-scale modelling
Wilhelm-und-Else-Heraeus Physics School on Density Functional Theory and its Applications in Crystallography, 7.-11.02.2010, Aachen, Germany

16. Gemming, S.
Conductivity in DFT
Wilhelm-und-Else-Heraeus Physics School on Density Functional Theory and its Applications in Crystallography, 7.-11.02.2010, Aachen, Germany

17. Gemming, S.
From molecular chemistry to solid state physics – chemical concepts in material science
Institutskolloquium - Institut für Chemie und Biochemie / Physikalische und Theoretische Chemie der Freien Universität Berlin und Kolloquium des Graduiertenkollegs 788, 3.06.2010, Berlin, Germany

18. Gemming, S.; Erbe, A.; Facsko, S.
Nanostructures - small and beautiful
Physikalisches Kolloquium, 7.07.2010, Freiberg, Germany

19. Grenzer, J.; Biermanns, A.; Akhmadaliev, C.; Bischoff, L.
X-ray Investigations on $CoSi_2$ nano wires manufactured by focused ion beam synthesis
Science with X-ray Nano-beams, 9.-12.02.2010, Grenoble, France

20. Grenzer, J.
In-situ X-ray scattering: A tool to investigate the formation of nanostructures
Swiss Light Source (SLS) Seminar, 19.02.2010, Villigen, Switzerland

21. Kolitsch, A.
Ions for nanotechnology
Jahresempfang der Slowakischen Technischen Universität Bratislava, 21.01.2010, Trnava, Slovak Republic

22. Kosmata, M.; Munnik, F.; Neelmeijer, C.; Heller, R.; Vieluf, M.; Merchel, S.; Möller, W.
Analyse ultradünner Schichten und deren Grenzflächen mit Nanometertiefenauflösung
Seminar am Institut für Halbleiter- und Mikrosysteme, TU Dresden, 25.02.2010, Dresden, Germany

23. Körner, M.; Lenz, K.; Liedke, M. O.; Strache, T.; Keller, A.; Facsko, S.; Fassbender, J.
Morphology induced magnetic phenomena
Group Seminar, TU München, 9.06.2010, München, Germany

24. Martin, N.; Schäfer, R.; Fassbender, J.; Schultz, L.; McCord, J.
Herstellung und Charakterisierung magnetisch heterogener, dünner Schichten
VAC-Kolloqium, 9.-10.12.2010, Hanau, Germany

25. McCord, J.
Blending magnetic properties - hybrid magnetic thin films
Colloquium of the "Sonderforschungsbereich 855" - Magnetoelektrische Verbundwerkstoffe - Biomagnetische Schnittstellen der Zukunft, 1.07.2010, Kiel, Germany

26. McCord, J.; Hamann, C.; Strache, T.; Martin, N.; Mönch, I.; Mattheis, R.; Kaltofen, R.; Quandt, E.; Fassbender, J.
Magnetic hybrid films - magnetic property patterning by ion irradiation
„Struktur und Eigenschaften kondensierter Materie“ Seminar der TU Chemnitz, 23.11.2010, TU Chemnitz, Germany

27. Merchel, S.
Ungeduldige Wissenschaftler: Bestimmung langlebiger Radionuklide mittels Beschleunigermassen-spektrometrie (AMS)
Glaziologie-Seminar, Alfred-Wegener-Institut für Polar- und Meeresforschung, 18.02.2010, Bremerhaven, Germany

28. Munnik, F.; Heller, R.
Ion Beam Analysis at FZD: Achievements and perspectives
Materials Science Seminar, 19.01.2010, Dresden, Germany

29. Munnik, F.; Heller, R.
Channeling as a means to obtain information on crystal quality and structure
New detector technologies for advanced materials research using ion beam analysis, 25.-26.10.2010, Plitvice Lakes, Croatia

30. Neelmeijer, C.
Ionen als Agenten und Detektive
Schülervortrag, 1.02.2010, Dresden, Germany

31. Neelmeijer , C.
Kunstwerke - zerstörungsfreie Materialanalyse
Vorlesung, 24.02.2010, Dresden, Germany

32. Neelmeijer, C.; Pietsch, U.; Ulbricht, H.
Das Arcanum von Meissner Porzellan: Beharrung oder Wandel?
DGZfP Arbeitskreis 2010, 9.12.2010, Residenzschloss Dresden, Germany

33. Neudert, A.; Schäfer, R.; McCord, J.
Domains and Dynamics in NiMnGa
SPP Convention Tutzing, 29.09.2010, Tutzing, Germany

34. Posselt, M.
Experimentelle und theoretische Untersuchungen zur elektrischen Aktivierung von Dotanden und zur Festphasenepitaxie in Ge
Seminar des Instituts für Materialphysik der Universität Münster, 1.06.2010, Münster, Germany

35. Posselt, M.
Kinetics and thermodynamics of defects, impurities, nanostructures and interfaces
Seminar Talk, SRMP, Department des Materiaux pour le Nucleaire, CEA Saclay, 10.12.2010, Saclay/Paris, France

36. Schmidt, B.; Haberjahn, M.; Lange, H.; Hanf, D.
Ion-implanted silicon detectors - Silicon strip detectors
1st SPIRIT Workshop on New detector technologies for advanced materials research using ion beam analysis, 25.-26.10.2010, Plitvice Lakes, Croatia

37. Schmidt, H.
Electrical characterization of semiconductors on the mm-nm length scale
Fraunhofer IZFP-Kolloquium, 25.10.2010, Saarbrücken, Germany

38. Schneider, H.
Ultrafast and nonlinear terahertz spectroscopy of semiconductor quantum structures
Condensed Matter Physics Colloquium, 21.09.2010, Hefei, China

39. Schreiber, M.; Steinbach, G.; Gemming, S.
Density-functional investigation of the electronic structure at surfaces and interfaces of gallium phosphide
Arbeitstreffen GaP-based Devices, 12.11.2010, Berlin, Germany

40. Skorupa, W.
Doping issues of Si nanowires
27. Deutsches Nutzertreffen RTP und Heissprozesse, 5.05.2010, Erlangen, Germany

41. Skorupa, W.
Doping of vertical Si nanowires by ion implantation
43. Deutsches Nutzertreffen Ionenimplantation, 6.05.2010, Erlangen, Germany

42. Skorupa, W.
Doping & annealing issues of electronic materials
SPIRIT Tutorial "Ion Implantation and Irradiation", 13.-14.12.2010, Dresden, Germany

43. Vinnichenko, M.; Cornelius, S.; Rogozin, A.; Shevchenko, N.; Gago, R.; Kolitsch, A.; Möller, W.
Electrical properties, structure and phase composition of transparent conducting oxide thin films: effect of elevated temperatures
Invited Lecture, Department "Solare Brennstoffe", Helmholtz-Zentrum Berlin für Materialien und Energie GmbH, 22.01.2010, Berlin, Germany

44. Vinnichenko, M.
Capabilities and limitations of spectroscopic ellipsometry for characterization of functional thin films
Invited lecture during visit to "Next Energy" EWE-Forschungszentrum für Energietechnologie e.V., 10.-11.02.2010, Oldenburg, Germany

45. Vinnichenko, M.; Cornelius, S.; Rogozin, A.; Shevchenko, N.; Gago, R.; Kolitsch, A.; Möller, W.
Properties, structure and phase composition of transparent conductive oxide thin films grown by magnetron sputtering
Invited lecture during visit to "Next Energy" EWE-Forschungszentrum für Energietechnologie e.V., 10.-11.02.2010, Oldenburg, Germany

46. Zhou, S.; Bürger, D.; Baumgart, C.; Skorupa, W.; Timm, C.; Oesterlin, P.; Helm, M.; Schmidt, H.
Manganese doped germanium: From clustering to carrier-mediated ferromagnetism
Invited Talk at the Institute of Physics, Chinese Academy of Sciences, 13.04.2010, Beijing, China

47. Zhou, S.
Transition metal implanted ZnO: Have we obtained a diluted magnetic semiconductor?
Invited Talk at Shanghai Institute of Microsystem and Information Technology, Chinese Academy of Sciences, 8.11.2010, Shanghai, China

Workshops

1. Merchel, S., Faßbender, J., Helm, M., Facsko, S.
International Workshop „Ion Beam Physics“
29.-31.03.2010, Dresden-Rossendorf, Germany

2. Helm, M., Wosnitza, J., Zvyagin, S., Schneider, H., Winnerl, S., Stehr, D., van der Zande, W., Engelkamp, H.
Terahertz Spectroscopy and its High-Field Applications & EuroMagNET II User Meeting
14.-16.06.2010, Dresden-Rossendorf, Germany

3. Baumgart, C., Schmidt, H.
Common FZD / FZJ Workshop „Silicon Nanowire Structures“
29.04.2010, Dresden-Rossendorf, Germany

4. **IEEE Magnetics Society Summer School**
Local Organizers: Fassbender, J., Mc.Cord, J., Gutfleisch, O.
16.-20.08.2010, Dresden, Germany

5. Merchel, S. (FZD), Knappik, R. (VKTA)
6. Workshop RCA (Radiochemische Analytik bei Betrieb und Rückbau kerntechnischer Anlagen, der Deklaration von Abfällen und im Strahlenschutz) **& 23. SAAGAS** (Seminar Aktivierungsanalyse und Gammaspektroskopie)
6.-9.09.2010, Dresden, Germany

6. Wagner, A., Potzger, K.
Workshop on Positron Annihilation Spectroscopy
19.10.2010, Dresden-Rossendorf, Germany

Patents

1. Kolitsch, A.; Yankov, R.; Donchev, A.; Schütze, M.
Erhöhung der von TiAl-Legierungen und daraus bestehenden Bauteilen durch PI³
Patent DE102008028990A1 / 11.02.2010

2. Rebohle, L.; Skorupa, W.
Silizium-basierter Lichtermitter auf SOI-Substraten
Patent: DE102008037225A1 / 25.02.2010

3. Voelskow, M.; Kanjilal, A.; Skorupa, W.
Verfahren zur Herstellung von Halbleiterstrukturen auf Silizium-Germanium-Basis mit erhöhter Effizienz
Patent: DE 10 2008 035 846 A1 / 4.02.2010

PhD Theses

1. Cantelli, V.
Growth, structure and magnetic properties of magnetron sputtered FePt thin films
TU Dresden, 15.03.2010

2. Cherkouk, C.
Östrogennachweis in wässrigen Lösungen mit Hilfe Silizium-basierter Lichtemitter
TU Dresden, 6.10.2010; Wissenschaftlich-Technische Berichte FZD-542/2010.

3. Marko, D.
Magnetostatics and dynamics of ion irradiated NiFe/Ta multilayer films studied by VNA-FMR
TU Dresden, 25.11.2010

4. Peter, F.
Advanced emitters and detectors for terahertz time-domain spectroscopy
TU Dresden, 4.06.2010; Wissenschaftlich-Technische Berichte FZD 538/2010.

5. Talut, G.
Ferromagnetismus in mit Fe implantierten GaN und TiO_2
TU Dresden, 1.03.2010

6. Thieme, M.
Investigations of the binary system Vanadium:Silicon - DFT-simulations based on experimental results
TU Dresden, 3.06.2010

7. Vieluf, M.
Hochauflösende Rutherford-Streuspektrometrie zur Untersuchung von ZrO_2-Schichtwachstum im Anfangsstadium
TU Dresden, 3.06.2010; Wissenschaftlich-Technische Berichte FZD-537/2010.

8. Wagner, M.
Terahertz studies on semiconductor quantum heterostructures in the low and high field regime
TU Dresden, 23.03.2010; Wissenschaftlich-Technische Berichte FZD-532/2010.

Diploma Theses

1. Mittendorf, M.
Messung der komplexen Leitfähigkeit von Halbleiterproben im THz-Bereich
Hochschule Darmstadt, 28.09.2010

Colloquia

1. Cuniberti, G.
Institue of Materials Science, University of Technology Dresden, Germany
Molecular electronics: "In weiter Ferne, so nah!"
22.04.2010

2. Ganteför, G.
Fachbereich Physik, Universität Konstanz, Germany
Small is different. Nanoparticles with surprising properties
10.06.2010

3. Gao, F. (FZD Fellow 2008)
Pacific Northwest Laboratory, Richland, USA

4. **Materials behavior under extreme conditions: Multi-scale computer simulations**
30.07.2010 (FZD-Colloquium)

5. Malerba, L.,
Reactor Materials Research, Belgian Nuclear Research Centre, Mol, Belgium
Modelling nanostructural changes in metals under irradiation
12.01.2010

6. Michel, J.
Microphotonics Center, Massachusetts Institute of Technology, Cambridge, MA, USA
Ge optoelectronic devices for silicon photonics
8.07.2010

7. Mikolajick, T.
Chair of NamLab, University of Technology Dresden, Germany
Semiconductor memories: Current status and a look into the future
4.02.2010

8. Muenzenberg, M.
I. Physikalisches Institut, Universität Göttingen, Germany
Ferromagnets stirred up
20.05.2010

9. O'Grady, K.
Department of Physics, University of York, Heslington, York, UK
A new paradigm for exchange bias in polycrystalline films
12.08.2010

10. Osten, H.-J.
Institut of Electronic Materials and Devices, Leibniz University Hannover, Germany
Epitaxial oxides on silicon for CMOS and beyond
14.01.2010

11. Schmidt, G.
Institut für Physik, Martin-Luther-Universität Halle-Wittenberg, Germany
Using anisotropic crystalline ferromagnets for spintronics
4.11.2010

12. Smith, R.
Department of Mathematical Sciences, Loughborough University, UK
Multiscale modelling: From nanoindentation to thin film growth
27.05.2010

13. Stöhlker, T.,
Atomic Physics Department, Helmholtz-Zentrum für Schwerionenforschung GSI, Darmstadt, Germany
Heavy ions at GSI: From fundamental physics to applications
11.02.2010

14. Trautmann, C.
Helmholtz-Zentrum für Schwerionenforschung GSI, Darmstadt, Germany
Materials research and nanotechnology with MeV-GeV ion beams
29.04.2010

Theory / Materials Science Seminar

1. Heinig, K.-H.
Kinetic Lattice Monte Carlo Simulations (KLMCS) in materials science
11.03.2010

2. Munnik, F. and Heller, R.
Ion beam analysis at FZD: Achievements and perspectives
19.01.2010

3. Posselt, M.
Molecular dynamics in materials science
04. 03. 2010

4. Zhou, S.
Ferromagnetic semiconductors prepared by magnetic ion implantation and pulsed laser annealing
18.05.2010

Seminars

1. Andermann, C.
TU Bergakademie Freiberg, Germany and Université de Rennes, France
Erosian in the Himalaya from cosmogenic nuclides
15.06.2010

2. Bald, I.
Interdisciplinary Nanoscience Center, Aarhus University, Denmark
Low-energy processes in DNA radiation damage – Site and energy selective bond breaking induced by electrons and ions
27.10.2010

3. Bauer, C.
Physikalische Chemie III, Universität Bielefeld, Germany
Differenzspektroskopie an Bacteriorhodopsin im fernen Infrarot
20.12.2010

4. Basov, D.N.
University of California, San Diego, USA
Correlated electron matter at the nanoscale: Electronic phase separation and memory effects
23.08.2010

5. Bogdanovic Radovic, I.
Experimental Physics Division, Rudjer Boskovic Institute, Zagreb, Croatia

Analysis and modification of thin layers by heavy ion beams
31.03.2010

6. Bristowe, P.D.
Department of Materials Science and Metallurgy, Cambridge University, UK
Atomistic studies of interfacial failure in optical multilayer coatings
9.03.2010

7. Diesing, D.
Universität Duisburg-Essen, Germany
The detection of ion induced excited electrons in deeper layers of metal substrates
26.05.2010

8. Dubois, C. and Prudon, G.
CNRS & Université de Lyon, France
SIMS measurement of high concentrations of elements in semiconductors using the Isotopic Comparative Method (ICM)
22.07.2010

9. Eder, F.
Atominstitut Wien, Austria
Vulkanglas unter Beschuss: Ionenstrahl- und Neutronenaktivierungsanalyse
12.08.2010

10. Gensch, M.
BESSY at Helmholtz-Center Berlin, Germany
Low energy excitations: Experiments with THz radiation from accelerator-based sources
3.06.2010

11. Günther, M.
Institut für Physik, TU Chemnitz, Germany
SiCN Abscheidung mittels PECVD
20.03.2010

12. Hirakawa, K.
Tokyo University,Japan
Fabrication and novel physics in ultrasmall nanogap-electrode / quantum-nanostructure junctions
14.04.2010

13. Kalathiparambil, K. K.
Institute for Plasma Physics and Facilitation Center for Plasma Technologies Bhat, Ghandinagar, India
Structural properties of Ti based nanocomposite coatings
1.04.2010

14. Khurgin, J.
Johns Hopkins University, Baltimore MD , USA
Plasmonic enhancement of optical properties: Figures of merit
13.01.2010

15. Kleiner, A.
Institut für halbleiter- und Mikrosystemtechnik, TU Dresden, Germany
Herstellung und Charakterisierung und Vergleich von Antihaftschichten auf Si, SiO_2 und Chromoberflächen für das UV-Nanoimprinting
22.10.2010

16. Kokkoris, M.
Faculty of Applied Sciences, National Technical University of Athens, Greece
On the implementation of nuclear data for the study of fundamental channelling parameters
10.06.2010

17. Lindner, J.
Experimentalphysik, Universität Duisburg-Essen, Germany
Spin dynamics in nanomagnets from ensemble to single structure investigations
21.04.2010

18. Maydell, K. von
NEXT ENERGY EWE-Forschungszentrum für Energietechnologie e. V.,
Carl von Ossietzky Universität Oldenburg
Thin film silicon solar cell research and development at NEXT ENERGY
23.03.2010

19. Mc Vitie, S.
Department of Physics and astronomy, University of Glasgow, UK
TEM studies of domain walls
8.03.2010

20. Mukherjee, S
Institute for Plasma Research, Ghandinagar, India
Industrial plasma application at the facilitation Centre for Industrial Plasma Technologies
10.09.2010

21. Nazarov, A.N
Institute of Semiconductor Physics, National Academy of Sciences of Ukraine, Kiev, Ukraine
Electrical diagnostics of high-k dielectric silicon structures
13.12.2010

22. Nembach, H. T.
Magnetics Group, Electromagnetics Division, National Institute of Standards and Technology, Boulder, USA
Dependence of the magnetic properties of Co_2MnGe on Ge content and annealing temperature
29.03.2010

23. Poll, I. and Bugoi, R.
National Institute for Nuclear Physics and Engineering, Bucharest, Romania
Glass bracelets discovered in archaeological centers from Romania (3rd century BC – 18th century AC)
12.08.2010

24. Ritter, R.
Institute for Applied Physics, TU Vienna, Austria
Systematic studies of ion-induced defects on polymethylmetacrylate (PMMA) and titanium oxide TiO_2
1.07.2010

25. Rugel, G.
Physik-Department, TU München, Germany
Beschleuniger-Massenspektrometrie mit mittelschweren Isotopen am Münchner Tandembeschleuniger
2.12.2010

26. Salvan, S.
Physics Department, Chemnitz University of Technology, Chemnitz, Germany
Magneto-optical Kerr effect spectroscopy applied to the study of thin molecular films
23.11.2010

27. Schalley, C.A.
Institut für Chemie und Biochemie der Freien Universität Berlin, Germany
Tandem-Massenspektrometrie als Methode zur Untersuchung von Struktur und Reaktivität in der Gasphase
18.11.2010

28. Schnohr, C.
Institut für Festkörperphysik, Friedrich-Schiller-Universität Jena, Germany
Amorphous phase formation and structure in III-V semiconductors
18.11.2010

29. Wang, T.
University of Lanzhou, China
Introduction to nuclear research activities in Lanzhou, China
27.07.2010

30. Yildirim, C.
GeoForschungsZentrum Potsdam, Germany
Topology and cosmogenic nuclides
15.06.2010

31. Zahn, P.
Institut für Physik, Universität Halle-Wittenberg, Germany
Electrons in magnetic nanostructures: Properties and transport coefficients
8.11.2010

SPIRIT Visitors

1. Barlak, M.
   Soltan Institute for Nuclear Studies, Swierk, Poland; 24.-28.05., 17.-30.10.2010
2. Barradas, N.P.
   Nuclear and Technological Institute Sacavem, Portugal; 22.-27.11.2010
3. Bochenska, K.
   Soltan Institute for Nuclear Studies, Swierk, Poland; 17.-23.10.2010
4. Bugoi, R.-N.
   Hulubei National Institute for Nuclear Physics and Engineering, Bucharest, Rumania; 8.-15.08.2010
5. Caciolli, A.
   National Institute for Nuclear Physics, Department of Physics, Padua, Italy; 30.05.-5.06., 8.-17.11.2010
6. de Diego Velasco, G.
   CIEMAT Madrid, Spain; 24.-30.10.2010
7. Decoster, S.
   Catholic University Leuven, Institute for Nuclear and Radiation Physics, Leuven, Belgium; 1.-6.08.2010
8. Dekov, V.
   Department of Geology and Palaeontology, University of Sofia, Bulgaria; 19.09.-2.10.2010
9. Dubios, C.
   Lyon Institute of Nanotechnology, Lyon, France; 20.-22.07.2010
10. Eder, F.
    Institute of Atomic and Subatomic Physics, TU Vienna, Austria; 1.-14.08.2010
11. Eric, M.
    Laboratory of Physics, Vinca Institute of Nuclear Sciences, Belgrade, Serbia; 6.-12.06.2010
12. Fülöp, Z.
    Institute of Nuclear Research, Hungarian Academy of Sciences, Debrecen, Hungary; 27.06.-1.07., 8.-11.11.2010
13. Gago Fernandez, R.
    Institute for Materials Science, CIEMAT Madrid, Spain; 6.-10.09.2010
14. Hernandez-Mayoral, M.
    Institute for Materials Science, CIEMAT Madrid, Spain; 30.05.-4.06.2010
15. Jakiela, R.
    Institute of Physics, Polish Academy of Sciences, Warsaw, Poland; 8.-13.08.2010
16. Karlusic, M.
    Experimental Physics Division, Ruder Boskovic Institute Zagreb, Croatia; 20.-24.09., 21.-27.11.2010
17. Kokkoris, M.
    National Technical University of Athens, Greece; 6.-12.06.2010
18. Lü, B.
    Linköping University, Sweden; 7.-9.12.2010
19. Martins, R.M.S.
    Nuclear and Technological Institute Sacavem, Portugal; 6.-13.11.2010
20. Meunier, C.
    University of Franche-Comte Montbeliard, France; 4.-8.07.2010
21. Nekvindova, P.
    Institute of Chemical Technology, Prague, Czech Republic; 24.-28.05.2010
22. Petrovic, S.
    Laboratory of Physics, Vinca Institute of Nuclear Sciences, Belgrad, Serbia; 6.-12.06.2010
23. Poll, I.
    City Museum of Bucharest, Rumania; 7.-14.08.2010
24. Prudon, G.
    Institute for Nanotechnologies Lyon, France; 20.-22.07.2010

25. Redondo Cubero, A.
Institute for Materials Science, CIEMAT Madrid, Spain; 5.-10.9.2010
26. Ritter, R.
Institute for Applied Physics, TU Vienna, Austria; 27.06.-2.07., 15.-20.08., 7.-12.11.2010
27. Romero-Gomez, P.
Materials Science Institute, University of Seville, Spain; 25.-30.07.2010
28. Saez Maderuelo, A.
Institute for Materials Science, CIEMAT Madrid, Spain; 24.-30.10.2010
29. Sterba, J.
Institute of Atomic and Subatomic Physics, TU Vienna, Austria; 12.-17.04.2010
30. Svecova, B.
Institute of Chemical Technology, Prague, Czech Republic; 24.-28.05.2010
31. Szücs, T.
Institute of Nuclear Research, Hungarian Academy of Sciences, Debrecen, Hungary; 21.-25.06., 1.-11.11.2010
32. Torres, M.
Materials Science Institute Madrid, Spain; 19.-24.09.2010
33. Vladimirova, M.
Department of Geology and Palaeontology, University of Sofia, Bulgaria; 19.09.-2.10.2010
34. Werner, Z.
Andrzej Soltan Institute for Nuclear Studies, Swierk, Poland; 23.-29.05., 24.-30.10.2010

FEL-Visitors

1. Balocco, C.
University of Manchester, UK; 27.-29.04., 18.-21.06.2010
2. Dean, N.
University of Oxford, UK; 15.05.-2.06.2010
3. Fromherz, T.
Institute of Semiconductor and Solid State Physics, University of Linz, Austria; 24.-31.05.2010
4. Kasjoo, S.R.
University of Manchester, UK; 27.-29.04.2010
5. Kehr, S.C.
School of Physics & Astronomy, University of St. Andrews, UK; 24.04.-6.05.2010
6. Kossacki, P.
National High Field Laboratory Grenoble, France; 28.6.-5.07.2010
7. Plochocka, P.
National High Field Laboratory Grenoble, France; 28.6.-5.07.2010
8. Rauter, P.
Institute of Semiconductor and Solid State Physics, University of Linz, Austria; 25.-31.05.2010
9. Zhang, L.
University of Manchester, UK; 18.-21.06.2010

ROBL-MRH Visitors

1. Barchasz, C.
Laboratory of Innovation for New Energy Technologies and Nanomaterials, CEA-LITEN, Grenoble, France; 23.-26.10.2011
2. Bayer, B.
Department of Engineering, University of Cambridge, UK; 17.-23.02.2010
3. Boulieau, A.
Laboratory of Innovation for New Energy Technologies and Nanomaterials, CEA-LITEN, Grenoble, France; 23.-26.10.2011

4. Braz Fernandes, F.M.
CENIMAT Caparica and New University of Lisbon, Portugal; 12.-16.02., 14.-22.06.2010
5. Brunken, S.
Institute Solar Fuels, Helmholtz-Zentrum Berlin, Germany; 17.-20.11.2010
6. Buljan, M.
Materials Science Division, Ruder Boskovic Institute Zagreb, Croatia; 27.10.-2.11.2010
7. Chacravarty, S.
Institute of Metallurgy, TU Clausthal, Clausthal-Zellerfeld, Germany; 24.02.-1.03.2010
8. Craciunescu, C.
Department of Structural Materials, CENIMAT Caparica, Portugal; 14.-22.06.2010
9. Colin, J.F.
Electrochemical Laboratory, Paul Scherrer Institute, Villigen, Switzerland; 23.-26.10.2011
10. Devillers, T.
Institute of Semiconductor and Solid State Physics, University of Linz, Austria; 8.-14.12.2010
11. Gonzalo, E.
Department of Solid State Chemistry and Materials Science, San Pablo University, Madrid, Spain; 19.-23.10.2010
12. Gruber, W.
Institute of Metallurgy, TU Clausthal, Clausthal-Zellerfeld, Germany; 24.02.-1.03.2010
13. Gutel, T.
Laboratory of Innovation for New Energy Technologies and Nanomaterials, CEA-LITEN, Grenoble, France; 23.-26.10.2011
14. Hofmann, S.
Department of Engineering, University of Cambridge, UK; 17.-23.02.2010
15. Horak, L.
Materials Science Division, Ruder Boskovic Institute Zagreb, Croatia; 27.10.-2.11.2010
16. Husak, M.
Department of Solid State Chemistry, Institute of Chemical Technology Prague, Czech Republic; 14.-18.05.2010
17. Kalinichenka, S.
Fraunhofer Institut IFAM, Dresden, Germany; 7.-13.04.2010
18. Kuhn, A.
Department of Solid State Chemistry and Materials Science, San Pablo University, Madrid, Spain; 19.-23.10.2010
19. Mahesh, K.K.
Department of Structural Materials, CENIMAT Caparica, Portugal; 12.-16.02., 14.-22.06.2010
20. Martin, J.F.
Institute of Materials, CNRS, Nantes, France; 23.-26.10.2011
21. Navarro Quezeda, A.
Institute of Semiconductor and Solid State Physics, University of Linz, Austria; 8.-14.12.2010
22. Perez Flores, J.C.
Department of Solid State Chemistry and Materials Science, San Pablo University, Madrid, Spain; 19.-23.10.2010
23. Plasis, J.
National Museum Prague, Czech Republic; 14.-18.05.2010
24. Radic, N.
Materials Science Division, Ruder Boskovic Institute Zagreb, Croatia; 27.10.-2.11.2010
25. Radvanyi, E.
Laboratory of Innovation for New Energy Technologies and Nanomaterials, CEA-LITEN, Grenoble, France; 23.-26.10.2011
26. Ratayski, U.
Institute of Materials Science, TU Bergakademie Freiberg, Germany; 16.-20.12.2010
27. Rey, M.
Laboratory of Innovation for New Energy Technologies and Nanomaterials, CEA-LITEN, Grenoble, France; 23.-26.10.2011
28. Roentzsch, L.
Fraunhofer Institut IFAM, Dresden, Germany; 7.-13.04.2010

29. Rohlicek, J.
Department of Solid State Chemistry, Institute of Chemical Technology Prague, Czech Republic; 14.-18.05.2010
30. Schimpf, C.
Institute of Materials Science, TU Bergakademie Freiberg, Germany; 16.-20.12.2010
31. Schmidt, H.
Institute for Technical Chemistry, TU Clausthal, Clausthal-Zellerfeld; Germany; 24.02.-1.03.2010
32. Schubert, J.
Institute for Bio- and Nanosystems, Forschungszentrum Jülich, Germany; 20.-23.11.2010
33. Schuhknecht, T.
Institute of Materials Science, TU Bergakademie Freiberg, Germany; 16.-20.12.2010
34. Silva, R.J.C.
Department of Structural Materials, CENIMAT Caparica, Portugal; 12.-16.02.2010
35. Simonin, L.
Laboratory of Innovation for New Energy Technologies and Nanomaterials, CEA-LITEN, Grenoble, France; 23.-26.10.2011
36. Weatherup, R.
Department of Engineering, University of Cambridge, UK; 17.-23.02.2010
37. Wintersberger, E.
Institute of Semiconductor and Solid State Physics, University of Linz, Austria; 8.-14.12.2010
38. Wirth, C.
Department of Engineering, University of Cambridge, UK; 17.-23.02.2010

Other Guests

1. Behar, M.
Universidade Federal do Rio Grande do Sul, Porto Alegre, Brazil; 12.-19.07.2010
2. Dekel, E. J.
Q. Bialik, Israel; 10.08.-30.09.2010
3. Gao, F.
Pacific Northwest National Laboratory, Richland, WA, USA; 24.07.-7.08.2010
4. Ghosh, S.
Indian Institute of Technology, Delhi, India; 19.06.-18.07.2010
5. Li, L.
Peking University, China; 1.01.-31.12.2010
6. Markov, A.,
Institute of High Current Electronics, Tomsk, Russia; 13.10.-15.11.2010
7. Mazalski, P.
Institute of Experimental Physics, University of Bialystok, Poland; 23.01.-7.02., 21.03.-10.04.2010
8. Maziewski, A.
Institute of Experimental Physics, University of Bialystok, Poland; 25.-31.01.2010
9. Nazarov, A.
Institute for Semiconductor Physics, UAS, Kiev, Ukraine; 2.-16.12.2010
10. Rice, W.
Rice University, Houston, TX, USA; 29.07.-7.11.2010
11. Rihawi, M.S.
Atomic Energy Commission, Damascus, Syria; 1.10.-31.12.2010
12. Smith, R.
Loughborough University, UK; 15.02.-31.07.2010
13. Tyagulskiy, S.
Institute for Semiconductor Physics, UAS, Kiev, Ukraine; 18.7.-13.8.2010
14. Varun, J.
Institute of Technology, Manipal, India; 15.01.-15.05.2010

15. Wassouf, A.
Atomic Energy Commission, Damascus, Syria; 28.02.-31.05.2010
16. Yao, S.
University of Chengdu, China; 1.01.-31.12.2010

Laboratory Visits

1. Abrasonis, G.
Advanced Light Source, Berkeley, USA; 1.-10.05.2010
2. Akhmadaliev, Sh.
CEREGE, Aix-en-Provence, France; 3.-7.05.2010
ETH Zürich, Switzerland; 4.-7.10.2010
3. Banholzer, A.
Swiss Light Source, PSI Villigen, Switzerland; 5.-15.10.2010
4. Bernert, K.
Swiss Light Source, PSI Villigen, Switzerland; 13.-19.03., 8.-12.11.2010
5. Borany, J. von
ESRF Grenoble, France; 5.-11.05., 18.-23.11.2010
6. Buhl, M.
Swiss Light Source, PSI Villigen, Switzerland; 13.-19.03., 8.-19.11.2010
7. Bunce, C.
Swiss Light Source, PSI Villigen, Switzerland; 23.-30.06., 5.-15.10.2010
8. Cornelius, S.
Canadian Light Source, Saskatoon, Canada; 14.-21.05.2010
9. Drachenko, O.
LNCMP Toulouse, France; 12.02.-7.03., 8.-23.05.2010
Institute for Microstructures, RAS, Nizhny Novgorod, Russia; 13.-28.03.2010
10. Erbe, A.
Universität Konstanz, Germany; 13.-19.04., 6.-9.06.2010
Swiss Light Source, PSI Villigen, Switzerland; 11.-19.11.2010
11. Facsko, S.
University of Cosenza, Calabria, Italy; 24.-27.11.2010
12. Franke, C.
BESSY, Berlin, Germany; 7.-12.06.2010
13. Friedrich, D.
Bilkent University Ankara, Turkey; 25.10.-11.11.2010
14. Grebing, J.
Universität Konstanz, Germany; 1.-12.06.2010
15. Grenzer, J.
ESRF Grenoble, France; 8.-16.02., 7.-14.06., 7.-15.09., 25.10.-2.11., 16.-23.11.2010
16. Haberjahn, M.
University of Surrey, UK; 13.-18.06.2010
17. Hanf, D.
CEREGE, Aix-en-Provence, France; 3.-7.05., 8.-11.11.2010
18. Hanisch, A.
DESY, Hamburg, Germany; 1.-8.03.2010
19. Heinig, K.H.
Bilkent Universität Ankara, Turkey; 25.-28.10.2010
20. Heller, R.
CEREGE, Aix-en-Provence, France, 3.-7.05., 8.-11.11.2010
21. Henschel, T.
Swiss Light Source, PSI Villigen, Switzerland; 12.-19.11.2010

22. Kelling, J.
KFKI Research Institute for Particle and Nuclear Physics, Budapest, Hungary; 6.-13.12.2010

23. Klare, S.
ETH Zürich, Switzerland; 4.-7.10.2010

24. Körner, M.
Swiss Light Source, PSI Villigen, Switzerland; 13.-19.03., 23.-30.06.2010

25. Kosmata, M.
University of Surrey, UK; 13.-18.06.2010
ESRF Grenoble, France; 18.-23.11.2010

26. Lehmann, J.
University of Porto Alegre, Brazil; 21.10.-2.12.2010

27. Merchel, S.
CEREGE, Aix-en-Provence, France; 3.-7.05., 8.-12.11., 6.-10.12.2010

28. Möller, W.
University of Sydney, Australia; 30.10.-3.12.2010

29. Munnik, F.
ETH Zürich, Switzerland; 4.-7.10.2010

30. Neubert, A.
Swiss Light Source, PSI Villigen, Switzerland; 17.-24.06.2010
Diamond Light Source, Didcot, UK; 26.-31.05., 1.-6.12.2010

31. Roshchupkina, O.
ESRF Grenoble, France; 8.-16.02., 7.-14.06., 7.-15.09., 16.-23.11.2010

32. Schneider, H.
Universität Freiburg, Germany; 24.-28.05.2010
BESSY, Berlin, Germany; 6.-12.06.2010
X'ian University, Beijing, China; 18.-27.09.2010
Hebrew University, Jerusalem, Israel; 2.-9.10.2010

33. Schönherr, T.
Swiss Light Source, PSI Villigen, Switzerland; 13.-19.03.2010

34. Shalimov, A.
ESRF Grenoble, France; 7.-15.09.2010

35. Strache, T.
Swiss Light Source, PSI Villigen, Switzerland; 13.-19.03., 17.-30.06., 5.-15.10.2010
Glasgow University, UK; 15.-19.11.2010

36. Talut, G.
Svedberg Laboratory, University of Uppsala, Sweden; 13.-16.04., 24.-27.05.2010

37. Wiesenhütter, U.
Swiss Light Source, PSI Villigen, Switzerland; 8.-12.11.2010

38. Wieser, M.
Universität Konstanz, Germany; 1.-12.06.2010

39. Winnerl, S.
BESSY, Berlin, Germany; 6.-11.06.2010

40. Wintz, S.
Advanced Light Source, Berkeley, USA; 23.02.-8.03., 26.04.-12.05., 15.-30.09.2010
Swiss Light Source, PSI Villigen, Switzerland; 13.-19.03., 17.-30.06., 5.-15.10., 8.-19.11.2010

41. Vinnichenko, M.
Bilkent Universität Ankara, Turkey; 25.-28.10.2010

42. Zschintzsch, M.
ESRF Grenoble, France; 5.-11.05.2010

Projects

The projects are listed with respect to the funding institution and the project starting date. In addition the institute has also several bilateral service collaborations with industrial companies and research institutes. These activities are not included in the following overview.

European Projects

1. 04/2005 – 09/2010 European Union — EU
PRONANO – Technology for the production of massively parallel intelligent cantilever-probe platforms for nanoscale analysis and synthesis
Dr. B. Schmidt *Phone: 0351 260 2726* *bernd.schmidt@hzdr.de*

2. 09/2005 – 02/2010 European Union — EU
FOREMOST – Fullerene-based opportunities for robust engineering: Making optimised surfaces for tribology
Prof. A. Kolitsch *Phone: 0351 260 3348* *a.kolitsch@hzdr.de*

3. 01/2006 - 06/2010 European Union — EU
ITS-LEIF - Ion technology and spectroscopy at low energy ion beam facilities
Dr. S. Facsko *Phone: 0351 260 2987* *s.facsko@hzdr.de*

4. 04/2006 - 03/2010 European Union — EU
AIM - Center for application of ion beams to materials research
Prof. A. Kolitsch *Phone: 0351 260 3348* *a.kolitsch@hzdr.de*

5. 03/2009 – 02/2013 European Union — EU
SPIRIT – Support of Public and Industrial Research using Ion Beam Technology
Prof. W. Möller *Phone: 0351 260 2245* *w.moeller@hzdr.de*

6. 03/2009 – 08/2011 European Union — EU
ELISA – European Light Sources Activities: Synchrotrons and Free Electron Lasers
Prof. M. Helm *Tel. 0351 260 2260* *m.helm@hzdr.de*

German Science Foundation Projects

7. 06/2005 – 03/2010 Deutsche Forschungsgemeinschaft — DFG
Mössbauerspektroskopie an ionenimplantierten magnetischen Halbleitern
Dr. H. Reuther *Phone: 0351 260 2898* *h.reuther@hzdr.de*

8. 04/2007 - 11/2010 Deutsche Forschungsgemeinschaft — DFG
Ion-beam induced rippling at the amorphous-crystalline interface in silicon
Dr. J. Grenzer *Phone: 0351 260 3389* *j.grenzer@hzdr.de*

9. 05/2007 - 08/2010 Deutsche Forschungsgemeinschaft — DFG
Strukturübergänge eingebetteter magnetischer Nanopartikel
Dr. K. Potzger *Phone: 0351 260 3148* *k.potzger@hzdr.de*

10. 07/2007 - 01/2013 Deutsche Forschungsgemeinschaft — DFG
Hybride magnetische Materialien
Prof. J. Fassbender *Phone: 0351 260 3096* *j.fassbender@hzdr.de*

11. 08/2007 - 11/2010 Deutsche Forschungsgemeinschaft — DFG
Nanostrukturierung von Oberflächen mit direkter Extraktion der Ionen aus Plasmaquellen
Dr. S. Facsko *Phone: 0351 260 2987* *s.facsko@hzdr.de*

12. 08/2007 - 10/2010 Deutsche Forschungsgemeinschaft — DFG
Selbstorganisierte Nanostrukturen durch niederenergetische Ionenstrahlerosion
Dr. K.-H. Heinig *Phone: 0351 260 3288* *k.h.heinig@hzdr.de*

13. 08/2007 - 08/2010 Deutsche Forschungsgemeinschaft — DFG
Ferromagnetism in transition metal doped ZnO
Dr. H. Schmidt *Phone: 0351 260 2724* *heidemarie.schmidt@hzdr.de*

14. 09/2007 - 10/2010 Deutsche Forschungsgemeinschaft — DFG
Infrared scattering near-field optical microscopy near dielectric (polaritonic) resonances using a free-electron laser
Prof. M. Helm *Phone: 0351 260 2260* *m.helm@hzdr.de*

15. 01/2008 - 03/2010 Deutsche Forschungsgemeinschaft DFG
Bildung, Stabilität und Struktur nanoskaliger Phasen in funktionellen Oxiden und ihre Auswirkung auf die Materialwissenschaft (Oxidkristalle)
Dr. S. Gemming *Phone: 0351 260 2470* *s.gemming@hzdr.de*

16. 02/2008 - 11/2010 Deutsche Forschungsgemeinschaft DFG
Adsorption von Molekülen an strukturierten Fluid-Feststoff-Grenzflächen
Dr. S. Gemming *Phone: 0351 260 2470* *s.gemming@hzdr.de*

17. 07/2008 - 06/2011 Deutsche Forschungsgemeinschaft DFG
Morphologie-induzierte magnetische Anisotropie- und Dämpfungsphänomene
Prof. J. Fassbender *Phone: 0351 260 3096* *j.fassbender@hzdr.de*

18. 02/2009 – 09/2011 Deutsche Forschungsgemeinschaft DFG
Electric-field control of magnetoresistance (Ferromagnetism II)
Dr. H. Schmidt *Phone: 0351 260 2724* *heidemarie.schmidt@hzdr.de*

19. 02/2009 – 01/2012 Deutsche Forschungsgemeinschaft DFG
Magnetismus von nanoskaligen CoCrPt-SiO_2-Filmen in templatbedingt geometrisch eingeschränkten Dimensionen (MAGTEMPLAT)
Prof. J. Fassbender *Phone: 0351 260 3096* *j.fassbender@hzdr.de*

20. 09/2009 – 08/2012 Deutsche Forschungsgemeinschaft DFG
Bestimmung der elektronischen Struktur von Punktdefekten mittels DAFS
Dr. S. Gemming *Phone: 0351 260 2470* *s.gemming@hzdr.de*

21. 11/2009 – 10/2012 Deutsche Forschungsgemeinschaft DFG
Electric field control of magnetoresistance (TCOMR)
Dr. H. Schmidt *Phone: 0351 260 2724* *heidemarie.schmidt@hzdr.de*

22. 02/2010 – 08/2010 Deutsche Forschungsgemeinschaft DFG
Electron-electron interaction effects
Dr. O. Drachenko *Phone: 0351 260 3593* *o.drachenko@hzdr.de*

23. 03/2010 – 08/2010 Deutsche Forschungsgemeinschaft DFG
Cyclotron resonance spectroscopy
Dr. O. Drachenko *Phone: 0351 260 3593* *o.drachenko@hzdr.de*

24. 04/2010 – 03/2011 Deutsche Forschungsgemeinschaft DFG
Oxidkristalle II
Dr. S. Gemming *Phone: 0351 260 2470* *s.gemming@hzdr.de*

25. 04/2010 – 03/2013 Deutsche Forschungsgemeinschaft DFG
Strukturbildende Prozesse in amorphen Kohlenstoffschichten
Dr. L. Bischoff *Phone: 0351 260 2963* *l.bischoff@hzdr.de*

26. 05/2010 – 03/2011 Deutsche Forschungsgemeinschaft DFG
Dynamic metallographic and magneto-optical polarization microscopy of magnetic shape memory systems (MSMA)
Dr. J. McCord *Phone: 0351 260 3709* *j.mccord@hzdr.de*

27. 05/2010 – 02/2013 Deutsche Forschungsgemeinschaft DFG
Hybride magnetische Materialien
Dr. J. McCord *Phone: 0351 260 3709* *j.mccord@hzdr.de*

28. 08/2010 – 09/2013 Deutsche Forschungsgemeinschaft DFG
Supraleitung in hochdotierten Gruppe IV Halbleitern (SuSi)
Dr. V. Heera *Phone: 0351 260 3343* *v.heera@hzdr.de*

29. 09/2010 – 08/2013 Deutsche Forschungsgemeinschaft DFG
Terahertz non-linear detection and quantum optical studies by resonant two-photon transitions in semiconductor quantum wells (TERATOP)
Dr. H. Schneider *Phone: 0351 260 2880* *h.schneider@hzdr.de*

30. 11/2010 – 12/2013 Deutsche Forschungsgemeinschaft DFG
Relaxation dynamics in graphene
Dr. S. Winnerl *Phone: 0351 260 3522* *s.winnerl@hzdr.de*

31. 11/2010 – 10/2013 Deutsche Forschungsgemeinschaft DFG
Ionenstrahlerosion II
Dr. K.-H. Heinig *Phone: 0351 260 3288* *k.h.heinig@hzdr.de*

FRG R&D Projects

32. 07/2008 - 12/2010 Bundesministerium für Bildung und Forschung BMBF
WTZ Russland: Duplexbehandlung rostfreier Stähle
Prof. A. Kolitsch *Phone: 0351 260 3348* *a.kolitsch@hzdr.de*

33. 07/2008 - 08/2011 Bundesministerium für Bildung und Forschung BMBF
Multifunktionale Speicherkonzepte
Prof. J. Fassbender *Phone: 0351 260 3096* *j.fassbender@hzdr.de*

34. 05/2009 – 04/2011 Bundesministerium für Bau, Verkehr und Stadtentwicklung BMBVS
FZR- Applikationslabor Ionentechnologie
Prof. A. Kolitsch *Phone: 0351 260 3348* *a.kolitsch@hzdr.de*

35. 06/2009 – 05/2012 Bundesministerium für Bildung und Forschung BMBF
Rezeptor-selektive Anreicherung und Bio-LED-Sensorik zur Detektion von (anti-) östrogen- und (anti-) androgenwirkenden Substanzen (BIO-LED-Sensorik)
Dr. L. Rebohle *Phone: 0351 260 3368* *l.rebohle@hzdr.de*

36. 06/2009 – 05/2011 AG Industrieller Forschungsvereinigungen (AiF) BMWi
Unterdrückung der Sauerstoffversprödung von Titanlegierungen (II)
Prof. A. Kolitsch *Phone: 0351 260 3348* *a.kolitsch@hzdr.de*

37. 01/2010 – 12/2011 AG Industrieller Forschungseinrichtungen (AiF) BMWi
Advanced coatings to suppress environmental embrittlement of TiAl alloys (ACETAL)
Prof. A. Kolitsch *Phone: 0351 260 3348* *a.kolitsch@hzdr.de*

38. 03/2010 – 04/2011 Bundesministerium für Wirtschaft BMWi
Exist – Gründerstipendium SAXRAY
Dr. S. Gemming *Phone: 0351 260 2470* *s.gemming@hzdr.de*

39. 04/2010 – 03/2013 Bundesministerium für Bildung und Forschung BMBF
RainbowEnergy
Dr. K-.H. Heinig *Phone: 0351 260 3288* *k.h.heinig@hzdr.de*

40. 05/2010 – 10/2012 AG Industrieller Forschungseinrichtungen (AiF) BMWi
TCO Grenzflächenoptimierung
Prof. A. Kolitsch *Phone: 0351 260 3348* *a.kolitsch@hzdr.de*

41. 07/2010 – 06/2013 Gesellschaft für Chemische Technik und Biotechnologie DECHEMA
Ionenimplantation von TiAl-Proben
Prof. A. Kolitsch *Phone: 0351 260 3348* *a.kolitsch@hzdr.de*

42. 12/2010 – 12/2011 Gesellschaft für Chemische Technik und Biotechnologie DECHEMA
Cl-Ionenimplantation von Proben Nickelbasislegierungen
Prof. A. Kolitsch *Phone: 0351 260 3348* *a.kolitsch@hzdr.de*

43. 10/2010 – 09/2013 Bundesministerium für Bildung und Forschung BMBF
Photoinitiated dynamics studied in the fs to ns time and the THz to PHz frequency domain: Picosecond beamline at FELBE (PIDID)
Dr. H. Schneider *Phone: 0351 260 2880* *h.schneider@hzdr.de*

Saxony R&D Projects

44. 07/2009 – 06/2012 Sächsische Aufbaubank SAB
High-k Gate Dielektrika 2. Generation (KZWEI)
Dr. W. Skorupa *Phone: 0351 260 3612* *w.skorupa@hzdr.de*

45. 12/2010 – 05/2013 Sächsische Aufbaubank SAB
Kelvin-Kraft-Mikroskopie
Dr. H. Schmidt *Phone: 0351 260 2724* *heidemarie.schmidt@hzdr.de*

Personnel Exchange Projects

46. 01/2009 – 12/2010 Deutscher Akademischer Austauschdienst DAAD
Projektbezogener Personenaustausch mit Polen (University Bialystok)
Prof. J. Fassbender *Phone: 0351 260 3096* *j.fassbender@hzdr.de*

47. 05/2009 – 04/2011 Alexander-von-Humboldt-Stiftung AvH
Gastaufenthalt Frau Bhattacharyya (Tatar State University, Russia)
Dr. H. Schneider *Phone: 0351 260 2880* *h.schneider@hzdr.de*

48. 07/2009 – 06/2011 Deutscher Akademischer Austauschdienst DAAD
Projektbezogener Personenaustausch mit Großbritannien (University of Glasgow)
Prof. J. Fassbender Phone: 0351 260 3096 j.fassbender@hzdr.de

49. 09/2009 – 02/2011 Alexander-von-Humboldt-Stiftung AvH
Gastaufenthalt Dr. El-Said (MansouraUniversity, Egypt)
Dr. S. Facsko Phone: 0351 260 2987 s.facsko@hzdr.de

50. 10/2009 – 06/2010 Heraeus Stiftung HS
WE-Heraeus-Physikschule 2010
Dr. S. Gemming Phone: 0351 260 2470 s.gemming@hzdr.de

51. 01/2010 – 12/2011 Deutscher Akademischer Austauschdienst DAAD
Projektbezogener Personenaustausch mit Frankreich (CEREGE Aix-en-Provence)
Dr. S. Merchel Phone: 0351 260 2802 s.merchel@hzdr.de

52. 01/2010 – 12/2011 Deutscher Akademischer Austauschdienst DAAD
Projektbezogener Personenaustausch mit Brasilien (University Porto Allegre)
Dr. L. Rebohle Phone: 0351 260 3368 l.rebohle@hzdr.de

53. 03/2010 – 05/2010 International Atomic Energy Agency IAEA
IAEA-Gastaufenthalt Mr. Wassouf (AEC of Syria, Damaskus, Syria)
Dr. S. Merchel Phone: 0351 260 2802 s.merchel@hzdr.de

54. 06/2010 – 07/2010 Deutscher Akademischer Austauschdiens DAAD
DAAD-Gastaufenthalt Prof. Ghosh (VIT University, Vellore, India)
Prof. M. Helm Phone: 0351 260 2260 m.helm@hzdr.de

55. 10/2010 – 12/2010 International Atomic Energy Agency IAEA
IAEA-Gastaufenthalt Dr. Rihawy (AEC of Syria, Damaskus, Syria)
Dr. S. Merchel Phone: 0351 260 2802 s.merchel@hzdr.de

Bilateral Projects

56. 11/2007 - 10/2010 Eifeler GmbH Industry
Technologietransfer c-BN II
Prof. A. Kolitsch Phone: 0351 260 3348 a.kolitsch@hzdr.de

57. 05/2008 - 04/2012 FHR Anlagenbau Ottendorf-Okrilla/IHP Frankfurt/O. Industry
Blitztemperung 200
Dr. W. Skorupa Phone: 0351 260 3612 w.skorupa@hzdr.de

58. 09/2008 - 06/2011 TU Dresden TUD
Modellieren der Bedeckung keramischer Oberflächen mit Wachstumsproteinen (BIOMIN)
Dr. S. Gemming Phone: 0351 260 2470 s.gemming@hzdr.de

59. 07/2009 – 06/2011 TU Bergakademie Freiberg TU-BA
Eigenschaften nano- und mikrokristalliner Si-Dünnfilme
Dr. W. Skorupa Phone: 0351 260 3612 w.skorupa@hzdr.de

60. 04/2010 – 03/2012 FHR Anlagenbau / Centrotherm Industry
Entwicklung industrietauglicher Temperaturmessung
Dr. W. Skorupa Phone: 0351 260 3612 w.skorupa@hzdr.de

61. 05/2010 – 06/2011 Brehm Präzisionstechnik Ulm GmbH Industry
Osteofit 2030
Prof. A. Kolitsch Phone: 0351 260 3348 a.kolitsch@hzdr.de

62. 10/2010 – 09/2013 DTF Technology Dresden Industry
DTF- Industriedoktoranden
Prof. A. Kolitsch Phone: 0351 260 3348 a.kolitsch@hzdr.de

Experimental Equipment

1. Accelerators, Ion Implanters and Ion-Assisted-Deposition

⇒	Van de Graaff Accelerator	(VdG)	1,8 MV	*TuR Dresden, DE*
⇒	Tandem Accelerator	(Td)	5 MV	*NIIEFA, RU*
⇒	Tandetron Accelerator	(Tdt)	3 MV	*HVEE, NL*
⇒	Tandetron Accelerator (commissioning)		6 MV	*HVEE, NL*
⇒	Low-Energy Ion Implanter		0.5 - 50 kV	*Danfysik, DK*
⇒	High-Current Ion Implanter		20 - 200 kV	*Danfysik, DK*
⇒	High-Energy Ion Implanter		40 - 500 kV	*HVEE, NL*
⇒	Plasma Immersion Ion Implantation		5 - 60 keV	*GBR, DE/Home-built*
⇒	Focused Ion Beam (15 nm, variable ions)		30 keV, 10 A/cm^2	*Orsay Physics, FR*
⇒	Highly-Charged Ion Facility		25 eV – 25 keV×q q = 1…40 (Xe)	*Home-built*
⇒	Dual-Beam Magnetron Sputter Deposition			*Roth & Rau, DE*
⇒	Ion-Beam-Assisted Deposition			*Danfysik, DK*
⇒	Ion-Beam Sputtering		200 - 2000 V	*Home-built*
⇒	UHV Ion Irradiation (Ar, He, etc.)		0 - 5 keV Scan 10×10 mm^2	*VG, USA*

2. Ion Beam Analysis (IBA)

A wide variety of advanced IBA techniques are available at the MeV accelerators (see figure).

⇒	RBS	Rutherford Backscattering	(1), (2), (3), (8)	*VdG, Td, Tdtr*
⇒	RBS/C	RBS + Channelling	(1), (2), (3), (8)	*VdG, Td, Tdtr*
		High-Resolution RBS/C	(7), (10)	*Tdtr*
⇒	ERDA	Elastic Recoil Detection Analysis	(2), (4), (5)	*VdG, Td*
		High-resolution ERDA	(7)	*Td*
⇒	PIXE	Proton-Induced x-ray Emission	(3)	*Td*
⇒	PIGE	Proton-Induced γ Emission	(3)	*Td*
⇒	NRA	Nuclear Reaction Analysis	(4)	*Td*
⇒	NRRA	Nuclear Resonance Reaction Analysis	(6)	*Td*
⇒	NμP	Nuclear Microprobe	(9)	*Tdtr*
⇒	AMS	Accelerator Mass Spectrometry	(commissioning)	
		focused to cosmogenic radionuclides:	^{10}Be, ^{26}Al, ^{36}Cl, ^{41}Ca, ^{129}J	

Some stations are equipped with additional process facilities which enable *in-situ* IBA investigations during ion irradiation, sputtering, deposition, annealing etc.

3. Other Particle Based Analytical Techniques

⇒	SEM	Scanning Electron Microscope	1 - 30 keV + EDX	*Hitachi, JP*
⇒	TEM	Transmission Electron Microscope (Titan 80-300 with Image Corrector)	80 - 300 keV + EDX, +GIF	*FEI, NL*
⇒	FIB/SEM	Focused Ion / Electron Cross Beam (NVision 40 with Elphy Plus Litho)	0.5 – 30 keV + IL, + EDX	*Zeiss-NTS, DE* *Raith, Bruker, DE*
⇒	AES	Auger Electron Spectroscopy	+ XPS	*Fisions, UK*
⇒	CEMS	Mössbauer Spectroscopy	^{57}Fe source	*Home-built*
⇒	PAS	Positron Annihilation Spectroscopy	^{22}Na source 30 V - 36 kV	*Home-built*

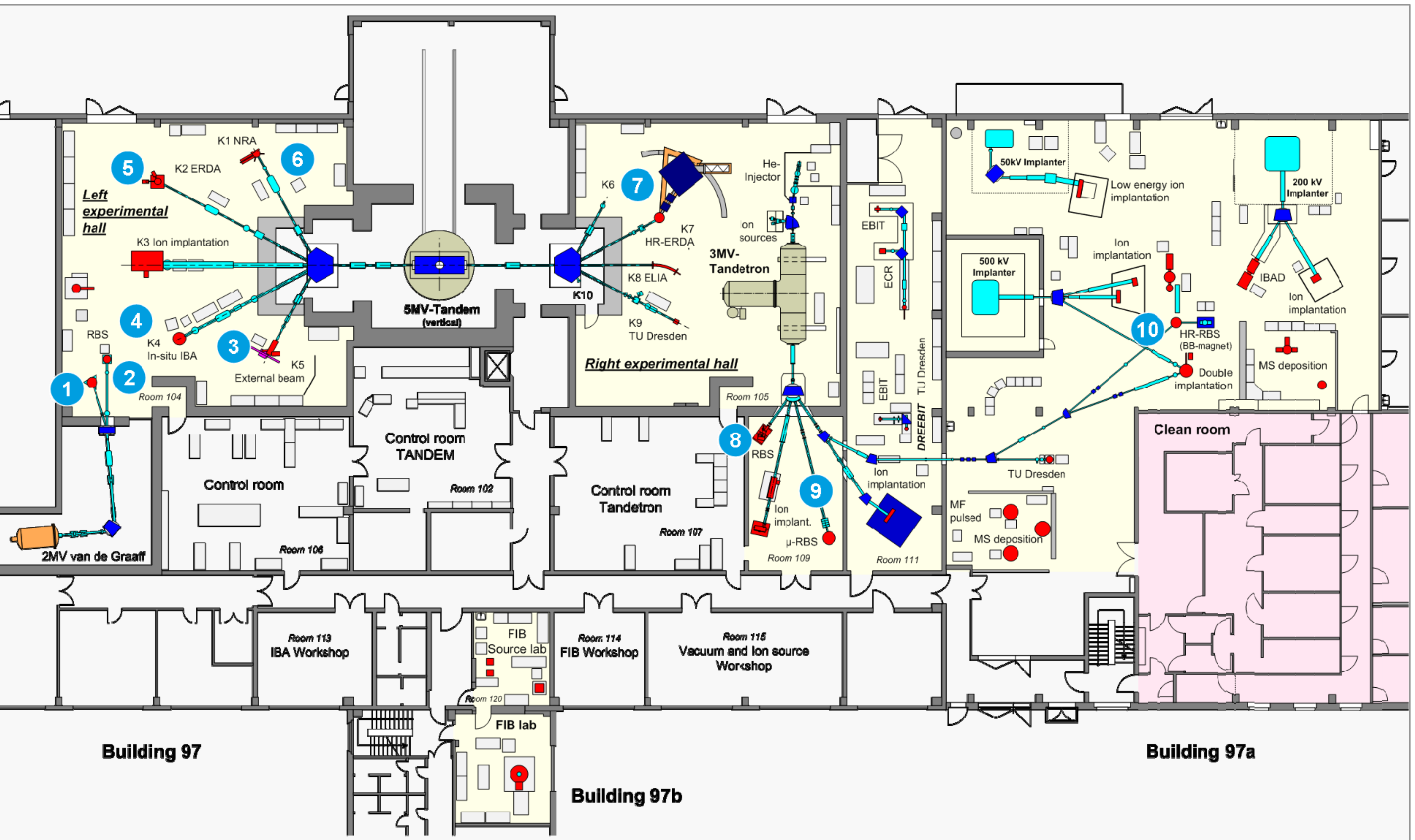

Ion Beam Centre: Schematic Overview of Installations.

4. Photon Based Analytical Techniques

⇒	XRD/XRR	X-Ray Diffraction and Reflection	Cu-K_α	*Bruker axs, DE*
	HR-XRD	High-Resolution XRD	Cu-K_α	*GE Inspection, DE*
⇒	XRD/XRR	with Synchrotron Radiation	5 – 35 keV	*ROBL at ESRF, FR*
⇒	SE	Spectroscopic Ellipsometry	250 - 1700 nm	*Woolam, US*
⇒	FTIR	Fourier-Transform Infrared Spectr.	600 - 7000 cm^{-1}	*Nicolet, US*
⇒	FTIR	Fourier-Transform Infrared Spectr.	50 - 15000 cm^{-1}	*Bruker, DE*
⇒		Ti:Sapphire Femtosecond Laser		*Spectra Physics, US*
⇒		Femtosecond Optical Parametric Osci.		*APE, DE*
⇒		Ti:Sapphire Femtosecond Amplifier		*Femtolasers, AT*
⇒		Femtosecond Optical Parametric Amplifier		*Light Conversion, LI*
⇒	THz-TDS	Terahertz Time-Domain Spectroscopy	0.1 - 4 THz	*Home-built*
⇒	Raman	Raman Spectroscopy	45 cm^{-1} shift	*Jobin-Yvon-Horiba, FR*
⇒	PL	Photoluminescence	300 - 1500 nm	*Jobin-Yvon-Horiba, FR*
⇒	TRPL	Time-Resolved PL	τ = 3 ps - 2 ns	*Hamamatsu Phot., JP*
			τ > 5 ns	*Stanford Research, US*
⇒	EL	Electroluminescence (10-300 K)	300 - 1500 nm	*Jobin-Yvon-Horiba, FR*
		Optical Split-Coil Supercond. Magnet	7 T	*Oxford Instrum., UK*
⇒	PR	Photomodulated Reflectivity	300 - 1500 nm	*Jobin-Yvon-Horiba, FR*
⇒	PLE	Photoluminescence Excitation	300 - 1500 nm	*Jobin-Yvon-Horiba, FR*

5. Magnetic Thin Film Deposition and Analysis

⇒	MBE	Molecular Beam Epitaxy with in-situ FIB		*CreaTec, DE*
⇒	MBE	Molecular Beam Epitaxy		*Home-built*
⇒	PLD	Pulsed Laser Deposition		*SURFACE, DE*
⇒	MFM	Magnetic Force Microscope	~ 50 nm resol.	*VEECO / DI, US*
⇒	SQUID	Supercond. Quantum Interf. Device	± 7 T	*Quantum Design, US*
⇒	MOKE	Magneto-Optic Kerr Effect (in-plane)	± 0.35 T	*Home-built*
⇒	MOKE	Magneto-Optic Kerr Effect (perpend.)	± 2 T	*Home-built*
⇒	SKM	Scanning Kerr Microscope		*Home-built*
⇒	TR-MOKE	Time-Resolved MOKE (Pump-Probe)		*Home-built*
⇒	VNA-FMR	Vector Network Analyzer Ferromagnetic Resonance		*Agilent / Home-built*
⇒	ME	Magnetoellipsometer		*LOT, DE; AMAC, US*

6. Other Analytical and Measuring Techniques

⇒	STM	Scanning Tunneling Microscope (with AFM-Option)		*DME, DK*
⇒	STM	*In-situ* Scanning Tunneling Microscope (T variable)		*Omicron, DE*
⇒	AFM	Atomic Force Microscope (Tapping Mode)		*SIS, DE*
⇒	AFM	Atomic Force Microscope (with c-AFM, SCM-Module)		*Veeco Instruments, UK*
⇒	KFM	Kelvin Probe Force Microscopy		*Anfatec, DE*
⇒		Dektak Surface Profilometer		*Veeco, US*
⇒		Micro Indenter / Scratch Tester		*Shimatsu, JP*
⇒		Wear Tester (pin-on disc)		*Home-built*
⇒	HE	Hall Effect Equipment	(2 - 400 K, ≤ 9 T)	*LakeShore, US*
⇒	RS	Sheet-Rho-Scanner		*AIT, South Korea*
⇒	DLTS	Deep Level Transient Spectroscopy	(+ IU / CV) (10 - 300 K, 1 MHz)	*PhysTech, DE*
⇒		Photocapacitance (+I-U/G-V)	(250 - 2500 nm)	*Home-built*
⇒		I-V and C-V Analyzer		*Keithley, US*
⇒		I-V and C-V Semi-Automatic Prober	(-60°C - +300°C)	*Süss, DE; Keithley, US*

7. Processing and Preparation Techniques

⇒ Etching / Cleaning	incl. Anisotropic Selective KOH Etching	
⇒ Photolithography	Mask-Aligner, 2 µm-level	*Süss, DE*
⇒ Thermal Treatment	Room Temperature - 2000°C	
• Furnace		*InnoTherm, DE*
• Rapid Thermal Annealing		*ADDAX, FR*
• Flash-Lamp Units (0.5 – 20 ms)		*Home-built; FHR, DE*
• RF Heating (Vacuum)		*JIP.ELEC, FR*
⇒ Physical Deposition	Sputtering DC / RF, Evaporation	*Nordiko, UK*
	Electron Beam Evaporation System	*Leybold Optics, DE*
	Thermal Evaporation	*Bal-Tec, LI*
⇒ Chemical Deposition	Plasma Enhanced CVD (for a-Si, SiO_2, SiON, Si_3N_4)	*Oxford Instruments, UK*
⇒ Dry Etching	Plasma and RIE Mode	*Sentech, DE*
⇒ Bonding Techniques	Ultrasonic Wire Bonding	*Kulicke&Soffa, US*
⇒ Cutting, Grinding, Polishing		*Bühler, DE*
⇒ TEM Sample Preparation	Plan View and Cross Section incl. Ion Milling Equipment	*Gatan, US*

SPIRIT

The Institute of Ion Beam Physics and Materials Research is coordinating the Integrated Infrastructure SPIRIT under the FP7 Capacities Programme of the European Union. The duration of the project is from March 2009 to February 2013, the total funding is 6.991.000 €.

SUPPORT OF **P**UBLIC AND **I**NDUSTRIAL **R**ESEARCH USING **I**ON BEAM **T**ECHNOLOGY

Integrated Activity, EU Project No. 227012
www.spirit-ion.eu

SPIRIT integrates 11 leading ion beam facilities from 6 European Member States and 2 Associated States. Seven of the partners provide Transnational Access to European researchers and industry at their infrastructures. Ion beams in an energy range from ~10 keV to ~100 MeV are supplied for modification and analysis of solid surfaces, interfaces, thin films and nanostructured systems, being mainly applied in research related to materials, biomedicine, environment, and cultural heritage. SPIRIT aims at increasing user access and the quality of research by sharing best practice, balancing supply and demand, harmonizing procedures and extending the services into new emerging fields and to new users especially from the New European Member States and industry. The project comprises a management section (4% of the total funding) and three interlinked activities, which are Transnational Access (45%), Networking (19%) and Joint Research (32%).

Potential users from public of industrial research are invited for free use of the ion beam facilities at the SPIRIT partners laboratories, either by conducting experiments personally or by sending samples in case of standard ion implantation or ion beam materials analysis. Regularly, access is given on a transnational basis, i.e. the user has to be employed in a European Member or Associate State in which the specific infrastructure is not situated. However, there are exceptions in particular in case of industrial use and/or non-conventional use of ion technologies.

Proposals may be turned in continuously through the SPIRIT website and will be evaluated promptly by an international User Selection Panel. Any successful proposer will be granted free access to the infrastructure, with the associated travel costs and daily expenses being covered by the European Commission.

Until 31-March-2010, the institute was providing Transnational User Access under the FP6 project AIM, which then has followed up by access under SPIRIT.

Helmholtz-Zentrum Dresden-Rossendorf	Germany
CNRS – CENBG Bordeaux	France
Katholieke Universiteit Leuven	Belgium
Jozef Stefan Institut Ljubljana	Slovenia
Universität der Bundeswehr München	Germany
CEA – JANNUS Saclay and CIMAP Caen	France
University of Surrey	U.K.
Institute Tecnologico e Nuclear Lisboa	Portugal
University de Pierre et Marie Curie Paris	France
Ruder Boskovic Institute Zagreb	Croatia
Swiss Federal Institute of Technology Zurich	Switzerland

The SPIRIT Consortium.
The top seven partners provide Transnational Access.

Free Electron Laser FELBE

ELBE is an acronym for the free-electron laser (FEL) at the Electron Linear accelerator with high Brilliance and Low Emittance (ELBE) located at the Helmholtz-Zentrum Dresden-Rossendorf, Germany. The heart of ELBE is a superconducting linear accelerator operating in cw mode with a pulse repetition rate of 13 MHz. The electron beam (40 MeV, 1 mA max.) is guided to several laboratories where secondary beams (particle and electromagnetic) are generated. Two free-electron lasers (U27-FEL and U100-FEL) produce intense, coherent electromagnetic radiation in the mid and far infrared, which is tunable over a wide wavelength range (4 – 250 µm) by changing the electron energy or the undulator magnetic field. Main parameters of the infrared radiation produced by FELBE are as follows:

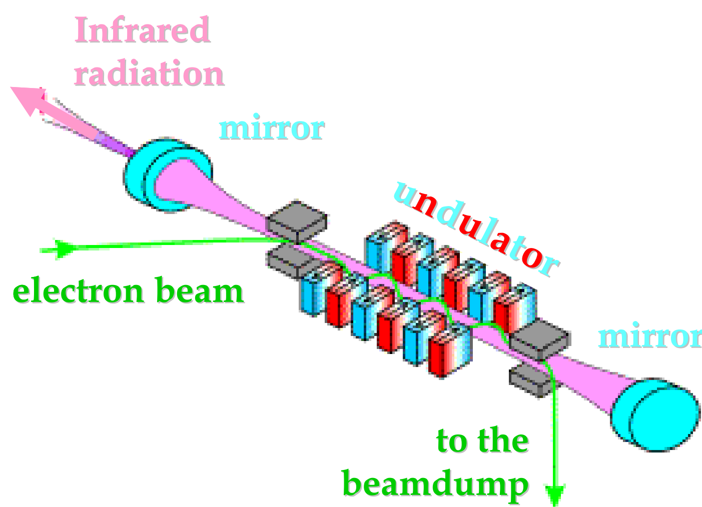

Wavelength λ	4 - 22 µm 18 – 250 µm	FEL with undulator U27 FEL with undulator U100
Pulse energy	0.01 – 2 µJ	depends on wavelength
Pulse length	1 – 25 ps	depends on wavelength
Repetition rate	13 MHz	3 modes: cw / macropulsed (> 100 µs, < 25 Hz) / single pulsed (Hz…kHz)

The free electron laser is a user facility. Applications for beam time can be submitted twice a year, typically by April, 15 and October, 15. User from EU countries can receive support through the FP7 Integrated Infrastructure Initiative (I3) ELISA (**E**uropean **LI**ght **S**ources **A**ctivities). Typical applications are picosecond pump-probe spectroscopy (also in combination with several other femtosecond lasers, which are synchronized to the FEL), near-field microscopy and nonlinear optics. The FELBE facility also serves as a far-infrared source for experiments at the High-Field Laboratory Dresden (HLD) involving pulsed magnetic fields up to 70 Tesla.

Beamtime Distribution at ELBE 2010
Scheduled: 5.940 h, Used: 4.990 h)

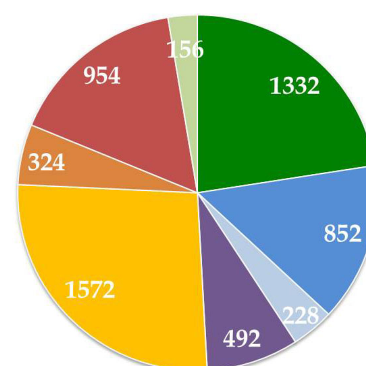

The statistics shows that the FEL used 1896 hours beamtime of the ELBE accelerator. This corresponds to 38% of total beamtime, which is again distributed among internal and external users as shown in the graph.

For further information please contact Prof. Manfred Helm (m.helm@hzdr.de) or visit the FELBE webpage www.hzdr.de/FELBE.

ROBL

The **RO**ssendorf **B**eam**L**ine (ROBL), operated by the HZDR since 1998, is a bending magnet synchrotron beam line located at the European Synchrotron Radiation Facility (ESRF) in Genoble, France. The set-up and main parameters are sketched as follows:

Energy range	6 – 35 keV
Energy resolution	$< 5 \times 10^{-4}$
Photon flux density	8×10^{9} phot./(s·mm²)
Divergence	(0.08 x 2.5) mrad
Beam size (typ.)	(0.4 x 5) mm²

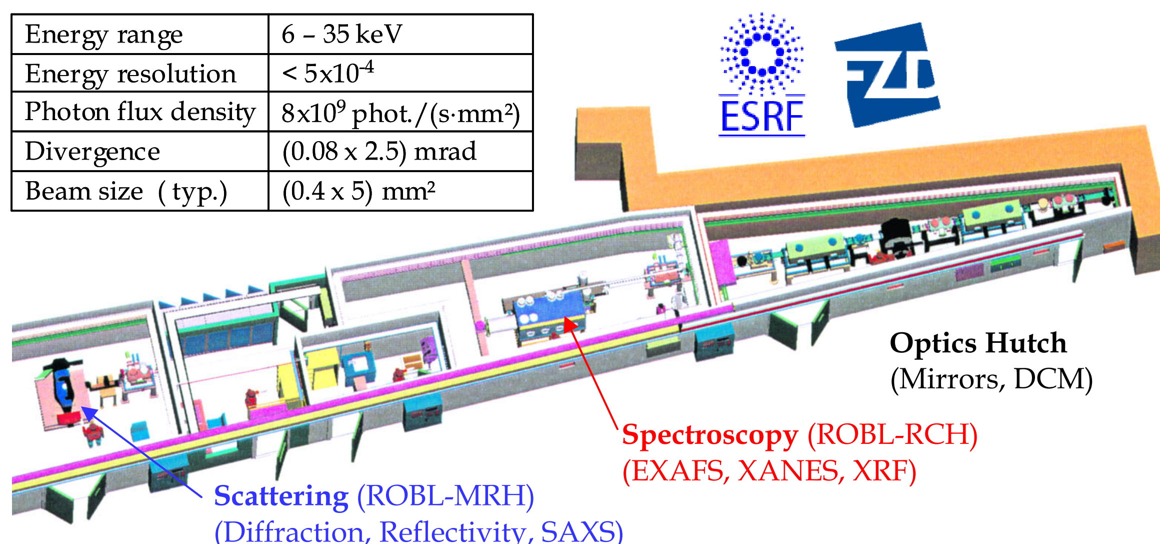

The activeness of ROBL is based upon the high specialization of its two end-stations for Radiochemistry (RCH) and Materials Research (MRH). ROBL-RCH is one of only two stations in Europe dedicated to X-ray absorption spectroscopy of actinides and other radionuclides. The core competence of ROBL-MRH is the analysis of thin films, multilayers and (ion-beam-synthesized) nanostructures using X-ray scattering techniques. Main aspects are the analysis of phase formation or transformations, nanostructure evolution, surface and interface characterization or strain/stress investigations at thin films. A continuously increasing number of experiments are performed as *in-situ* X-ray studies using process chambers for magnetron sputter deposition, ion irradiation or annealing under vacuum or various (including reactive) atmospheres, respectively.

ROBL has the status of an user facility. Applications for ROBL beam time can be submitted twice a year, typically by March, 1 and September, 1 via the official ESRF proposal submission portal. Successfully reviewed proposals will be financially supported by the ESRF by covering the travel and accommodation costs. In addition, there is also the possibility to use in-house research beam time for collaborative experiments between external users and FZD scientists for studies of common interest.

With more than 5000 beam time hours per year ROBL belongs to the most reliable and booked beam lines at the ESRF. The diagram at the right plots the beam time distribution of ROBL which reveal an availability of about 90% for experimental research studies.

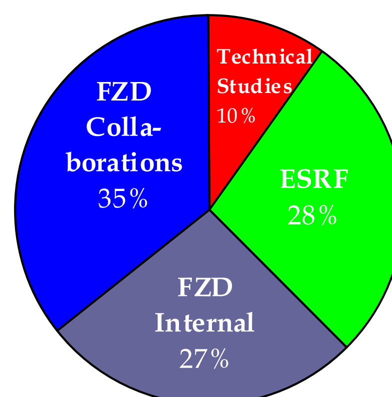

For further information please contact

Dr. A. Scheinost (ROBL-RCH): scheinost@esrf.fr
Dr. C. Bähtz (ROBL-MRH): baehtz@esrf.fr

or visit the ROBL webpage www.hzdr.de/ROBL.

Services

Main Areas of Competence:

- Ion implantation in a broad range of ion energy (~ 200 eV to ~ 50 MeV) and substrate temperature
- Advanced ion beam technologies (high energy ion implantation, plasma immersion ion implantation, focused ion beam) for (micro)electronic applications
- Deposition of functional coatings using ion-assisted physical vapor deposition
- Development and fabrication of sensors and detectors for charged particle spectroscopy
- High energy ion implantation service for power devices and laser structures
- Doping of semiconductors, in particular wide bandgap semiconductors
- Surface analysis of solid materials with high energy ion beams
- Computer simulation of ion beam interaction with materials
- Optical characterization of materials (luminescence, FTIR, Raman)

Offers:

- Consultation and problem evaluation for ion beam applications
- Process development for ion beam processing of metals, ceramics, semiconductors, thin films
- Preparation and treatment of material samples, tools or complex parts of devices
- Ion implantation and ion beam analysis services
- Fabrication of silicon radiation sensors under clean room conditions
- Structural diagnostics of materials surfaces including e-beam- (SEM, TEM, AES) and X-ray techniques (XRD, XRR with both Cu-K and Synchrotron (5-35 keV) radiation).

Contact:

Please direct your inquiry about the application of ion beams for modification and analysis of materials to one of the following experts:

Field of application	Name	Phone / Fax	E-mail
Ion implantation (metals, ceramics, polymers, biomaterials)	Prof. Andreas Kolitsch	3348 / 2703	a.kolitsch@hzdr.de
(High-energy) Ion implantation in semiconductors	Dr. Johannes von Borany	3378 / 3438	j.v.borany@hzdr.de
Thin film deposition	Prof. Andreas Kolitsch	3348 / 2703	a.kolitsch@hzdr.de
High-energy ion beam analysis	Dr. Silke Merchel	2802 / 3701	s.merchel@hzdr.de
Semiconductor preparation Detector / Sensor fabrication	Dr. Bernd Schmidt	2726 / 3285	bernd.schmidt@hzdr.de
Focused ion beams	Dr. Lothar Bischoff	2963 / 3285	l.bischoff@hzdr.de
Structural diagnostics	Dr. Johannes von Borany	3378 / 3438	j.v.borany@hzdr.de
Materials research with Synchrotron radiation at ROBL (ESRF)	Dr. Carsten Bähtz	2367	baehtz@esrf.fr
Optical materials characterization	Dr. Harald Schneider	2880 / 3285	h.schneider@.de

For all phone/ fax-numbers choose the country / local code: +49 351 260 - xxxx (for HZDR)
+33 47 688 - xxxx (for ROBL)

The institute also recommends the homepages of its spin-off companies

- "GeSiM mbH" Si- Microsystems www.gesim.de
- "APT Dresden" Applied Pulse Technology www.apt-dresden.de
- "DFT GmbH" Thin Film Technology www.dtf-technology.de

Helmholtz – Zentrum Dresden – Rossendorf e.V.

Institute of Ion Beam Physics and Materials Research (IIM)

P.O. Box 51 01 19
01314 Dresden
Phone: +49 351 260 2345
Fax: + 49 351 260 3285
http://www.hzdr.de/FWI

DIRECTORS

Prof. Dr. Manfred Helm (- 2260) / Prof. Dr. Jürgen Fassbender (-3096)
Prof. Dr. Wolfhard Möller (-2245) (ret.)

DIVISIONS

SEMICONDUCTOR MATERIALS
Dr. Wolfgang Skorupa / 3612 — **FWIM**

- Semiconductor Nanostructures
- Nanophotonics
- Subsecond Thermal Processing
- Magnetic Semiconductors

ION BEAM ANALYSIS
Dr. Silke Merchel / 2802 — **FWIA**

- MeV Accelerator Operation
- High-Energy Ion Beam Analysis
- Accelerator Mass Spectrometry
- Non-destructive Analysis of Art Objects

SEMICONDUCTOR SPECTROSCOPY
Dr. Harald Schneider / 2880 — **FWIH**

- Semiconductor Quantum Structures
- Terahertz Spectroscopy
- Femtosecond Spectroscopy
- Free Electron Laser at ELBE
- Optical Characterization (PL, FTIR, Raman)

ION TECHNOLOGY
Prof. Dr. Andreas Kolitsch / 3326 — **FWII**

- Ion Implanter / PIII operation
- Ion Beam and Plasma Assisted Deposition
- Transparent Conductive Oxides
- Biotechnological Materials
- Industrial Services and Projects

STRUCTURAL DIAGNOSTICS
Dr. Johannes von Borany / 3378 — **FWIS**

- Electron Microscopy (TEM, SEM)
- Electron Spectroscopy (AES, XPS)
- SEM / FIB Cross Beam Techniques
- X-ray Analysis / Mössbauer Spectroscopy
- Materials Research with Synchr. Radiation

NANOMAGNETISM
Dr. Jeff McCord / 3709 — **FWIN**

- Modification of Magnetic Materials
- Nano-Spintronics
- Magnetization Dynamics
- Magnetism at Interfaces
- High Anisotropy Nanoparticles

THEORY
Dr. Matthias Posselt / 3279 — **FWIT**

- Atomistic Computer Simulations
- Defects, Impurities, Nanostructures, Surfaces and Interfaces
- Formation, Evolution and Self-Organization
- Energetics and Kinetics

NANOSTRUCTURES
Dr. Sibylle Gemming / 2470 — **FWIO**

- Ion Induced Nanostructure Formation
- Slow Highly-Charged Ions
- Transport Phenomena in Nanostructures
- DFT Modelling of Nanostructured Matter
- Nanocomposite Materials

PROCESS TECHNOLOGY
Dr. Bernd Schmidt / 2726 — **FWIP**

- Clean Room Operation
- Semiconductor Technology and Processing
- Focused Ion Beam Technology
- Si Detector and Sensor Development
- Electrical Device Characterization

List of Personnel 2010

Directors:
Prof. M. Helm, Prof. J. Fassbender
Prof. W. Möller (ret.)

Office:
S. Kirch, A. Schiemann,
S. Vogelgesang

Scientific Staff:

Permanent:
Dr. G. Abrasonis
Dr. C. Akhmadaliev
Dr. C. Bähtz
Dr. L. Bischoff
Dr. J. von Borany
Dr. S. Facsko
Dr. S. Gemming
Dr. J. Grenzer
Dr. V. Heera
Dr. K.-H. Heinig
Dr. R. Kögler
Prof. A. Kolitsch
Dr. J. McCord
Dr. S. Merchel
Dr. A. Mücklich
Dr. F. Munnik
Dr. C. Neelmeijer
Dr. M. Posselt
Dr. K. Potzger
Dr. L. Rebohle
Dr. H. Reuther
Dr. B. Schmidt
Dr. H. Schneider
Dr. W. Skorupa
Dr. D. Stehr
Dr. M. Voelskow
Dr. S. Winnerl

Post Docs:
Dr. R. Heller
Dr. N. Jeutter
Dr. G. Kovacs
Dr. M. Wagner

Projects:
Dr. J. Bhattacharyya
Dr. C. Bunce
Dr. W. Bürger
Dr. C. Cherkouk
Dr. O. Drachenko
Dr. A. S. El-Said
Dr. A. Erbe
Dr. M. Friedrich
Dr. J. Grebing
Dr. M. Haberjahn
D. Henke
M. Herrmann
Dr. A. Kanjilal
G. Krahl (SAXRay)
Dr. M. Krause
Dr. T. Leisegang
Dr. K. Lenz
Dr. M. O. Liedke
Prof. W. Möller
Dr. J. Neidhart
Dr. A. Neudert
Dr. X. Ou
Dr. W. Pilz
Dr. J. Potfajova
Dr. S. Prucnal
Dr. A. Rogozin
Dr. H. Schmidt
Dr. A. Shalimov
Dr. G. Talut
Dr. M. Vinnichenko
Dr. R. Yankov
Dr. S. Zhou
Dr. M. Zier

PhD Students:
D. Ball
A. Banholzer
C. Baumgart
K. Bernert
M. Buhl
D. Bürger
S. Cornelius
R. Endler
J. Fiedler
M. Fritzsche
S. Germer
A. Hanisch
M. Höwler
R. Jacob
T. Kaspar
M. Körner
M. Kosmata
A. Kranz
T. Kunze
J. Lehmann
B. Liedke
D. Markó
N. Martin
A. Martinavicius
M. Mittendorff
K. M. Mok
M. Neubert
S. Numazawa
X. Ou
F. Peter
P. Philipp
M. Ranjan
D. Reichel
O. Roshchupkina
C. Scarlat
M. Schmidt
T. Strache
M. Teich
M. Thieme
A. Thorn
M. Vieluf
U. Wiesenhütter
M. Wieser
C. Wilde
S. Wintz
C. Wündisch
M. Zschintzsch
M. Zschornak
S. Zybell

Diploma Students:
M. Baudisch
S. Berger
R. Böttger
S. Dießner
C. Franke
F. Göttfert
F. Großmann
A. Haase
J. Kelling
T. Henschel
J. Krause
M. Langer
R. Mertzig
A. Mrotzek
I. Ronneberger
A. Neubert
J. Osten
E. Ritter
T. Schönherr
M. Schuster
S. Streit
R. Wenisch
R. Wiemann
R. Wilhelm

Technical Staff:

Permanent:

Ry. Aniol
Rb. Aniol
E. Christalle
S. Eisenwinder
B. Gebauer
H.-J. Grahl
D. Hanf
J. Haufe
A. Henschke
H. Hilliges
S. Klare
J. Kreher
A. Kunz
H. Lange
U. Lucchesi
F. Ludewig
R. Mester
M. Mißbach
C. Neisser
S. Probst
A. Reichel
M. Roch
B. Scheumann
G. Schnabel
A. Schneider
A. Scholz
T. Schumann
M. Steinert
U. Strauch
K. Thiemig
A. Vetter
J. Wagner
R. Weidauer
A. Weise
J. Winkelmann
U. Strauch
G. Winkler
I. Winkler
L. Zimmermann
J. Zscharschuch

Projects:

C. Frenzel
M. Kretzschmar
V. Kühn
T. Putzke
I. Skorupa
A. Weißig